NISTIR 5870

Shear Design of High-Strength Concrete Beams: A Review of the State-of-the-Art

Dat Duthinh
Nicholas J. Carino

August 1996
Building and Fire Research Laboratory
National Institute of Standards and Technology
Gaithersburg, MD 20899

U.S. Department of Commerce
Michael Kantor, *Secretary*
Technology Administration
Mary L. Good, *Under Secretary for Technology*
National Institute of Standards and Technology
Arati Prabhakar, *Director*

TABLE OF CONTENTS

ABSTRACT

This state-of-the-art review of the shear design of high-strength concrete (HSC) beams consists of four parts. In the first part, various analysis methods are presented:
a) The plastic solution assumes that both concrete, modeled as a modified Mohr-Coulomb material, and steel reinforcement are at yield. Under shear loading, the concrete web develops an inclined compression field which satisfies both upper and lower bound theorems. A plastic solution of shear friction is also discussed.
b) Both the compression field theory and the modified compression field theory (MCFT) are "exact"theories in the sense that they satisfy equilibrium, compatibility of displacements and stress-strain relationships. The MCFT accounts for the contribution of the tensile strength of concrete to shear resistance.
c) Other "exact" solutions are also discussed, that do not assume that the principal stress and principal strain directions are aligned with each other, as the MCFT does.
d) The 45° truss, the variable angle truss (VAT) and strut-and-tie models (STM) belong to a class of solutions that only satisfy equilibrium.

The second part of the report is a comparison of various National Codes:
a) The ACI Code is semi-empirical and based on the 45° truss with a correction term called the concrete contribution. For shear-friction, the ACI Code only accounts for a friction term.
b) The Canadian Code (CSA) and the AASHTO Code are more "rational" and based on the MCFT. STM are acceptable for "D" regions near supports, loads or sudden changes in geometry. For shear-friction, the CSA Code accounts for a friction and a cohesion term.
c) The Norwegian (NS) Code's general design method is also based on the MCFT. However, the VAT method and a simplified method are also allowed. Again, STM are acceptable for D regions. For shear-friction, the Norwegian Code accounts for a friction and a cohesion term.
d) The Japanese Code is based on an equilibrium theory and considers shear resistance as a combination of arch action and (variable angle) truss action.
e) The CEB-FIP Code is based on the VAT, and
f) so is the French Prestressed Concrete Code which includes a concrete contribution term.
g) However, the French Reinforced Concrete Code is based on the 45°truss with a concrete contribution term.

The third part of the report is a review of research results:
a) Beam test results are surveyed and compared to various empirical and design code equations.
b) Panel tests are reviewed, that simulate the state of biaxial tension and compression in beam webs.
c) Shear friction measurements and theories are discussed and
d) Size effect is briefly covered, with the help of fracture mechanics.

The last part of the report discusses future work. We recommend that emphasis be placed on experimental measurement of the shear friction properties of HSC. Biaxial behavior is also important, but would require a major commitment in funding. In addition, we recommend that NIST perform a parametric study of the strength of HSC beans, using the MCFT, to determine the influence of various models of shear friction and biaxial tension-compression softening; and that the work on automation of strut-and-tie modeling be expanded.

Keywords: building technology; compression field theory; design codes; high-strength concrete; reinforced concrete; shear strength; strut-and-tie model; truss model.

ERRATA

Page	Line	Is	Should be
vi	3rd from bottom	HSC beans	HSC beams
2	2nd §, end	Test results to date of HSC indicate a reduction in shear friction of up to 35 % compared to NSC.	Test results to date indicate that shear friction in HSC can be as low as 35 % of that in NSC.
60, 61		μ	μ_f
61, 62		f'_c	f_c
62		τ_o	τ_{f0}
62	before last	that given by Vecchio	the shear friction given by Vecchio
102	4th table	See Fig. 3.16. If $\sigma_{cr} = 0$, NS and Collins agree.	See Fig. 3.16.
103	midpage	NS does not provide any guidance on the calculation of θ and is even more general than MCFT:	NS uses the 1986 version of the MCFT, which is slightly more general than the 1991 version:
144	Fig. 4.15		Frame should be moved to the left to envelop all data points and lines.
151	last §	$0.012 < \varepsilon_1 < 0.0044$	$0.0012 < \varepsilon_1 < 0.0044$
165	midpage	... shear friction ... is reduced by 35 % for HSC	... shear friction ... is reduced to 35 % for HSC
165	near bottom	$\frac{v_u}{f'_c} = 0.43\sqrt{\omega}$	$\frac{v_u}{f'_c} = 0.23\sqrt{\omega}$

"Shear Design of High-Strength Concrete Beams: A Review of the State-of-the-Art"
NISTIR 5870 by Dat Duthinh and Nicholas J. Carino

1. INTRODUCTION

In the last 30 years, the compressive strength of concrete that can be produced reliably in the field has more than doubled, from 35 MPa (5000 psi) to 85 MPa (12 000 psi). Strengths as high as 140 MPa (20 000 psi) can be achieved in the laboratory and on rare occasions in the field[1]. Very high strengths have been achieved with Reactive Powder Concrete which is made of powders with no aggregate (200 MPa when hot water cured at 90°C and 800 MPa - twice the strength of most steels - when dry heated at 400°C. Bonneau et al 1996). These advances have been made possible by two major developments: the introduction of high range water-reducing admixtures (superplasticizers) and the use of silica fume. The admixtures allow the production of workable concrete mixtures with very low water-cement ratios, and the silica fume can produce cement paste with very low porosity.

High-strength concrete (HSC) will be used more and more frequently, to mention a few examples, in columns which can be made smaller and thus result in more useable floor space than if normal-strength concrete (NSC) were used (Walthers 1989); in joints between precast columns, which can then develop their full strength; in offshore structures where mass and buoyancy need to be considered (Jakobsen 1989); and in structures where durability (resistance to corrosion and abrasion) is important because HSC is less permeable than NSC. When strength is not the only consideration, the term high-performance concrete[2] (HPC) is preferred to high-strength concrete (HSC). In addition, early strength development of HSC can accelerate construction schedules significantly. For example, a 105-MPa HSC is as strong after one day as a 35-MPa NSC is after one month (Walraven 1995). Also, HPC exhibits excellent workability and an ability to self- desiccate, thus reducing or eliminating moisture problems due to concrete "sweating".

As far as shear strength is concerned, high-strength concrete presents three main challenges:

1) Current American Concrete Institute (ACI) code provisions for shear strength design rely on empirical rules whose data base is largely below 40 MPa (6000 psi). New design rules would have to rely on either rational methods or on tests that cover a higher range of strengths. Much progress has been made in the last 20 years on rational methods for shear design and there is hope that the rules can be made more understandable from first principles of mechanics, such as has been achieved for flexure. Moreover, it is likely that the rules can be made simple enough that they will gain adoption by the design community in the not-too-distant future. The Canadian

---

[1]Two Union Square in Seattle employs 130-MPa concrete, the highest strength used up to 1989 in a conventional building. Concrete with strength of 160 MPa has been used experimentally in Norway to armor pavement subjected to studded tires. The ice shield on the piers of the bridge that will link New Brunswick to Prince Edward Island in Canada uses 100 MPa concrete. The bridge is scheduled to be completed in 1997.

[2]The term "high-performance concrete" means concrete having special properties that are tailored to a specific application and which cannot be obtained by using only the basic ingredients of cement, water and aggregates.

Code (CSA 1994) and the Norwegian Code (NS 1992) are two pioneering examples of such efforts.

2) Shear failure surfaces in high-strength concrete members are smoother than in normal-strength concrete members, with cracks propagating *through* coarse aggregate particles rather than *around* them. Since one of the shear transfer mechanisms across cracks is by *aggregate interlock* this mechanism needs to be re-examined for high-strength concrete. Test results to date of HSC indicate a reduction in shear friction of up to 35% compared to NSC.

3) In the cracked web of a beam under shear, the portions of concrete between cracks act as compression struts that are also subjected to transverse tension, which reduces their compression capacity. Modeling of this softening behavior is based on tests. Softening shows a dependence on concrete strength that needs to be extended to HSC. However, test results to date indicate no marked difference in biaxial tension-compression behavior between HSC and NSC.

This report reviews in detail the literature on the shear problem in beams, with particular attention devoted to beams made of HSC. Chapter 2 surveys solution methods, starting with plasticity analyses, continuing with more exact solutions (such as the modified compression field theory) and ending with truss solutions often used in design (strut and tie). Chapter 3 compares various national concrete design codes. Some codes have remained basically unchanged for the last 30 years and still rely on the 45° truss with a concrete correction term, whereas other codes have achieved a remarkable level of rationality founded on more exact solutions. Chapter 4 reviews research results, mostly experimental: beam tests from around the world; panel tests (biaxial tension-compression) from Canada, the U.S.A., Europe and Japan; and shear friction tests from Europe and the U.S.A.. Fracture mechanics and size effect are also mentioned in Chapter 4, but they are topics that deserve a separate review. Finally, Chapter 5 is a proposal for work that NIST could perform in the next several years to improve the solution of shear problems in HSC beams, with a view to updating design and construction standards.

2. ANALYSIS METHODS

2.1 Elastic Solution — Uncracked RC Beams

In the uncracked state, reinforced concrete (RC) can be considered as a homogenous, elastic material. For a simply-supported, uniformly loaded beam, the combination of shear stresses, which are high at the supports, and bending stresses, which are high at midspan, cause the principal stress trajectories to change directions along the length of the beam (Fig. 2.1a), as shown, for example, by Mörsch (1909). For a brittle material such as concrete, reinforcement is provided to carry the tensile stresses. The elastic stress distribution provides the basis for using inclined reinforcing bars to resist the effect of shear, as shown in Fig. 2.1b.

Modern design methods, however, account for cracking in a reinforced concrete member, even under loads well below the ultimate strength of the member.

2.2 Plastic Solution — Cracked RC Beams

Designers are often more interested in designing a safe structure than in tracking its complete behavior over its loading history. This approach is called *limit state design*. The theory of plasticity offers useful tools for establishing the carrying capacity of structural members. Application of the theory of plasticity to structural engineering is based on the following two theorems:

1. If a load path can be found where equilibrium is satisfied, the boundary conditions are fulfilled and the material does not exceed the yield condition anywhere, then the structure is safe. This is the *lower bound theorem* of the theory of plasticity. The stress field can be continuous, as for example in the compression field theory, or it can be discontinuous, as for example in the strut-and-tie method.

2. On the other hand, the load that causes a failure mechanism compatible with the geometrical constraints of the structure is an *upper bound* of the strength of the structure.

Whereas the reinforcing steel exhibits a definite plastic behavior and a readily defined yield point (Fig. 2.2a), plain concrete exhibits strain-softening and a rather brittle behavior in compression (Fig. 2.2b). Concrete behavior can be idealized to have a yield plateau at $f_c = \nu f'_c$, where ν is a factor less than 1.0, whose value depends on the cylinder compressive strength f'_c, the ultimate strain ε_u and the application. ν is calculated by equating the area under the stress-strain curve for the real and the elastic-plastic curve, as shown in Fig. 2.2c. This *rigid-plastic* idealization has been found to be useful in soil mechanics and in the analysis of reinforced concrete behavior. For shear in RC beams with stirrups, an *average* empirical value is:

$$\nu = 0.8 - \frac{f'_c}{200}$$

A *safe* value is:

$$\nu = 0.7 - \frac{f'_c}{200}$$

which gives $\nu = 0.5$ for $f'_c = 40$ MPa. On the other hand, for punching shear,

$$\nu = \frac{3.2}{\sqrt{f'_c}}$$

(Nielsen 1984), which also gives $\nu = 0.5$ for $f'_c = 40$ MPa. It should be noted that the majority of

reinforced concrete members are under-reinforced and their strength is essentially determined by the yield strength of the reinforcement. The concrete model, i.e. the choice of ν, does not have a pronounced effect, except in over-reinforced cases. If an appropriate concrete compression strength (i.e. adjusted by tests) is taken into account, limit analysis leads to quite satisfactory strength predictions even for over-reinforced cases.

A model of concrete strength that has proved to be very useful is the *Mohr-Coulomb failure criterion*. According to the Coulomb theory, sliding failure occurs when (Fig.2.3a):

$$|\tau| = c - \mu\,\sigma = c - \sigma \tan\phi \tag{2.1}$$

where τ = shear stress,
σ = normal stress (tension is positive),
c = cohesion intercept (typical value for concrete = $f_c / 4$),
μ = $\tan\phi$ = friction coefficient, and
ϕ = friction angle (typical value for concrete = 37°).

If, in addition, a separation (fracture) failure criterion, such as

$$\sigma = f_t$$

can be defined, the material is called a *modified Mohr-Coulomb* material. From Fig. 2.3a:

$$AB = OB - OA$$

or

$$\frac{1}{2}(\sigma_1 - \sigma_3) = c\cos\phi - \frac{1}{2}(\sigma_1 + \sigma_3)\sin\phi$$

$$\left(\mu + \sqrt{1+\mu^2}\right)^2 \sigma_1 - \sigma_3 = 2c\left(\mu + \sqrt{1+\mu^2}\right)$$

$$k\,\sigma_1 - \sigma_3 = 2c\sqrt{k} \tag{2.2}$$

with

$$k = \left(\mu + \sqrt{1+\mu^2}\right)^2 = \tan^2\left(\frac{\pi}{4} + \frac{\phi}{2}\right) \tag{2.3}$$

The constants can be determined from a compression test, which according to this theory, involves sliding failure:

$$\sigma_1 = \sigma_2 = 0 \text{ and } \sigma_3 = -f_c$$

Substituting into Eq. 2.2, gives

$$-\sigma_3 = 2c\sqrt{k} = f_c \tag{2.4}$$

Therefore, Eq. 2.2 can be rewritten as

$$k\,\sigma_1 - \sigma_3 = f_c \tag{2.5}$$

Figure 2.3b shows the modified Mohr-Coulomb failure criterion plotted in terms of shear stress versus normal stress. If the Mohr's circle of stress touches the inclined boundary, failure is by sliding

as indicated by the circles representing uniaxial and triaxial compression. If the circle touches the tension cut-off, failure is by separation, as indicated by the circle representing uniaxial tension.

The Mohr-Coulomb criterion for sliding failure considers only the maximum shear stress, which is related to the difference between the largest and smallest principal stresses. Another way to view the failure envelope is in terms of principal stresses, which is shown in Fig. 2.4a for biaxial stress states. If tensile strength is neglected, the failure envelope is as shown in Fig. 2.4b.

2.2.1 Lower Bound Solution

Figure 2.5 shows a reinforced concrete beam with two concentrated loads applied at distance a from the supports. The portions of the beam between the supports and load points are subjected to a shear force equal to P. The yield envelope for the beam is reached when one or more of the following is attained:

- the longitudinal steel *(x)* yields,
- the transverse (stirrups) steel *(y)* yields, or
- the concrete "yields".

The following example, taken from Nielsen (1984), shows best how the method works.

Equilibrium— Consider shear loading only for the beam in Fig. 2.5, and assume that the concrete web develops a diagonal compression field making an angle θ to the x-axis. The stirrups and the lower stringer are in tension, whereas the upper stringer is in compression.

If the stirrups are closely spaced with horizontal spacing s, the stirrup stress σ_s can be replaced by an equivalent stirrup stress σ_{ys} distributed over the concrete area.

$$\sigma_{ys} = \frac{A_s \sigma_s}{b s} = r \sigma_s$$

where A_s is the stirrup area crossing the concrete area bs, and r is the reinforcement ratio. Upon transformation of the concrete diagonal compressive stress σ_c into the x-y coordinates, the total stress carried by the concrete and the stirrups are:

$$\sigma_x = -\sigma_c \cos^2\theta$$
$$\sigma_y = -\sigma_c \sin^2\theta + r \sigma_s$$
$$\tau = \sigma_c \sin\theta \cos\theta$$

These equations can be rewritten as

$$\sigma_c = \frac{\tau}{\sin\theta \cos\theta} = \tau (\tan\theta + \cot\theta)$$

$$\sigma_x = -\tau \cot\theta$$

Vertical equilibrium requires $\sigma_y = 0$, therefore,

$$r \sigma_s = \sigma_c \sin^2\theta = \tau \tan\theta \qquad (2.6)$$

Yield Conditions — If the upper and lower stringers are strong enough, the lower bound solution must satisfy the material conditions:

$$\sigma_c = \tau (\tan\theta + \cot\theta) \le f_c \qquad (2.7)$$
$$\sigma_s \le f_y$$

where f_c = concrete "yield" strength and
f_y = stirrup yield strength.
The best lower bound solution is the largest load satisfying those conditions. From Eqs. 2.6 and 2.7:

$$\tan\theta = \frac{r\,\sigma_s}{\tau} = \frac{r\,\sigma_s}{\sigma_c}\,\frac{\sigma_c}{\tau} = \xi\,(\tan\theta + \cot\theta)$$

from which

$$\tan\theta_l = \sqrt{\frac{\xi}{1-\xi}} \tag{2.8}$$

with the notation

$$\xi = \frac{r\,\sigma_s}{\sigma_c} \tag{2.9}$$

where ξ is the degree of shear reinforcement and θ_l is the lower bound solution for the strut angle. From Eqs. 2.7 and 2.8,

$$\frac{\tau}{\sigma_c} = \frac{1}{(\tan\theta + \cot\theta)} \tag{2.10}$$

$$\frac{\tau}{\sigma_c} = \sqrt{\xi(1-\xi)} \tag{2.11}$$

or

$$\left(\frac{\tau}{\sigma_c}\right)^2 + \left(\xi - \frac{1}{2}\right)^2 = \frac{1}{4} \tag{2.12}$$

Eq. 2.12 represents a circle in the $(\tau/\sigma_c, \xi)$ coordinate system. In the range $0 \le \xi < ½$, the right hand side of Eq. 2.11 is a positive and monotonically increasing function of ξ. Therefore, τ is maximum for $(\sigma_c)_{max} = f_c$ and for

$$\xi_{max} = \frac{r\,(\sigma_s)_{max}}{f_c} = \frac{r\,f_y}{f_c} = \psi \tag{2.13}$$

i.e., the web crushes and the stirrups yield simultaneously (Fig. 2.6). The longitudinal reinforcement, however, remains elastic. For $\xi \ge ½$, Eq. 2.11 or 2.12 gives the best lower bound solution as $\tau_{max} = ½f_c$, i.e., a straight line as shown in Fig. 2.6, and Eq. 2.9 gives $\sigma_s = f_c / (2r) < f_y$. Equations 2.8 and 2.11 show that when $0 \le \psi \le 0.5$, the compressive stress direction is $0 \le \theta \le 45°$. For $\psi > 0.5$, $\tau_{max} = 0.5\,f_c$, and $\theta = 45°$ (from Eq. 2.11). The lower bound solution thus produces a diagonal compression field at an angle that varies depending on the reinforcement ratio and does not exceed 45° to the longitudinal axis. Notice that the above solution neither discusses displacement compatibility, as this is not required in a lower bound solution, nor the special conditions at the concentrated loads.

Eq. 2.10 can be rewritten as

$$\frac{\tau}{\sigma_c} = \frac{1}{\tan\theta + \tan(90° - \theta)}$$

and produces the same numerical result for θ and $(90° - \theta)$.

This lower bound solution was first published by Nielsen in November 1967 in the Danish Journal of Structural Engineering, Vol. 38, No. 2, pp. 33-58.

2.2.2 Upper Bound Solution

The following also follows Nielsen (1984). Figure 2.7 shows the shear failure mechanism of a beam under two concentrated loads. An upper bound solution is sought whereby the central portion of the beam slides along straight yield lines at angle θ to the horizontal and displaces by a vertical distance u. The number of stirrups crossing the yield line is $h\,(\cot\theta)\,/\,s$. They have cross-sectional area A_s and stretch a distance u at yield. The internal work of the stirrups is (Fig. 2.8):

$$W_s = \frac{h\cot\theta}{s} A_s f_y u = r f_y b h \cot\theta\, u \tag{2.14}$$

The internal work of the concrete compression strut is more difficult to evaluate. Assume concrete is a modified Mohr-Coulomb material with zero tensile strength, and whose failure envelope is represented by Fig. 2.4b. Energy dissipation per unit volume is:

$$W = \sigma_1 \varepsilon_1 + \sigma_2 \varepsilon_2 + \sigma_3 \varepsilon_3 \tag{2.15}$$

where the subscripts correspond to the three principal directions. For a rigid-plastic Coulomb material, the failure condition of the frictional hypothesis is (see Eq. 2.5):

$$f = k\sigma_3 - \sigma_1 - f_c = 0 \quad \text{for} \quad \sigma_3 \geq \sigma_2 \geq \sigma_1 \tag{2.16}$$

There are five similar equations depending on the relative magnitudes of σ_1, σ_2, and σ_3. If we use the yield condition Eq. 2.16 as the associated flow rule, the normality condition states that

$$\varepsilon_i = \lambda \frac{\partial f}{\partial \sigma_i}$$

where λ is an arbitrary constant. Thus the strains corresponding to Eq. 2.16 are:

$$\varepsilon_1 = -\lambda; \quad \varepsilon_2 = 0; \quad \varepsilon_3 = \lambda k \tag{2.17}$$

This is represented as plane 2 in Fig. 2.4b. By addition of the principal strains:

$$\varepsilon_1 + \varepsilon_2 + \varepsilon_3 = \lambda (k - 1) \tag{2.18}$$

The energy dissipation therefore is (from Eqs. 2.15, 2.16, 2.17 and 2.18):

$$W = -\lambda \sigma_1 + \lambda k \sigma_3 = \lambda (-\sigma_1 + k \sigma_3)$$

$$W = \lambda f_c = \frac{f_c}{k-1} (\varepsilon_1 + \varepsilon_2 + \varepsilon_3)$$

The same operation is performed on the other planes, edges and apexes of the yield surface in the (σ_1, σ_2, σ_3) space. In all cases,

$$W = \frac{f_c}{k-1} (\varepsilon_1 + \varepsilon_2 + \varepsilon_3) \tag{2.19}$$

Disregarding the apex, summation gives

$$W = \frac{f_c}{k} \sum \varepsilon^+ = f_c \sum |\varepsilon^-| \tag{2.20}$$

and therefore

$$k = \frac{\Sigma\ \varepsilon^+}{\Sigma\ |\varepsilon^-|} \tag{2.21}$$

where $\sum \varepsilon^+$ is the sum of positive principal strains and $\sum |\varepsilon^-|$ is the sum of the absolute values of the negative principal strains. Next, consider a line of discontinuity (yield line) where there is a jump in displacement between two parallel planes separated initially by a distance δ (Fig. 2.10). Part I has displacements (u_n , u_t) with respect to part II. In the volume, the strains are:

$$\varepsilon_n = \frac{u_n}{\delta} = \frac{u \sin \alpha}{\delta}$$

$$\varepsilon_t = 0$$

$$\gamma_{nt} = \frac{u_t}{\delta} = \frac{u \cos \alpha}{\delta}$$

The principal strains are:

$$\begin{pmatrix} \varepsilon_1 \\ \varepsilon_2 \end{pmatrix} = \frac{1}{2} \frac{u \sin \alpha}{\delta} \pm \frac{1}{2} \sqrt{\frac{u^2 \sin^2 \alpha}{\delta^2} + \frac{u^2 \cos^2 \alpha}{\delta^2}} = \frac{1}{2} \frac{u}{\delta} (\sin \alpha \pm 1) \tag{2.22}$$

From Eq. 2.21:

$$k = \frac{\varepsilon_1}{\varepsilon_2} = \frac{1 + \sin \alpha}{1 - \sin \alpha} \tag{2.23}$$

For plane strain, Eqs. 2.19 and 2.23 give

$$W = f_c \frac{1}{2} \frac{u}{\delta} (1 - \sin \alpha) \tag{2.24}$$

The dissipation per unit length in the t-direction is:

$$W_l = W\ b\ \delta = \frac{1}{2} f_c\ u\ b\ (1 - \sin \alpha) \tag{2.25}$$

It turns out that Eq. 2.24 is also valid for plane stress. From Eq.2.25 and Fig. 2.9, where the displacement vector is u, the length of the yield line is $h/\sin \theta$, and the beam width is b, the work of

the concrete is

$$W_c = \frac{1}{2} f_c \, b \, (1 - \cos\theta) \, \frac{h}{\sin\theta} \, u \tag{2.26}$$

Dissipation formulas for yield lines in Coulomb materials and modified Coulomb materials were first derived by Jensen and by Nielsen and others. A more complete and detailed derivation can be found in Nielsen (1984).

Neglecting the contribution of the longitudinal reinforcement, the work equation for the reinforced concrete beam with vertical stirrups failing under constant shear is, from Eqs. 2.14 and 2.26:

$$P u = r f_y \, b \, h \cot\theta \, u + \frac{1}{2} f_c \, b \, (1 - \cos\theta) \, \frac{h}{\sin\theta} \, u$$

from which

$$\frac{\tau}{f_c} = \frac{P}{b \, h \, f_c} = \psi \cot\theta + \frac{1 - \cos\theta}{2 \sin\theta} \tag{2.27}$$

where $\psi = r f_y / f_c$ is the shear reinforcement mechanical ratio. If τ / f_c is minimized with respect to θ, we obtain the upper bound solution:

$$\frac{\tau}{f_c} = \sqrt{\psi \, (1 - \psi)} \tag{2.28}$$

which is identical to the lower bound Eq. 2.11, and is therefore the "exact" solution within our assumptions (concrete is a modified Mohr - Coulomb material with zero tensile strength, longitudinal steel performs no work). The best upper bound of Eq. 2.28 above is obtained for

$$\tan\theta_u = \frac{2\sqrt{\psi \, (1 - \psi)}}{1 - 2\psi} \tag{2.29}$$

where θ_u is the upper bound solution for the strut angle. This is twice the crack angle found by the lower bound solution Eq. 2.8:

$$\theta_u = 2 \, \theta_l$$

Braestrup (1994) explains what this means physically. For a strut angle of θ_l, the applied shear force equals the force in the stirrups over the length $h\cot\theta_l$. Once the stirrups yield, increasing loads can only be carried by an increase in $\cot\theta_l$, i.e. a flattening of the strut inclination. This causes the concrete stress to increase, since its vertical component remains constant to balance the stirrup stresses, until compression failure occurs. The beam fails by sliding failure along yield lines inclined at θ_u, exactly twice the strut angle θ_l.

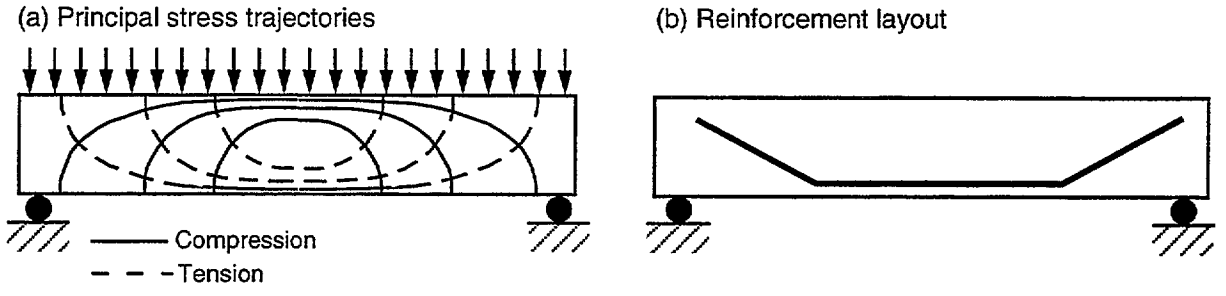

Figure 2.1 — (a) Principal stress trajectories for a simply-supported beam; (b) reinforcement layout to carry principal tensile stresses.

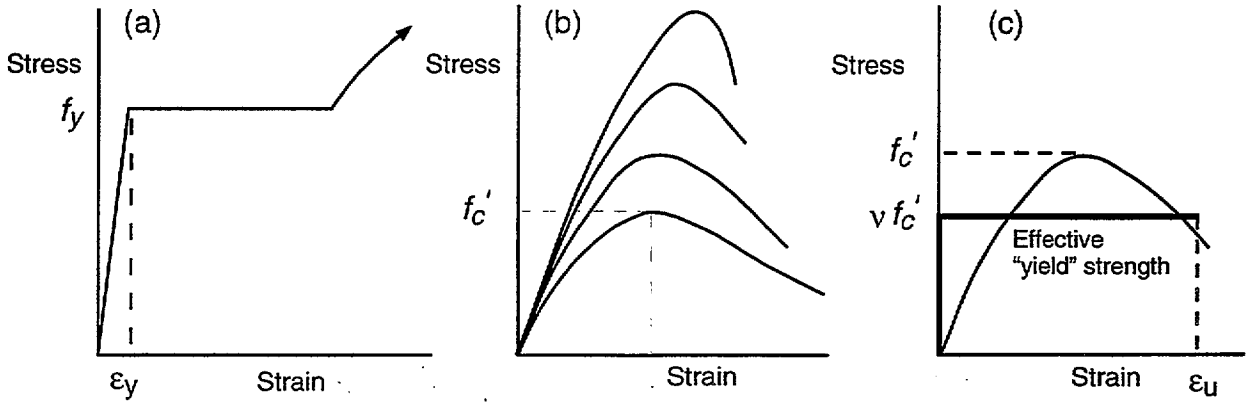

Figure 2.2 — Schematic stress-strain curves: (a) structural steel: (b) concrete with different compressive strengths; and (c) rigid-plastic idealization of concrete used in plasticity analysis.

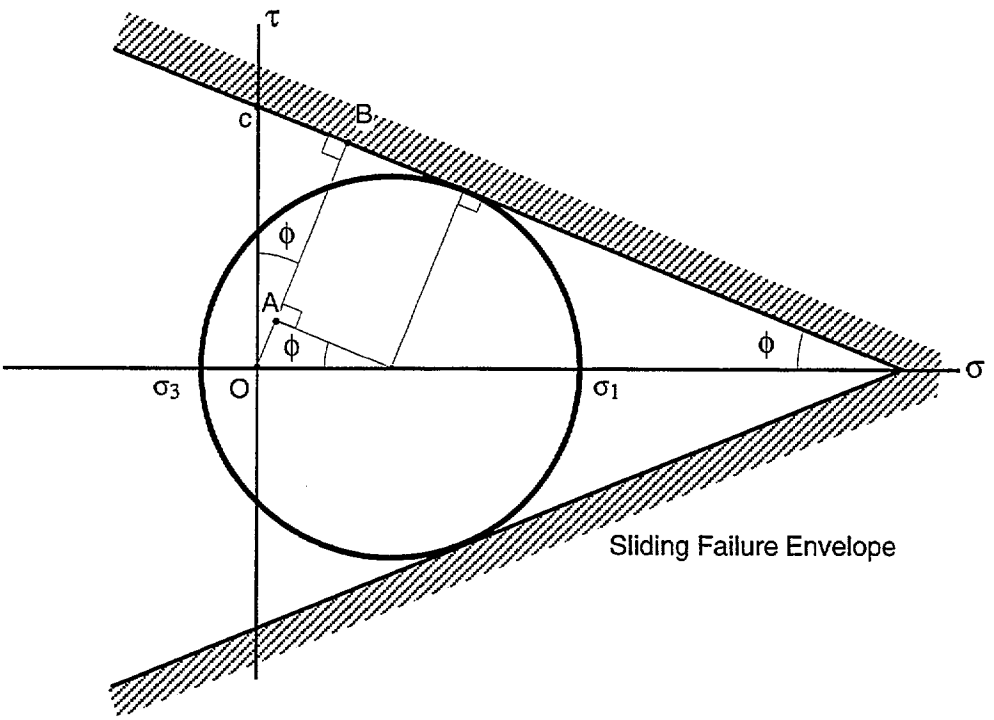

Figure 2.3 — (a) Mohr-Coulomb envelope for sliding failure.

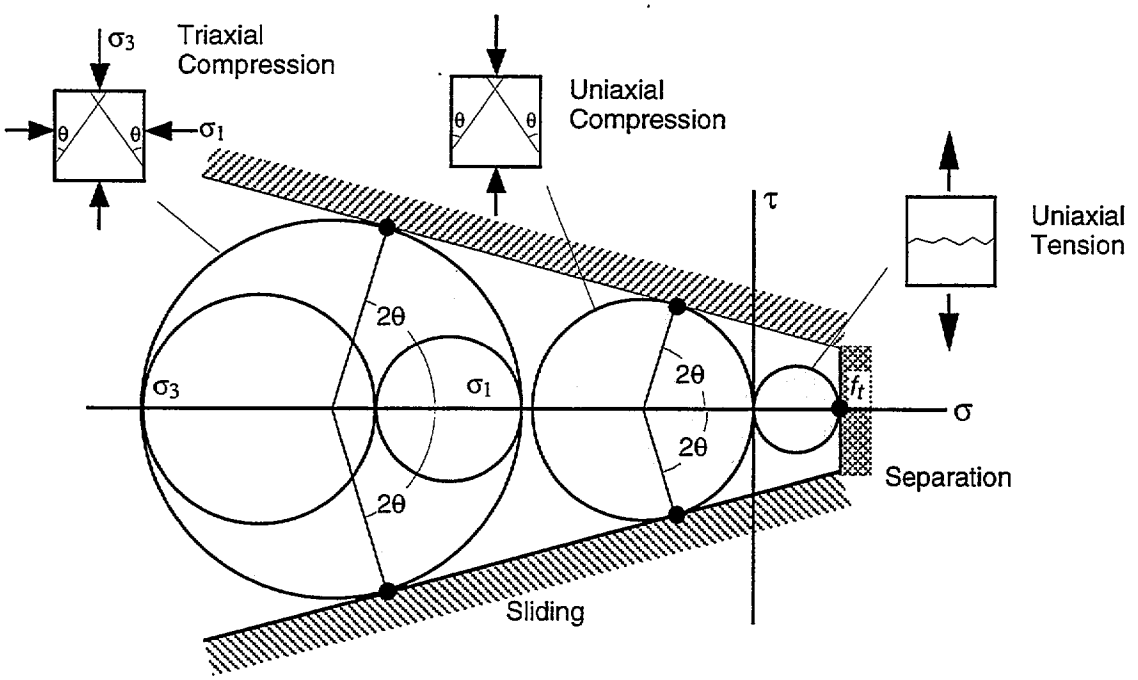

Figure 2.3 — (b) Modified Mohr-Coulomb failure criterion with tension cut-off showing failure under uniaxial tension, uniaxial compression, and triaxial compression.

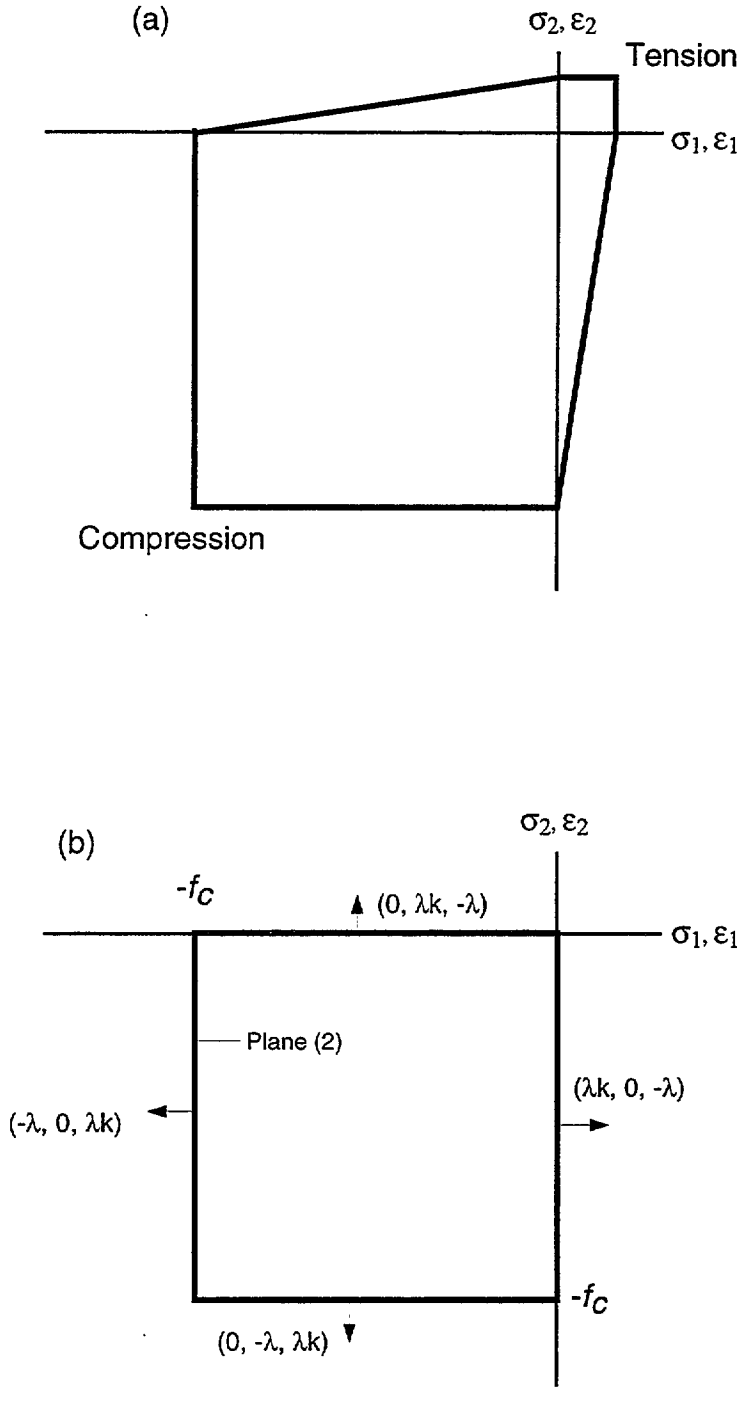

Figure 2.4 — Biaxial stress failure envelopes based on modified Mohr-Coulomb failure theory; (a) tensile strength included and (b) tensile strength neglected.

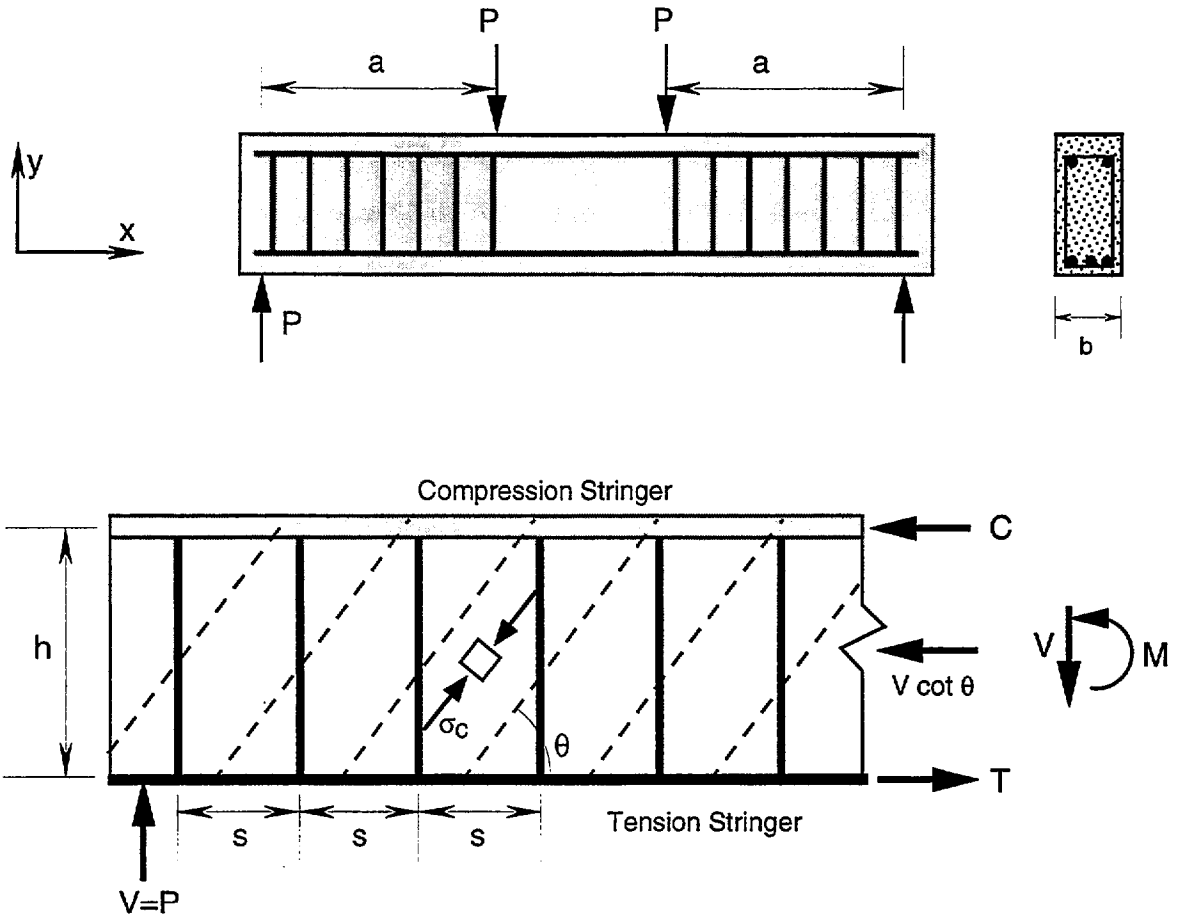

Figure 2.5 — Lower bound solution of beam under shear loading.

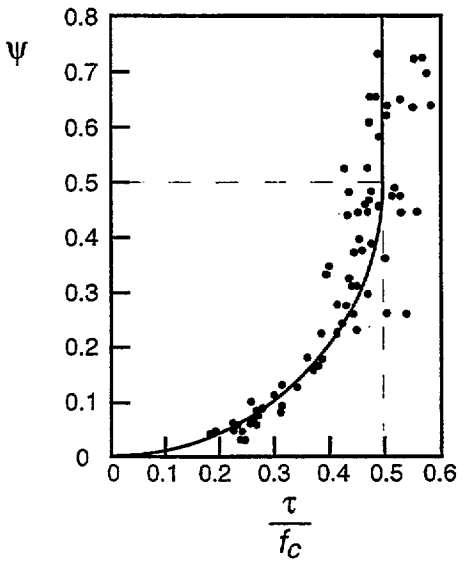

Figure 2.6 — Relationship between shear strength and reinforcement ratio compared with test results (Nielsen 1984).

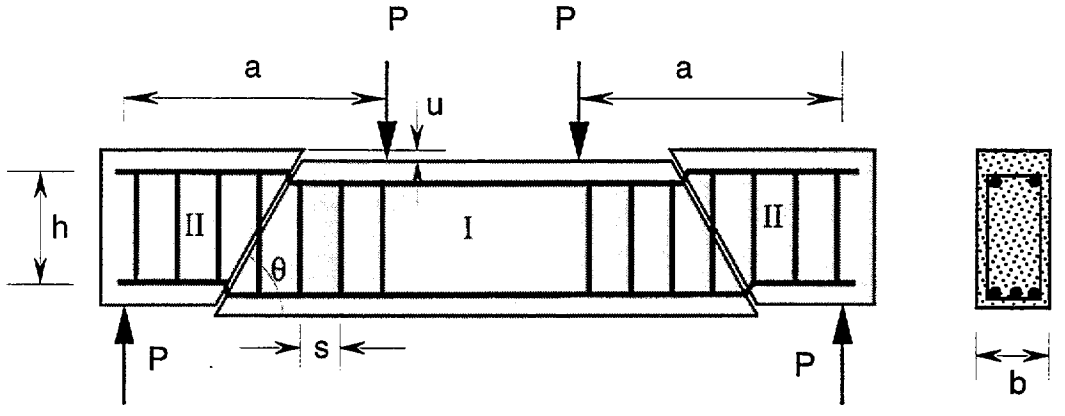

Figure 2.7 — Shear failure mechanism of beam subjected to concentrated loads.

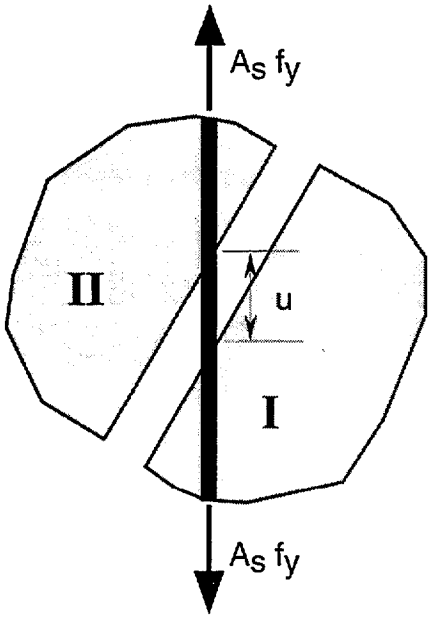

Figure 2.8 — Strain energy of stirrup.

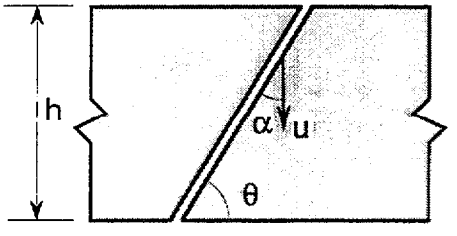

Figure 2.9 — Internal work of concrete.

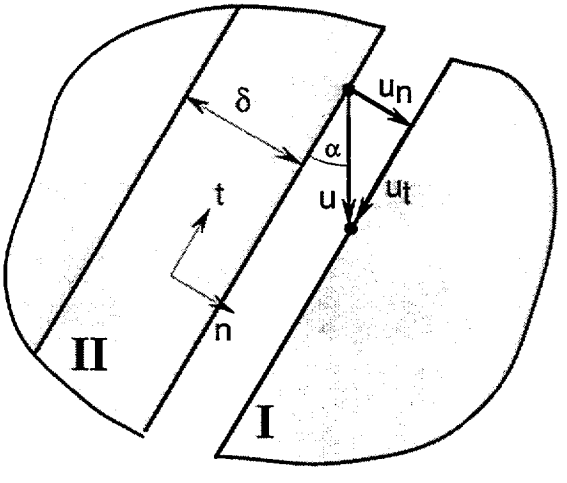

Figure 2.10 — Yield line (crack) in concrete web.

2.3 Plastic Theory of Shear Friction

The plastic theory of shear friction was also developed by the "Copenhagen Shear Group" and the following is adapted from Nielsen (1984).

2.3.1 Upper bound solution

Fig. 2.11 shows a shear friction test where a failure mechanism has formed along the line of loading. The relative displacement of the two halves is u, at an angle α to the yield line. The external work is:

$$W_E = P u \cos\alpha$$

Both steel reinforcement and concrete contribute to the dissipation of energy. The reinforcing steel of area A_s is at yield in the ultimate limit state. Neglecting the dowel effect of the steel reinforcement, here perpendicular to the crack, the steel dissipation is:

$$W_s = A_s f_y u \sin\alpha$$

The concrete dissipation is evaluated in the same way as in § 2.2.2, Fig. 2.9, but with the yield line length as h. From Eq. 2.25:

$$W_c = W_l h = \frac{1}{2} f_c u b h (1 - \sin\alpha)$$

Depending on the direction α of the relative displacements, consideration of energy balance gives rise to the following values of shear strength:

$\underline{\alpha = 0}$ Since the displacement is perpendicular to the reinforcement, $W_s = 0$ and

$$P u = \frac{1}{2} f_c u b h$$

$$\text{or} \qquad \frac{\tau}{f_c} = \frac{P}{b h f_c} = \frac{1}{2} . \tag{2.30}$$

$\underline{0 < \alpha < \phi}$ where ϕ is the friction angle of concrete.

$$P u \cos\alpha = \frac{1}{2} f_c u b h (1 - \sin\alpha) + A_s f_y u \sin\alpha$$

$$\text{or} \qquad \frac{\tau}{f_c} = \frac{1 - \sin\alpha}{2 \cos\alpha} + \psi \tan\alpha \tag{2.27a}$$

where ψ is the degree of reinforcement

$$\psi = \frac{A_s f_y}{b h f_c} .$$

The minimum value of Eq. 2.27a is:

$$\frac{\tau}{f_c} = \sqrt{\psi (1 - \psi)} \tag{2.28}$$

which occurs for

$$\sin\alpha = 1 - 2\psi \tag{2.29a}$$

Since $0 < \alpha < \phi$, Eq. 2.28 applies in the interval

$$\frac{1-\sin\phi}{2} < \psi < \frac{1}{2}$$

In the $(\tau / f_c, \psi)$ coordinate system, Eq. 2.28 represents a circle with radius 0.5 centered at (0 , 0.5). Eq. 2.30 is a tangent to this circle at (0.5, 0.5). See Fig. 2.6.

<u>$\alpha = \phi$</u> The work equation is:

$$P u \cos\phi = \frac{1}{2} f_c u b h (1 - \sin\phi) + A_s f_y u \sin\phi$$

$$\text{or} \qquad \frac{\tau}{f_c} = \frac{1-\sin\phi}{2\cos\phi} + \psi \tan\phi \tag{2.31}$$

From Eqs. 2.3 and 2.4:

$$\frac{f_c}{2c} = \tan\left(\frac{\pi}{4} + \frac{\phi}{2}\right) = \frac{1+\tan(\phi/2)}{1-\tan(\phi/2)} = \frac{1+\cos\phi+\sin\phi}{1+\cos\phi-\sin\phi} = \frac{\sin\phi+1-\cos\phi}{\sin\phi-1+\cos\phi} = \frac{2\cos\phi}{2-2\sin\phi}$$

So

$$\frac{\tau}{f_c} = \frac{c}{f_c} + \psi \tan\phi \tag{2.32}$$

Eq. 2.32 is tangent to the circle Eq. 2.28 at

$$\left(\frac{1-\sin\phi}{2}, \frac{\cos\phi}{2}\right).$$

Fig. 2.12 shows good agreement with experimental results.

<u>$\alpha > \phi$</u> This case involves the concrete tensile strength and Eqs. 2.20 and 2.21 are generalized to:

$$W = f_c \sum|\varepsilon^-| + f_t(\sum\varepsilon^+ - k\sum|\varepsilon^-|) \tag{2.33}$$

when

$$\frac{\sum\varepsilon^+}{\sum|\varepsilon^-|} > k\,. \tag{2.34}$$

Eq. 2.20 is a special case of Eq. 2.33 when condition Eq. 2.21 is satisfied. From Eqs. 2.22 and 2.33:

$$W_l = W b \delta = \frac{1}{2} f_c u b \left[1 - \sin\alpha + \frac{f_t}{f_c}[1 - k + (1+k)\sin\alpha]\right]$$

From Eq. 2.3

$$k - 1 = \frac{2\sin\phi}{1-\sin\phi} \qquad \text{and} \qquad k + 1 = \frac{2}{1-\sin\phi}$$

and the dissipation is

$$W_l = \frac{1}{2} f_c u b \left(1 - \sin\alpha + 2 \frac{f_t}{f_c} \frac{\sin\alpha - \sin\phi}{1 - \sin\phi} \right) \tag{2.35}$$

which can be written more compactly as:

$$W_l = \frac{1}{2} f_c u b (l - m \sin\alpha)$$

with

$$l = 1 - \frac{f_t}{f_c}(k - 1) = 1 - 2 \frac{f_t}{f_c} \frac{\sin\phi}{1 - \sin\phi} \tag{2.36}$$

$$m = 1 - \frac{f_t}{f_c}(k + 1) = 1 - 2 \frac{f_t}{f_c} \frac{1}{1 - \sin\phi} \tag{2.37}$$

The work equation is:

$$P u \cos\alpha = \left[\frac{1}{2} f_c (1 - \sin\alpha) + \frac{\sin\alpha - \sin\phi}{1 - \sin\phi} f_t \right] u b h + A_s f_y u \sin\alpha$$

or

$$\frac{\tau}{f_c} = \frac{1 - \sin\alpha}{2 \cos\alpha} + \frac{\sin\alpha - \sin\phi}{(1 - \sin\phi)\cos\alpha} \frac{f_t}{f_c} + \psi \tan\alpha$$

The minimum value is found to be:

$$\frac{\tau}{f_c} = \sqrt{\left(\psi + \frac{f_t}{f_c} \right) \left(1 - 2 \frac{f_t}{f_c} \frac{\sin\phi}{1 - \sin\phi} - \psi - \frac{f_t}{f_c} \right)} \tag{2.38}$$

occurring for:

$$\sin\alpha = 1 - 2 \frac{\psi + \dfrac{f_t}{f_c}}{1 - 2 \dfrac{f_t}{f_c} \dfrac{\sin\phi}{1 - \sin\phi}}$$

Eq. 2.38 is a circle of

$$\text{radius} = \frac{1}{2} - \frac{f_t}{f_c} \frac{\sin\phi}{1 - \sin\phi}.$$

and Eq. 2.31 is tangent to this circle.

Eq. 2.38 can be written in a more compact form:

$$\frac{\tau}{f_c} = \frac{1}{2} \sqrt{l^2 - (m - 2\psi)^2}$$

with l and m defined in Eqs. 2.36 and 2.37.

When $f_t = 0$, Eq. 2.38 becomes identical to Eq. 2.27a and Eq. 2.31 vanishes. In this case the load-carrying capacity is the same as for beams, where the tensile strength is assumed to be 0 (see §

2.2.2).

Experimental results agree well with the above equations. The effectiveness factor is less for cracked ($\nu' = 0.45$) than for monolithic concrete ($\nu = 2/3$), but the friction angles are the same ($\phi = \phi' = 37°$). In Fig. 2.13, curves for cracked and uncracked concrete are shown. Where the curve for cracked concrete exceeds that of uncracked concrete, the latter governs.

2.3.2 Lower bound solution

A statical interpretation can be given to the upper bound solution shown above, although it is not a true lower bound solution because the stress fields are defined only along the yield line.

The compressive normal stress in the concrete due to the reinforcement is:

$$\sigma = \frac{A_s f_y}{b h} = \psi f_c \tag{2.39}$$

The average shear stress is given by:

$$\tau = \frac{P}{b h} \tag{2.40}$$

We now use a modified Mohr-Coulomb material with a circular cut-off (Fig. 2.14):

$$\left(\sigma + \frac{1}{2} f_c + \frac{f_t}{1 - \sin\phi}\right)^2 + \tau^2 = \frac{1}{2} f_c - f_t \frac{\sin\phi}{1 - \sin\phi} \tag{2.41}$$

Inserting Eq. 2.39 into Eq. 2.41 gives the shear strength Eq. 2.38.

In Fig. 2.14, the straight line has the equation:

$$\tau = c - \sigma \tan\phi \tag{2.1}$$

Inserting Eq. 2.39 into Eq. 2.1 gives Eq. 2.32.

When we assume plane stress, one of the principal stresses is always 0. When there is no tension, the greatest Mohr circle (Fig. 2.3b) passes through $(\sigma,\tau) = (0,0)$ and $(\sigma,\tau) = (f_c, 0)$ and has the equation

$$\left(\sigma + \frac{1}{2} f_c\right)^2 + \tau^2 = \left(\frac{1}{2} f_c\right)^2 \tag{2.42}$$

Inserting Eq. 2.39 into Eq. 2.42 gives Eq. 2.27a.

For degrees of reinforcement greater than ½, the reinforcement does not yield because the shear strength of the concrete is limited to $\tau / f_c = ½$, which is Eq. 2.30.

These statical solutions are thus shown to be identical to the upper bound solutions.

2.3.3 Axial Forces

With axial forces N, all equations are still valid if we replace ψ by:

$$\psi^* = \psi - \frac{N}{b h f_c}$$

where N is positive for tension.

2.3.4 Design Recommendations

Nielsen (1984) recommends the following values:

- For cleaned and rough joints $c'/f'_c = 0.05$ to 0.06 and $\tan \phi' = 0.75$.
- For smooth joints $c' = 0$ and $\tan \phi' = 0.6$.

(The $'$ on c' and ϕ' indicates cracked, as opposed to monolithic concrete).

In the introduction to his book, Nielsen (1984) wrote: "...the concrete world, in the early days of concrete history was forced to develop its own methodology with sparse connections to classical mechanics with its roots in linear elastic theories. Since only little progress can be made by identifying concrete with a linear elastic body, the world of mechanics in its classical sense and the world of concrete have been and still are very separated." By solving the shear problem using rigorous plasticity theorems, Nielsen and his "Copenhagen shear group" have made a very important contribution to the unification of the two worlds.

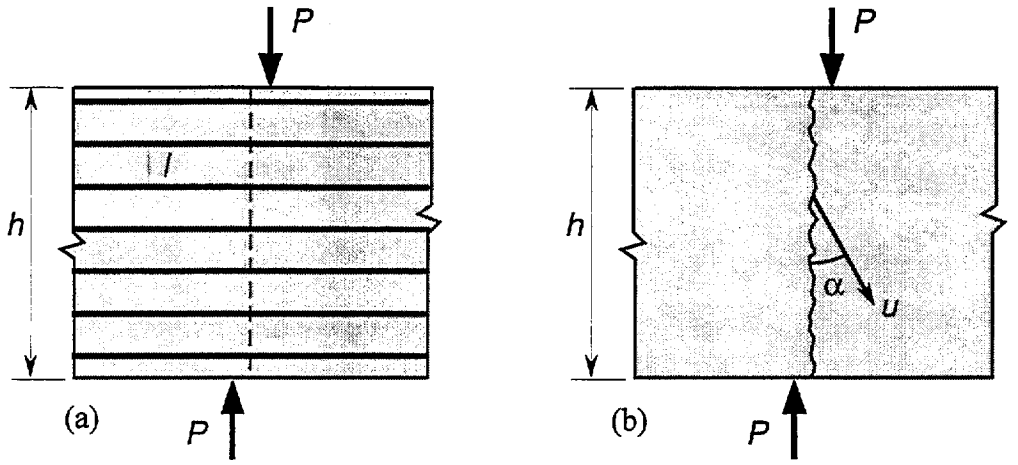

Figure 2.11 — (a) Disk subjected to shear and (b) failure mechanism (from Nielsen 1984)

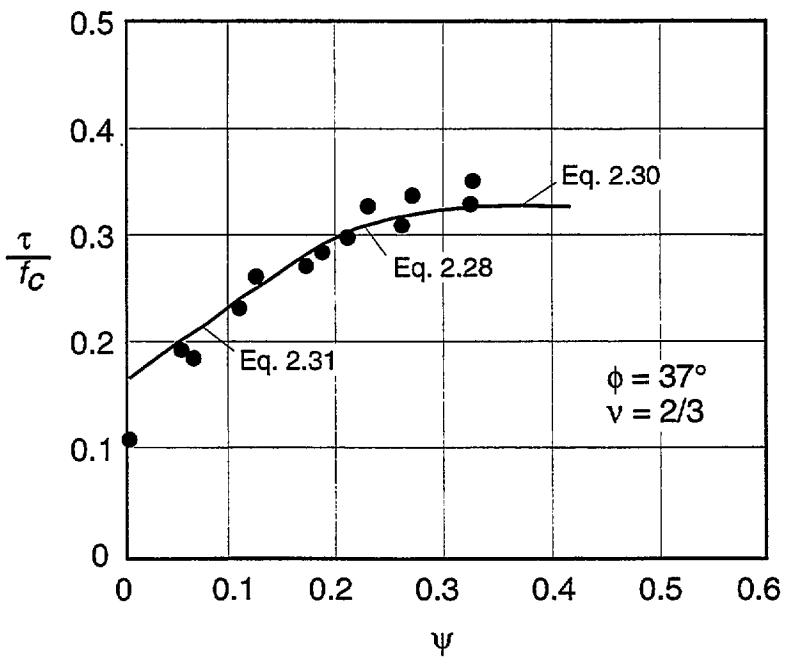

Figure 2.12 — Test results for monolithic concrete (Nielsen 1984)

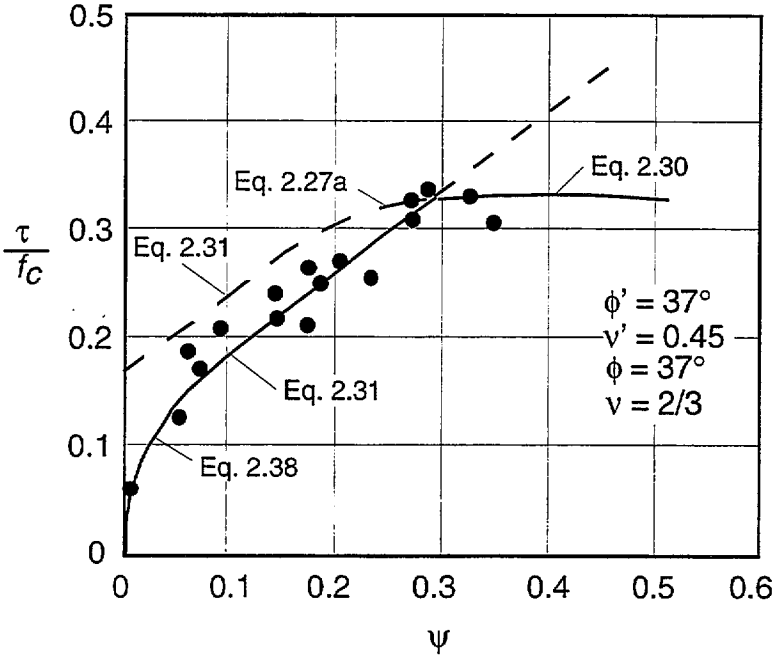

Figure 2.13 — Test results for a cracked specimen (Nielsen 1984)

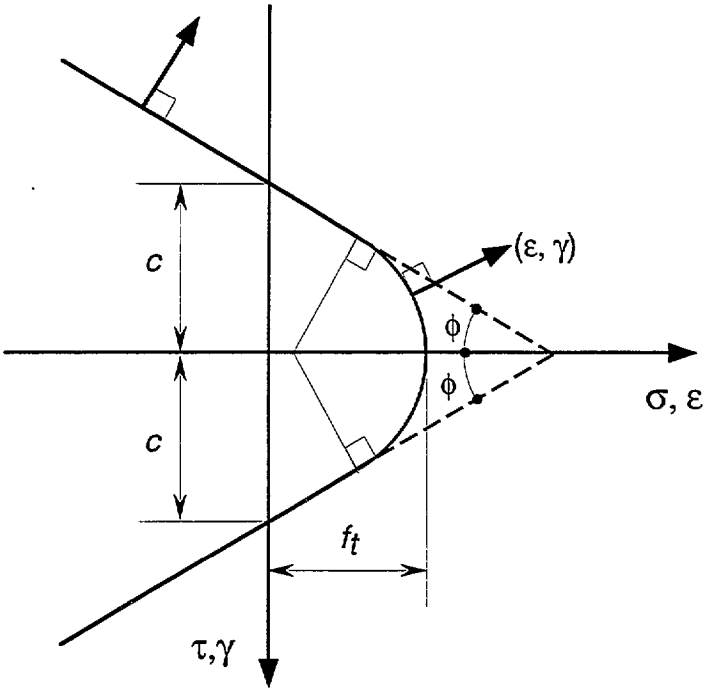

Figure 2.14 — Dissipation in a yield line for a modified Mohr-Coulomb material with a circular tension cut-off (Nielsen 1984)

2.4 "Exact" Solutions – Compression Field Theories

2.4.1 Compression Field Theory

The compression field theory is an "exact" solution because it satisfies equilibrium, strain compatibility and stress-strain relationships. It was developed by Mitchell and Collins (1974) following the "tension field theory" invented by Wagner (1929) to describe the post-local buckling behavior of thin webs of steel girders, and is similar to Nielsen's (1967) lower bound solution. In contrast to the limit-state analysis of plasticity theory, compression field theory describes shear behavior through the entire cracked range up to failure. Therefore, neither the concrete nor the reinforcement are at their limiting stress in a typical case. Compression field theory idealizes cracked concrete as a material with coinciding principal stress and strain axes which are free to adapt their direction as required by the applied loads.

Equilibrium — This is similar to developments shown for the lower bound solution of the plasticity theory. Consider the equilibrium at a cross-section in a reinforced concrete beam where the bending moment is zero, as shown in Fig. 2.15a.

Concrete: The vertical component of the diagonal compressive force in the concrete, which is inclined at θ to the longitudinal axis, must equal the applied shear force (Fig. 2.15a).

$$V = D \sin\theta = (f_2 \, b_w \, jd \cos\theta) \sin\theta$$

$$f_2 = \frac{V}{b_w \, jd} (\tan\theta + \cot\theta) \tag{2.43}$$

Stirrups: In turn, the diagonal compression in the concrete transfers vertical force to the stirrups (Fig. 2.15b).

$$A_v f_v = (f_2 \, b_w \, s \sin\theta) \sin\theta$$

$$\frac{A_v f_v}{s} = \frac{V}{jd} \tan\theta \tag{2.44}$$

Stringers: The longitudinal component of the diagonal compression in the concrete is equilibrated by tension in the "stringers":

$$N_v = A_x f_x = V \cot\theta$$

Two important assumptions are made:

- the concrete carries no tension after cracking.
- the angle of inclination of the diagonal compressive stress coincides with the angle of inclination of the principal compressive strain. This is the exact converse of Wagner's hypothesis for the diagonal tension field theory. In reality, the principal directions for stress differ from those for strain after the concrete cracks (as will be discussed).

Strain Compatibility: The strain compatibility relationships in the cracked web are established using the geometrical transformations represented by Mohr's circle of strain as shown in Fig. 2.16b.

From triangle 2Bx in Fig. 2.16b:

$$\gamma_{xt} = 2\,(\varepsilon_x - \varepsilon_2)\,\cot\theta$$

while from triangle 2At:

$$\gamma_{xt} = 2\,(\varepsilon_t - \varepsilon_2)\,\tan\theta$$

where ε_x = longitudinal strain of web (tension is positive),
ε_t = transverse strain,
γ_{xt} = shear strain, and
ε_2 = principal compressive strain (negative).

From both equations above, we obtain the angle of inclination of the diagonal compression:

$$\tan^2\theta = \frac{\varepsilon_x - \varepsilon_2}{\varepsilon_t - \varepsilon_2}$$

Since the above strain compatibility relationship was derived using Mohr's circle, the diagonal compression field theory is also sometimes referred to as the Mohr-compatibility truss (Hsu 1993). However, this latter name lacks the physical and historical appeal of the former one.

The first strain invariant also provides a useful relationship:

$$\varepsilon_1 + \varepsilon_2 = \varepsilon_x + \varepsilon_t$$

Note that, for cracked concrete, these compatibility relationships are expressed in terms of "average" strains, i.e., strains measured over base lengths long enough to include several cracks.

Stress-strain Relationships of Cracked Concrete — The concrete web is not only in compression in direction 2, but also in tension in direction 1 (Fig. 2.16a). Vecchio and Collins (1982) tested reinforced concrete panels under biaxial stresses (including pure shear) and found that the principal compressive stress in the concrete, f_2, is a function not only of the principal compressive strain ε_2, but also of the coexisting principal tensile strain ε_1.

They suggested the following parabolic stress-strain relationship (Fig.2.17):

$$f_2 = f_{2\max}\left[2\left(\frac{\varepsilon_2}{\varepsilon'_c}\right) - \left(\frac{\varepsilon_2}{\varepsilon'_c}\right)^2\right]$$

where

$$\frac{f_{2\max}}{f'_c} = \frac{1}{0.8 + 170\,\varepsilon_1} \le 1.0.$$

The presence of transverse tensile strain reduces the compression capacity of the concrete. For this reason, this model is sometimes referred to as the softened truss model (Hsu 1993). In addition, the reinforcing steel behaves elastically:

$$f_y = E_s\,\varepsilon_t$$
$$f_x = E_s\,\varepsilon_x$$

Thus we have three equilibrium equations, two strain-compatibility equations, and three stress-strain relations to solve for the three stress unknowns f_2, f_v, f_x, four strain unknowns ε_x, ε_t, ε_1, ε_2 and the angle of the diagonal compression θ, or a total of eight equations for eight unknowns. With these relationships, it is possible not only to predict the strength (limit-state) but also the load-deformation response of reinforced concrete members subjected to shear.

It would be interesting to simplify the stress-strain relationship of concrete to linearly elastic-plastic and then compare this "exact" solution to the previous plasticity solutions which neglect elastic deformations. For consistency with the plasticity solutions, we assume that the stringers are elastic $f_x = E_s \varepsilon_x < f_y$, but that the stirrups and the concrete have just reached their elastic limit.

$$f_v = f_y; \quad \varepsilon_t = \varepsilon_y = \text{yield strain}$$

$$f_2 = f_c; \quad \varepsilon_2 = -\varepsilon_c \quad (\varepsilon_2 \text{ is a negative quantity})$$

The shear stress is now the unknown. From Eq. 2.10:

$$\frac{\tau}{f_c} = \frac{\tan\theta}{\tan^2\theta + 1}.$$

From Eq. 2.44:

$$\tan\theta = \frac{A_v}{b\,s}\frac{f_y}{\tau} = \frac{A_v}{b\,s}\frac{f_y}{f_c}\frac{f_c}{\tau} = \psi\frac{f_c}{\tau}$$

$$\text{where} \quad \psi = \frac{A_v}{b\,s}\frac{f_y}{f_c} = \text{shear reinforcement mechanical ratio,}$$

from which

$$\left(\frac{\tau}{f_c}\right)\left(\psi^2\frac{f_c^2}{\tau^2} + 1\right) = \psi\frac{f_c}{\tau}$$

$$\psi^2 + \left(\frac{\tau}{f_c}\right)^2 = \psi$$

$$\frac{\tau}{f_c} = \sqrt{\psi\,(1 - \psi)}$$

$$\tan\theta = \sqrt{\frac{\psi}{(1 - \psi)}}$$

So we retrieve the lower bound solution of the theory of plasticity, Eqs. 2.11 and 2.8, as we should, without making use of strain compatibility.

2.4.2 Modified Compression Field Theory

The compression field theory neglects the contribution of tensile stresses in the cracked concrete and consequently overestimates deformations and underestimates strengths. This is corrected in the

modified compression field theory (Vecchio and Collins 1986). The key simplifying assumption of the modified compression field theory is that the principal strain directions coincide with the principal stress directions. This assumption is justified by experimental measurements which show that the principal directions of stress and strain are parallel within ±10° (Fig. 2.18). Also, concrete struts are at a shallower angle than cracks, and the compressive stress field must be transferred across the cracks, thus reducing concrete strength from its uncracked state and inducing shear stress across the crack faces (Collins 1978).

Equilibrium between cracks — Fig. 2.19 is used to establish the equations of equilibrium. Shear in the section is resisted by the diagonal compressive stresses f_2 together with the diagonal tensile stresses f_1. The tensile stresses vary from 0 at the cracks to a maximum between cracks. The average value is used in the equilibrium formulation.

From the Mohr circle (Fig. 2.19c):

$$\text{In triangle At1 : A1} = v \tan\theta$$

$$\text{In triangle At2 : A2} = v \cot\theta$$

$$f_1 + f_2 = \text{A1} + \text{A2} = v\,(\tan\theta + \cot\theta) \tag{2.45}$$

where

$$v = \frac{V}{b_w\, jd}$$

Compared with the previous equilibrium equation, Eq. 2.43 of the compression field theory, concrete tensile stresses contribute to carrying the load. The diagonal compressive stresses push apart the flanges of the beam while the diagonal tensile stresses pull them together. The vertical imbalance is carried by tension in the web reinforcement.

$$A_v f_v = (f_2 \sin^2\theta - f_1 \cos^2\theta)\, b_w\, s \tag{2.46}$$

From Eqs. 2.45 and 2.46

$$v = \frac{f_1}{\tan\theta + \cot\theta} + \frac{1}{\tan\theta + \cot\theta}\left(\frac{A_v f_v}{b_w\, s} + f_1 \cos^2\theta\right)\frac{1}{\sin^2\theta}$$

$$V = v\, b_w\, jd = \frac{A_v f_v\, b_w\, jd}{b_w\, s}\,\frac{\cos^2\theta + \sin^2\theta}{(\tan\theta + \cot\theta)\sin^2\theta} + \frac{f_1\, b_w\, jd}{\tan\theta + \cot\theta}\,(1 + \cot^2\theta)$$

$$V = \frac{A_v f_v}{s}\, jd\,\frac{\cot^2\theta + 1}{\tan\theta + \cot\theta} + f_1\,\frac{\tan\theta + \cot\theta}{\tan\theta\,(\tan\theta + \cot\theta)}\, b_w\, jd$$

$$V = \frac{A_v f_v}{s}\, jd\,\frac{\tan\theta + \cot\theta}{\tan\theta\,(\tan\theta + \cot\theta)} + f_1\, b_w\, jd\,\cot\theta$$

$$V = \frac{A_v f_v}{s}\, jd\,\cot\theta + f_1\, b_w\, jd\,\cot\theta$$

$$V = V_s + V_c = \text{Steel Contribution} + \text{Concrete Contribution}$$

So the steel contribution is based on the variable angle truss model (§ 2.6.1), whereas the concrete contribution is the shear resisted by tensile stresses in diagonally cracked concrete.

Similarly, the longitudinal imbalance f_l between the diagonal tension and compression in the concrete must be carried by the longitudinal steel.

$$A_{sx} f_l = (f_2 \cos^2 \theta - f_1 \sin^2 \theta)\, b_w jd = V \cot \theta - f_1 b_w jd$$

Equilibrium Across Cracks — In checking the condition at a crack, the actual complex crack pattern is idealized as a series of parallel cracks, all occurring at angle θ (the strut angle) to the longitudinal reinforcement (Collins 1993). At low shear values, tension is transmitted across cracks by local increases in reinforcement stresses. At a certain shear force the stresses in the web reinforcement will just reach yield at the crack locations. At higher shear forces, transmitting tension across cracks will require local shear stress, v_{ci}, on the crack surface. The two sets of stresses, at a crack and between cracks, must be statically equivalent (see Fig. 2.20). Equivalence of vertical forces at the two locations shown in Fig. 2.20a and 2.20b requires:

$$A_v f_v \left(\frac{jd}{s \tan \theta} \right) + f_1 \frac{b_w jd}{\sin \theta} \cos \theta = A_v f_{vy} \left(\frac{jd}{s \tan \theta} \right) + v_{ci} b_w jd$$

To maintain this equality, the average tensile stress, f_1, must be:

$$f_1 = v_{ci} \tan \theta + \frac{A_v}{b_w s} (f_{vy} - f_v)$$

The concrete contribution, which depends on f_1, is thus tied to the shear that can be transmitted across cracks by aggregate interlock. The ability of the crack interface to transmit the shear stress v_{ci} depends on the crack width w. Vecchio and Collins (1986) suggest the following limiting value of v_{ci}

$$v_{ci} = \frac{0.18 \sqrt{f'_c}}{0.3 + \frac{24w}{a + 16}}$$

where f'_c = compressive strength of concrete in MPa, and
a = maximum aggregate size in mm.

This equation is based on Walraven's (1981) experiments performed on concretes with cube strengths of 13, 37, and 59 MPa and maximum aggregate size of 32 mm (see § 4.3.2). This formula will require further investigation because, for high f'_c, the aggregate may fracture, whereas for low f'_c, fracture goes around the aggregate.

The use of the above formula for design requires an estimate of the crack width w. It can be taken as the product of the principal tensile strain ε_1 and the average spacing of the diagonal cracks, $s_{m\theta}$:

$$w = \varepsilon_1 s_{m\theta}$$

The spacing of the inclined cracks depends upon the crack control characteristics of both the longitudinal and the transverse reinforcement. Referring to Fig. 2.21, the diagonal crack spacing can be related to crack widths in the vertical and horizontal directions:

$$s_{m\theta} = \frac{1}{\frac{\sin \theta}{s_{mx}} + \frac{\cos \theta}{s_{mv}}}$$

Crack spacing is estimated from the provisions of the CEB-FIP Model Code:

$$s_{mx} = 2\left(c_x + \frac{s_x}{10}\right) + 0.25\, k_1 \frac{d_{bx}}{\rho_x}$$

$$s_{mv} = 2\left(c_v + \frac{s}{10}\right) + 0.25\, k_1 \frac{d_{bv}}{\rho_v}$$

where d_b = bar diameter,
c = distance to reinforcement,
s = bar spacing,
ρ_v = $A_v/(b_w s)$,
ρ_x = A_{sx}/A_c, and
k_1 = 0.4 for deformed bars or 0.8 for plain bars.

Fig. 2.22 further defines the parameters influencing crack spacing.

Finally, equality of the horizontal forces at a crack and between cracks also limits the magnitude of the concrete tension to the value corresponding to yielding of longitudinal steel at a crack.

$$A_{sx} f_y \geq A_{sx} f_{sx} + f_1 b_w jd + \left(f_1 - \frac{A_v}{b_w s}(f_{vy} - f_v)\right) b_w jd \cot^2 \theta$$

Compatibility — The compatibility equations for the average concrete strains are the same as described in the compression field theory.

Stress-Strain Relationship of Cracked Concrete — In addition to having the diagonal compressive stress f_2 as a function of the principal strains ε_1 and ε_2 as in the compression field theory, the modified compression field theory also has the diagonal tensile stress f_1 as a function of ε_1. Based on Vecchio and Collins's (1986) tests of reinforced panels made with concrete having a compressive strength less than 35 MPa, Collins and Mitchell (1991) recommend:

$$\text{If } \varepsilon_1 \leq \varepsilon_{cr} \quad \text{then} \quad f_1 = E_c\, \varepsilon_1$$

$$\text{If } \varepsilon_1 > \varepsilon_{cr} \quad \text{then} \quad f_1 = \frac{\alpha_1 \alpha_2 f_{cr}}{1 + \sqrt{500\, \varepsilon_1}}$$

where ε_{cr}, f_{cr} = cracking strain and strength of concrete,
α_1, α_2 = factors accounting for the bond characteristics of the reinforcement (deformed or smooth bars) and the type of loading (short term, cyclic, or sustained).

The above equations for equilibrium, compatibility, and stress-strain properties provide a complete solution by which to predict the shear strength of a reinforced concrete element.

Comparison with Data — Figure 2.23 shows that the modified compression theory offers a marked improvement over the compression field theory and a good prediction of experimental results. See also § 3.2.5, Fig.3.12 and § 4.1.15, Fig. 4.23 - 4.25.

Vecchio (1991) notes that: "The simplicity of the modified compression field theory formulations has allowed them to be easily adopted into various analytical algorithms. Procedures have been developed for the nonlinear analysis of membranes, beams, plane frames, plates and shells, and three

dimensional solids. In applying the analysis procedures to the modeling of more complex structural systems, generally good correlation was found between predicted and observed responses. The theory was found to provide accurate modeling of crack patterns, deformation, reinforcement stresses, ultimate strengths, and failure modes. This was achieved by an accurate description of the constitutive behavior of structural concrete in a simple, transparent, and easy to implement formulation. It can be said that the modified compression field theory represents a unified, rational analysis approach that can be applied to structural concrete in many of its various forms and applications."

2.4.3 Extended Modified Compression Theory

The MCFT was developed for shear and axial loads. Nakamura and Higai (1995) extended it to shear, axial and flexural loads. An outline of their method follows:

1- Divide the cross-section into layers.
2- Distribute the axial force N and shear force V uniformly over the cross-section.
3- Assume a longitudinal strain ε_{xi}. For a given curvature ϕ, the strain ε_{xi} in each layer located at y_{ci} is calculated from an assumed linear distribution over the section depth h and an assumed strain ε_c at the top fiber:

$$\varepsilon_{xi} = (h - y_{ci})\,\phi + \varepsilon_c$$

4- Satisfy equilibrium and compatibility for the known quantities τ_{xy} and ε_{xi} in each layer.
5- Repeat Step 4 for all layers.
6- Calculate stress in longitudinal reinforcement from strain.
7- Calculate resultant of longitudinal stresses and check equilibrium of axial force. If equilibrium is not satisfied, adjust ε_c and go back to Step 3.
8- Calculate moment from longitudinal stresses and check equilibrium of moments.

Step 4 is further detailed as follows:

a- Assume principal tensile strain ε_1.
b- Calculate principal tensile stress σ_1 from ε_1 and concrete stress-strain relationship.
c- Calculate the inclination θ of σ_1 and ε_1 with respect to the longitudinal axis from equilibrium in the transverse direction. From equilibrium, the stress in the transverse steel is:

$$f_{sy} = -\frac{\sigma_y b_w s}{A_w} = -\frac{b_w s}{A_w(\sigma_1 - \tau_{xy}\tan\theta)}$$

where A_w = area of transverse steel,
s = spacing of transverse steel,
b_w = width of web,
σ_y = normal stress in y direction.

On the other hand, from compatibility and the stress-strain relationship of the transverse steel:

$$f'_{sy} = E_{sy}\varepsilon_y = E_{sy}[\varepsilon_1 - (\varepsilon_1 - \varepsilon_x)\tan^2\theta]$$

θ is solved by setting $f_{sy} = f'_{sy}$. This provides a quadratic equation in $\tan\theta$ before yielding of the steel bar, or a linear equation after yielding.

d- Calculate the principal compressive strain ε_2, the transverse strain ε_y, and the shear strain γ_{xy} from Mohr circle.

e- Calculate the longitudinal stress σ_x, transverse stress σ_y, and principal compressive stress σ_2 from Mohr circle.
f- Calculate σ'_2 from ε_2 using concrete stress-strain relationship.
g- If $\sigma_2 \neq \sigma'_2$, try another value of ε_1 and return to Step a.

The solution algorithm used by Collins and Mitchell (1991) involves the convergence of ε_2 and θ for each layer, and that of the longitudinal strain distribution for the cross-section. In comparison, the procedure described above only requires convergence of ε_1 in each layer and ε_c for the cross-section. Computation is therefore faster. Two possible ultimate states are attained as the curvature increases under constant axial and shear forces:
1- flexural failure: the maximum compressive strain in the section reaches - 0.002 (strain at ultimate concrete strength), or
2- shear failure: no solution satisfying equilibrium for the given ε_x and τ_{xy} is obtained in at least one layer, even if equilibrium of axial force is satisfied.

Stress-strain curve for concrete

In tension, stress increases linearly with strain up to the tensile strength. After that, Collins's (1978) equation is modified by a factor α, which accounts for the non-uniform distribution of the reinforcement in the beam.

$$\sigma_1 = \frac{f_t}{1 + \alpha\sqrt{200\,(\varepsilon_1 - \varepsilon_{cr})}}$$

where ε_{cr} = cracking strain of concrete, and
f_t = concrete tensile strength.

In compression, the stress-strain curve is a quadratic parabola up to the compressive strength f_{2max} which is a function of the principal strain ε_1 as proposed by Collins (1978). However, following Miyahara (1988, see § 4.3) f_{2max} is assumed constant for $\varepsilon_1 > 40\,\varepsilon_{cr}$.

Verification

The analytical model is verified against Niwa's empirical formula for shear strength:

$$V = 0.94(f'_c)^{1/3}\,(100\rho_w)^{1/3}\,(d/100)^{-1/4}\,(0.75 + 1.4d/a)\,b_w d$$

where f'_c = concrete compressive strength,
ρ_w = longitudinal reinforcement ratio,
d = effective depth,
a = shear span, and
b_w = width of cross-section.

Collins's (1978) equation ($\alpha = 1$) overestimates the shear strength. However, $\alpha = 2$ shows good agreement with Niwa's equation in the range of diagonal tension failure $a/d > 3$. Agreement is also good with the moment capacity curve in the range of $a/d > 6$, and with the shear failure curve for $3 < a/d < 6$. For $a/d < 3$ the strength is underestimated. This is due to the effect of compressive stress in the transverse direction (arching effect).

Parametric Study

Size Effect

Good agreement is obtained with Niwa's equation if the influence of effective depth on the shear strength is modeled by:

$$\alpha = 3\,(d/16)^{1/3}$$

Longitudinal reinforcement ratio

The shear strength obtained by this analysis is proportional to $(\rho_w)^{1/4}$ whereas Niwa's equation is proportional to $(\rho_w)^{1/3}$. For the range of reinforcement used in practice, $0.3\ \% < \rho_w < 3\ \%$, the difference between the two formulations is less than 10 %.

Longitudinal reinforcement stiffness

Results indicate that the effect of longitudinal reinforcement stiffness is similar to the effect of longitudinal reinforcement ratio:

$$V = V_c\,(E_i/E_s)^{1/4}$$

where E_i = modulus of elasticity of non-steel reinforcement,
E_s = modulus of elasticity of steel,
V_c = shear strength of steel reinforced beam,
V = shear strength of concrete beam reinforced with bars of stiffness E_i.

Results of experiments conducted in the range $0.12 < \rho_w\,(E_i/E_s) < 0.22$ show good agreement with analytical predictions.

Concrete Strength

Shear strength is rather insensitive to f'_c. However, it is approximately proportional to $f_t^{2/3}$. Since f_t is proportional to $(f'_c)^{1/2}$ according to ACI, or $(f'_c)^{2/3}$ according to JSCE (Japanese Society of Civil Engineers), this implies that V is proportional to $(f'_c)^{1/3}$ according to the ACI formula, or $(f'_c)^{4/9}$ according to the JSCE formula. This is close to Niwa's equation.

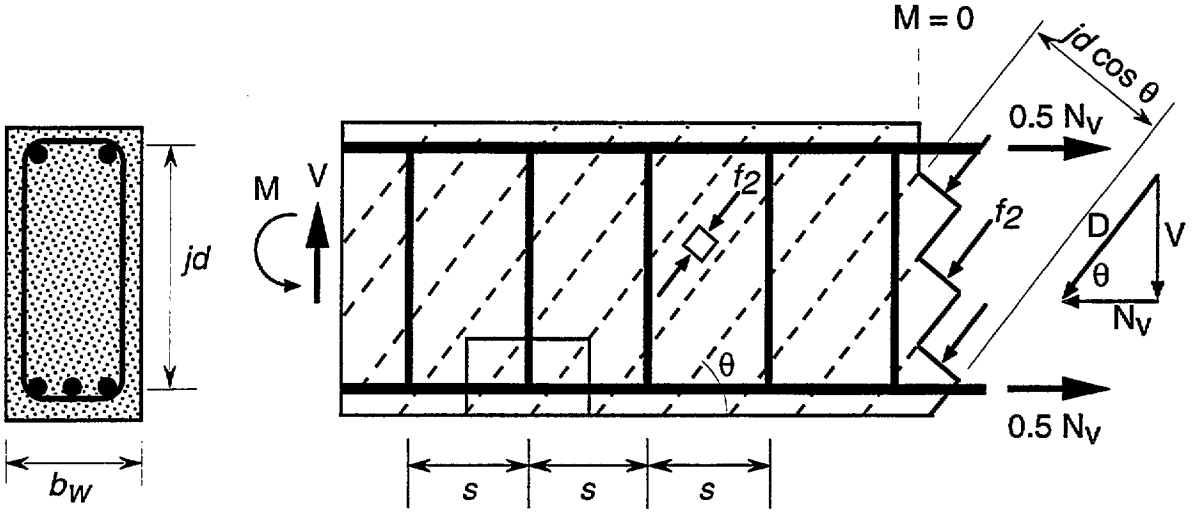

(a) Diagonal stresses and longitudinal equilibrium

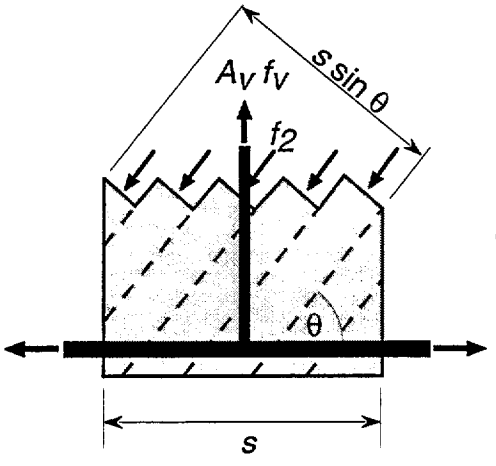

(b) Stirrup force

Figure 2.15— Equilibrium condition for variable angle truss used in the compression field theory (Collins and Mitchell 1991).

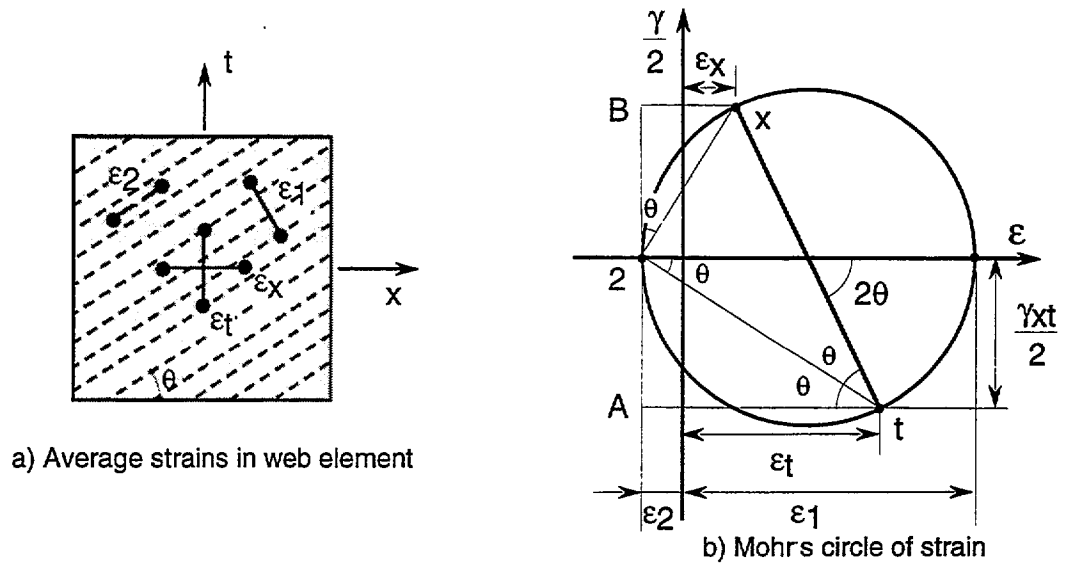

a) Average strains in web element

b) Mohr's circle of strain

Figure 2.16 — Strain compatibility for cracked web (Collins and Mitchell 1991).

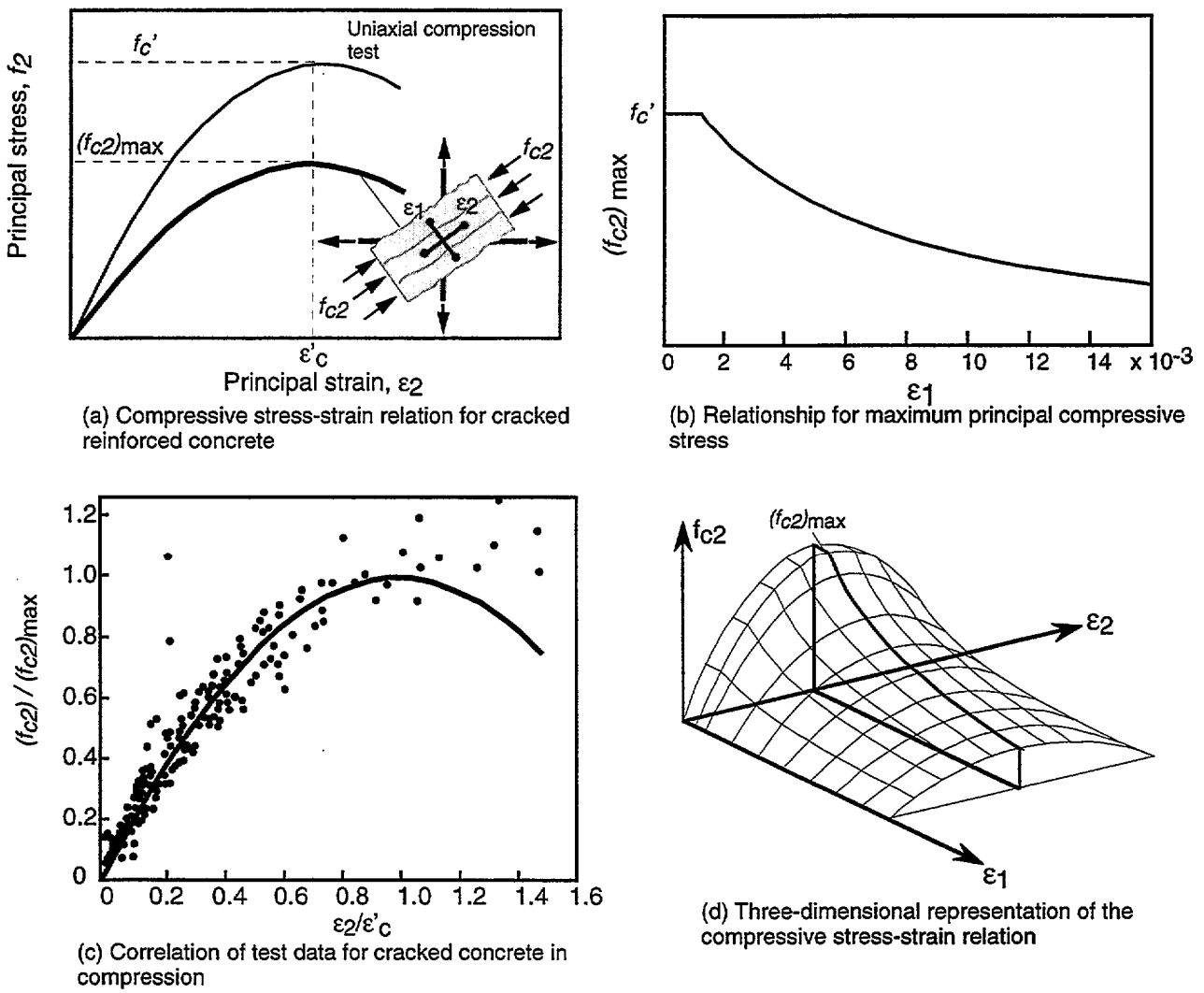

(a) Compressive stress-strain relation for cracked reinforced concrete

(b) Relationship for maximum principal compressive stress

(c) Correlation of test data for cracked concrete in compression

(d) Three-dimensional representation of the compressive stress-strain relation

Figure 2.17— Compressive stress-strain relationships for cracked concrete (Collins and Mitchell 1991).

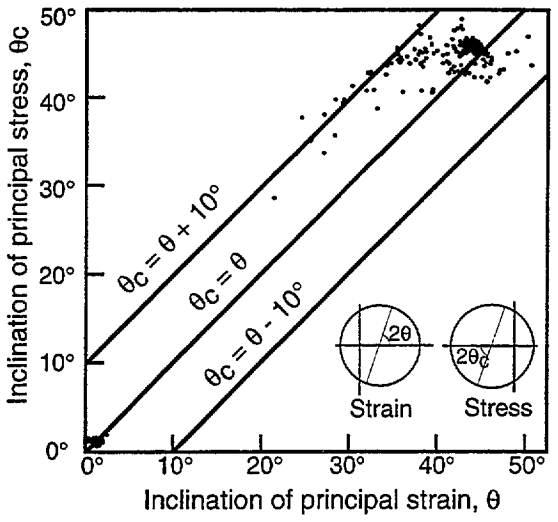

Figure 2.18 — Comparison of principal stress and principal strain directions (Vecchio and Collins 1986).

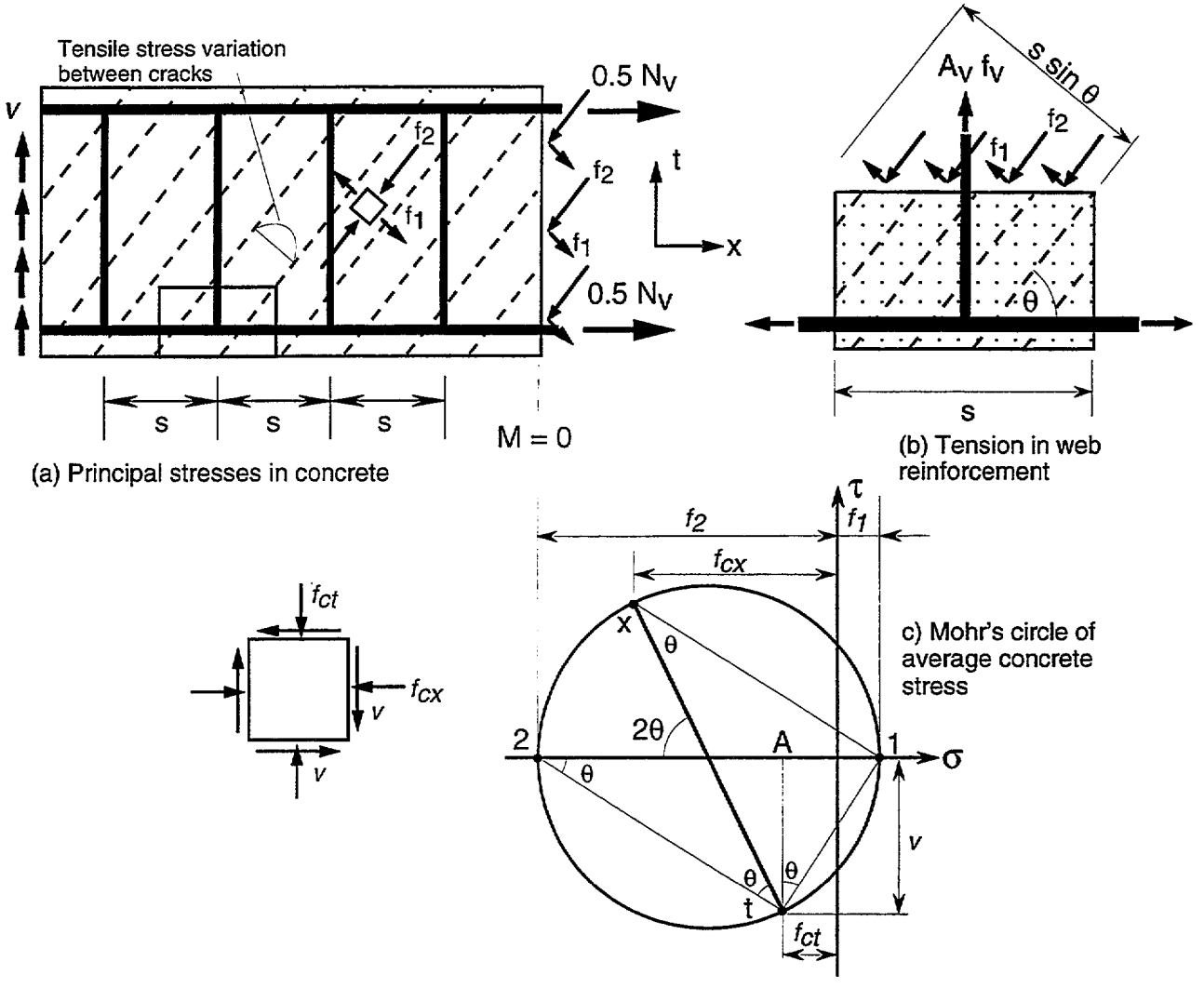

Figure 2.19 — Equilibrium conditions for modified compression field theory (Collins and Mitchell 1991).

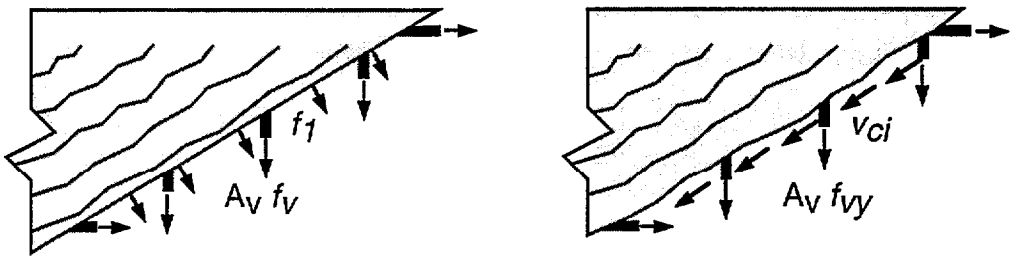

(a) Calculated average stresses

(b) Local stresses at a crack

Figure 2.20— Force transmission across cracks (Collins and Mitchell 1991).

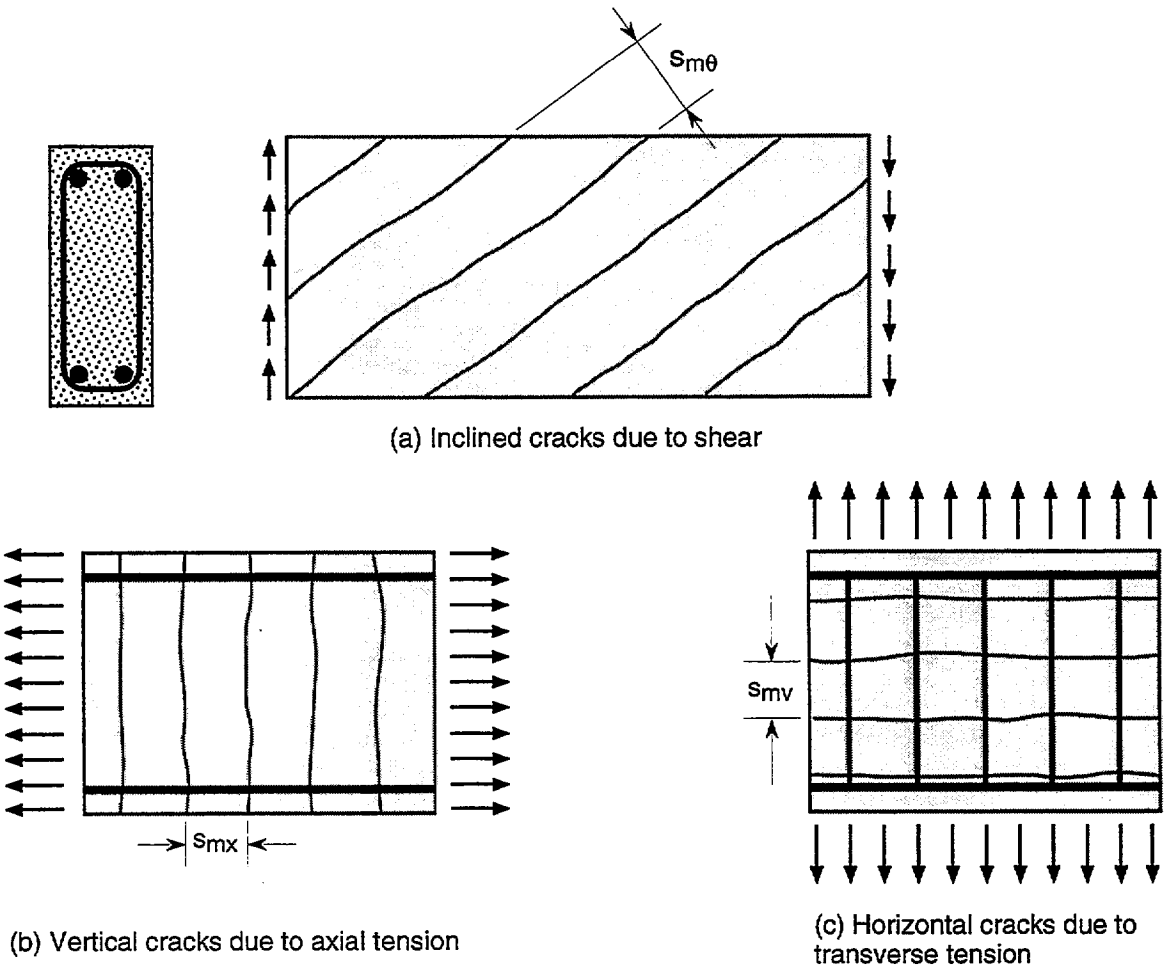

(a) Inclined cracks due to shear

(b) Vertical cracks due to axial tension

(c) Horizontal cracks due to transverse tension

Figure 2.21 — Crack spacings in reinforced concrete (Collins and Mitchell 1991).

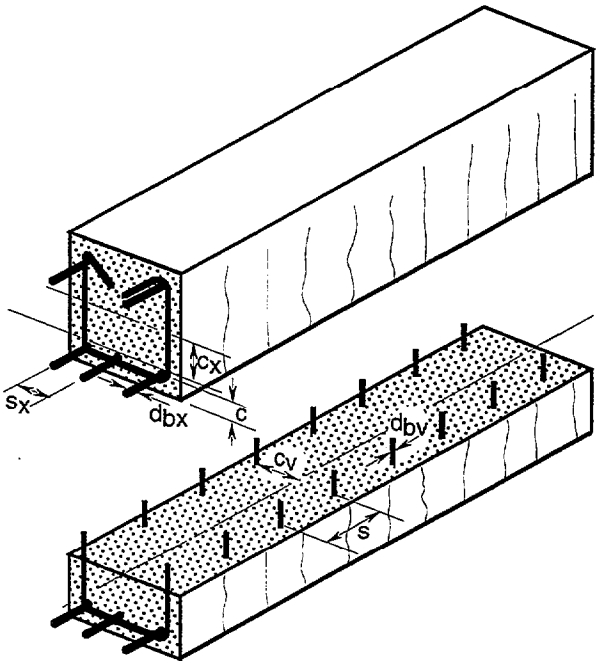

Figure 2.22 — Parameters affecting crack spacing (Collins and Mitchell 1991).

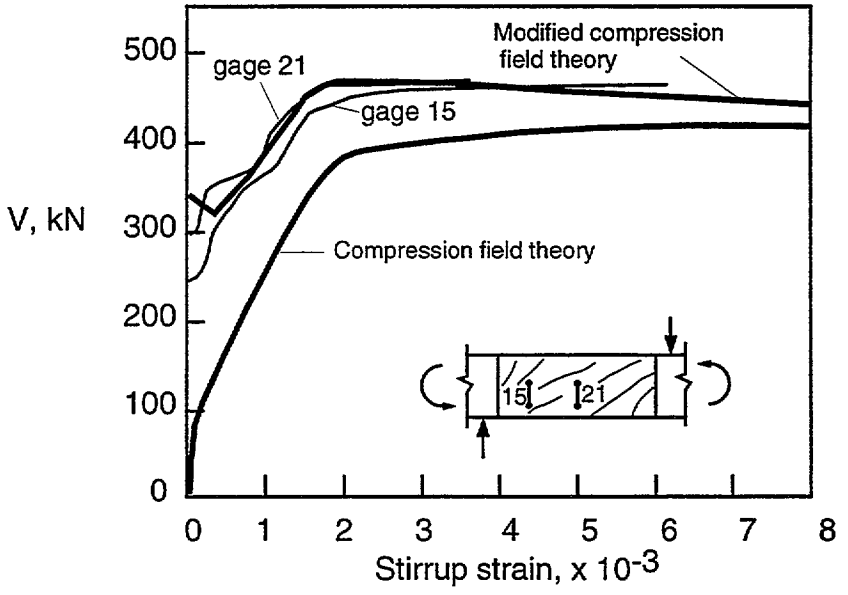

Figure 2.23 — Comparison of measured and predicted stirrup strains (Collins and Mitchell 1991).

2.5 Other "Exact" Solutions where the Directions of Principal Stresses and Strains Differ

2.5.1 Analysis of Kupfer, Mang and Karavesyroglou

Kupfer, Mang and Karavesyroglou (1983) developed an "exact" theory for the shear resistance of reinforced concrete beams that accounts for equilibrium, strain compatibility and stress-strain relationships. The major difference between this theory and the *modified compression field theory* is that here, the principal stresses and principal strains are not assumed to be parallel. In general, the principal stress and strain axes do not coincide (and they also deviate from the crack direction), but these deviations are small, as shown in Fig. 2.18.

The paper by Kupfer et al. (1983) is presented in its essential elements because it has had a major influence on European concrete codes, and is not readily accessible to English readers. The following notation is used:

f'_c = short term, cylinder strength of concrete (β_c in original paper),
f_y = yield strength of stirrup steel (β_s in original paper),
f_2 = long term strength of diagonal (cracked) compression field (β_2 in original paper),
f_t = tensile strength of concrete (β_{bz} in original paper),
v, w = crack sliding (tangential) and opening (normal, crack width),
ε_b, γ_b = normal and shear strains of concrete between cracks,
ε, γ = normal and shear strains due to smeared-out crack displacements,
ε_{bs} = concrete shrinkage strain,
ε_s = stirrup strain at diagonal crack,
ε_t = $\alpha_s\varepsilon_s + \Delta\varepsilon_s + \varepsilon_{bs}$ = effective stirrup strain,
$\alpha_s\varepsilon_s$ = stirrup strain averaged over crack spacing ,
$\Delta\varepsilon_s$ = anchorage slip smeared over stirrup length,
σ = normal stress in concrete web,
σ_2 = principal compressive stress in strut,
τ = applied shear stress,
τ_1 = bond strength of reinforcement,
τ_{xy}, τ_{dr} = shear stress of concrete in *x-y* and *d-r* coordinate system,
$\Delta\tau_1$ = $\tau_{dr} - \sigma_r \cot \phi$ = shear resistance due to aggregate interlock,
$\Delta\tau_2$ = shear resistance due to strut bending,
μ_s = $nA_{s1} / (sb_o)$ = geometric shear reinforcement ratio,
n-legged stirrups spaced at interval *s*, measured *perpendicular* to stirrups,
β = inclination of stirrup with respect to longitudinal axis,
θ = inclination of compressive strut with respect to longitudinal axis (α in original paper),
ϕ = inclination of crack with respect to longitudinal axis (α_r in original paper).

See also Fig. 2.24 for the notation of the dimensions and directions used in the derivations. Units used are N and mm.

Equilibrium — At a joint between stirrup, concrete strut, and bottom chord (Fig. 2.25 and 2.26):
Force:

$$\sigma_2 = \frac{\tau}{\sin^2\theta\,(\cot\theta + \cot\beta)}$$

$$\mu_s f_y = \frac{\tau}{\sin^2\beta\,(\cot\beta + \cot\theta)}$$

Moment:

$$\tan\theta = \frac{1 - \dfrac{\Delta\tau_1}{\tau}}{\cot\phi + \cot\beta\,\dfrac{\Delta\tau_1}{\tau}}$$

For $\Delta\tau_1 = 0$, i.e. no aggregate interlock, the strut angle θ equals the crack angle ϕ.
Therefore,

$$\mu_s f_y = \frac{\tau - \Delta\tau_1}{\sin^2\beta\,(\cot\beta + \cot\phi)}$$

For a crack inclination of 45°:

$$\mu_s f_y = \frac{\tau - \Delta\tau_1}{\sin^2\beta\,(\cot\beta + 1)} < \frac{\tau}{\sin^2\beta\,(\cot\beta + 1)} = \text{CEB requirement}$$

Thus, accounting for the shear resistance due to aggregate interlock reduces the stirrup requirement.

From Mohr's stress circle and for a crack inclination of 45° (Fig. 2.27):

$$\tau_{xy} - \sigma_y = \tau_{dr} - \sigma_r = \Delta\tau_1$$

with $\quad \sigma_y = \mu_s f_y \sin^2\beta$

and $\quad \tau_{xy} = \tau - \mu_s f_y \sin\beta\cos\beta$

Compatibility — When cracks form, the effective stirrup strain ε_t is greater than the corresponding strain in the compression field, ε_{bt}; likewise, the longitudinal strain ε_x of the panel is often different from the strain ε_{bx} of the compression field.

$$\Delta\varepsilon_t = \varepsilon_t - \varepsilon_{bt} \quad \text{and} \quad \Delta\varepsilon_x = \varepsilon_x - \varepsilon_{bx} \tag{2.47}$$

For cracks inclined at 45°, the smeared strain due to crack sliding v is (Fig. 2.28):

$$-\varepsilon_{x,v} = \varepsilon_{y,v} = \frac{v\sqrt{2}}{2a}$$
$$\gamma_{xy,v} = 0$$

Also, for cracks inclined at 45°, the smeared strain due to crack opening w is (Fig. 2.28):

$$\varepsilon_{r,w} = \frac{w\sqrt{2}}{a}$$
$$\varepsilon_{d,w} = 0$$
$$\varepsilon_{x,w} = \varepsilon_{y,w} = \frac{\gamma_{xy,w}}{2} = \frac{w\sqrt{2}}{2a}$$

Two cases are considered:

Case a: $\varepsilon_x = \varepsilon_{bx}$ and $\beta = 90°$ (stirrups are perpendicular to beam axis, Fig. 2.29).
This case assumes that the average strains of both flanges equal the longitudinal component of the normal strain, ε_{bx}, of the compression struts. This situation arises in prestressed beams.

$$\gamma_{xy} = \gamma_{b,xy} + \gamma_{xy,v} + \gamma_{xy,w} = \gamma_{b,xy} + 0 + \frac{w\sqrt{2}}{a}$$
$$\gamma_{dr} = \gamma_{b,dr} + \gamma_{dr,v} + \gamma_{dr,w} = \gamma_{b,dr} + \frac{v\sqrt{2}}{a} + 0$$

From Mohr's circle, and because

$$\varepsilon_d - \varepsilon_x = \varepsilon_{bd} - \varepsilon_{bx}$$

then $\gamma_{dr} - \gamma_{xy} = \gamma_{b,dr} - \gamma_{b,xy}$

$$\varepsilon_y = \varepsilon_{by} + \varepsilon_{y,v} + \varepsilon_{y,w} = \varepsilon_{by} + \frac{v\sqrt{2}}{2a} + \frac{w\sqrt{2}}{2a} = \varepsilon_{by} + \frac{v\sqrt{2}}{a} \qquad (2.48)$$

From which

$$v = \frac{a}{\sqrt{2}}(\varepsilon_y - \varepsilon_{by}) = w \qquad (2.49)$$

$$\varepsilon_{by} = \frac{\varepsilon_{b2} + \varepsilon_{b1}}{2} - \frac{\varepsilon_{b2} - \varepsilon_{b1}}{2}\cos 2\theta = \varepsilon_{b2}\left(\frac{1-\nu}{2} - \frac{1+\nu}{2}\cos 2\theta\right) \qquad (2.50)$$

Case b: $\varepsilon_x = 0$ and $\beta = 90°$. In this case the average strain of both chords is 0 (Fig. 2.30).

$$\varepsilon_x = \varepsilon_{bx} + \varepsilon_{x,v} + \varepsilon_{x,w} = \varepsilon_{bx} - \frac{v\sqrt{2}}{2a} + \frac{w\sqrt{2}}{2a} = 0 \qquad (2.51)$$

$$\varepsilon_y = \varepsilon_{by} + \varepsilon_{y,v} + \varepsilon_{y,w} = \varepsilon_{by} + \frac{v\sqrt{2}}{2a} + \frac{w\sqrt{2}}{2a}$$

From Eqs. 2.47, 2.48, and 2.51:

$$v = \frac{a}{\sqrt{2}}(\varepsilon_y + \varepsilon_{bx} - \varepsilon_{by}) = \frac{a}{\sqrt{2}}(\Delta\varepsilon_t - \Delta\varepsilon_x)$$

$$w = \frac{a}{\sqrt{2}}(\varepsilon_y - \varepsilon_{bx} - \varepsilon_{by}) = \frac{a}{\sqrt{2}}(\Delta\varepsilon_t + \Delta\varepsilon_x)$$

Substituting ε_{by} from Eq. 2.50 and

$$\varepsilon_{bx} = \frac{\varepsilon_{b2} + \varepsilon_{b1}}{2} + \frac{\varepsilon_{b2} - \varepsilon_{b1}}{2}\cos 2\theta = \varepsilon_{b2}\left(\frac{1-\nu}{2} + \frac{1+\nu}{2}\cos 2\theta\right)$$

results in

$$v = \frac{a}{\sqrt{2}}\left(\varepsilon_y - (1+\nu)\,|\varepsilon_{b2}|\,\cos 2\theta\right)$$

$$w = \frac{a}{\sqrt{2}}\left(\varepsilon_y + (1-\nu)\,|\varepsilon_{b2}|\right)$$

Determination of crack spacing a (measured parallel to beam axis):

$$a_{\min}\, u\, \tau_1 = f_t\, A_b$$

where u = circumference of stirrups,
A_b = concrete area per stirrup, and
d_s = stirrup diameter.

$$\frac{A_b}{u} = \frac{s\, b_o}{n\,\pi\, d_s} = \frac{1}{\mu_s}\frac{d_s}{4}$$

$$a_{\min} = \frac{f_t}{\tau_1}\frac{1}{\mu_s}\frac{d_s}{4}$$

The mean crack spacing a is approximately $1.5\, a_{min}$. For ribbed stirrups $f_t / \tau_1 = 0.4$ and $a = 0.15\, d_s / \mu_s$. For end-anchored stirrups with no bond, $a \le 0.75\, z$.

Constitutive relations of cracks — From experiments performed on concrete with compressive strength of 25 MPa and for $v > 0.20$ mm:

$$\frac{\Delta \tau_1}{f'_c} = 0.117 - 0.085\, v \qquad \text{for case (a):} \quad (v = w)$$

$$\frac{\Delta \tau_1}{f'_c} = 0.017 + 0.1\, \frac{v}{w} - 0.085\, v \qquad \text{for case (b):} \quad (v \neq w)$$

Constitutive relations of concrete — For uniaxially compressed concrete with a crushing strain of $\varepsilon_{bu} = -0.002$

$$\varepsilon_b = -2 \times 10^{-3} \left(1 - \sqrt{1 - \frac{\sigma_2}{f_2}} \right)$$

$$f_2 = 0.8 \times 0.85 \times f'_c \approx \frac{2}{3} f'_c$$

0.8 is a long-term load factor and 0.85 is an experimental factor.

Solution — Case a: $\varepsilon_x = \varepsilon_{bx}$ and $\beta = 90°$
For Poisson's ratio = 0.25, using Eqs. 2.49 and 2.50, and since the effective stirrup strain is:

$$\varepsilon_t = \varepsilon_y = \alpha_s\, \varepsilon_s + \Delta \varepsilon_s + \varepsilon_{bs}$$

one obtains

$$w = \frac{a}{\sqrt{2}} \left[\alpha_s\, \varepsilon_s + \Delta \varepsilon_s + |\varepsilon_{bs}| + 0.625\, |\varepsilon_{b2}|\, (0.6 - \cos 2\theta) \right]$$

The solution is arrived at by iteration.

Case b: $\varepsilon_x = 0$ and $\beta = 90°$

$$v = \frac{a}{\sqrt{2}} \left(\alpha_s\, \varepsilon_s + \Delta \varepsilon_s + |\varepsilon_{bs}| - 1.25\, |\varepsilon_{b2}|\, \cos 2\theta \right)$$

$$w = \frac{a}{\sqrt{2}} \left(\alpha_s\, \varepsilon_s + \Delta \varepsilon_s + |\varepsilon_{bs}| + 0.75\, |\varepsilon_{b2}| \right)$$

The solution is also obtained by iteration.

Comparison with experimental results — Fig. 2.31 compares experimental data with predictions for cases a and b using vertical stirrups ($\beta = 90°$) of diameters 10 mm or 6 mm. Code equations and Mörsch's prediction are also shown. Satisfactory agreement is obtained between predicted and measured values. Kupfer et al. observed that, at low shear, deviations from experiments are greater than at high shear, and attribute this to the neglected bending of the struts and the lack of uniformity of crack spacing at low shear. Also, experiments vary widely in beam depth, concrete strength and stirrup yield strength.

Estimation of influence of bending of concrete struts — For low applied shear and shallow beams, strut bending further reduces the stirrup requirement by $\Delta\tau_2 \approx 0.25\ \tau$ (for $a = 0.75\ z$, $\phi = 45°$, and $\beta = 90°$).

Conclusion — In this paper, Kupfer et al. (1983) show that aggregate interlock across the diagonal cracks of reinforced or prestressed concrete beams is responsible for carrying a portion $\Delta\tau_1$ of the applied shear. This concrete contribution is separate from the concrete contribution in the concrete compression zone and depends on the magnitude of the shear stress. For small shear stresses, important parameters for $\Delta\tau_1$ are the beam depth and longitudinal strain, and the stirrup strain, diameter and inclination. Furthermore, constitutive relations for cracks are obtained from experiments and the bending stiffness of the concrete strut is neglected.

There results a uniform compression field whose inclination is somewhat shallower than that of the shear cracks. Consequently, the aggregate interlock force crosses the cracks at a shallow angle. The authors also derive strain compatibility from Mohr's circle and estimate the influence of strut bending. The resulting concrete contribution is somewhat higher than that given in the German (DIN 4227) or European (CEB) codes.

2.5.2 Analysis by Kupfer and Bulicek

Kupfer and Bulicek (1991) updated the work of Kupfer, Mang and Karavesyroglou (1983) by incorporating improved constitutive relations for biaxial strength of concrete and shear friction. Also, the shear reinforcement is limited to being vertical and only "case a" is treated, i.e., the longitudinal strain in the web equals the average strains in the chords. As in the previous model, an important feature is that the crack angle ϕ is different from the strut angle θ, which is also the direction of principal compression in the web. The following notation is used, in addition to that defined at the beginning of Section 2.5.1:

σ_c = normal stress perpendicular to cracks,
σ_d = normal stress in struts parallel to shear cracks,
σ_{xf} = axial stress due to load effect at onset of cracking,
σ_y = vertical normal stress in web concrete due to stirrup forces,
τ_c = shear stress parallel to cracks,
τ_f = shear stress due to load effect at onset of cracking,
ω = mechanical shear reinforcement ratio, $\omega = 2A_{sw}f_y / (bsf_2)$
f_{cube} = cube compressive strength of concrete.

In contrast to the previous paper, the crack spacing a is now measured *perpendicular* to the cracks and the stirrup spacing s is now *parallel* to the beam axis.

Crack angle — Cracks initiate perpendicularly to the direction of principal tension in the previously uncracked concrete. Under applied stress σ_{xf} and $\tau_f = \sigma_{xf}/n$, the crack angle is found from Mohr's circle

$$\cot\phi = -\frac{n}{2} + \sqrt{1 + \frac{n^2}{4}}$$

Equilibrium — Horizontal and vertical equilibrium requires (Fig. 2.32a):

$$\sigma_d = \frac{2\,\tau}{\sin 2\,\phi} + 2\,\tau_c \cot 2\phi + \sigma_c$$

$$\sigma_y = (\tau - \tau_c) \tan \phi + \sigma_c$$

From Mohr's circle (Fig. 2.32b,c), the following relations are derived:

$$\sigma_y = -\tau \tan \phi + \sigma_1$$

$$\begin{pmatrix} \sigma_1 \\ \sigma_2 \end{pmatrix} = \frac{1}{2}\left(\sigma_d + \sigma_c \pm \sqrt{(\sigma_d - \sigma_c)^2 + 4\,\tau_c^2}\right)$$

$$\tan 2\delta = \frac{2\tau_c}{\sigma_c - \sigma_d}$$

The last relation gives the strut angle: $\theta = \phi - \delta$.

Kinematic conditions of strains — The overall smeared strain ε of the web results from the pure concrete strain ε_o and the smeared average strains ε_w and ε_v due to crack opening w and crack slip v:

$$\varepsilon = \varepsilon_o + \varepsilon_w + \varepsilon_v$$

From Mohr circles and denoting the crack spacing by a, now measured perpendicularly to the cracks:

$$\frac{w}{a} = \varepsilon_x + \varepsilon_y - \varepsilon_{10} - \varepsilon_{20}$$

$$\frac{v}{a} = -\varepsilon_x \cot \phi + \varepsilon_y \tan \phi - \varepsilon_{10} \frac{\sin^2 \phi - \sin^2 \theta}{\sin \phi \cos \phi} + \varepsilon_{20} \frac{\cos^2 \phi - \sin^2 \theta}{\sin \phi \cos \phi}$$

where ε_x is either given or derived as:

$$\varepsilon_x = \frac{1}{2}\left(\varepsilon_{x,\,\text{top chord}} + \varepsilon_{x,\,\text{bottom chord}}\right)$$

and ε_{10}, ε_{20} are principal strains defined below. The overall vertical strain ε_y of the web is the factored sum of the strain ε_s of the stirrup, anchorage slip $\Delta\varepsilon_s$ and shrinkage strain $\varepsilon_{cs} < 0$.

$$\varepsilon_y = (\varepsilon_s + \Delta\varepsilon_s - \varepsilon_{cs})\, k\,.$$

The factor k is due to tension stiffening.

Constitutive relations — The web is biaxially loaded by σ_1 and σ_2. From experiments performed with concrete having a uniaxial compressive strength of 40 MPa, the strength f_2 is given by:

$$f_2 = f'_c \times 0.85 \times 0.75\left(1 - \frac{f'_c}{250}\right)$$

where 0.85 = factor for sustained load,

0.75 = factor for irregular crack trajectory, and
$(1 - f'_c/250)$ = difference between cylinder strength and uncracked concrete prism.
The principal strains ε_{10} and ε_{20} are given by:

$$\varepsilon_{10} = \frac{\sigma_1 + \sigma_2}{9 K_s} + \frac{2\sigma_1 - \sigma_2}{6 G_s}$$

$$\varepsilon_{20} = \frac{\sigma_1 + \sigma_2}{9 K_s} + \frac{2\sigma_2 - \sigma_1}{6 G_s}$$

where the secant shear modulus G_s, the secant compressive modulus K_s, and the octahedral shear stress τ_o are as follows:

$$G_s = 13000 \left(1 - 3.5 \left(\frac{\tau_o}{f_2} \right)^{2.5} \right) \text{ MPa}$$

$$K_s = 17000 \left(1 - 1.6 \left(\frac{\tau_o}{f_2} \right)^{1.8} \right) \text{ MPa}$$

$$\tau_o = \frac{\sqrt{2}}{3} \sqrt{\sigma_1^2 + \sigma_2^2 - \sigma_1 \sigma_2} \text{ MPa}$$

Shear reinforcement — The shear reinforcement yields at the cracks. The average concrete tensile stress is assumed to be $0.20 f_t$ along the stirrups, which leads to:

$$k = 1.0 - 0.20 \frac{f_t}{\mu f_y} = 1 - \frac{f_t}{f_2} \frac{1}{w}$$

Assuming $f_t/f_2 = 0.15$, $k = 1 - 0.06/w$.

Aggregate interlock — The relationships between crack stresses and displacements are from Walraven (1981) and Walraven and Reinhardt (1981). See § 4.3.2.

$$\tau_c = -\frac{f_{cube}}{30} + \left(1.8\ w^{-0.8} + (0.234\ w^{-0.707} - 0.20) f_{cube}\right) v \geq 0$$

$$\sigma_c = \frac{f_{cube}}{20} - \left(1.35\ w^{-0.63} + (0.191\ w^{-0.552} - 0.15) f_{cube}\right) v \leq 0$$

where the units are MPa and mm.

Shear crack spacing a — Factors influencing shear crack spacing a, measured perpendicularly to the cracks, are the reinforcement ratio, the stirrup diameter d_s and the inner lever arm z. From experiments:

$$\frac{1}{a} = \frac{5\mu}{d_s} + \frac{2}{z} = \frac{2.5\omega f_2}{d_s f_y} + \frac{2}{z}$$

where μ is the geometrical shear reinforcement ratio defined for a stirrup spacing measured parallel

to the beam axis.

Numerical evaluation — A numerical evaluation is made for crack angles $35° \le \phi \le 55°$ and average axial strain $-0.001 \le \varepsilon_x \le 0.001$. The results indicate that (Fig. 2.33):

- The plastic method (§ 2.2) represents an upper bound of the shear capacity.
- σ_1 is negligible.
- Axial tension decreases and axial compression increases the shear capacity.
- Practical designs $-0.002 \le \varepsilon_x \le 0.002$ fall between the Ritter-Mörsch straight line and the plastic solution quarter circle.
- The crack angle has little influence for moderate shear but a marked influence for small or high applied shear. The authors propose a formula for the strut angle θ that results from a linear interpolation between $\tan\theta_R = 1$ and $\tan\theta_P$ in terms of ε_x by taking into account unfavorable crack inclination ϕ:

$$\tan\theta = 1 - \frac{2 - 1000\,\varepsilon_x}{4}(1 - \tan\theta_P) \ge \frac{1}{3}$$

and

$$\tan\theta \ge \tan\theta_P = \frac{1 - \sqrt{1 - \nu^2}}{\nu}$$

where $\nu = 2\tau / f_{c2}$ is the acting shear stress ratio.

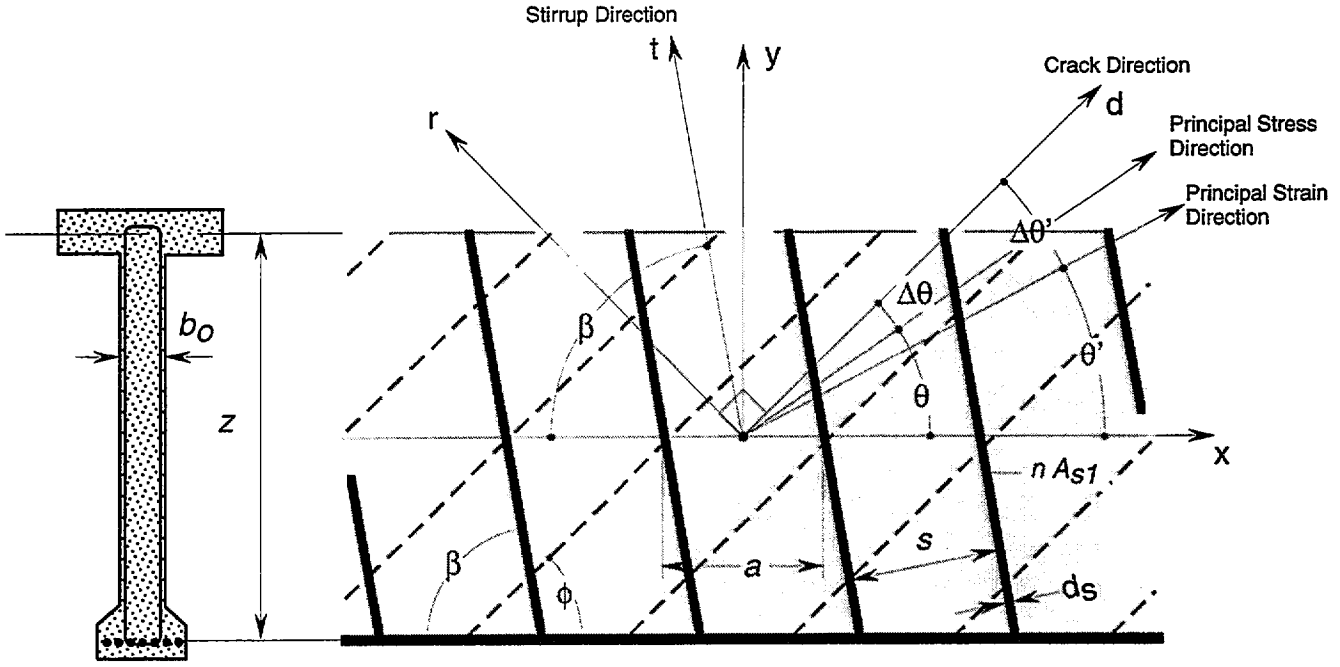

Figure 2.24 — Dimensions and directions in beam web (Kupfer et al. 1983).

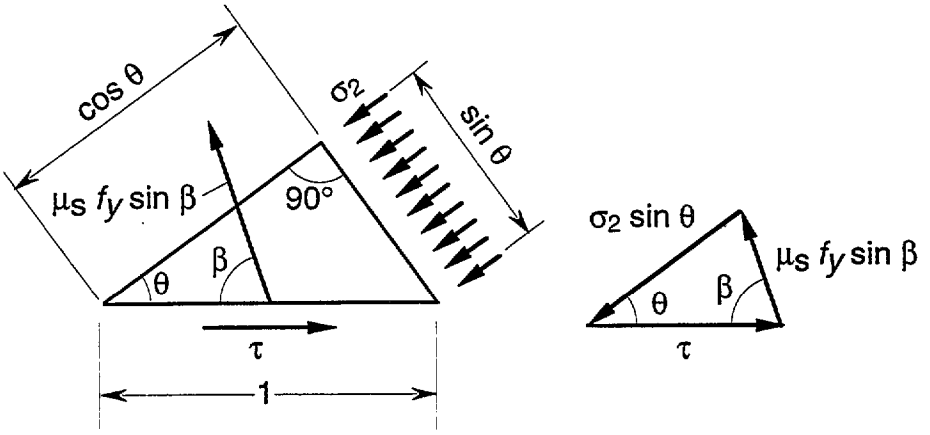

Figure 2.25 — Forces on a web element due to shear (Kupfer et al. 1983).

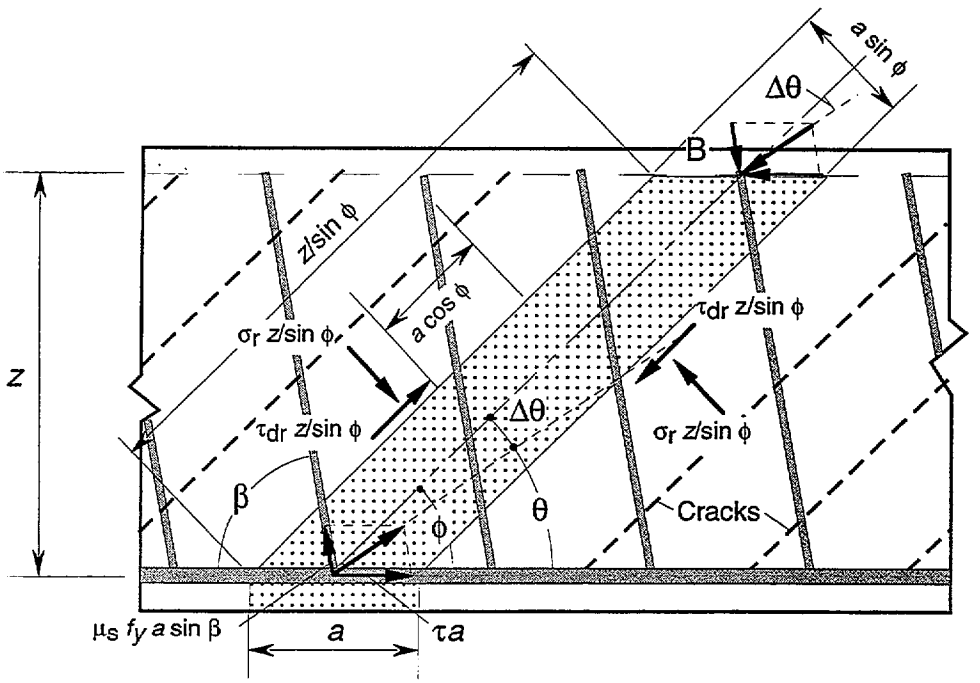

Figure 2.26 — Forces acting along compressive strut neglecting bending (Kupfer et al. 1983).

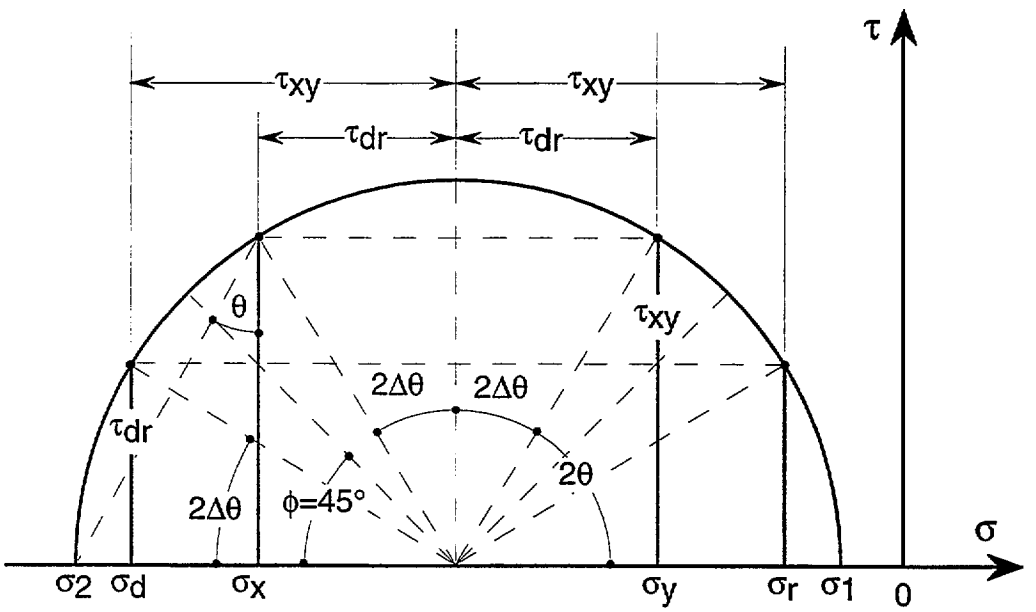

Figure 2.27 — Mohr's circle of stress for element in compression for $\phi = 45°$ (Kupfer et al. 1983).

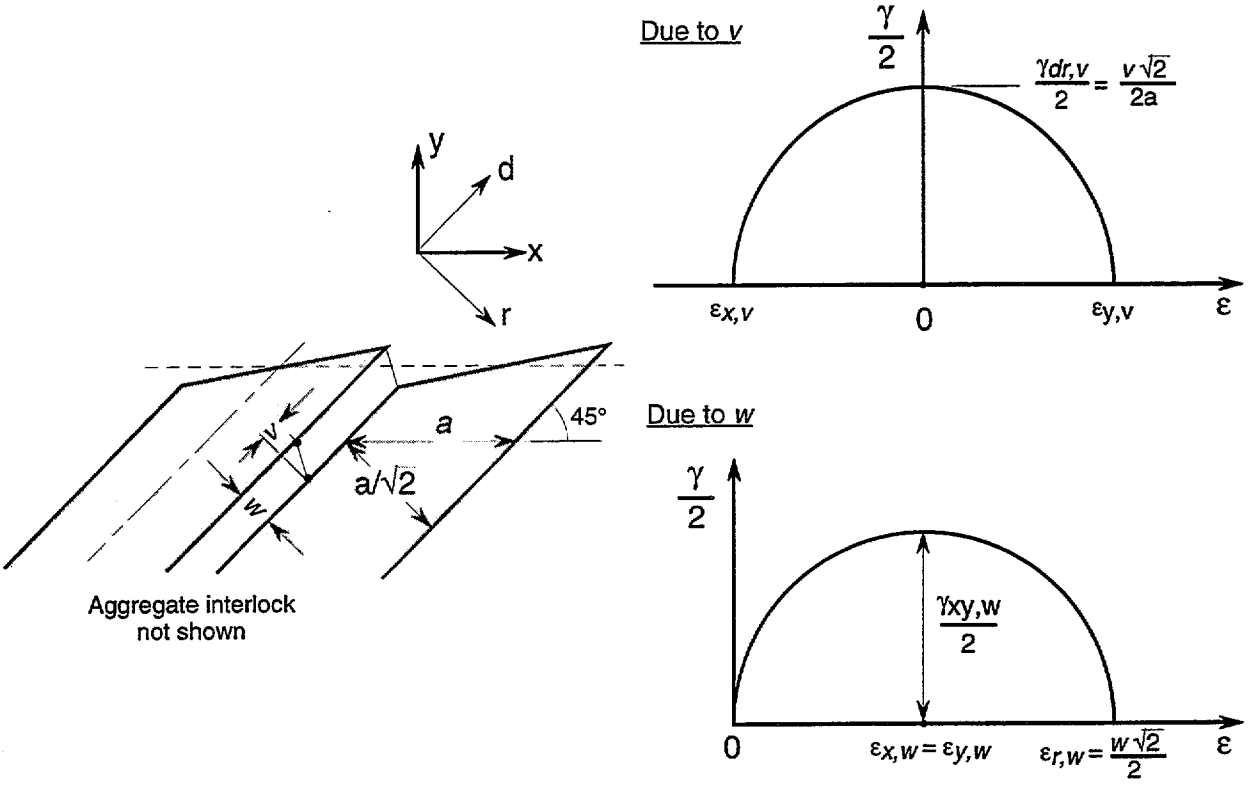

Figure 2.28 — Smeared strains due to opposing edge displacements v and w at a crack (Kupfer et al. 1983).

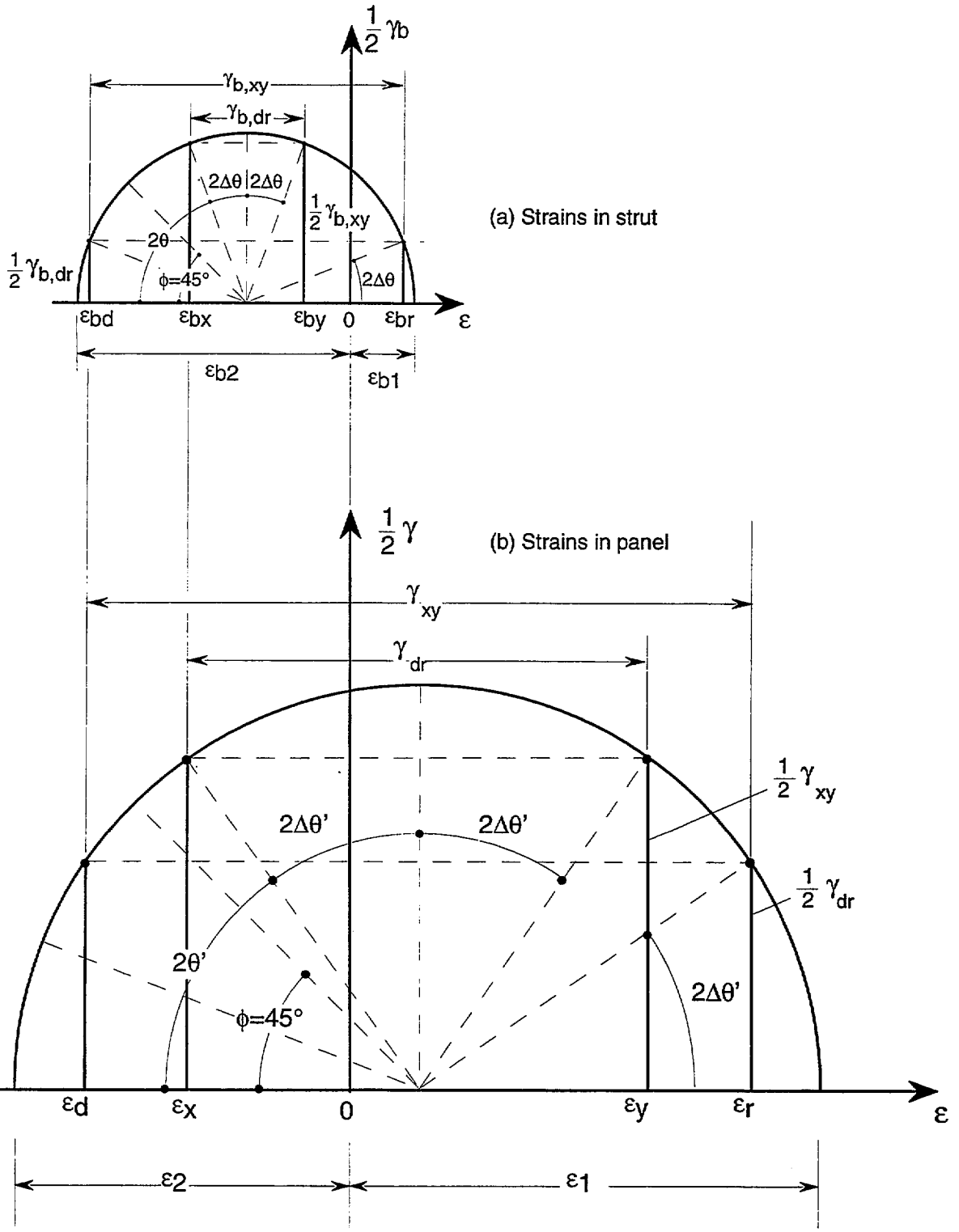

Figure 2.25 — Mohr's circles of strain: (a) in strut and (b) in panel with smeared crack strains: Case (a), $\varepsilon_x = \varepsilon_{bx}$ and $\phi = 45°$ (Kupfer et al. 1983).

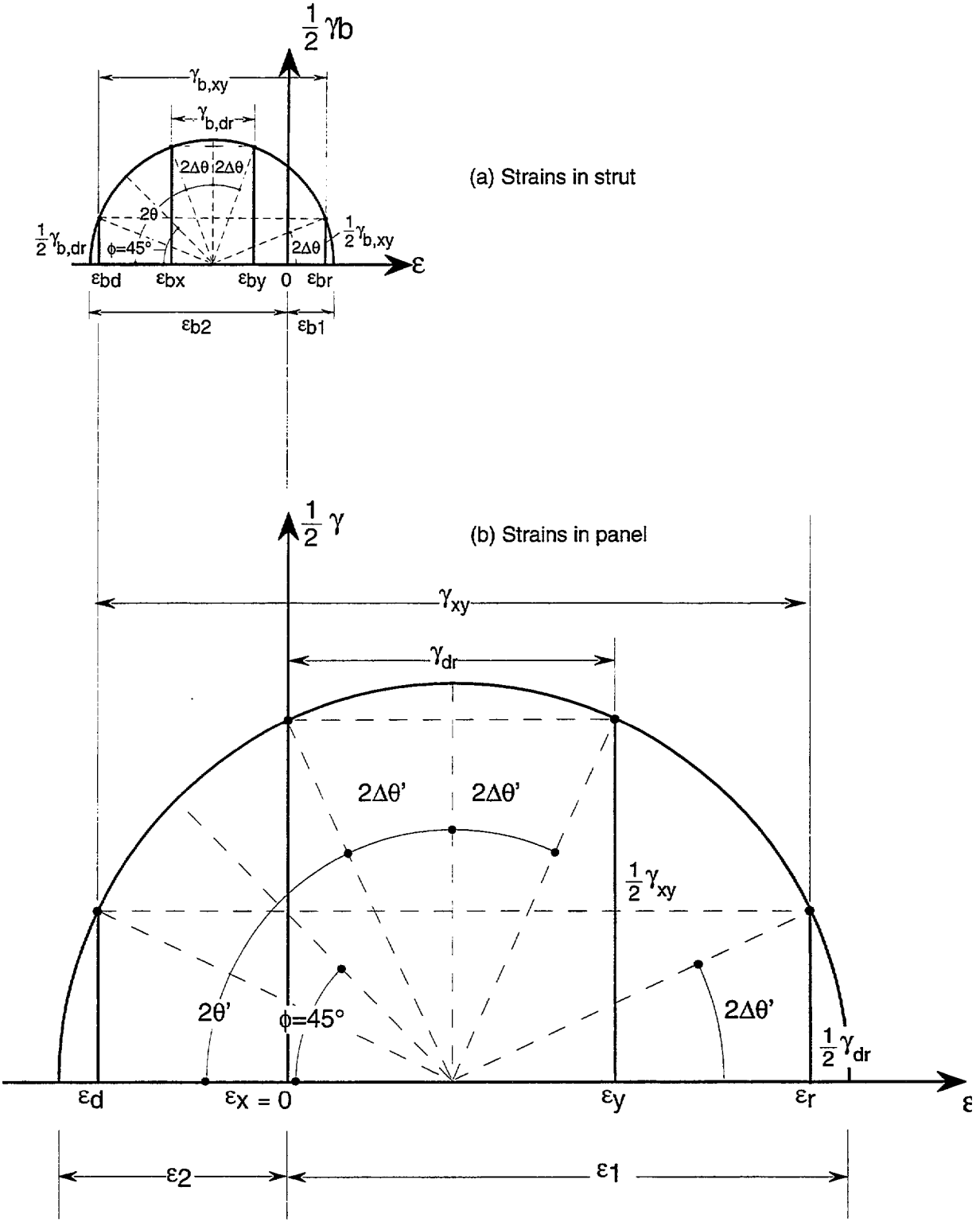

Figure 2.30 — Mohr's circles of strain: (a) in strut and (b) in panel with smeared crack strains: Case b, $\varepsilon_x = 0$ and $\phi = 45°$ (Kupfer et al. 1983)

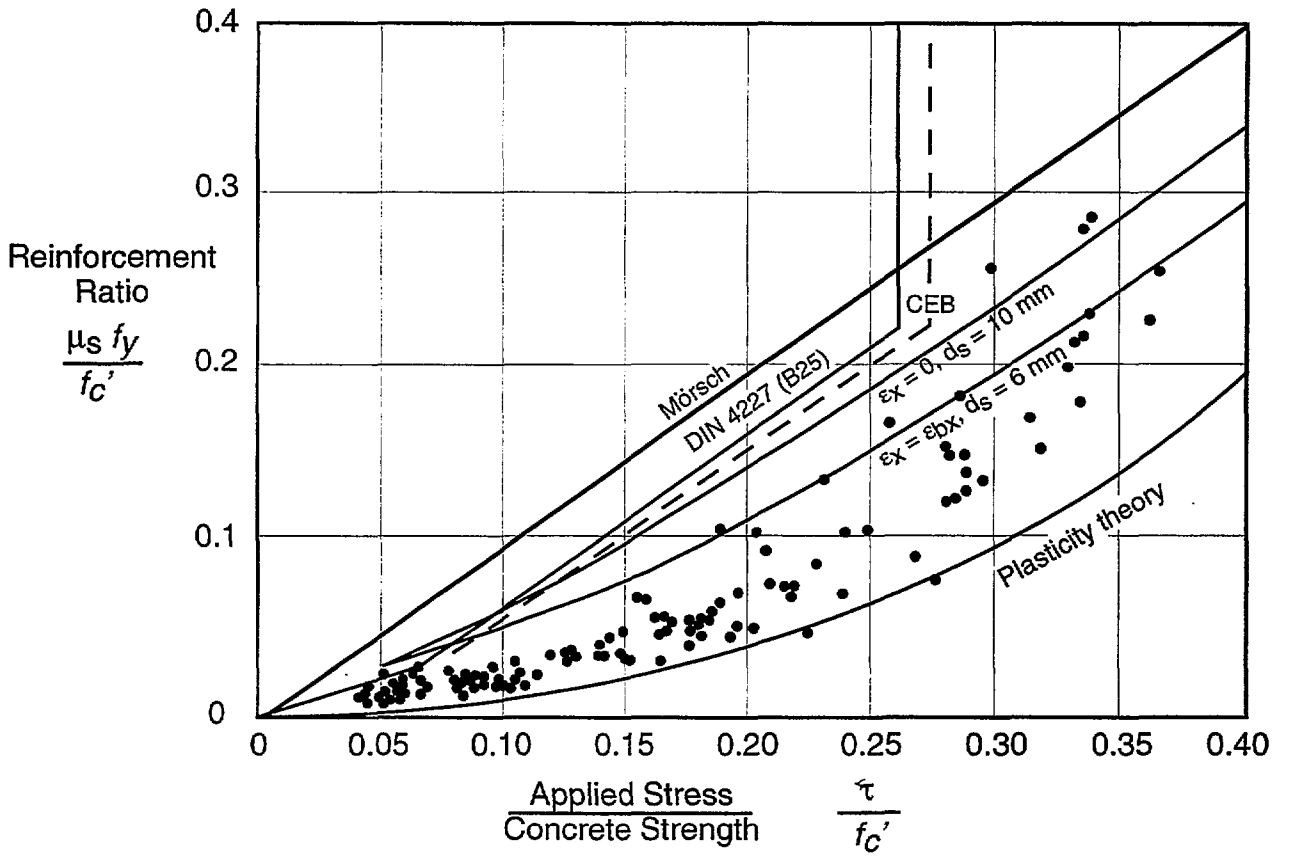

Figure 2.31 — Comparison of shear reinforcement ratio calculated by various methods with experimental data (Kupfer et al. 1983).

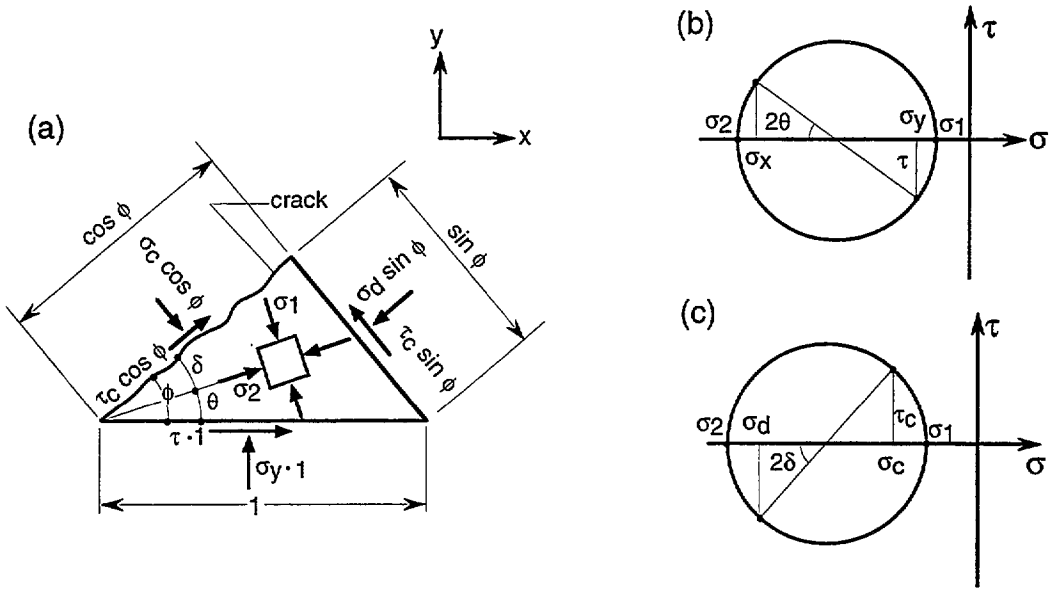

Figure 2.32 — Stress state in web concrete (Kupfer and Bulicek 1991)

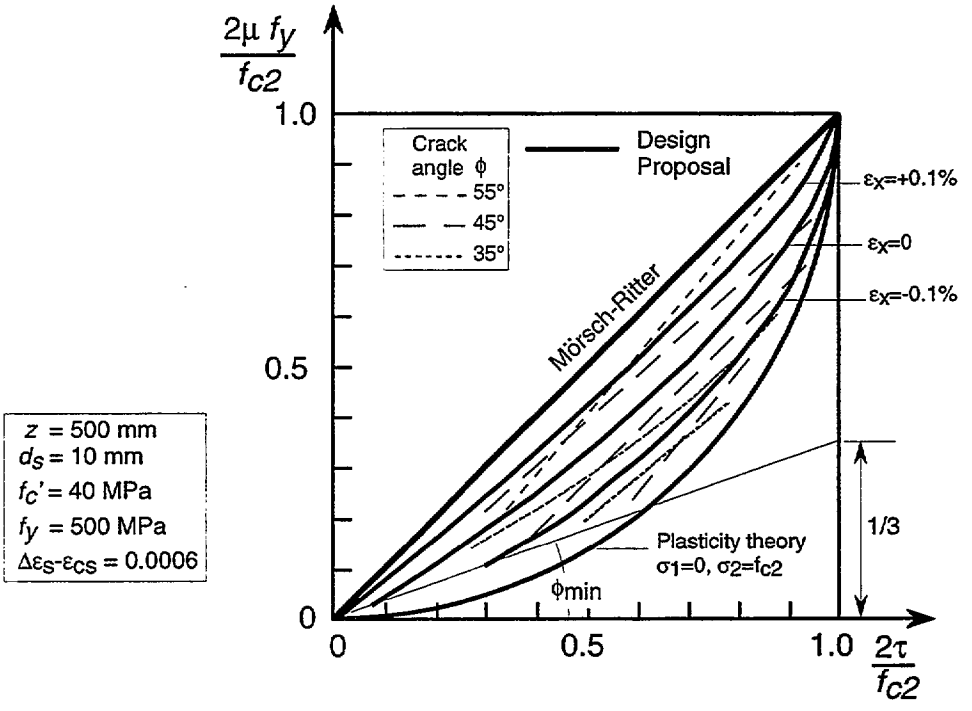

Figure 2.33 — Shear strength versus reinforcement ratio (Kupfer and Bulicek 1991)

2.5.3 Analysis of Dei Poli, Gambarova, and Karakoç (1987)

Dei Poli , Gambarova, and Karakoç (1987) developed an original version of the compression field theory. The major difference between this theory and the Modified Compression Field Theory (MCFT) is that here the principal stresses and principal strains are not parallel. The crack faces transmit not only shear stress, as in the MCFT, but also normal compressive stress (confinement). Dei Poli et al. adopted an approach similar to that of Kupfer et al. (1983) but used a different aggregate interlock relationship. The following notation is used:

A_{st} = area of stirrup per span length s,
b = web width,
d_{st} = diameter of one leg of stirrup,
f_{sy} = yield stress of shear reinforcement,
f_c^* = reduced concrete compressive strength,
f_{ct} = concrete tensile strength,
f_b = stirrup-concrete bond stress,
s = stirrup spacing,
z = lever arm of internal moment,
ε^c = concrete strain,
ε^{sc}, ε_2^{sc}, ε_x^{sc} = strain, principal compressive strain, and longitudinal strain in solid concrete,
ε^{cr}, ε_x^{cr} = strain due to crack and longitudinal strain due to crack,
ε' = smeared strain due to crack opening,
ε'' = smeared strain due to crack slip,
ε^*, ε_x^* = strain due to load and longitudinal strain due to load,
ε^{sh} = concrete shrinkage strain,
ε_{cu}^* = concrete strain at maximum compressive stress,
ε^s = stirrup strain,
ε_{sy} = yield strain of stirrups,
$\Delta\varepsilon^s$ = anchorage slip of stirrups,
σ_{nt} = shear stress on crack faces,
σ_{nn} = normal stress on crack faces (compressive),
σ_2 = principal compressive stress in concrete strut,
τ_u = $Vu/(bz)$ = ultimate shear stress,
$\Delta\tau$ = aggregate interlock contribution to the ultimate shear stress,
ν = Poisson's ratio,
θ = strut inclination with respect to the longitudinal axis,
ϕ = crack inclination with respect to the longitudinal axis,
ρ_{st} = $A_{st}/(bs)$ = shear reinforcement ratio.

The theory includes the following components:

Equilibrium — Refer to Fig. 2.34.

Along a crack:

$$\tau_u = \rho_{st} f_{sy} \cot\phi + \Delta\tau$$

where

$$\Delta\tau = \sigma_{nt} - \sigma_{nn} \cot\phi$$

Between stirrup and diagonal strut:

In the longitudinal direction

$$\sigma_2 = \frac{\tau_u}{\sin\theta \cos\theta}$$

In the transverse direction

$$\frac{\tan\theta}{\tan\phi} = 1 - \frac{\Delta\tau}{\tau_u}$$

Strain Compatibility —

Concrete strains:

Concrete strains, ε^c, are the sum of load induced strains, ε^*, and shrinkage strains, ε^{sh}:

$$\varepsilon^c = \varepsilon^* + \varepsilon^{sh}$$

The load induced strains are, in turn, the sum of strains in the solid concrete between cracks ε^{sc} and the smeared strains ε^{cr} at the cracks.

$$\varepsilon^* = \varepsilon^{sc} + \varepsilon^{cr}$$

The smeared strain due to cracks has components due to crack opening (normal) ε' and crack slip (tangential) ε'':

$$\varepsilon^{cr} = \varepsilon^{/} + \varepsilon^{//}$$

The struts are in a state of uniaxial compression σ_2 (for comparison the modified compression field theory assumes a biaxial state of stress) and

$$\varepsilon_1^{sc} = -\nu\, \varepsilon_2^{sc}$$

Stirrup strains: The average stirrup strain is a fraction α_s of its yield strain plus some anchorage slip:

$$\varepsilon^s = \alpha_s\, \varepsilon_{sy} + \Delta\varepsilon^s$$

Compatibility: Two cases are considered:

1) Near the ends of the beam span, where shear-tension dominates, the longitudinal strain contribution due to crack slip compensates that due to crack opening:

$$\varepsilon_x^{cr} = 0$$

2) Near midspan, where flexure-shear dominates, the top of the web is in compression, the bottom in tension and the average strain due to load is zero:

$$\varepsilon_x^{*} = 0$$

Constitutive Equations —

Concrete: A parabolic stress-strain curve is assumed:

$$\frac{\sigma_2}{f'_c} = 2\,\frac{\varepsilon_2^{sc}}{\varepsilon_{cu}^{*}} - \left(\frac{\varepsilon_2^{sc}}{\varepsilon_{cu}^{*}}\right)^2$$

The strength is reduced by 15% due to the presence of bonded bars in tension crossing the struts. Therefore, some account of the biaxial state of stress is taken.

Cracks: Aggregate interlock is a function of crack slip, crack opening, crack angle, aggregate size and concrete strength. Two alternative theories are offered: the rough crack model and the two-phase model. The latter accounts for the friction between the aggregate and the mortar. These theories will be discussed further in Section 4.3.6.

Crack spacing:

$$s = \frac{5}{8} \frac{f_{ct}}{f_b} \frac{d_{st}}{\rho_{st}}$$

Results — Iterative solution of the above equations for a crack angle $\phi = 45°$ shows that:

- As the ultimate shear τ_u increases, so does the strut angle α which asymptotically approaches the crack angle ϕ but is always less than it.
- Aggregate interlock contributes between 25% and 35% of the shear resistance of rectangular sections. This contribution is larger at the ends of the span than at midspan.
- The shear resistance contribution of aggregate interlock is greater for 40 MPa concrete than for 25 MPa concrete. This obviously depends on the crack constitutive equations used and should not be generalized.
- Comparisons with ACI and CEB code equations and with experimental data show satisfactory agreement. A judicious choice of all the parameters in the theory is necessary.

Subsequent Refinement — The method outlined above was refined further by Dei Poli, Prisco and Gambarova (1990) to account for the additional effects of bending stiffness and shear in the concrete compression bands (in comparison, the modified compression field theory assumes the concrete struts are in a state of biaxial tension-compression). The following notation is used, in addition to that mentioned in the previous discussion:

f_c' = cylinder compressive strength of concrete,
m = moment per unit length due to aggregate interlock,
N^*, V^* = axial and shear forces in inclined bands,
x' = eccentricity of axial force in inclined band of concrete web,
σ_2, θ = principal compressive stress according to compression field theory and associated angle,
σ_1', σ_2' = actual principal stresses in web,
$\Delta\tau_{BND}$ = shear stress due to bending stiffness of band,
$\Delta\tau_{INT}$ = shear stress due to aggregate interlock.

The essential elements of this refined approach are:

Equilibrium:

Moment equilibrium. A web *band* that is bounded by two diagonal cracks inclined at angle ϕ to the longitudinal axis carries a distributed moment m, shear V^*, and axial force N^* (in contrast to a concrete *strut* which is inclined at angle θ and carries only uniaxial compression σ_2). See Fig. 2.35.

$$\tau_u = \frac{N^* x'}{b\ s\ z} + \rho_{st} f_{sy} \cot\phi + \frac{m}{b\ s \sin\phi}$$

where

$$\Delta \tau_{BND} = \frac{N^* x'}{b s z}$$

$$\Delta \tau_{INT} = \frac{m}{b s \sin \phi} = \sigma_{nt} - \sigma_{nn} \cot \phi$$

Force equilibrium: Equilibrium of the band requires that:

$$N^* \cos \phi = \tau_u b s - V^* \sin \phi$$

where

$$V^* = b s \sin \phi \left(\Delta \tau_{BND} + \Delta \tau_{INT} \right)$$

Equilibrium of a concrete band is calculated at its intersection with a stirrup (one stirrup per band; stirrup spacing is not an input, but rather an output of the calculations):

Longitudinally:

$$\sigma_2 = \frac{\tau_u}{\sin \theta \cos \theta}$$

Transversely:

$$\frac{\tan \theta}{\tan \phi} = 1 - \frac{\Delta \tau_{INT}}{\tau_u} - \frac{\Delta \tau_{BND}}{\tau_u}$$

Strains and compatibility — The strain and compatibility equations are the same as in the previous method (Dei Poli, Gambarova and Karokoç 1987).

Constitutive laws:

Concrete: The same parabolic stress-strain curve for uniaxial compression is assumed as previously (Dei Poli, Gambarova and Karakoç 1987). In addition, a linear failure envelope is assumed for concrete in biaxial tension-compression:

$$\frac{\sigma_2'}{f_c'} = \frac{\sigma_1'}{f_{ct}} - 0.85$$

This relationship is used for the concrete, which is in a state of impending failure at the tip of the cracks near the compression flange, to calculate the eccentricity of the axial compressive force in the concrete band.

Cracks: The same rough crack model is used as previously to model aggregate interlock.

$$\sigma_{nn} = 0.62 \frac{r \sqrt{\delta_n} \sigma_{nt}}{\left(1 + r^2\right)^{0.25}}$$

$$\sigma_{nt} = \tau_0 \left(1 - \sqrt{\frac{2 \delta_n}{d_a}} \right) r \frac{a_3 + a_4 |r|^3}{1 + a_4 r^4}$$

where

δ_n , δ_t = crack opening and crack slip displacements,
d_a = maximum aggregate size,
a_3 = $2.45/\tau_0$ $\quad$ a_4 = $2.44\,(1 - 4/\tau_0)$
r = δ_t/δ_n $\quad$ τ_0 = $0.25 f_c'$

Crack spacing; The crack spacing is taken as the stirrup spacing, and is given by the following:

$$s = 0.133 \frac{d_{st}}{\rho_{st}} \cot \phi$$

Bond-slip law: From chemical adhesion and mechanical interaction between the concrete and the deformed stirrups, the average stirrup strain is obtained.

Results:

- The inclination of the uniaxial compression field, θ , is significantly less than the crack inclination, ϕ, for all practical designs, but tends asymptotically to ϕ. The value of θ is affected by aggregate interlock, and at small values of shear, also by strut bending stiffness and stirrup-concrete bond.
- The diagonal compression field is a valid concept. The transverse tension in the concrete strut is negligible.
- Within the range of practical designs ($0.2 > \tau_u / f'_c > 0.1$), the contributions of stirrup-concrete bond and strut bending stiffness to shear resistance are far from negligible (from 25-50% of aggregate interlock contribution for $\varepsilon_x^* = \varepsilon_x^{sc}$ to 10-15% for $\varepsilon_x^* = 0$). The combination of bending stiffness and bond is more than additive because it improves aggregate interlock.
- Also, within the range of practical designs, the stirrups are subjected to tension-stiffening (i.e. the surrounding concrete in tension helps) and displacements along shear cracks are greatly reduced.

— *Further Refinement*

Prisco and Gambarova (1995) further refined their method by accounting for the dowel action of the longitudinal reinforcement, the non-uniform distribution of the crack displacements and the plastic strain accumulation in the stirrups where they cross shear cracks. These effects are in addition to the effects of cantilever, aggregate interlock, tension-stiffening in the stirrups and biaxial behavior in shear compression present in the previous models. The framework is that of a truss, where the strut angle is shallower than the crack angle, and which fails by ductile failure in shear based on the simultaneous yielding of the stirrups and collapse of the end sections of the inclined struts.

Dowel action varies between a strong mechanism and a weak mechanism. In the strong mechanism, the dowel bar pushes against the concrete core, while in the weak mechanism, it pushes against the concrete cover and the stirrups. The behavioral model is that of a non-linear spring, which accounts for the interaction between dowel force and tensile force in the longitudinal reinforcement, and is limited by concrete splitting or the ultimate capacity in compression, bending and shear of the bottom end section of the concrete.

Crack slip and opening are given reasonable but arbitrary formulations with no slip at the crack tip.

Local yielding of stirrups at cracks

Stirrups are assumed to exceed yield but be less than 5 % over a length equal to one bar diameter on either side of each inclined crack.

Strength of struts

A different formulation is used than in previous models. To account for the effects of transverse reinforcement in tension, the concrete strength is reduced to:

$$f_c = 0.75 f_c'$$

$$\text{or} \quad f_c = \frac{0.9 f_c'}{\sqrt{1 + 600\varepsilon_1}} \geq \frac{f_c'}{2}$$

where ε_1 is the tensile strain perpendicular to the diagonal compression field (Hsu 1993).

Computation

The model requires the iterative solution of a 17 equation non-linear system:

- Eight equilibrium equations: one for the section, two regarding bending and interlock contributions, two for the diagonal compression field, and three for the strut;
- Two compatibility equations;
- Seven constitutive equations: two for aggregate interlock, one each for solid concrete, tension stiffening in the stirrups, crack and stirrup spacing, plastic strains in the stirrups, and dowel action.

Results

28 RC and PC beams were examined. The agreement between model predictions and tests is quite good, both for normal and HSC. However, the model applies to shear sensitive beams developing a truss-like mechanism and under-estimate the shear capacity when the arch mechanism comes into play (direct strut from load to support). It should also be noted that the efffects of plastic strain in the stirrups turned out to be negligible.

For $\tau_u / f'_c > 0.22$, where τ_u is the ultimate shear stress, agreement is very good because, in this region, the truss mechanism is predominant.

For $\tau_u / f'_c \leq 0.22$, agreement is satisfactory, provided the truss mechanism prevails. As a rule, for stirrup ratios $\rho_v < 0.5$ %, the proposed model falls short of the experimental shear capacity by 30-35 %, because of the importance of the arch mechanism. However, for $\rho_v > 0.75$ %, predictions are very close to test data.

On the whole, the mean prediction of the proposed model is closer to test results (mean 89 %, standard deviation ± 12 %) than Euro-Code 2 predictions (mean 80 %, standard deviation ± 17 %) or ACI predictions (mean 62 %, standard deviation ± 9 %).

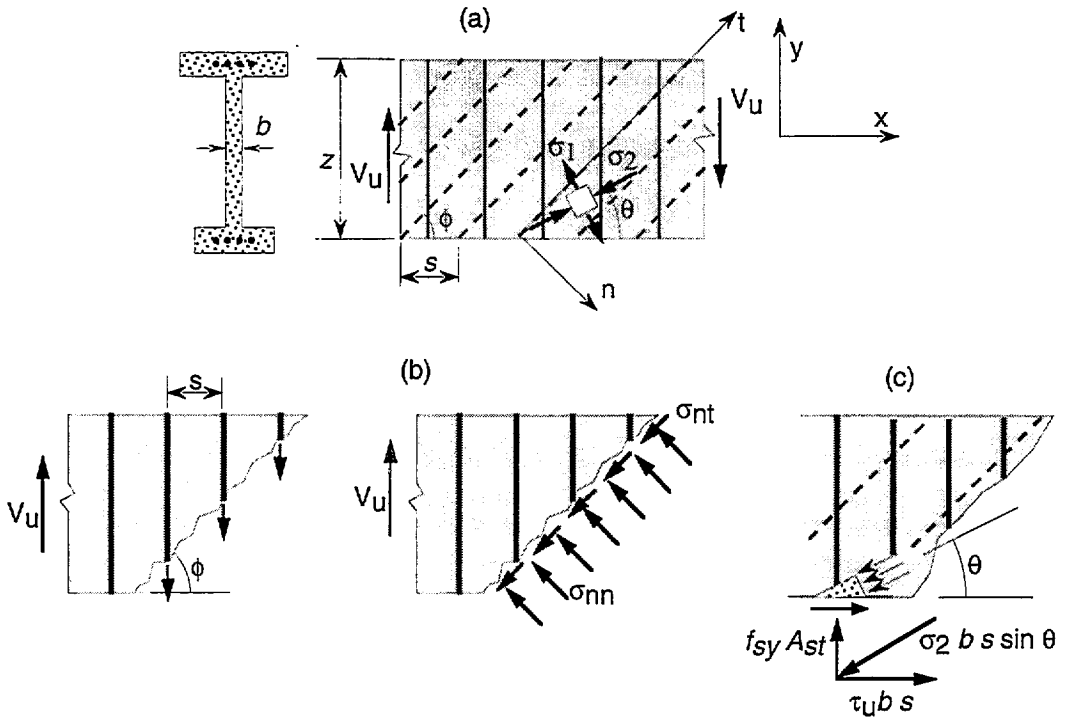

Figure 2.34 — (a) Truss analogy; (b) forces present at diagonal cracks; and (c) equilibrium at stirrup (Dei Poli et al. 1987)

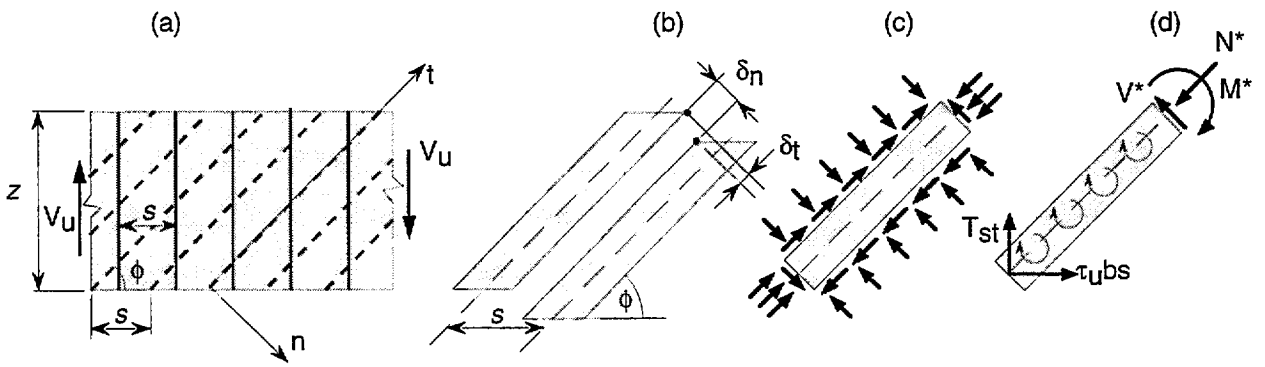

Figure 2.35 — (a) Truss analogy; (b) displacements at diagonal cracks; (c) simplified representation of band between cracks; and (d) free body diagram of band between cracks (Dei Poli et al. 1990)

2.5.4 Analysis of Reineck

Reineck (1982,1991a) presents a variation of the modified compression field theory (MCFT). The principal difference with Vecchio and Collins's MCFT is that the direction of the principal strain does not coincide with that of the compression field. Rather, the strut is at a shallower angle than the crack, whose faces transmit shear and compressive stresses. This is similar to Kupfer, Mang and Karavesyroglou (1983) and Dei Poli, Gambarova and Karakoç (1987) except that here the compression across the cracks is due to the biaxial state of stress in the web rather than a uniaxial compression field at a flatter inclination than the cracks. Rather than determining the compression field direction from an aggregate interlock consideration, Reineck and Hardjasaputra (Reineck 1989) assume that the cracks open perpendicularly to the compression field direction. Thus, the crack direction and compression field direction are characteristics of the strain field and the associated principal directions bisect the angles formed by the cracks and the compression struts. Taking the additional compressive strain in the concrete struts into account, Reineck concludes that the average principal compressive strain direction is somewhat closer to the strut direction than the crack direction. His analysis is similar to that of Kupfer et al. (1983).

Also, in contrast to the MCFT, the compressive strength of the struts is independent of the transverse tensile strain and is limited to $0.80 f_c'$. This is based on Kolleger and Mehlhorn's (1987) work. The shear friction across the cracks is of the form $\tau_f = \tau_{f0} + \mu\sigma_f$ where τ_{f0} is a cohesion term, $\mu = 1.7$ is a friction coefficient and both τ_{f0} and σ_f depend on crack opening and sliding.

In Reineck's (1991a) model, the tensile stresses occur in the concrete web due to the friction of the crack faces, which is taken into account by assuming flatter inclinations for the struts than the cracks. The dowel force of the longitudinal reinforcement is neglected for simplicity. See Fig. 2.36.

Equilibrium:

The appplied shear V is resisted by a steel component V_s and a concrete friction component V_f.

$$V = V_s + V_f$$

$$V_s = \frac{A_{sw}}{s_w}\sigma_{sw} z \cot\beta$$

$$V_f = b_w z\left[\tau_{f0} + \tau_{f\sigma}\left(1 - \frac{\cot\beta}{\mu}\right)\right]$$

$$\tau_f = \tau_{f0} + \tau_{f\sigma} = \tau_{f0} + \mu\sigma_f$$

$$\mu = \cot\psi = 1.7$$

where A_{sw} = area of web reinforcement,
s_w = spacing of web reinforcement,
z = distance between tension and compression chords,
β = crack angle,
μ = concrete - concrete friction coefficient,
ψ = friction angle ($\mu = \cot\psi$),
σ_f = compressive stress normal to crack face,
σ_{sw} = stress in web reinforcement,
τ_f = shear friction across cracks,
τ_{f0} = cohesion term of friction,

$\tau_{f\sigma}$ = friction term proportional to normal stress.

τ_f depends on the crack displacements. The rather high value of μ comes from Walraven's work (1981).

The truss action shown in Fig. 2.37 develops from the stirrups and the uniaxial compression field between the cracks. From equilibrium:

$$C_\eta = \frac{A_{sw}}{s_w}\sigma_{sw}\frac{s_{cr}}{\sin\beta}$$

or

$$\frac{\sigma_\eta}{f_c} = -\frac{\omega_w}{\sin^2\beta}\frac{\sigma_{sw}}{f_{sy}}$$

$$\sigma_\xi = \tau_{\xi\eta} = 0$$

where s_{cr} = crack spacing,

C_η, σ_η = strut compressive force and stress,

f_{sy} = yield strength of web reinforcement,

ω_w = web reinforcement ratio

$$\omega_w = \frac{A_{sw} f_{sy}}{b\, s_w f_c'}$$

The stress fields due to friction (Fig. 2.38) are considered separately. The shear stress τ_f results in a biaxial tension-compression field with the compression field inclined at $\beta/2$ to the longitudinal axis. The superposition of a normal stress σ_f, normal to the crack faces, results in a biaxial stress field.

<u>τ_f stress field</u> (Fig. 2.38a) :

$$\sigma_\xi = 0 \qquad \sigma_\eta = \frac{2\tau_f}{\tan\beta} \qquad \tau_{\xi\eta} = \tau_f$$

<u>σ_f stress field</u> (Fig 2.38b) :

$$\sigma_\xi = \sigma_f = \frac{\tau_{f\sigma}}{\mu} \qquad \sigma_\eta = \tau_{f\sigma}\frac{\cot^2\beta}{\mu} \qquad \tau_{\xi\eta} = 0$$

<u>Superimposed stress field</u> (Fig 2.38c):

The principal stresses σ_1 and σ_2 are oriented at :

$$\tan\phi_1 = \frac{\tau_{\xi\eta}}{\sigma_1 - \sigma_\eta}$$

The resultant stress field in the web (Figs. 2.37 and 2.38) shows a principal compression at an angle shallower than the crack angle. This state of stress results in the two load paths that Schlaich et al. (1987) referred to: the well-known truss model formed by a concrete uniaxial compression field and the stirrups (Fig. 2.44a) and a truss model with concrete tensile ties (Fig. 2.44b).

Reineck shows that the "shear friction" theory leading to the concrete term V_c (or V_f here) is statically equivalent to the truss analogy. In the truss analogy the discrete cracks are not modelled. However, one must examine them in order to calculate the tensile stress in the web which only depends on the friction stresses along the crack. Reineck's model shows a clear transition from

transversely unreinforced to transversely reinforced members and is therefore a consistent treatment of both member types (see also Reineck 1991b,c).

Compatibility

The complete state of strain of a beam element in a B-region (see § 2.6.2) is :

- longitudinal strain in the middle of the web:

$$\varepsilon_x = \frac{\varepsilon_s - \varepsilon_c}{2}$$

- curvature:

$$\bar{\kappa} = \kappa z = \frac{\varepsilon_s + \varepsilon_c}{2}$$

- vertical strain = stirrup strain:

$$\varepsilon_z = \varepsilon_{sw}$$

- shear strain :

$$\gamma_{xz} = \frac{\varepsilon_x}{\tan\beta} + \frac{\varepsilon_{cw}}{\sin\beta\cos\beta} + \varepsilon_{sw}\tan\beta$$

where ε_s and ε_c are the strains (both positive) in the tensile (steel) and compressive (concrete) chords and ε_{sw} is the stirrup strain.

The crack width n and the crack slip s in the middle of the web are:

$$\frac{\Delta n}{s_{cr}} = (\varepsilon_x + \varepsilon_{sw} + \varepsilon_{cw})\sin\beta + \bar{\kappa}\frac{s_{cr}}{z}\cos\beta$$

$$\frac{\Delta s}{s_{cr}} = -\varepsilon_x\cos\beta + (\varepsilon_{sw} + \varepsilon_{cw})\frac{\sin^2\beta}{\cos\beta} + \bar{\kappa}\frac{s_{cr}}{z}\sin\beta - 2.4\frac{\tau_f}{E_c}\sin\beta$$

Stress-strain relationships

The concrete struts behave elastically:

$$\varepsilon_{cw} = \varepsilon_\eta = \frac{\sigma_\eta - 0.2\sigma_\xi}{E_c}$$

The strength of the struts is not lower than

$$f_{cw} = 0.80 f_c'$$

The constitutive equations for the friction of the crack faces are derived by Walraven (1981):

$$\frac{\tau_f}{f_c'} = \frac{\tau_o}{f_c'}\,\frac{\Delta s - 0.24\,\Delta n}{0.096\,\Delta n + 0.01} \qquad \text{MPa, mm}$$

The cohesion friction stress τ_o is the limiting value without normal stresses σ_f on the crack face:

$$\frac{\tau_o}{f_c'} = 0.45\,\frac{f_{ct}}{f_c'}\left(1 - \frac{\Delta n}{0.9}\right) \qquad \text{MPa, mm}$$

where f_{ct} = concrete tensile strength. This is much lower than that given by Vecchio and Collins (1986) and by Bhide and Collins (1986).

With these formulations the whole response of the B-region in a member may be determined from cracking until failure. Comparison with experimental results shows that the calculated values are very conservative because the tension stiffening effect is not considered for the stirrup strains.

2.5.5 " Fixed Angle" Model

Pang and Hsu (1996) assume that shear cracks are parallel to the principal direction of compressive stress *defined by the applied loads* (the so-called fixed angle). This would only be true in webs or shear walls with equal reinforcement in the longitudinal and transverse directions. Most practical situations are, however, anisotropic. Shear cracks form in the direction of the principal strains in the concrete (the so-called rotating angle) rather than the principal direction of applied stress.

The motivation of Pang and Hsu's (1996) paper was to derive a concrete contribution to shear resistance. For this purpose, Pang and Hsu had to derive constitutive laws for shear in reinforced concrete membranes from panel tests. Based on their model, they concluded that the concrete contribution to shear resistance was caused primarily by the shear stress and secondly by the tensile stress of concrete. If cracks were assumed to occur at the "rotating angle", then the shear stress contribution disappeared.

2.5.6 "Rotating Angle" Model

The re-orientattion of the principal strain direction is well observed in a sequence of pictures of panel tests (Fig. 2.39) performed by Bhide and Collins (1987). The panel, which was reinforced in the x-direction only, was subjected to tensile stresses in the x-direction and shear stresses. Initially, cracks formed in a direction normal to the principal tensile stresses in the concrete (Fig. 2.39a). Upon increased loading, the tips of the cracks turned into a new direction, the original cracks become smaller and new cracks opened. When the ultimate strength of the panel was reached (Fig. 2.39c), the original cracks were closed and the failure of the panel was governed by uncontrolled opening of the new cracks. During the course of the test, the principal tensile strain direction rotated from 30° to 74°.

			Rotating Cracks		Fixed Cracks
Panel	Axial / Shear Load Ratio	Experiment	Weak Dowel Action	Strong Dowel Action	Weak Dowel Action
PB 29	2.02	1.49 MPa	1.34 MPa	1.78 MPa	3.47 MPa
PB 30	2.96	1.48 MPa	1.22 MPa	1.60 MPa	2.78 MPa
PB 31	5.78	1.15 MPa	1.02 MPa	1.22 MPa	1.64 MPa

Table 2.1 Comparison of experimental and analytical failure shear stresses (experimental results from Bhide and Collins 1987)

Kollegger and Mehlhorn (1990) showed that the rotating crack model was capable of reproducing the actual behavior fairly well (Table 2.1), whereas the fixed-crack model considerably overestimated the experimental failure loads. In the fixed crack as well as in the rotating crack models the first crack

forms in the direction normal to the principal stress in concrete when the tensile strength is exceeded. While this direction remains constant for the fixed crack model, the principal tensile strain direction may change in each iteration step for the rotating crack model. Dowel action of the reinforcement was modelled with a bar fixed at both ends, subjected to an axial force, and with an effective length of 20 mm (strong action) or 40 mm (weak action).

In the modified compression field theory the changing crack inclination is considered, since the crack direction depends on the strains, which vary with the load level (Adebar and Collins 1996).

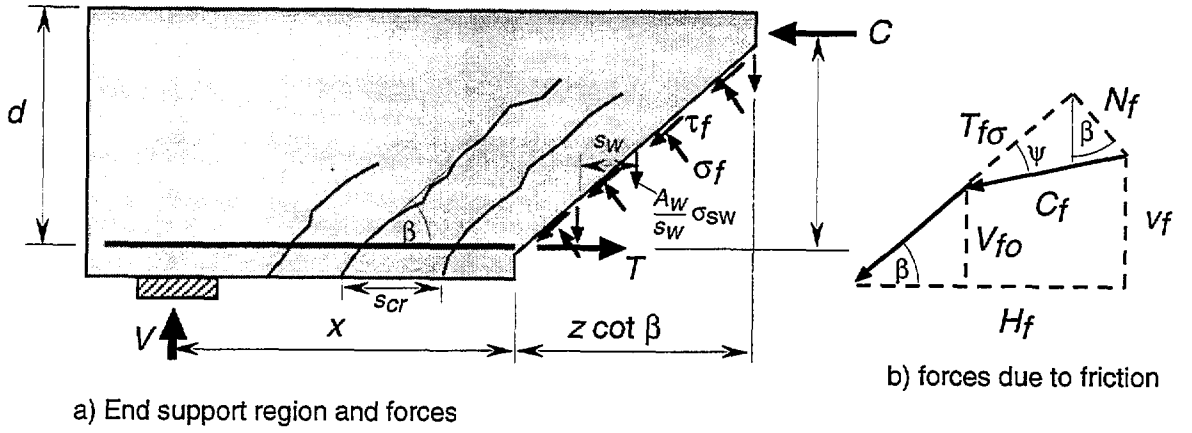

Fig. 2.36 Free-body diagram of end support region of beam (adapted from Reineck 1991a)

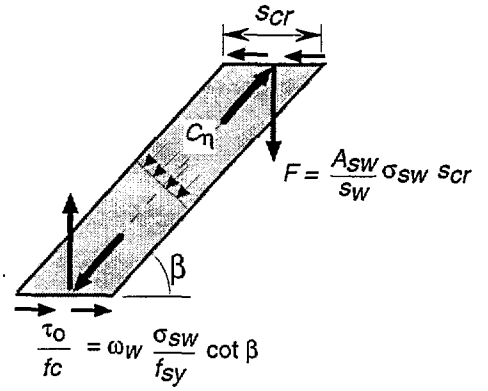

Figure 2.37 — Forces and concrete stress in strut between cracks due to truss action (adapted from Reineck 1991a)

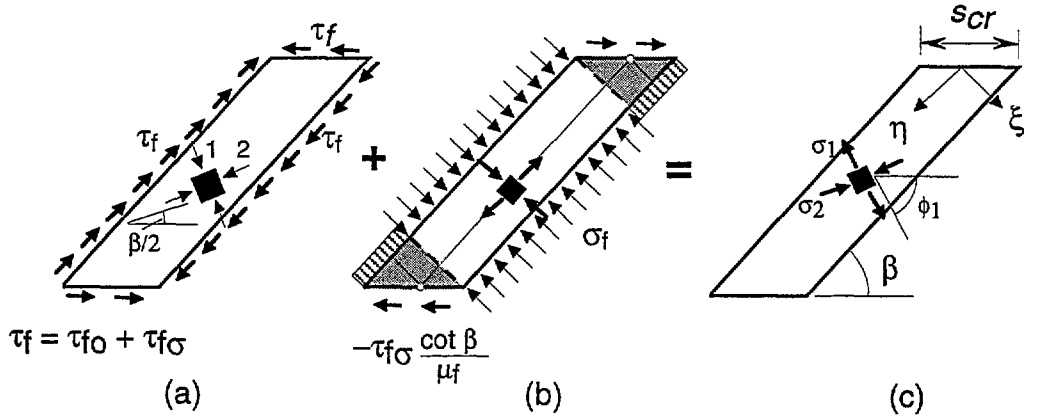

Figure 2.38 — Stresses in strut between cracks due to friction (adapted from Reineck 1991a)

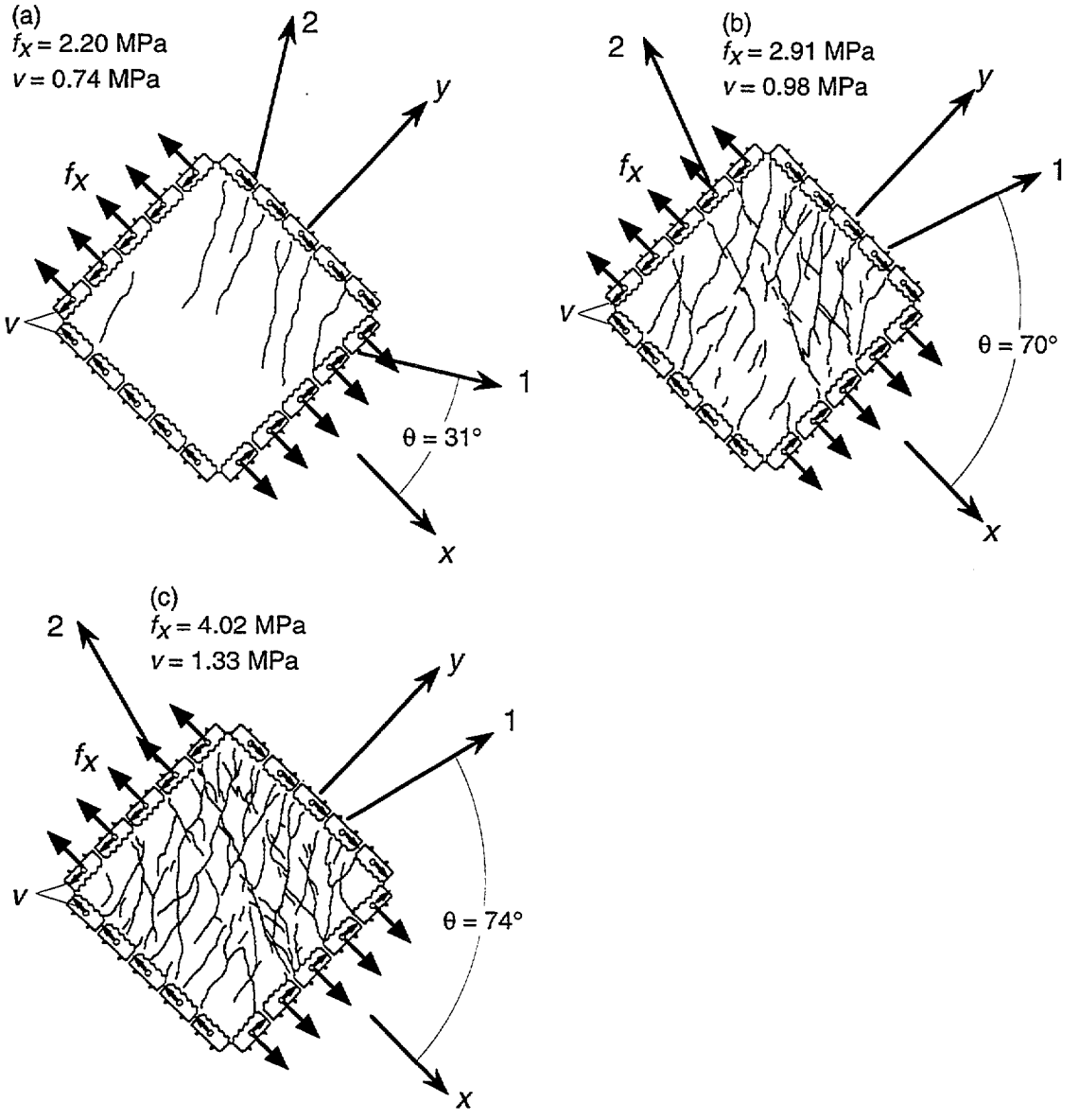

Fig. 2.39 Shift of principal strain direction in panel test of Bhide and Collins (adapted from Kolleger and Mehlhorn 1990)

2.6 Equilibrium Methods

2.6.1 Equilibrium Trusses

Due to their historical importance, relevance to present day codes, and usefulness in design, other theories are presented here. They satisfy equilibrium and are sometimes referred to as "equilibrium trusses" (Hsu 1993).

45 ° Truss Model — Ritter in 1899 and Mörsch in 1902 developed a reinforced concrete shear model that neglected the tensile stresses in the cracked concrete and assumed that the diagonal compression stress would remain at 45° after the concrete cracked (Fig. 2.40).

Equilibrium: The equilibrium equations (Eq. 2.43) for the compression field theory are specialized for $\theta = 45°$. Assuming a uniform distribution of shear in the web, the vertical component of the diagonal compression field must balance the applied shear:

$$f_2 = \frac{2V}{b_w j d}$$

The horizontal component of the diagonal compressive force is balanced by tension in the longitudinal reinforcement.

$$N_v = V$$

The diagonal compression force has a vertical component that must be balanced by the tension in the stirrups. From Eq. 2.44:

$$\frac{A_v f_v}{s} = \frac{V}{j d}$$

If the stirrups are assumed to yield, $f_v = f_y$, this last equation reduces to:

$$\frac{A_v f_y}{b s f_c'} = \frac{V}{b j d f_c'}$$

or

$$\mu_s \frac{f_y}{f_c'} = \frac{\tau}{f_c'}$$

which is represented by the Mörsch-Ritter straight line in Figs. 2.31 and 2.33.

Variable Angle Truss Model — The variable angle truss model is a refinement of the previous model and accounts for θ being typically less than 45°. The equilibrium equations are the same as for the compression field theory (see Section 2.4.1 and Fig. 2.15). Strain compatibility and concrete tensile stresses are ignored. If the reinforcement or the concrete reach their "yield" strength, the variable angle truss model is the same as the lower bound solution of the theory of plasticity mentioned earlier.

Modified Truss Model — Ramirez and Breen (1991) proposed a variable angle truss model with a concrete contribution term:

$$v_{MTM} = v_s + v_c$$

where v_{MTM} is the shear stress capacity of the Modified Truss Model.

The steel contribution v_s derives from a variable angle truss:

$$v_s = \frac{A_v}{b_w s} f_y \cot\alpha = r f_y \cot\alpha$$

where

α = inclination of truss model diagonals at failure,
A_v = area of transverse reinforcement,
b_w = web width,
f_y = specified yield strength of reinforcement,
r = transverse reinforcement ratio, and
s = stirrup spacing measured parallel to beam axis.

The concrete contribution v_c varies with the intensity of applied shear v, but is independent of α:

uncracked state:	$v_c = 2\sqrt{f_c'}$	for	$v \le 2\sqrt{f_c'}$		(psi)
	$v_c = 0.17\sqrt{f_c'}$	for	$v \le 0.17\sqrt{f_c'}$		(MPa)
transition state:	$v_c = (6\sqrt{f_c'} - v)/2$	for	$2\sqrt{f_c'} \le v \le 6\sqrt{f_c'}$		(psi)
	$v_c = (\sqrt{f_c'}/2 - v)/2$	for	$0.17\sqrt{f_c'} \le v \le \sqrt{f_c'}/2$		(MPa)
full truss state:	$v_c = 0$	for	$6\sqrt{f_c'} < v$		(psi)
	$v_c = 0$	for	$\sqrt{f_c'}/2 < v$		(MPa)

The strut angle must be within the limits $30° \le \alpha \le 65°$.
To prevent the concrete struts from crushing, the compression is limited by:

$$f_d = \frac{v}{\sin\alpha \cos\alpha} \le 30\sqrt{f_c'} \text{ psi} \quad (2.5\sqrt{f_c'} \text{ MPa})$$

The horizontal component H_u of the diagonal compression requires additional longitudinal reinforcement:

$$H_u = V_u \tan\alpha$$

where V_u is the factored shear force at the section. The horizontal force is distributed equally to the top and bottom chords. Thus, the required tension chord force becomes:

$$\phi_v A_{st} f_y \ge \frac{M_{umax}}{z} \ge \frac{M_u}{z} + \frac{H_u}{2}$$

where

ϕ_v = capacity reduction factor for shear,
A_{st} = area of longitudinal reinforcement,
M_u = factored moment in member due to factored loads, and
M_{umax} = maximum factored moment in member due to factored loads.

Comparison with ACI

The limiting compressive stress of $30\sqrt{f'_c}$ psi ($2.5\sqrt{f'_c}$ MPa) and the lower angle limit of 30° results in a maximum shear stress of $13\sqrt{f'_c}$ psi ($1.08\sqrt{f'_c}$ MPa). In terms of $V/(b_w d)$ with $d = z/0.9$, where d is the distance from the extreme compression fiber to the centroid of the longitudinal steel and z is the effective truss depth, this corresponds to $v_{max} = 11.7\sqrt{f'_c}$ psi ($0.972\sqrt{f'_c}$ MPa).

The current ACI shear provisions for members subjected to shear and flexure only limit the maximum shear stress to:

$$v_{max} = v_c(\max) + v_s(\max) = 2\sqrt{f'_c} + 8\sqrt{f'_c} = 10\sqrt{f'_c} \quad \text{(psi)}$$

$$v_{max} = v_c(\max) + v_s(\max) = 0.17\sqrt{f'_c} + 0.66\sqrt{f'_c} = 0.83\sqrt{f'_c} \quad \text{(MPa)}$$

In practical situations, with $v_c = 2\sqrt{f'_c}$ psi ($0.17\sqrt{f'_c}$ MPa), the proposed upper limit would allow the use of larger amounts of shear reinforcement, and hence somewhat smaller members.

rf_y psi (MPa)	n	test / model	mean	max.	min.	stand. dev.
0 - 50 (0-0.34)	10	test/MTM	1.35	1.61	1.08	0.227
		test/ACI	1.25	1.52	0.99	0.215
50 - 100 (0.34-0.69)	17	test/MTM	1.515	1.92	1.11	0.25
		test/ACI	1.45	1.92	1.04	0.247
100 - 200 (0.69-1.38)	3	test/MTM	1.87	2.25	1.33	0.48
		test/ACI	1.83	2.17	1.32	0.45
200 - 300 (1.38-2.07)	13	test/MTM	1.62	2.05	1.24	0.26
		test/ACI	1.64	2.00	1.32	0.23
300 - 400 (2.07-2.76)	4	test/MTM	1.13	1.19	0.99	0.094
		test/ACI	1.23	1.39	1.09	0.223
400 - 500 (2.76-3.45)	11	test/MTM	1.11	1.34	0.94	0.146
		test/ACI	1.29	1.52	1.10	0.156
500 - 600 (3.45-4.14)	1	test/MTM	1.09	—	—	—
		test/ACI	1.35	—	—	—

n = number of specimens. All 59 specimens are reinforced concrete beams with $a/d > 2.0$.
Overall statistics: mean = 1.42, standard deviation = 0.32, 95% confidence = 0.081.
ACI shear strength calculated with $v_c = 2\sqrt{f'_c}$ psi ($0.17\sqrt{f'_c}$ MPa). MTM assumes $\alpha = 30°$.

Table 2.2 Comparison between ACI and Modified Truss Model (MTM) predicted strengths

In comparing results of tests of 59 RC and 77 PC beams versus ACI design provisions or the proposed modified truss model (Table 2.2), one notes that:

- for $rf_y \leq 200$ psi (1.4 MPa), the modified truss model with $\alpha = 30°$ is slightly more conservative than ACI;
- for $200 < rf_y \leq 300$ psi ($1.4 < rf_y \leq 2.1$ MPa), the two procedures yield similar results; and
- for $300 < rf_y \leq 500$ psi ($2.1 < rf_y \leq 3.4$ MPa), the modified truss model yields better estimates than ACI does.

2.6.2 Strut-and-Tie Model (STM)

The strut and tie model is strictly an equilibrium model and is based on the lower bound theorem of the plasticity theory. In other words, there may exist other load paths which could carry a greater load. The designer must identify at least one load path and ensure that no part of it is over-stressed. If the designer can find, between the various elements of a member, an assumed distribution of load which satisfies equilibrium everywhere, and the stresses are at or below the material strength, the actual strength of the member will be at least as great as the calculated strength. This further assumes that material selection and detailing are adequate to ensure that yielding can occur without premature failure by over-straining, brittle fracture, or loss of anchorage.

The term "strut and tie" is reserved for *disturbed* or D-regions and the term "truss" is used for *beam* or B-regions, although both terms designate an assemblage of pin-jointed, uniaxially stressed compression or tension members. In B-regions, *b*eam behavior is expected, i.e., plane sections remain plane[1] and a uniform compression field can be found in response to shearing loads. In D-regions, complex load paths emanate from concentrated loads, converge towards supports, or flow around openings. Arch action, as opposed to beam action, is exhibited. As far as shear is concerned, the difference in behavior of the two regions can be expressed conveniently as follows (Park and Paulay 1975, MacGregor 1992, Fig. 2.41):

$$V = \frac{dM}{dx} = \frac{d}{dx}(T\,Z) = Z\,\frac{dT}{dx} + T\,\frac{dZ}{dx}$$

In B-regions, the lever arm remains constant and the tension force adjusts to provide the internal moment:

$$\frac{dZ}{dx} = 0 \quad \text{and} \quad V = Z\,\frac{dT}{dx}$$

The quantity dT/dx is the shear flow (shear stress multiplied by beam width) across any horizontal plane between the reinforcement and the compression zone and is typical of beam behavior.

In D-regions, the tension force remains constant and the lever arm adjusts to provide the internal moment:

$$\frac{dT}{dx} = 0 \quad \text{and} \quad V = T\,\frac{dZ}{dx}$$

This behavior is characteristic of arch action. This happens, for example, near the ends of a beam,

---

[1]B can also stand for Bernoulli in reference to Daniel Bernoulli, an eighteenth century Swiss mathematician associated with the hypothesis that plane sections remain plane under bending.

where shear flow is prevented by inclined cracks extending from the loads to the reactions.

Strut and tie or truss models provide a consistent design approach for B- and D-regions. For example, the same kind of model can be used to calculate tensile splitting reinforcement for short beams (D) or shear reinforcement for slender beams (B). If the level of accuracy and simplicity used in the design of D-regions were considered satisfactory for B-regions, the "endless discussion on shear can be put to bed" (Schlaich, Schäfer and Jennewein 1987). Although the models are consistent, the behaviors of short (or deep) beams and slender beams are different and it is important to account for arching action where it exists (Fig. 2.42). As the slenderness (shear span to depth) ratios for beams decreases, the role of web reinforcement changes from that of carrying primarily direct tension to that of serving primarily as shear friction reinforcement, preventing a sliding failure along the inclined crack. Figure 2.43 illustrates the different predictions from the truss model (or sectional model) and the strut-and-tie model for various shear span to depth ratios.

Strut-and-tie models are discrete representations of statically equivalent distributed stress fields, i.e., they condense the real stress fields by resultant straight lines and concentrate the curvature of the stress fields in nodes. The elastic stress fields serve as a guide in defining the geometry of the strut-and-tie model. Upon cracking of the concrete, a certain amount of stress redistribution occurs, limited by the plastic deformation capacity of the concrete (ductility requirement). It is therefore especially important in highly stressed regions to orient the strut-and-tie model along the internal forces predicted by the theory of elasticity. In less stressed regions, significant deviations from elasticity can be accommodated without exceeding the ductility of the structure. The selection of the appropriate truss is more important than the selection of a value for ν, the efficiency factor of concrete ($f_c = \nu f'_c$. See Section 2.2). This is because beams are typically under-reinforced and much of the flexural steel yields before the concrete fails in compression. Thus the actual failure strength of concrete is not nearly as significant as the correct determination of which steel yields.

Schlaich, Schäfer and Jennewein (1987) suggest two guides in selecting a workable strut-and-tie model:

1) The compatibility of deformations may be approximately considered by orienting the struts and ties within 15° of the force systems obtained from a linear elastic analysis of uncracked members and connections.
2) The most valid model tends to be the one that minimizes the amount of reinforcement since this corresponds to the minimum strain energy solution.

Marti (1985) recommends three rules in the use of strut-and-tie models:

1) Draw truss models to scale.
2) Visualize the force flow using consistent equilibrium considerations.
3) Ensure that truss member forces can be developed and transferred at the required locations.

Nodal Zones — The last rule needs emphasizing. Indeed, the nodes require special care, in particular, the angle between a strut and a tie entering a node should not be too small. The multi-axial state of stress in the nodes requires that different values of concrete strength be allowed. For example, the Canadian Code (CSA 1994) recommends:

For a compression-compression node (intersection of struts): $f_c = 0.85\,\Phi f'_c$
For a compression-tension node (intersection of strut and tie): $f_c = 0.75\,\Phi f'_c$
For a tension-tension node (intersection of ties): $f_c = 0.60\,\Phi f'_c$

where $\Phi = 0.70$ is a material resistance factor.

On the other hand, Schlaich et al. (1987) , Mac Gregor (1988) and Bergmeister et al. (Yun and Ramirez 1996) proposed values of effective stress levels of nodal zones listed in Table 2.3:

Effective stress level (MPa)	Nodes	Proposed by
$0.85f'_c$	Compression-compression-compression nodes	Schlaich et al. (1987)
$0.68f'_c$	Nodes where reinforcement is anchored in or crossing the node	
$0.85f'_c$	Nodes bounded by compressive struts and bearing areas	Mac Gregor (1988)
$0.65f'_c$	Nodes anchoring one tension tie	
$0.50f'_c$	Nodes anchoring tension ties in more than one direction	
$0.80f'_c$ for $f'_c \le 27.6$	Unconfined nodes without bearing plates	Bergmeister et al.
$(0.9 - 0.25f'_c/69)f'_c$ for $27.6 \le f'_c \le 69$		
$0.65f'_c$ for $f'_c \ge 69$		
$\nu f'_c (A/A_b)^{0.5} + \alpha (A_{core}/A_b) f_{lat} (1 - s/d)^2$	Confined nodes	
$\nu f'_c (A/A_b)^{0.5}$	Unconfined nodes without bearing plates	
$2.5f'_c$	Tri-axially confined nodes	

A, A_b, and A_{core} = area of confined concrete, bearing plate, and confined strut, respectively; f_{lat} = lateral pressure = $2f_y A_s/(ds)$ for $f'_c < 48.3$ MPa ; or $2f_s A_s/(ds)$ for $f'_c > 48.3$ MPa ; s = pitch or spacing of confining reinforcement; d = diameter of confined core; $\nu = 0.5 + 1.25/\sqrt{f'_c}$ α = 4.0 for spiral confinement, 2.0 for square closed hoop confinement anchored with longitudinal reinforcement, and 1.0 for square closed hoop confinement without longitudinal reinforcement anchorage.

Table 2.3 Effective Stress Levels in Nodal Zones (Yun and Ramirez 1996)

Based on test results of isolated 10 CCT and 9 CTT nodes (C = Compression and T = Tension), Jirsa et al. (Yun and Ramirez 1996) concluded that, if the effective concrete strut stress is limited to $0.8f'_c$, all predictions of nodal zones experiencing concrete failure were conservative. Adebar and Zhou (Yun and Ramirez 1996) limit the maximum bearing stress in deep members without sufficient reinforcement to:

$$f_c \le 0.6f'_c(1 + 2\alpha\beta) \le 1.8f'_c$$

where $\alpha = 0.33(\sqrt{A_2/A_1} - 1) \le 1.0$

$\beta = 0.33(h/b - 1) \le 1.0$

and $h/b > 1.0$

h/b is the height / width ratio of the struts, α accounts tor the amount of confinement and β accounts for the geometry of the compression stress field. A_1 and A_2 represent the loaded area and the supporting area respectively. If f'_c is significantly greater than 34.5 MPa, the bearing stress limit is

$$f_c \leq 0.6f'_c + 6\sqrt{f'_c}\,\alpha\beta \quad \text{MPa}$$

Struts:

Effective stress (MPa)	Concrete struts	Proposed by
$0.85f'_c$	Undisturbed and uniaxial state of compressive stress that may exist for prismatic struts.	Schlaich et al. (1987)
$0.68f'_c$	Tensile strains and/or reinforcement perpendicular to the axis of the strut may cause cracking parallel to the strut with normal crack width.	
$0.51f'_c$	Tensile strains causing skew cracks and/or reinforcement at skew angles to the strut axis.	
$0.34f'_c$	For skew cracks with extraordinary crack width. Skew cracks would be expected if strut-tie model departs significantly from the flow of internal forces predicted by the theory of elasticity.	
$0.50f'_c$	Isolated compression struts in deep beams or D-regions.	Mac Gregor (1988)
$0.25f'_c$	Severely cracked webs of slender beams with strut angle of 30°.	
$0.45f'_c$	Severely cracked webs of slender beams with strut angle of 45°.	
$0.85f'_c$	Moderately confined diagonal struts going directly from point load to support with shear span to depth ratio less than 2.0.	Alshegeir
$0.75f'_c$	Struts forming arch mechanism.	
$0.50f'_c$	Arch members in prestressed beams and fan compression members.	
$0.95f'_c$	Undisturbed and highly stressed compression struts.	

Table 2.4 Effective Stress Level in Concrete Struts (Yun and Ramirez 1996)

According to CSA 1994, concrete stress in struts must not exceed the crushing strength of cracked concrete, f_{2max}, given by:

$$f_{2max} = \frac{f'_c}{0.8 + 170\,\varepsilon_1} \leq 0.85\,f'_c$$

The principal tensile strain ε_1 depends on the strain condition of the concrete and the reinforcement

in the vicinity of the strut.

$$\varepsilon_1 = \varepsilon_s + (\varepsilon_s + 0.002)\cot^2\theta_s$$

where θ_s is the smallest angle between the compressive strut and the adjoining tensile ties and ε_s is the tensile strain in the tensile tie inclined at θ_s to the compressive strut. As θ_s decreases, ε_1 increases and f_{2max} decreases. In other words, a strut cannot be placed directly on top of a tie. This is the reason for the rapid drop in shear strength predicted by the STM for $a/d > 2.5$ in Fig. 2.43.

However, the allowable stress in struts is not always thought of as a function of the principal tensile strain ε_1 . Yun and Ramirez (1996) reviewed the effective stress levels allowed in concrete struts Table 2.4). Ramirez and Breen (1991) suggested 2.82 $\sqrt{f'_c}$ (MPa) as an estimate of the maximum diagonal compressive stress for beams and beam-type regions. Marti (1985) suggested an average value of effective stress level equal to $0.6f'_c$ for all types of struts and nodes. Bergmeister et al. (Yun and Ramirez 1996) proposed the following equation for the effective stress level of concrete struts:

$$f_c = \left(0.5 + \frac{1.25}{\sqrt{f'_c}}\right) f'_c \quad \text{for} \quad 20 < f'_c < 80 \quad \text{MPa}$$

Beam Shear — Truss models have formed the basis for beam shear design since the turn of the century, as mentioned earlier. The plasticity model and the modified compression field theory are truss models. What follows is a qualitative discussion adapted from Schlaich, Schäfer and Jennewein 1987 and consistent with what was presented earlier, that adds further insight into the shear behavior of beams

Fig. 2.44 shows a beam under shear loading. The web cracks after the principal tensile stress reaches the tensile strength of the concrete. Individual pieces of the cracked web tend to fall down, but are restrained by the stirrups. The compression C_c in the concrete strut is balanced by the tension T_s in the stirrups and additional tension in the longitudinal reinforcement. This is the principal load path 1 which disregards concrete tensile strength (Fig. 2.44a). In addition there exists load path 2 which takes into account concrete tension and aggregate interlock (Fig. 2.44b).

The relative movement of two pieces of web separated by a crack has two components (Fig. 2.44c): one perpendicular to the crack (opening) and one parallel to it (sliding). The sliding is resisted by force R parallel to the crack and due to aggregate interlock. The force R has two components: a concrete compression C_c with inclination $\theta < \phi$ (ϕ = crack angle) and a concrete tension T perpendicular to C_c (Fig. 2.44d). The chords (longitudinal reinforcement) are activated for equilibrium.

The concrete tension perpendicular to the strut alleviates the tension in the stirrups, which are required to carry only part of the shear load. Fig. 2.45 shows that the strut-and-tie model and the truss model require less shear reinforcement than the plasticity method, which neglects concrete tension. However, the tension also causes the concrete of the strut to be biaxially loaded, thus reducing its compressive strength. Also, in strut-and-tie models used in practice of members with transverse reinforcement, load path 2 is usually neglected.

Load path 2 (Fig. 2.44b) disappears when $\theta = \phi$. When this occurs, the concrete struts are loaded uniaxially and can then develop their maximum strength. Therefore, the maximum shear capacity of beams is achieved if the struts are parallel to the cracks and the required amounts of transverse and longitudinal reinforcements are provided.

The above discussion agrees, then, with the modified compression field theory and is also

confirmed by Dei Poli et al. (1987), who found that, as the shear strength increases, the strut angle approaches the crack angle.

The applicability of the strut-and-tie model is limited to small values of the shear span-to-depth ratio, *a/d* (Fig. 2.43). For large *a/d*, shear failure is related to concrete tensile strength and aggregate interlock, whereas practical strut and tie models only consider concrete in compression.

2.7 Summary

Great progress has been achieved since Mörsch's 45° truss, particularly in the last 20 years. The solution of shear problems in beams (B-regions) has achieved a remarkable level of rationality. For D-regions, strut-and-tie models provide designs which are rational and consistent with B-regions.

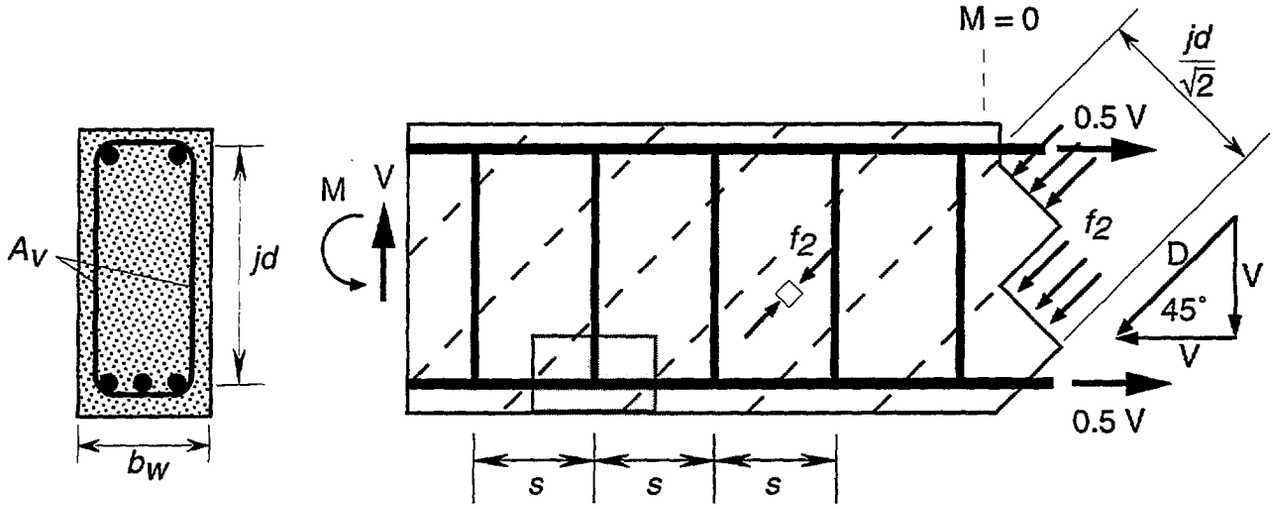

(a) Diagonal stresses and longitudinal equilibrium

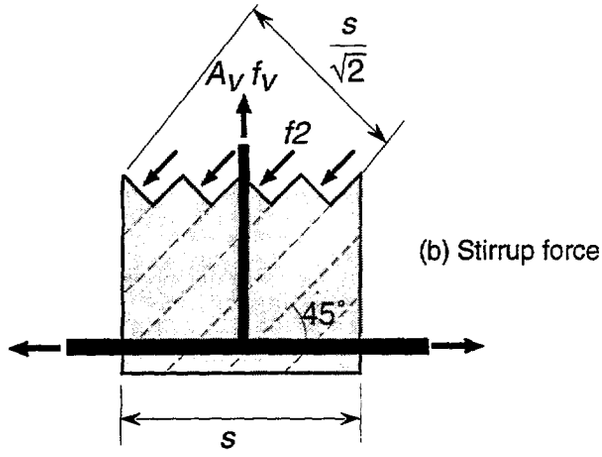

(b) Stirrup force

Figure 2.40 — Equilibrium condition for 45° truss model (Collins and Mitchell 1991).

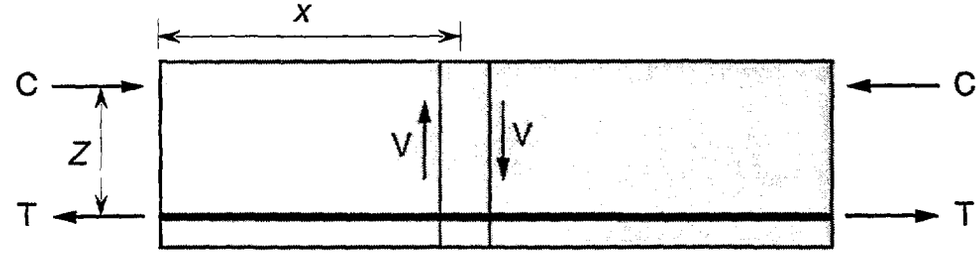

Figure 2.41 — Shear in a beam

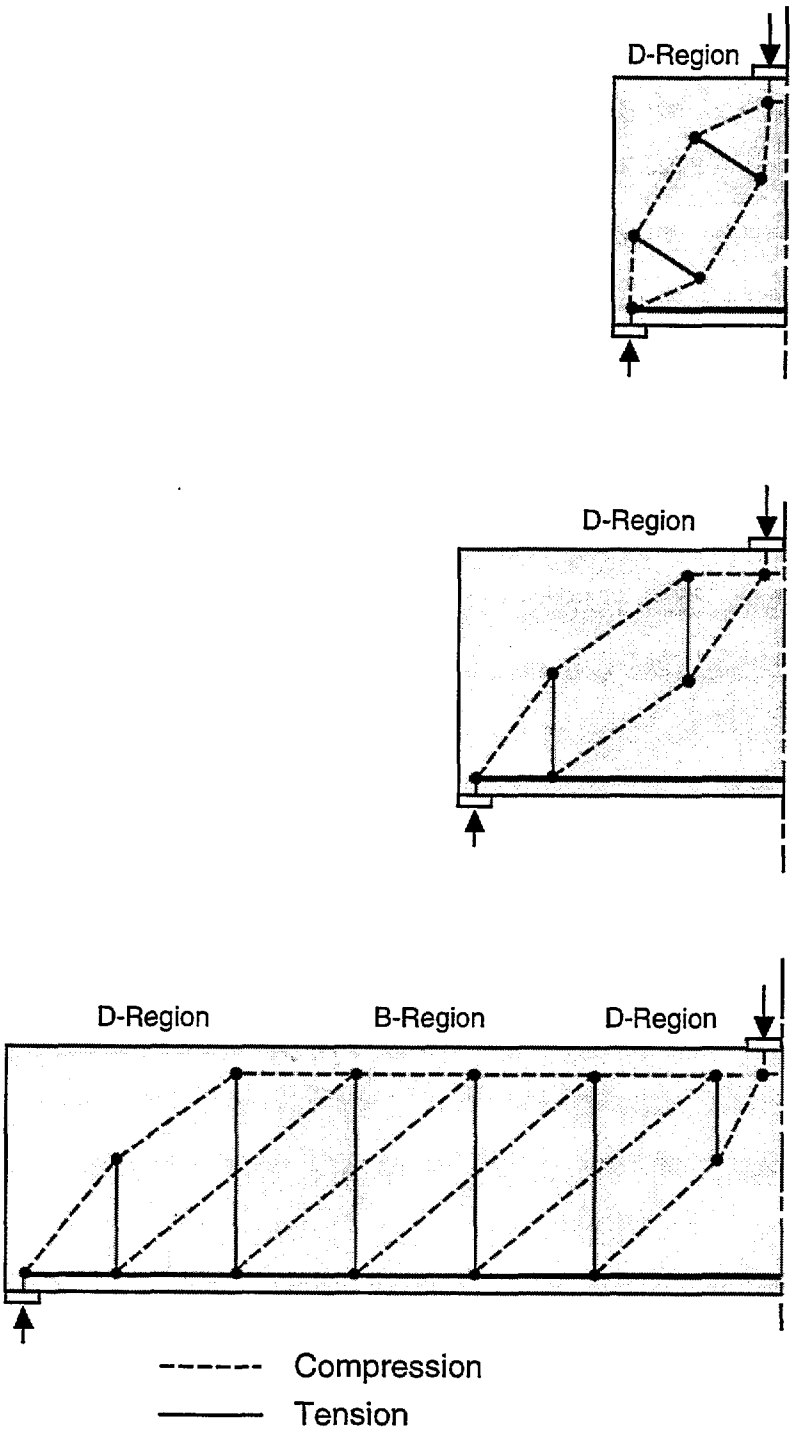

Figure 2.42 — Strut-and-tie models of beams with increasing shear-span-to-depth ratios (adapted from Schlaich et al. 1987).

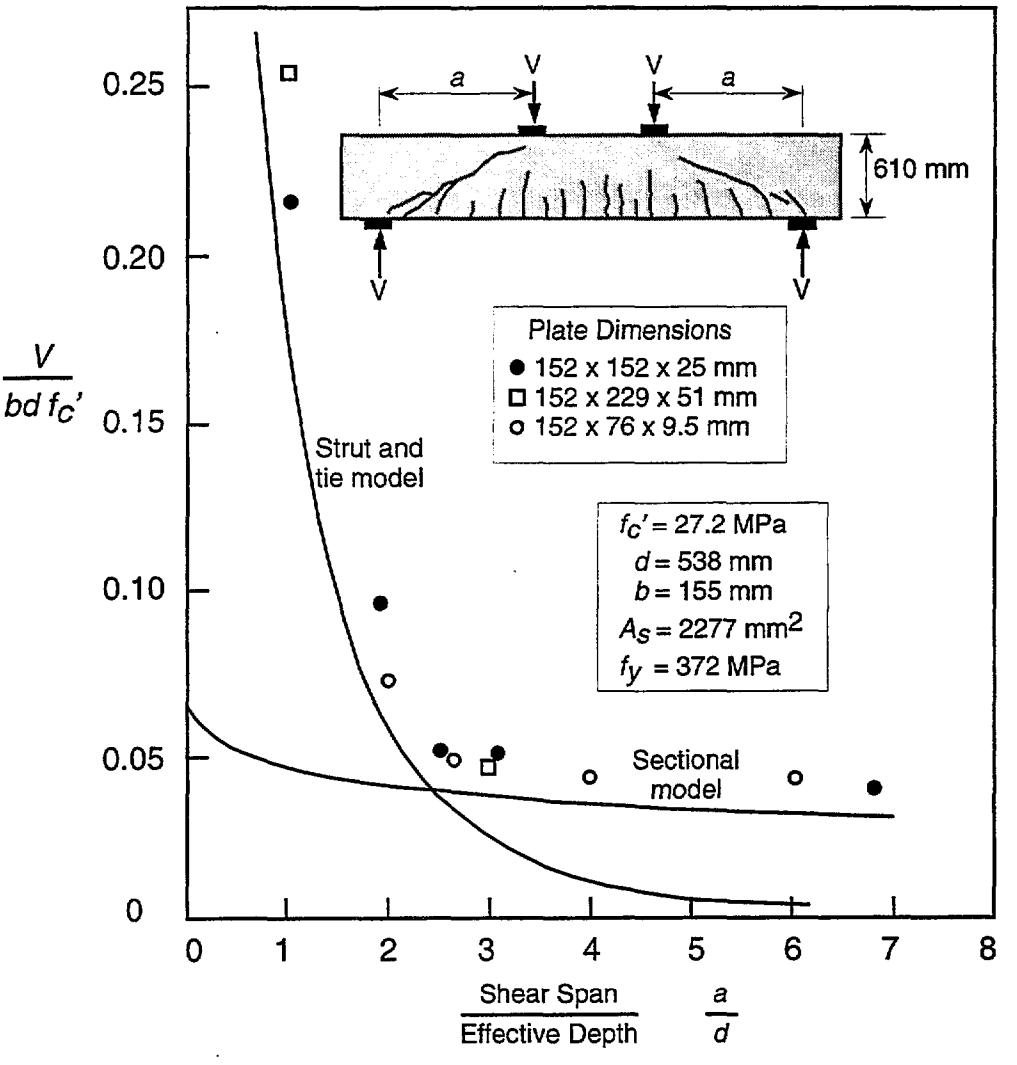

Figure 2.43 — Comparison of experimental shear capacity of beams with different shear-span-to-depth ratios with predictions by strut and tie models and sectional models (adapted from Collins and Mitchell 1991)

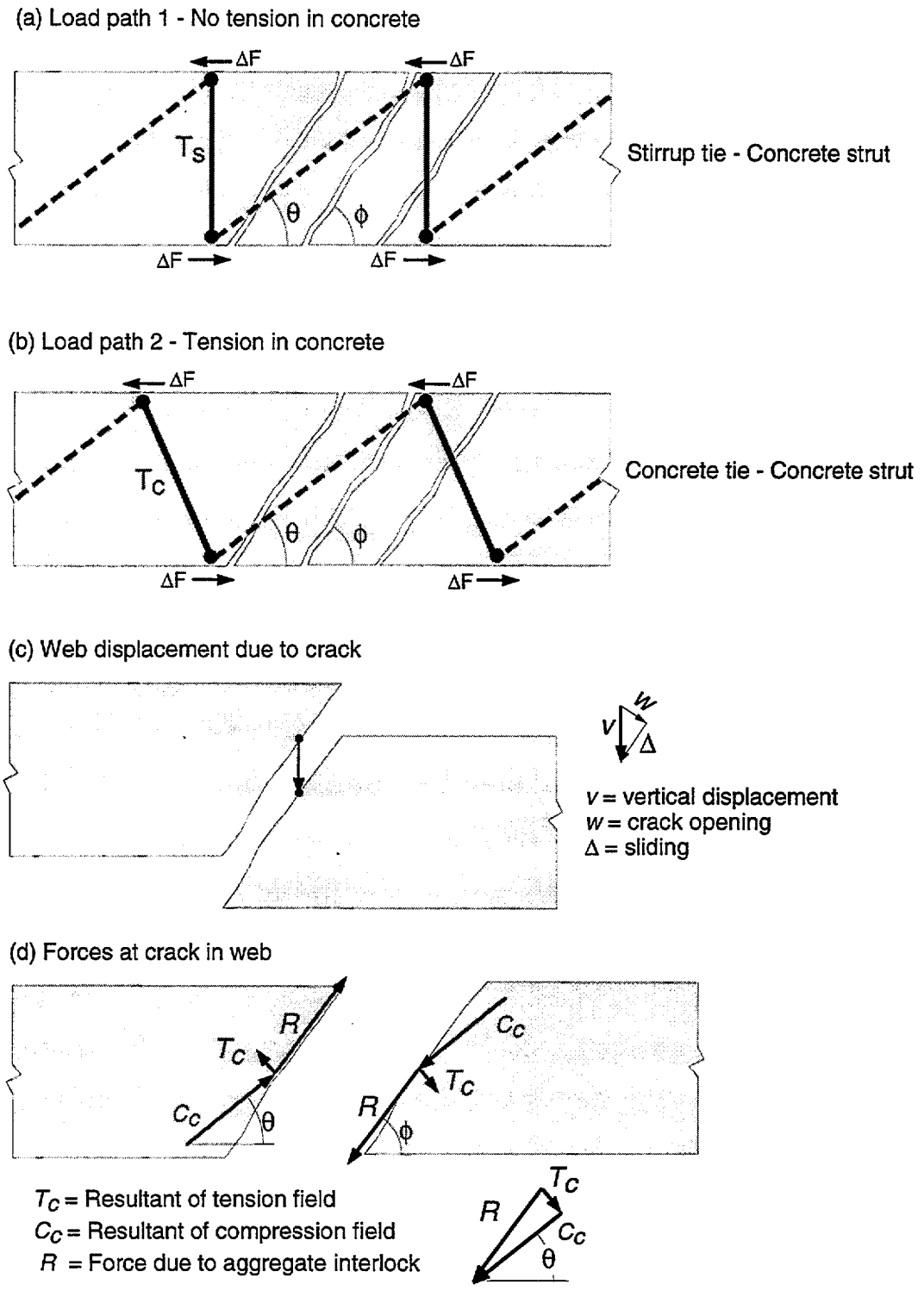

Figure 2.44 — Internal forces in beam due to shear (adapted from Schlaich et al. 1987).

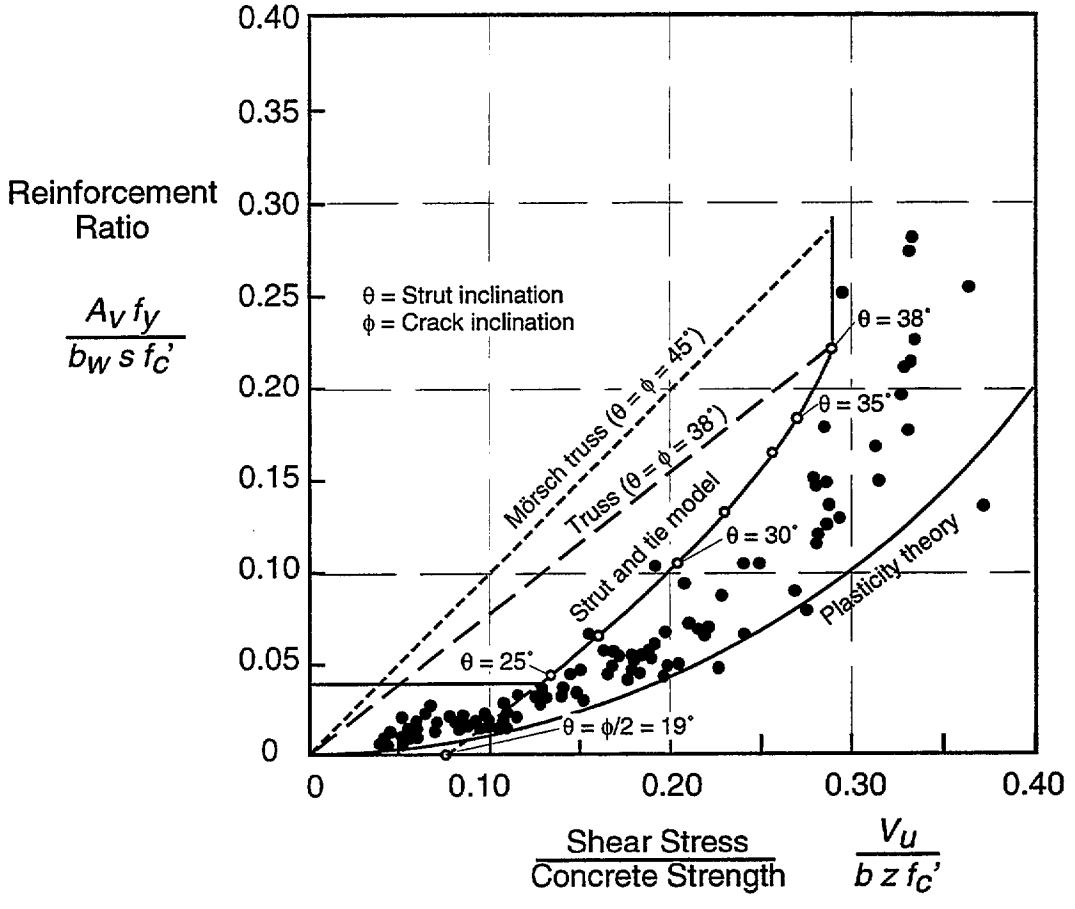

Figure 2.45 — Required vertical stirrups as a function of applied shear stress: comparison of strut and tie model ($\phi = 38°$), simple truss analogy, plasticity theory and experiments (adapted from Schlaich et al. 1987)

3. Comparison of Design Codes

3.1 ACI Code 318-95 (American Concrete Institute Building Code, 1995)

In a series of reports, ACI-ASCE Committee 326 on Shear and Diagonal Tension (1962) and its successor, ASCE- ACI Task Committee 426 (1973,1974, reapproved 1990) reviewed the fundamentals of shear behavior. These reports form the basis of the ACI code. The main parameters that govern the shear strength of beams, according to these reports, are summarized below.

3.1.1 Shear Strength Parameters

Beams without web reinforcement

Beams without web reinforcement fail when inclined cracking occurs or shortly afterwards. The inclined cracking load is affected by five principal variables, some included in design equations and others not.

1. Tensile strength of concrete

The stress state in the web of a beam involves biaxial principal tension and compression stresses. Also, the flexural cracking which precedes the inclined cracking disrupts the elastic stress field to such an extent that inclined cracking occurs at a principal stress, based on the cracked section, of roughly $f_{ct} / 3$, where f_{ct} is the concrete tensile strength.

2. Longitudinal reinforcement ratio

Fig. 3.1 (MacGregor and Gergely 1977) shows the shear capacity of simply supported beams without stirrups as a function of the steel ratio $\rho_w = A_s / (b_w d)$.

3. Shear span to depth ratio *a/d* or moment to shear ratio *M / (Vd)*

This is shown is Fig. 3.2 (ACI-ASCE Committee 326, 1962).

4. Size of beam

Fig. 3.3. (Collins and Mitchell 1991, Collins et al. 1996) shows the well-known size effect in beam shear. The Modified Compression Field Theory does a reasonable job at predicting the size effect, whereas the ACI provisions can be unconservative for large beams.

5. Axial forces

Axial tensile forces tend to decrease the inclined cracking load, while axial compressive forces tend to increase it. This is shown in Fig. 3.4 (MacGregor 1992).

Beam with web reinforcement

6. Yielding of the stirrups

Discussion of the truss model in the previous chapter shows this is an important failure mode.

7. Crushing of the web

Again the truss model explains this mode of failure. Some codes limit the ultimate shear stress to $0.2 f'_c$ in beams with vertical stirrups or $0.25 f'_c$ in beams with 45° stirrups. The ACI limit for

crack control

$$V_{smax} = 8\sqrt{f'_c}\, b_w d \quad \text{inch-pound system}$$
$$V_{smax} = 0.7\sqrt{f'_c}\, b_w d \quad \text{mm-Newton system} \qquad \text{(ACI § 11.5.6.8)}$$

provides adequate safety against web crushing.

8. Failure of the tension chord

The truss model shows that tension in the longitudinal reinforcement at a given point in the shear span is a function of the moment located approximately d (= effective depth) closer to the nearest section of maximum moment. This is why the ACI code requires that flexural reinforcement be extended a distance d past the point where it is no longer needed.

9. Failure of stirrup anchorage

Generally, the upper end of the inclined crack approaches very close to the compression face of the beam. At ultimate load, the stress in the stirrups approaches or equals the yield strength f_y at every point where an inclined crack intercepts a stirrup. Thus, the portion of stirrup above the crack must be able to anchor f_y. The ACI Code requires that stirrups be closed loops or anchored by hooks or T-heads.

10. Serviceability failure due to excessive crack widths at service loads.

ACI guards against this by limiting the maximum shear that can be transmitted by stirrups to that specified by ACI § 11.5.6.8 above.

3.1.2 Shear Resisting Mechanisms

The shear carried by the concrete, V_c, is the sum of :

- V_{cz} the shear carried by the compression zone,
- V_{ay} the vertical component of aggregate interlock, and
- V_d the dowel action of reinforcement crossing the crack.

The relative magnitude of all shear carrying mechanisms is shown in Fig. 3.5 (MacGregor 1992).

3.1.3 ACI Code Equations For Shear In Beams

In the ACI Code, the basic design equation for the shear capacity of a concrete beam is.

$$V_u \leq \Phi V_n$$

where V_u is the shear force due to the factored loads, Φ is the strength reduction factor, taken equal to 0.85 for shear, and V_n is the nominal shear resistance :

$$V_n = V_c + V_s \qquad \text{(ACI 11.2)}$$

V_c is the shear carried by the concrete and V_s, the shear carried by the stirrups, is based on the 45° truss.

The number of vertical stirrups spaced s apart crossed by a crack is therefore d/s, where d is the beam effective depth. Assuming that all stirrups yield at failure, the shear resisted by the stirrups is:

$$V_s = \frac{A_v f_y d}{s} \qquad \text{(ACI 11.15)}$$

where the stirrups have cross-sectional area A_v and yield strength f_y. However, tests have shown consistently that the stirrup stresses were considerably lower than those predicted by the 45° truss model (Hognestad 1952), which therefore underestimates the beam shear strength (Fig. 2.45).

The ACI code assumes that V_c is equal to the shear strength of a beam without stirrups, which in turn, is taken equal to the load at which inclined cracking occurs:

$$V_c = \left(1.9\sqrt{f_c'} + 2500\frac{\rho_w V_u d}{M_u}\right) b_w d \le 3.5\sqrt{f_c'} b_w d \quad \text{inch-pound system}$$

$$V_c = \left(0.16\sqrt{f_c'} + 17\frac{\rho_w V_u d}{M_u}\right) b_w d \le 0.29\sqrt{f_c'} b_w d \quad \text{mm-Newton system} \qquad \text{(ACI 11.5)}$$

where f'_c = concrete compressive strength,
ρ_w = longitudinal reinforcement ratio,
b_w = web width,
M_u = factored moment at section and
$M_u / (V_u d)$ expresses the shear span to depth ratio a/d.

This equation was developed by ACI-ASCE Committee 326 in 1962 and is still in current use. Taking V_c equal to the shear at inclined cracking is based on empirical observations and is approximately true if the truss angle θ is assumed to be 45°. If θ approaches 30°, as in the plastic truss model, V_c approaches 0, as assumed in that model (see Fig. 2.45).

The nechanism of shear failure of beams with shear reinforcement is totally different from beams without shear reinforcement. Yet, ACI and many other design codes, use the same V_c for both types of members. Thus, the shear resistance due to the concrete and stirrups are considered additive, when in fact they form part of a complex interaction (Chana 1987).

Eq. ACI 11.5 is plotted in Fig. 3.2 with its experimental basis. The same data are plotted in terms of reinforcement ratio in Fig 3.1, together with the following simplified version of Eq. ACI 11.5 allowed by the ACI code.

$$V_c = 2\sqrt{f_c'} b_w d \quad \text{inch-pound system}$$
$$V_c = \sqrt{f_c'} b_w d/6 \quad \text{mm-Newton system} \qquad \text{(ACI 11.3)}$$

3.1.4 Deep Beams

For deep beams with $a/d \le 2$, the ACI Code accounts for the increased shear resistance by the use of a multiplier:

$$V_c = \left(3.5 - 2.5\frac{M_u}{V_u d}\right)\left(1.9\sqrt{f_c'} + 2500\rho_w\frac{V_u d}{M_u}\right) b_w d \le 6\sqrt{f_c'} b_w d \quad \text{inch, lb}$$

$$V_c = \left(3.5 - 2.5\frac{M_u}{V_u d}\right)\left(0.16\sqrt{f_c'} + 17\rho_w\frac{V_u d}{M_u}\right) b_w d \le 0.5\sqrt{f_c'} b_w d \quad \text{mm, N} \qquad \text{(ACI 11.29)}$$

$$\text{with} \qquad 3.5 - 2.5\frac{M_u}{V_u d} \le 2.5$$

where M_u and V_u are calculated at a distance $a/2$ but not greater than d from the face of the support. a is the shear span or the distance between concentrated loads and support faces.

3.1.5 Proposed Revisions (1977)

Fig. 3.1 (MacGregor and Gergely 1977) also shows specifications from other codes (1977 or earlier versions) as well as revisions to Eqs. ACI 11.5 and 11.3 recommended by MacGregor and Gergely in 1977. Among the suggested revisions, the basic shear stress is changed to:

$$\lambda\sqrt{f_c'} \le v_b = (0.8 + 120\rho_w)\lambda\sqrt{f_c'} \le 2.3\lambda\sqrt{f_c'} \quad \text{inch-pound system}$$

$$0.083\lambda\sqrt{f_c'} \le v_b = (0.07 + 10\rho_w)\lambda\sqrt{f_c'} \le 0.19\lambda\sqrt{f_c'} \quad \text{mm-Newton system}$$

where $\lambda = 1.0$ for normal weight concrete, $\lambda = 0.85$ for "sand-lightweight" concrete, and $\lambda = 0.75$ for "all-lightweight" concrete.

The shear force V_c carried by the concrete is changed to:

$$V_c = v_b b_w d \quad \text{for} \quad \frac{a}{d} \ge 2$$

$$\text{and} \quad V_c = 2\frac{d}{a} v_b b_w d \ge v_b b_w d \quad \text{for} \quad \frac{a}{d} \le 2 \qquad (3.1)$$

The justification for Eq. 3.1 is presented in Fig. 3.6 (MacGregor and Gergely 1977). Further justification is that the meaning of $M/(Vd)$ for continuous beams is unclear (Fig.3.7, from Fergusson 1973). Thus, the influence of a/d or $M/(Vd)$ is neglected for $a/d > 2$. Although these revisions were not adopted, they are presented here because of their relevance to other national codes.

3.1.6 Axial Force

For axially loaded members, Eq. ACI 11.5 is modified as follows (Fig. 3.4, from MacGregor 1992). For axial compression $N_u > 0$ and with A_g denoting the gross area of the section, the simplified method limits V_c as follows:

$$V_c = 2\left(1 + \frac{N_u}{2000A_g}\right)\sqrt{f_c'} b_w d \quad \text{inch-pound system}$$

$$V_c = \left(0.166 + 0.012\frac{N_u}{A_g}\right)\sqrt{f_c'} b_w d \quad \text{mm-Newton system} \qquad (\text{ACI } 11.4)$$

whereas the detailed method specifies:

$$V_c = \left(1.9\sqrt{f_c'} + 2500\frac{\rho_w V_u d}{M_m}\right) b_w d \le 3.5\sqrt{f_c'} b_w d \sqrt{1 + \frac{N_u}{500A_g}} \quad \text{inch, lb}$$

$$V_c = \left(0.16\sqrt{f_c'} + 17\frac{\rho_w V_u d}{M_m}\right) b_w d \le 0.29\sqrt{f_c'} b_w d \sqrt{1 + \frac{N_u}{3.45A_g}} \quad \text{mm, N}$$

$$\text{with} \quad M_m = M_u - N_u\left(\frac{4h - d}{8}\right) \qquad (\text{ACI } \S 11.3.2.2)$$

For axial tension $N_u < 0$:

$$V_c = 2\left(1 + \frac{N_u}{500A_g}\right)\sqrt{f'_c}\,b_w d \qquad \text{inch-pound system}$$

$$V_c = \left(0.166 + 0.048\frac{N_u}{A_g}\right)\sqrt{f'_c}\,b_w d \qquad \text{mm-Newton system} \qquad \text{(ACI 11.8)}$$

3.1.7 f'_c Limits and Minimum Shear Reinforcement

Fig. 3.8 shows the limits of ACI current shear design provisions versus f'_c:

For long, shallow beams:

$$v_c = 1.9\sqrt{f'_c} \quad \text{psi} \qquad \text{or} \qquad 0.16\sqrt{f'_c} \quad \text{MPa}$$

For short, deep beams:

$$v_c = 3.5\sqrt{f'_c} \quad \text{psi} \qquad \text{or} \qquad 0.29\sqrt{f'_c} \quad \text{MPa}$$

It is seen that the tests that form the basis of the ACI equations were performed on members with concrete strengths of $f'_c \le 6000$ psi (40 MPa). Experiments suggest that the inclined cracking load of beams increases less rapidly than $\sqrt{(f'_c)}$ increases, for f'_c greater than about 8000 psi (55 MPa). This is offset by an increased effectiveness of stirrups in high-strength concrete beams. Other tests suggest that the required amount of web reinforcement increases as f'_c increases. For these reasons, the ACI code limits $\sqrt{(f'_c)}$ to 100 psi (8.3 MPa) unless the amount of minimum web reinforcement is increased according to Clause 11.1.2.1 by the ratio

$$f'_c \text{ (psi)} / 5000 \le 3 \quad [f'_c \text{ (MPa)} / 34.5 \le 3].$$

The minimum area of shear reinforcement for normal strength concrete is:

$$A_v = 50\frac{b_w s}{f_y} \qquad \text{inch-pound system}$$

$$A_v = 0.345\frac{b_w s}{f_y} \qquad \text{mm-Newton system} \qquad \text{(ACI 11.13)}$$

and for high strength concrete (ACI §11.1.2.1):

$$50\frac{b_w s}{f_y} \le A_v = 50\frac{f'_c}{5000}\frac{b_w s}{f_y} \le 150\frac{b_w s}{f_y}, \quad 10\,000 \le f'_c \qquad \text{inch-pound system}$$

$$0.345\frac{b_w s}{f_y} \le A_v = 0.010\frac{f'_c}{f_y}b_w s \le 1.035\frac{b_w s}{f_y}, \quad 69 \le f'_c \qquad \text{mm-Newton system}$$

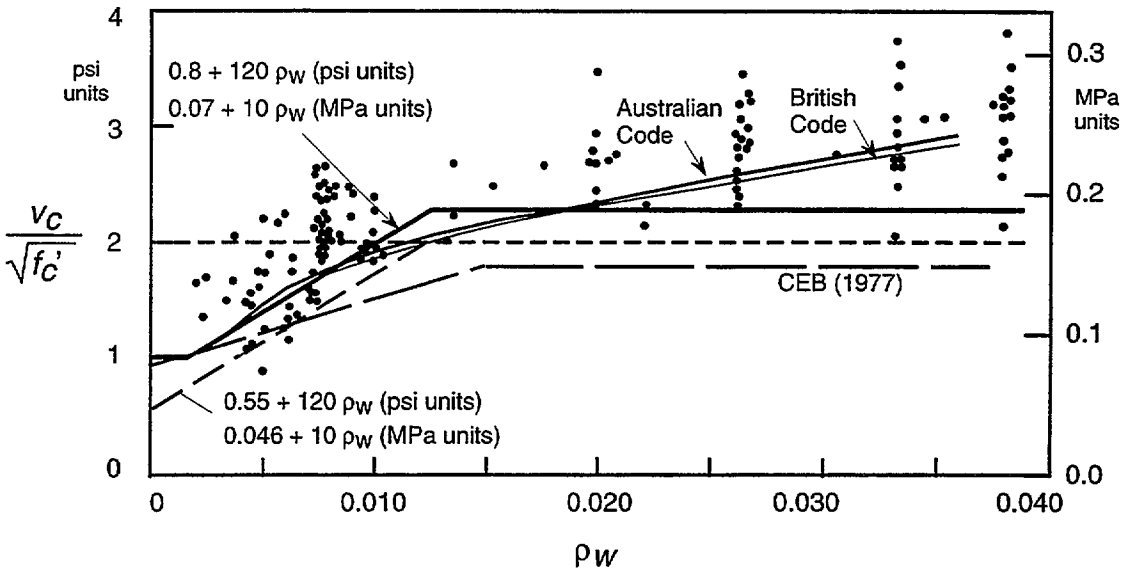

Figure 3.1 — Shear capacity of simply-supported beams (a/d > 2.5) without stirrups as a function of steel ratio (adapted from MacGregor and Gergely 1977)

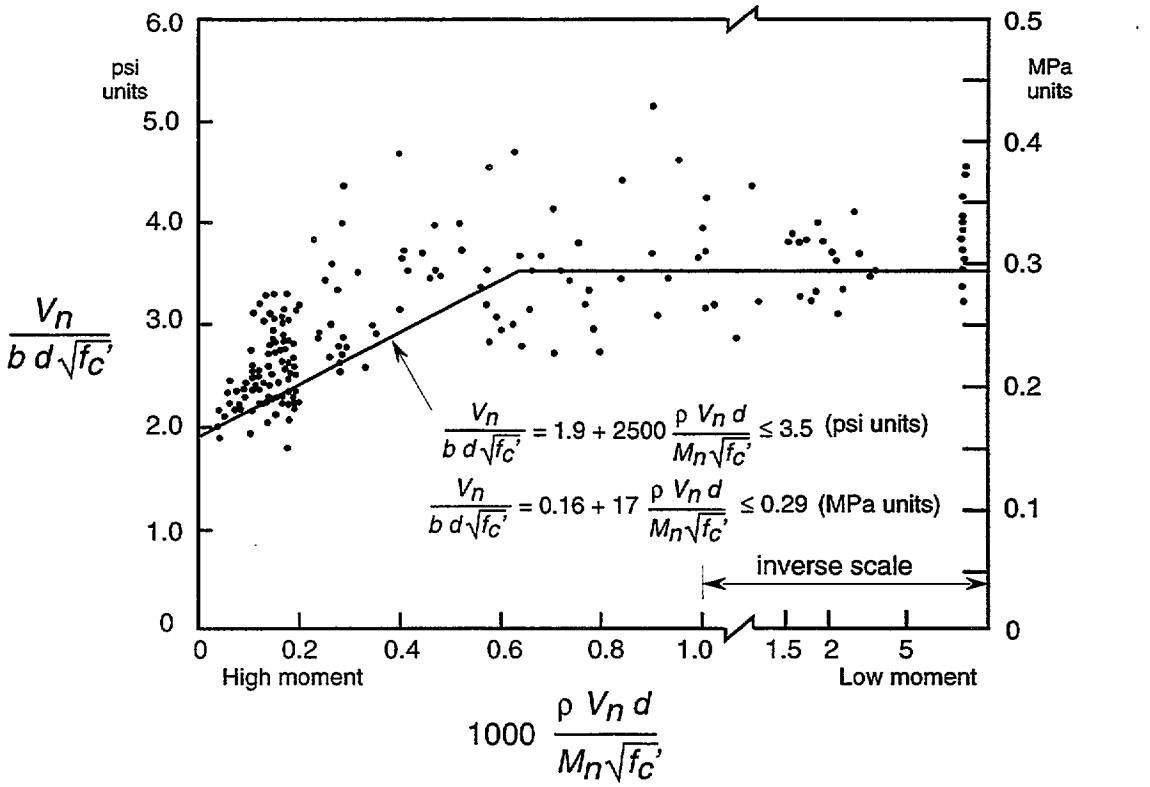

Figure 3.2 — Shear strength (flexural-shear cracking) as a function of the shear-to-moment ratio (adapted from ACI-ASCE 326, 1962)

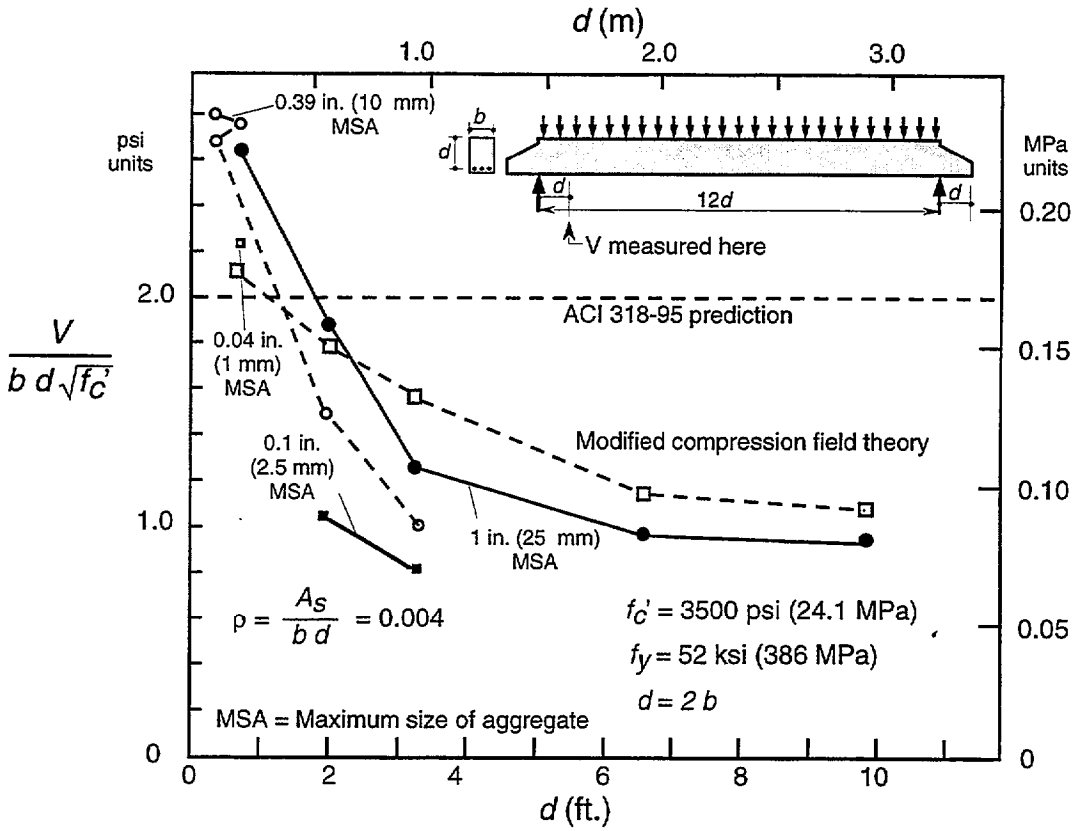

Figure 3.3 — Effect of beam size on shear stress at failure at distance d from support (adapted from Collins and Mitchell 1991 and Collins et al. 1996)

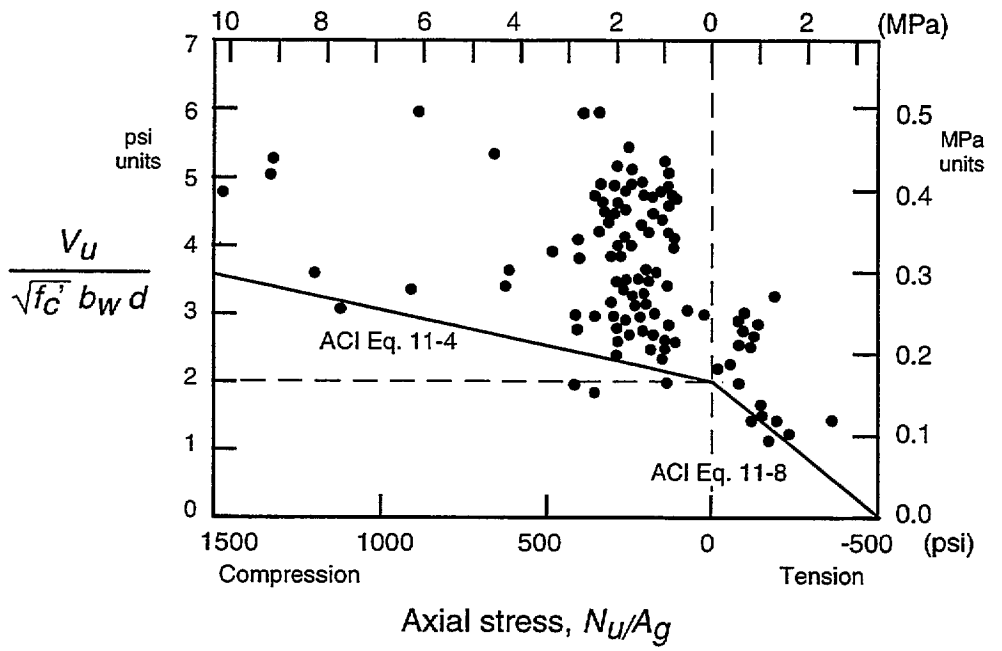

Figure 3.4 — Effect of axial force on shear force at inclined cracking (adapted from MacGregor 1992)

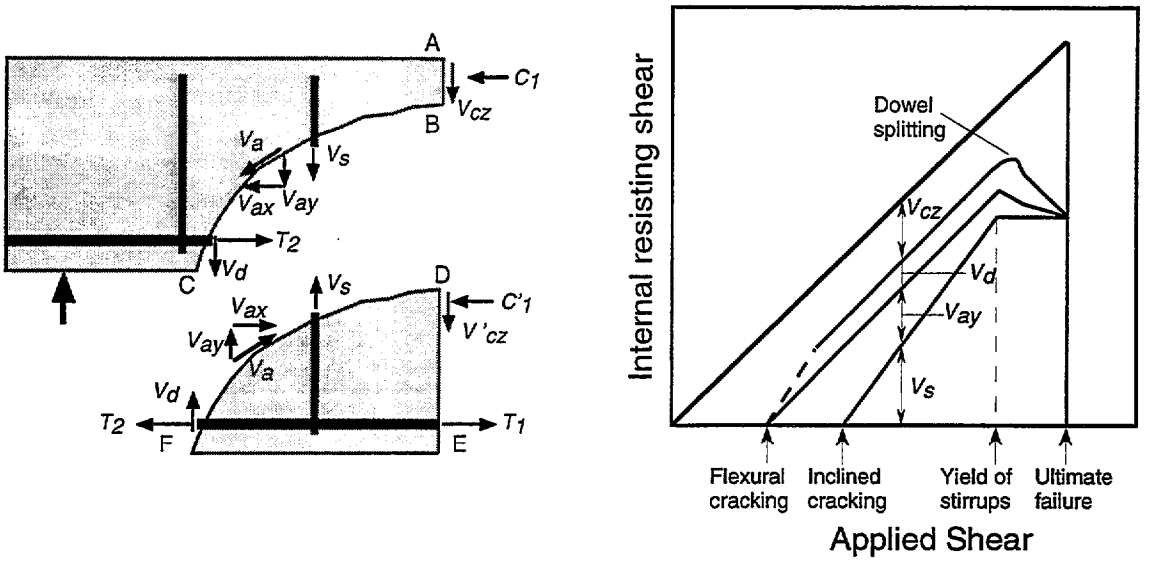

Figure 3.5 — (a) Internal forces in cracked beam with stirrups; (b) relative magnitude of shear carrying mechanisms (adapted from MacGregor 1992).

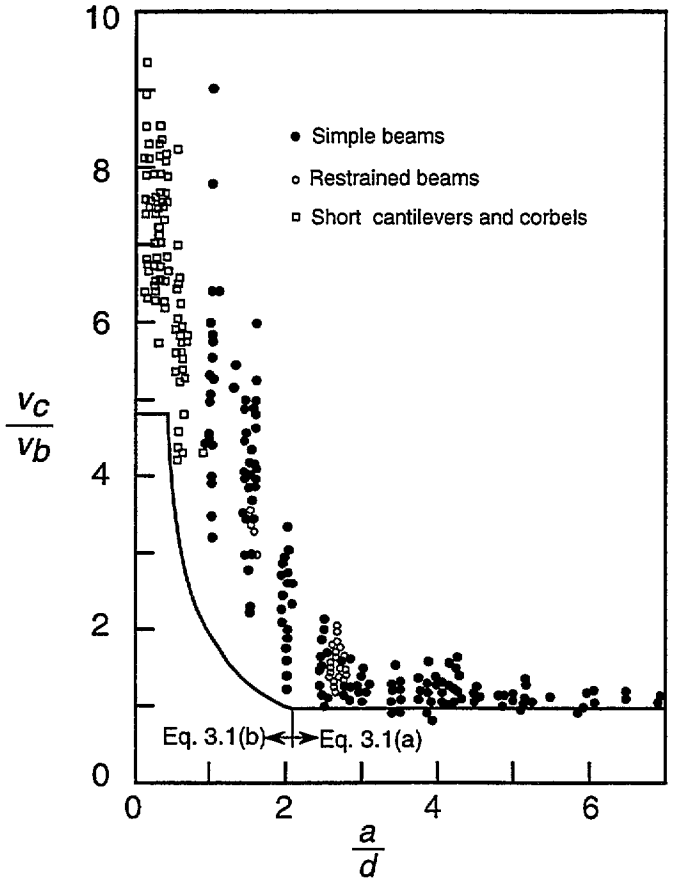

Figure 3.6 — Effect of *a/d* on shear strength of various beams (adapted from MacGregor and Gergely 1977)

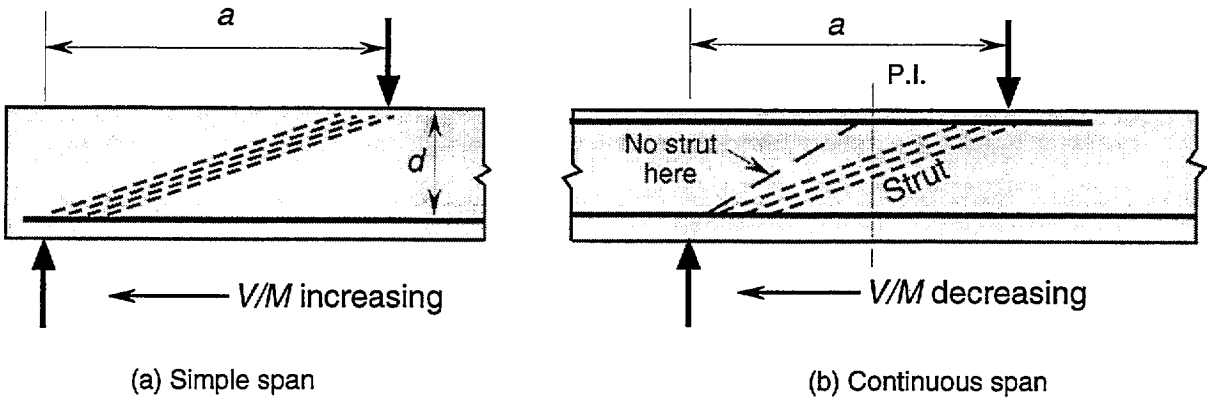

Figure 3.7 — Shear-to-moment ratio: (a) for simple span $Vd/M = d/a$; for continuous span $Vd/M = d/$[distance to point of inflection (P.I.)]$\neq d/a$ (adapted from Ferguson 1973).

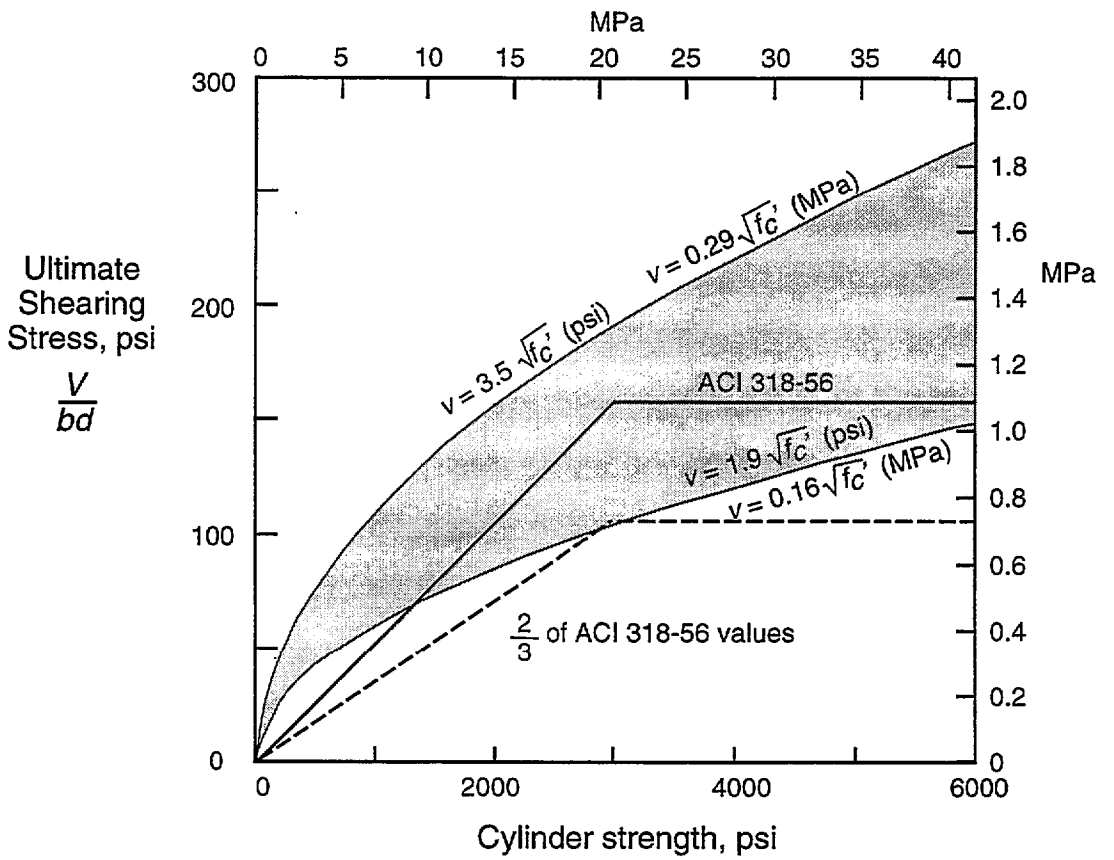

Figure 3.8 — Limits of concrete strength underlying the ACI shear design equations (adapted from ACI-ASCE 326 1962)

3.2 CSA A23.3-94 (Canadian Standards for the Design of Concrete Structures, Dec. 1994)

The latest CSA Code applies to concrete of compressive strength up to 80 MPa (11600 psi).

3.2.1 General Design Method

The *general design method* for shear and torsion in flexural regions is based on the Modified Compression Field Theory (MCFT). Adequate shear resistance is provided if :

$$V_{rg} \geq V_f$$

where V_{rg} is the factored shear resistance and V_f is the factored shear force at section.

The factored shear resistance is, for a non-prestressed section:

$$V_{rg} = V_{cg} + V_{sg} \leq 0.25\,\phi_c f'_c b_w d_v \qquad \text{(CSA 11.17)}$$

The limit on V_{rg} is intended to prevent concrete crushing in the web prior to yielding of the transverse reinforcement. In the above equation:

V_{cg} = concrete contribution,

$$V_{cg} = 1.3\,\lambda\,\phi_c\,\beta\sqrt{f'_c}\,b_w d_v \qquad \text{mm-Newton system}$$
$$V_{cg} = 1.3\,\lambda\,\phi_c\,(12\,\beta)\sqrt{f'_c}\,b_w d_v \qquad \text{inch-pound system} \qquad \text{(CSA 11.18)}$$

V_{sg} = steel contribution,

$$V_{sg} = \frac{\phi_s A_v f_y d_v (\cot\theta + \cot\alpha)\sin\alpha}{s} \qquad \text{(CSA 11.20)}$$

A_v = area of shear reinforcement within spacing s,
b_w = effective web width,
d = beam effective depth, or distance from the extreme compression fiber to the centroid of the longitudinal tension reinforcement,
d_v = lever arm of resisting flexural moment $\geq 0.9\,d$,
f'_c = specified compressive strength of concrete,
f_y = specified yield strength of reinforcement,
s = spacing of shear reinforcement,
α = angle of inclined stirrups to longitudinal axis,
β = factor accounting for shear resistance of cracked concrete,
λ = factor to account for low density concrete ($\lambda = 1$ for normal density concrete),
θ = angle of inclination of diagonal compressive stresses to the longitudinal axis of the member, and
ϕ_c, ϕ_s = material factors for concrete and steel ($\phi_c = 0.60$, $\phi_s = 0.85$).

The low value of ϕ_c is chosen to simplify the formulation of column design and is compensated for by the factor 1.3. The factor β and the angle θ are given in Tables 3.1 and 3.2 (11.1 and 11.2 CSA) and Figs. 3.9 and 3.10 (11.1 and 11.2 CSA) for sections with transverse reinforcement (i.e. greater than minimum required) and for sections without (i.e. less than minimum required). For β values in psi units, multiply the values in the tables by 12. The shear capacity of a member without stirrups is limited by the shear transfer of diagonal cracks (Adebar and Collins 1996)

The minimum area of shear reinforcement is proportional to $\sqrt{(f'_c)}$:

$$A_{vmin} = 0.06\sqrt{f_c'}\frac{b_w s}{f_y} \quad \text{mm-Newton system}$$

$$A_{vmin} = 0.02\sqrt{f_c'}\frac{b_w s}{f_y} \quad \text{inch-kips system} \qquad \text{(CSA 11.1)}$$

The use of these tables requires knowledge of the maximum longitudinal strain ε_x. As well, it requires knowledge of the spacing parameter s_z for sections without transverse reinforcement:

$$\varepsilon_x = \frac{0.5\,(N_f + V_f \cot\theta) + M_f/d_v}{E_s A_s} \le 0.002 \qquad \text{(CSA 11.22)}$$

where

N_f = factored axial load normal to cross-section, occurring simultaneously with V_f, with tension positive and compression negative,

V_f = factored shear force at section,

$M_f > 0$ factored moment at section,

E_s = modulus of elasticity of reinforcement,

A_s = area of reinforcement in tension zone,

$s_z \le 2000$ mm is the lesser of d_v and the maximum distance between layers of crack control reinforcement.

3.2.2 Simplified Design Method

The *simplified design method* for shear and torsion also determines shear resistance as the sum of a concrete and a steel contribution:

$$V_r = V_c + V_s \le V_c + 0.8\,\lambda\,\phi_c\sqrt{f_c'}\,b_w d \qquad \text{(CSA 11.5)}$$

For comparison with the last term, ACI 318-95 limits the maximum shear carried by stirrups to

$$8\sqrt{f_c'}\,b_w d \text{ pounds or } 0.7\sqrt{f_c'}\,b_w d \text{ Newton} \qquad \text{(ACI 11.5.6.8)}$$

The steel contribution is:

$$V_s = \frac{\phi_s A_v f_y d}{s} \quad \text{i.e. } \theta = 45° \text{ and } \alpha = 90° \text{ in Eq. CSA 11.20.}$$

For members having either a) at least the minimum amount of transverse reinforcement given by Eq. CSA 11.1 or b) an effective depth not exceeding 300 mm, the concrete contributiion can be calculated as:

$$V_c = 0.2\,\lambda\,\phi_c\sqrt{f_c'}\,b_w d \approx 1.3\,\lambda\,\phi_c\frac{2}{12}\sqrt{f_c'}\,b_w d \text{ Newton} \qquad \text{(CSA 11.6)}$$

This is comparable to ACI 1989 simplified shear resistance:

$$V_c = 2\sqrt{f_c'}\,b_w d \text{ pound} = \frac{2}{12}\sqrt{f_c'}\,b_w d \text{ Newton}$$

For members with effective depths greater than 300 mm and with transverse reinforcement less than that required by Eq. CSA 11.1:

$$V_c = \left(\frac{260}{1000 + d} \right) \lambda \phi_c \sqrt{f'_c} b_w d \geq 0.10 \lambda \phi_c \sqrt{f'_c} b_w d \qquad \text{(CSA 11.7)}$$

3.2.3 Longitudinal Reinforcement

The factored resistance of the longitudinal reinforcement N_r must be greater than or equal to the stress that can be developed in that reinforcement at all sections. The longitudinal reinforcement is designed to resist moment M_f and equivalent axial tension $N_v = V \cot \theta$ due to shear:

$$N_r > \frac{M_f}{d_v} + 0.5 N_f + (V_f - 0.5 V_{sg}) \cot \theta \qquad \text{(CSA 11.23)}$$

For disturbed regions near discontinuities, the Canadian Code recommends the use of strut-and-tie models.

3.2.4 Strut-and-Tie Method

The *strut-and-tie method* may be used to dimension RC members. The limiting compressive stress in the biaxially stressed strut is:

$$f_{cu} = \frac{f'_c}{0.8 + 170\varepsilon_1} \leq 0.85 f'_c \qquad \text{(CSA 11.30)}$$

where ε_1 is the principal tensile strain in cracked concrete due to factored loads and is calculated as:

$$\varepsilon_1 = \varepsilon_s + (\varepsilon_s + 0.002) \cot^2 \theta_s \qquad \text{(CSA 11.31)}$$

θ_s is the smallest angle between the compressive strut and the adjoining tensile ties and ε_s is the tensile strain in the tensile tie inclined at θ_s to the compressive strut. As θ_s decreases, ε_1 increases and f_{cu} decreases. In other words, there must be some difference in orientation between a strut and an intersecting tie, a strut cannot be placed directly on top of a tie.

Unless special confinement is provided, the calculated concrete compressive stress in the node region shall not exceed the following:

a) $0.85 \phi_c f'_c$ in node regions bounded by compressive struts and bearing areas,
b) $0.75 \phi_c f'_c$ in node regions anchoring a tension tie in only one direction, and
c) $0.65 \phi_c f'_c$ in node regions anchoring tension ties in more than one direction.

3.2.5 Beam versus Panel Tests

It is worth discussing at this point why the ACI has maintained its semi-empirical equations since 1962 even when more rational methods exist, such as the Modified Compression Field Theory (MCFT), which is now adopted, for example, in the Canadian, Norwegian and AASHTO LRFD Codes. Clearly, the fact that a whole generation of engineers has learned and used the present version (for shear) of the ACI code must be a factor. However, there is a fundamental difference in approach as well. According to ACI-ASCE Committee 326 (1962), "diagonal tension is a combined stress problem in which horizontal stresses due to bending as well as shearing stresses must be considered."

In "The Use of Rational Design Methods for Shear" (Collins 1993), the author of the Compression Field Theory (CFT) and the MCFT explains that this combination of flexure and shear is what has made the shear problem so intractable. He contrasts the traditional type of shear tests (beam), which are simple to perform, but difficult to analyze, with the more recent tests (panel) which

are more difficult to perform but simpler to analyze. See Fig. 3.11 (Collins 1993). In tests of beams, simply supported with two concentrated loads, the behavior of the member changes from section to section along the shear span and also over the depth of the beam. In contrast, the state of stress in a panel loaded in pure shear or a combination of shear and axial forces is uniform.

Because shear is studied independently of flexure, the shear carried by the compression zone V_{cz} does not exist in the CFT or MCFT. V_d, the shear carried by the dowel action of the longitudinal reinforcement is also neglected, but V_{ay}, the shear carried by aggregate interlock is accounted for.

V_d is rather small (see Fig. 3.5b), but V_{cz} can account for 25-30% of V_c in beams with typical longitudinal reinforcement ratios. Nevertheless, when the MCFT is applied to traditional beam tests, it fares rather well as a predictor of strength and has an even smaller coefficient of variation than the ACI equations do. See Fig 3.12 (Collins 1996). How can the results be so good ?

Vecchio and Collins performed a detailed analysis of a cross-section subjected to combined shear and moment. Fig. 3.13 shows the distribution of shear stress over the cross section. It also shows that the inclination of the principal compressive stress changes over the height of the beam. In the Canadian code the choice of the location (mid-depth) of ε_x reflects the redistribution of shear stress transferred from the most highly strained portions of the cross section to the less highly strained portion. It would be conservative to use the highest value of ε_x, as an increase in ε_x decreases the shear capacity. So, implicitly, the higher shear capacity of the uncracked or least strained region is taken into account.

Table 3.1 — Values of β and θ for sections with transverse reinforcement (CSA 1994)

$\frac{v_f}{\lambda \phi_c f'_c}$		Longitudinal strain, ε_x						
		≤ 0.0000	≤ 0.00025	≤ 0.0005	≤ 0.00075	≤ 0.0010	≤ 0.0015	≤ 0.0020
≤0.050	β	0.405	0.290	0.208	0.197	0.185	0.162	0.143
	θ	27.0°	28.5°	29.0°	33.0°	36.0°	41.0°	43.0°
≤0.075	β	0.405	0.250	0.205	0.194	0.179	0.158	0.137
	θ	27.0°	27.5°	30.0°	33.5°	36.0°	40.0°	42.0°
≤0.100	β	0.271	0.211	0.200	0.189	0.174	0.143	0.120
	θ	23.5°	26.5°	30.5°	34.0°	36.0°	38.0°	39.0°
≤0.125	β	0.216	0.208	0.197	0.181	0.167	0.133	0.112
	θ	23.5°	28.0°	31.5°	34.0°	36.0°	37.0°	38.0°
≤0.150	β	0.212	0.203	0.189	0.171	0.160	0.125	0.103
	θ	25.0°	29.0°	32.0°	34.0°	36.0°	36.5°	37.0°
≤0.200	β	0.203	0.194	0.174	0.151	0.131	0.100	0.083
	θ	27.5°	31.0°	33.0°	34.0°	34.5°	35.0°	36.0°
≤0.250	β	0.191	0.167	0.136	0.126	0.116	0.108	0.104
	θ	30.0°	32.0°	33.0°	34.0°	35.5°	38.5°	41.5°

Table 3.2— Values of β and θ for sections without transverse reinforcement (CSA 1994)

s_z		Longitudinal strain, ε_x					
		≤ 0.0000	≤ 0.00025	≤ 0.0005	≤ 0.0010	≤ 0.0015	≤ 0.0020
≤125	β	0.406	0.309	0.263	0.214	0.183	0.161
	θ	27°	29°	32°	34°	36°	38 °
≤250	β	0.384	0.283	0.235	0.183	0.156	0.138
	θ	30°	34°	37°	41°	43°	45°
≤500	β	0.359	0.248	0.201	0.153	0.127	0.108
	θ	34°	39°	43°	48°	51°	54°
≤1000	β	0.335	0.212	0.163	0.118	0.095	0.080
	θ	37°	45°	51°	56°	60°	63°
≤2000	β	0.306	0. 171	0.126	0.084	0.064	0.052
	θ	41°	53°	59°	66°	69°	72°

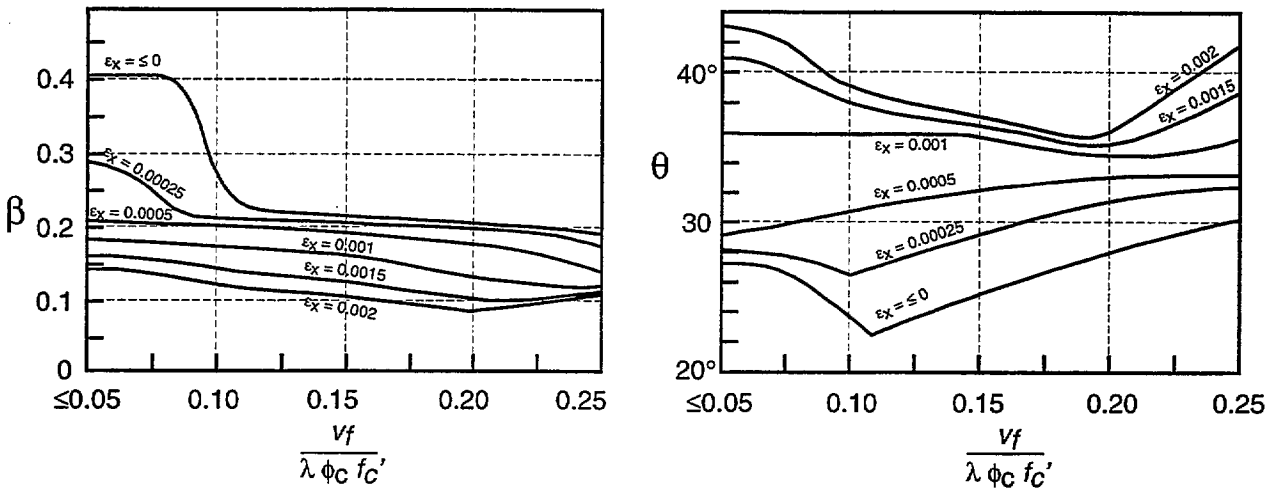

Figure 3.9 — Values of β and θ for sections with transverse reinforcement (adapted from CSA 1994)

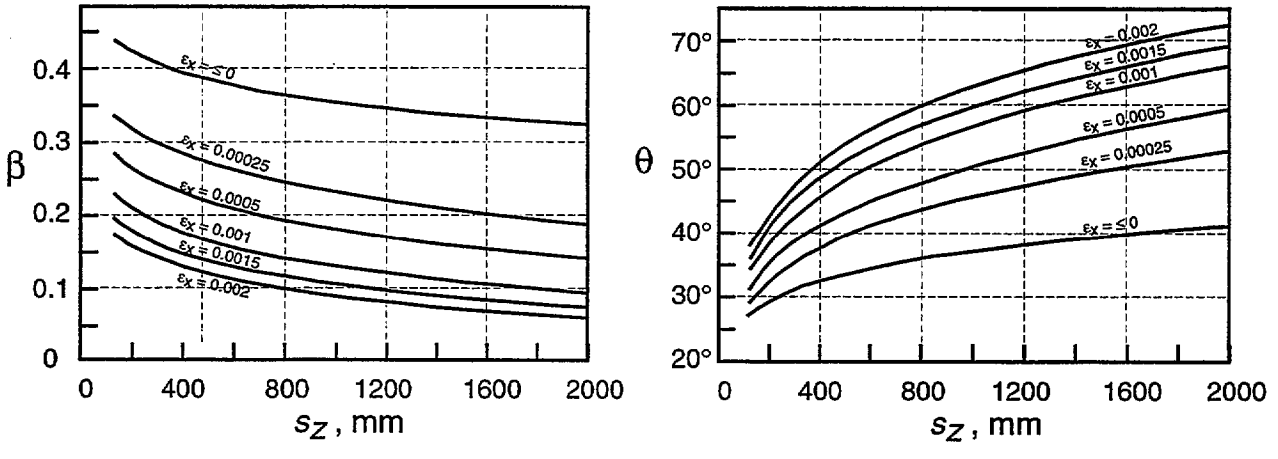

Figure 3.10 — Values of β and θ for sections without transverse reinforcement (adapted from CSA 1994)

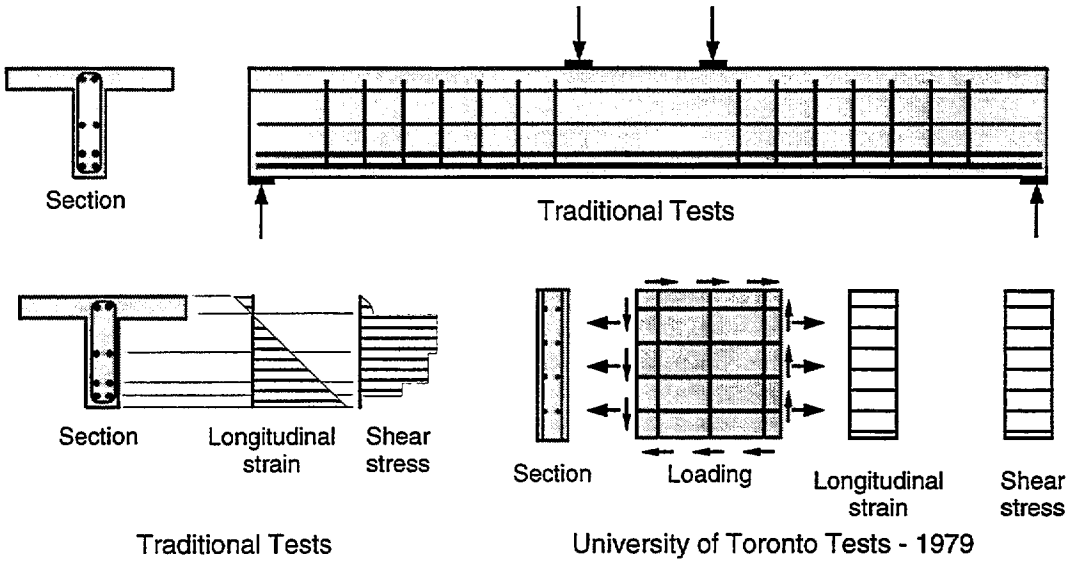

Figure 3.11 — Comparison of traditional beam tests with panel tests (adapted from Collins et al. 1993).

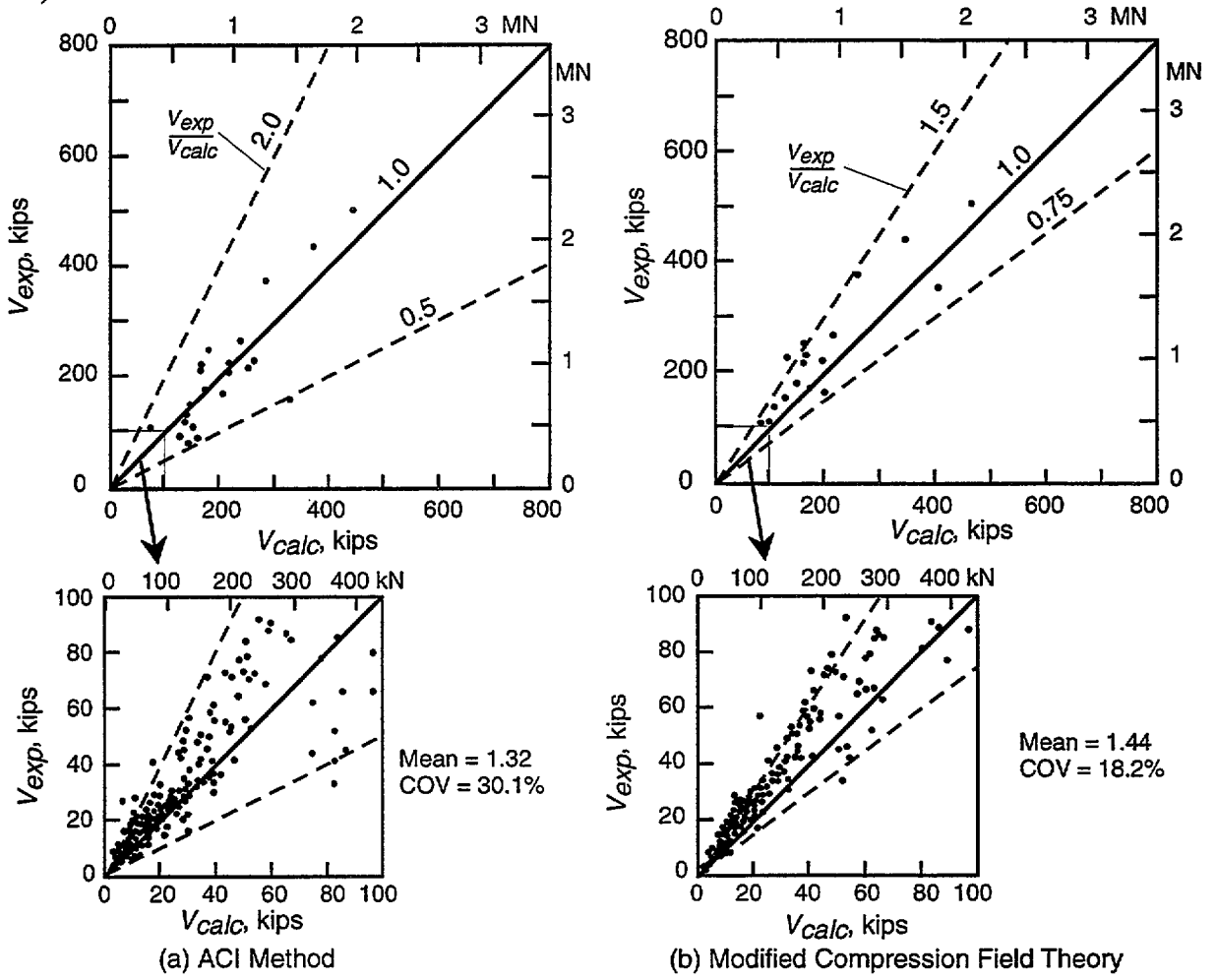

Figure 3.12 — Correlation of calculated and experimental shear strengths for 528 beam tests; (a) strength calculated according to ACI; (b) strength calculated according to modified compression field theory (adapted from Collins et al. 1996).

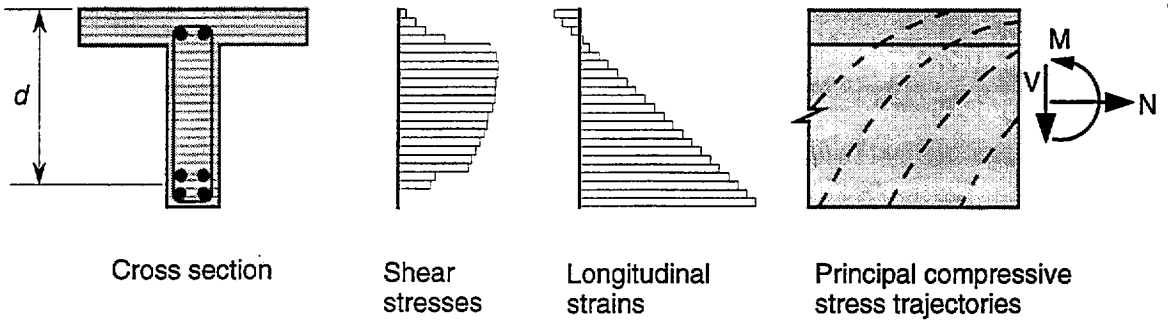

(a) Detailed Analysis

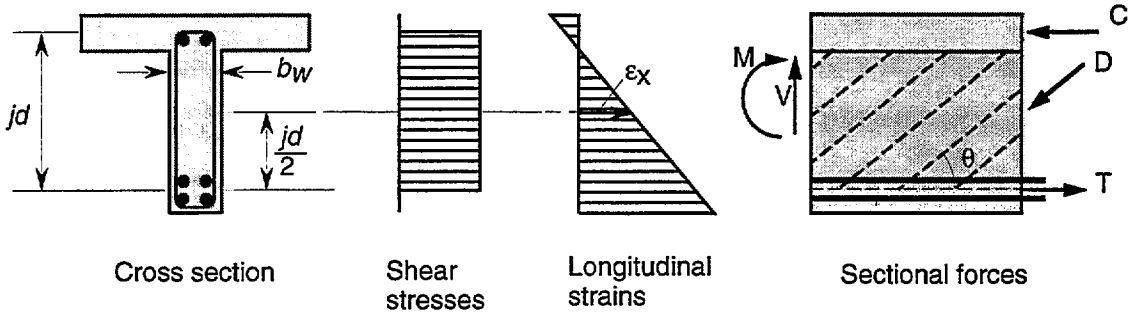

(b) Direct Procedure

Figure 3.13 — Distribution of shear stresses in (a) detailed analysis and (b) direct procedure (adapted from Collins and Mitchell 1991)

3.3 NS 3473E (Norwegian Standards, 4th. ed., Nov. 1992)

The Norwegian Code is applicable to concrete with strength up to 105 MPa = 15 200 psi (cube) or 94 MPa = 13 600 psi (cylinder) and allows three methods of shear design of increasing complexity:

1. A simplified method similar to ACI's $V_c + V_s$ (Clause 12.3.2),
2. A variable angle truss method (Clause 12.3.3), and
3. A general method based on the Modified Compression Field Theory (Clause 12.5 and A12.5).

In addition, strut-and-tie models are allowed for regions of discontinuity in geometry or loads (Clause 12.6).

Notation used in Norwegian Standards

A_c = Area of concrete,
A_s = Area of fully anchored tension reinforcement,
A_{sv} = Area of shear reinforcement unit,
$A_{sx,sy}$ = Area of longitudinal and transverse (vertical) reinforcement,
b_w = Web width,
d = Distance from extreme compression fiber to centroid of tension reinforcement,
D_o = Maximum aggregate size,
E_{cm} = Modulus of elasticity of concrete,
f_{cd} = Design compressive strength of concrete,
f_{c2d} = Reduced compressive design strength at simultaneous transverse tension,
f_{td} = Design tensile strength of concrete,
f_{sd} = Reinforcement design strength,
f_{sk} = Characteristic reinforcement strength defined as yield strength or 0.2 % proof test,
$f_{sdx, sdy}$ = Longitudinal and transverse (vertical) reinforcement design strength,
f_{tk} = Expected lower characteristic tensile strength of concrete,
I_c = Moment of inertia of uncracked concrete section,
M_f = Total moment in section acting in combination with shear force V_f,
M_o = $-N_f W_c / A_c$
s, s_y = Stirrup spacing,
S_c = Static moment about centroidal axis of one part of concrete section,
s_x = Depth of concrete web,
V_{ccd} = Shear capacity at compressive failure of concrete,
V_{cd} = Shear capacity at tensile failure of concrete,
V_{co} = Basic concrete shear strength,
V_f = Design shear force,
V_n = Nominal shear strength of section,
V_{sd} = Contribution of transverse reinforcement to shear resistance,
w = Mean crack width,
W_c = Section modulus of concrete cross-section about extreme tension fiber or fiber with least compression,
z = Internal moment arm of cross-section, $z = 0.9\,d$ if cross-section has a compressive zone,
z_1 = The greater of $0.7d$ and I_c/S_c,
α = Angle of reinforcement with longitudinal axis,
γ_c = Material coefficient for concrete,
$\varepsilon_{1,2}$ = Principal strains in concrete,

ε_{co} = Compressive strain in concrete corresponding to maximum stress,
ε_{ct} = Assumed strain at cracking of concrete,
$\varepsilon_{x,y}$ = Longitudinal or transverse strain,
σ_{cr} = Mean compressive stress normal to cracks,
$\sigma_{c1,2}$ = Principal stresses in concrete,
$\sigma_{sx,sy}$ = Mean stresses in longitudinal or (vertical) shear reinforcement,
$\sigma_{sxr,syr}$ = Stresses in longitudinal or (vertical) shear reinforcement at cracks,
τ = Shear stress,
τ_{cr} = Shear stress transferred by concrete in cracks,
τ_{rm} = Maximum shear stress which can be transmitted in a crack,
θ = Inclination of compression field to longitudinal axis.

3.3.1 Comparison of NS Simplified Method with ACI Method

NS 3473E §12.3.2 (Simplified Method)	ACI 318-95 (N, mm)
Members without Shear Reinforcement	
Tensile Failure in Shear	
$V_{cd} = V_{co} = 0.33\left(f_{td} + \frac{k_A A_s}{\gamma_c b_w d}\right) b_w d k_v \le 0.66 f_{td} b_w d k_v$ k_A = 100 MPa, A_s = fully anchored tension reinforcement, $1.0 \le k_v = 1.5 - \frac{d}{1\ meter} \le 1.4$ • NS uses concrete tensile strength explicitly rather than as a function of compressive strength (see Table 3.3). • NS accounts for the influence of the longitudinal reinforcement ratio but not of *a/d*, in a manner similar to ACI-ASCE Com. 426 (1977) revisions.	$V_c = \sqrt{f'_c} b_w d / 6$ (simple) • ACI assumes that flexural cracking occurs when the tensile strength reaches $0.5\sqrt{f'_c}$ MPa. • ACI recommends that the principal tensile stress at web shear cracking be taken as $0.33\sqrt{f'_c}$ MPa.
Tensile Failure in the Presence of Shear and Axial Compression	
$V_{cd} = V_{co} + 0.8\frac{M_o}{M_f} V_f \le \left(f_{td} k_v - \frac{0.25 N_f}{A_c}\right) b_w z_1$ $N_f / A_s < 0.4 f_{cd}$; $N_f < 0$ for compression. The additional term ($0.8 V_f M_O / M_f$) depends not only on the axial compression, but also on the ratio of shear to flexure at the design section. The axial compression is transformed into an equivalent moment.	$V_c = \left(0.166 + 0.012\frac{N_u}{A_g}\right)\sqrt{f'_c} b_w d$ (simple) $N_u > 0$ for compression

<table>
<tr><th colspan="2">Tensile Failure in the Presence of Shear and Axial Tension</th></tr>
<tr><td>$$V_{cd} = V_{co}\left(1 - \frac{N_f}{1.5 f_{td} A_c}\right) \geq 0$$
$N_f > 0$ for tension
Where there is a bending moment associated with the axial force, equation below should be used if it gives greater capacity than equation above.
$$V_{cd} = V_{co}\left(1 - \frac{M_o}{|M_f|}\right) \geq 0$$</td><td>$$V_c = \left(0.166 + 0.048\frac{N_u}{A_g}\right)\sqrt{f_c'}\, b_w d$$
$N_u < 0$ for tension</td></tr>
<tr><th colspan="2">Members with Shear Reinforcement</th></tr>
<tr><td>$$V_n = V_{cd} + V_{sd}$$
In calculating V_{cd}, set $k_v = 1.0$.
$$V_{sd} = \frac{A_{sv} f_{sd}}{s} z\,(1 + \cot\alpha)\sin\alpha$$</td><td>$$V_n = V_c + V_s$$
$$V_c = \left(0.16\sqrt{f_c'} + 17\frac{\rho_w V_u d}{M_u}\right) b_w d \leq 0.29\sqrt{f_c'}\, b_w d$$
(general)
$$V_s = \frac{A_v f_y (\sin\alpha + \cos\alpha)\, d}{s}$$
In the presence of axial compression:
$$V_c = \left(0.16\sqrt{f_c'} + 17\frac{\rho_w V_u d}{M_m}\right) b_w d \leq 0.29\sqrt{f_c'}\, b_w d \sqrt{1 + \frac{N_u}{3.45 A_g}}$$
with $M_m = M_u - N_u\left(\frac{4h - d}{8}\right)$
$N_u > 0$ for compression (general)</td></tr>
<tr><th colspan="2">Compression Failure In Shear</th></tr>
<tr><td>$$V_{ccd} = 0.25 f_{cd} b_w z\,(1 + \cot\alpha) \leq 0.45 f_{cd} b_w z$$
This implies
$$\cot\alpha \leq \frac{0.20}{0.25} \quad \text{or} \quad \alpha \geq 51°$$</td><td>No explicit provision. However
$$V_s \leq V_{smax} = 0.7\sqrt{f_c'}\, b_w d$$
for crack control, where V_s = shear force carried by stirrups.</td></tr>
</table>

The unfavorable effect of brittleness for the higher strength concrete is taken into account by keeping the tensile strength, and hence the design shear strength, constant from C85 upwards (cube strength 85 MPa, cylinder strength 74 MPa, in-situ tensile strength 2.70 MPa. See Table 3.3).

3.3.2 Variable Angle Truss Method (NS 3473E §12.3.3.1)

"The capacity for shear force only or in combination with other action effects can be calculated based on an assumed internal truss model with compressive concrete struts at an angle θ to the longitudinal axis of the beam. The shear reinforcement acts as tension ties, and the tensile and the compressive zones as chords in the assumed truss. A capacity portion V_{cd} like in Clause 12.3.2 shall not be included in the capacity."

3.3.3 General Design Method For Structural Members Subjected To In-Plane Force (NS 3473E §12.5.1)

The Modified Compression Field Theory (MCFT) is also an acceptable design method.

"Design for forces acting in the middle plane of a structural member may be performed by a method based on an assumed internal force model satisfying equilibrium conditions and compatibility requirements for the local region to be designed.

The concrete is assumed to transfer compression by compression fields, and the reinforcement in two or more directions transfers tension. Under certain conditions, a limited transfer of shear forces parallel to the cracks and tension in concrete between the cracks may be assumed.

Strains and stresses shall be calculated as average values over a cracked region. The strain can be assumed constant in local regions and through the thickness. Average strain in the reinforcement can be assumed equal to the average strain parallel to the direction of reinforcement for the region. Principal stress and principal strain of the concrete are assumed to have the same direction in the assumed compression field." (NS 3473E §12.5.1).

NS 3473E §12.5, A12.5 (General Method)	MCFT (Collins and Mitchell, 1991)
Uniaxial Compression	
$\sigma_{c2} = f_{c2d}\frac{\varepsilon_2}{\varepsilon_{co}}\left(2 - \frac{\varepsilon_2}{\varepsilon_{co}}\right)$ for $\lvert\varepsilon_2\rvert \le \lvert\varepsilon_{co}\rvert$ $\varepsilon_{co} = -0.002$; $\varepsilon_2 < 0$ for compression. See Fig. 3.14	$f_2 = f_{2\max}\left[2\left(\frac{\varepsilon_2}{\varepsilon'_c}\right) - \left(\frac{\varepsilon_2}{\varepsilon'_c}\right)^2\right]$ $\varepsilon'_c = 0.002$. See Figs. 2.17 a,c
Biaxial Tension-Compression	
$f_{c2d} = \frac{f_{cd}}{0.8 + 100\varepsilon_1} < f_{cd}$	$f_{2\max} = \frac{f'_c}{0.8 + 170\varepsilon_1} < f'_c$
Principal Tensile Strain in Concrete Web	
$\varepsilon_1 = \varepsilon_x + (\varepsilon_x - \varepsilon_2)\cot^2\theta$ For simplification $\varepsilon_2 = \varepsilon_o = -0.002$; $\varepsilon_x = 0.002$	$\varepsilon_1 = \varepsilon_x + (\varepsilon_x - \varepsilon_2)\cot^2\theta$

Principal Compressive Stress in Concrete Web	
$\sigma_{c2} = \sigma_{c1} - \tau(\tan\theta + \cot\theta)$	$-f_2 = f_1 - v(\tan\theta + \cot\theta)$
Mean Reinforcement Strain	
$\varepsilon_x = \varepsilon_1 \sin^2\theta + \varepsilon_2 \cos^2\theta$ $\varepsilon_y = \varepsilon_1 + \varepsilon_2 - \varepsilon_x$ Mohr circle	$\varepsilon_t = \varepsilon_1 + \varepsilon_2 - \varepsilon_x$
Mean Tensile Stress Between Cracks	
$\sigma_{c1} = \varepsilon_1 E_{cd}$ for $\varepsilon_1 < \varepsilon_{ot}$ $\sigma_{c1} = 0.5 f_{td}$ for $\varepsilon_1 \geq \varepsilon_{ot}$ where $\varepsilon_{ot} = f_{cd} / E_{cd}$ = assumed strain at cracking $E_{cd} = E_{cn} / \gamma_c$ See Fig. 3.15 a.	$f_1 = \varepsilon_1 E_c$ for $\varepsilon_1 \leq \varepsilon_{cr}$ $f_1 = \dfrac{\alpha_1 \alpha_2 f_{cr}}{1 + \sqrt{500\varepsilon_1}}$ for $\varepsilon_1 > \varepsilon_{cr}$ α_1, α_2 account for bond characteristics of the reinforcement and type of loading. See Fig. 3.15 b.
Shear Stress Across Cracks	
$\dfrac{\tau_{cr}}{\tau_{rm}} = 1 - 0.82\left(1 - \dfrac{\sigma_{cr}}{\tau_{rm}}\right)^2$ $\tau_{rm} = \dfrac{2 f_{td}}{0.31 + 24\dfrac{w}{D_o + 16}}$ See Fig. 3.16. If $\sigma_{cr} = 0$, NS and Collins agree.	$v_{ci} = \dfrac{0.18\sqrt{f_c'}}{0.3 + 24\dfrac{w}{a + 16}}$ $\sigma_{cr} = 0$ See Fig. 2.20.
Crack Spacing	
Mean crack spacing $\leq 0.8\,z$.	Crack spacing according to CEB-FIP. $s_{mx} = 2\left(c_x + \dfrac{s_x}{10}\right) + 0.25\,k_1 \dfrac{d_{bx}}{\rho_x}$ $s_{mv} = 2\left(c_v + \dfrac{s}{10}\right) + 0.25\,k_1 \dfrac{d_{bv}}{\rho_v}$

Stresses in Shear Reinforcement (Vertical) at Cracks:	
$\sigma_{syr} = \sigma_{sy} + \frac{\sigma_{c1} + \sigma_{cr} - \tau_{cr}\tan\theta}{\rho_y} \le f_{sdy}$ with $\rho_y = \frac{A_{sy}}{b_w s_y}$	f_v = yield at crack $f_1 = v_{ci}\tan\theta + \rho_v(f_{vy} - f_v)$ or $f_{vy} = f_v + \frac{f_1 - v_{ci}\tan\theta}{\rho_v}$ with $\rho_v = \frac{A_v}{b_w s}$ Since f_{vy} = yield, this equation gives f_1.
Stresses in Longitudinal Reinforcement at Cracks	
$\sigma_{sxr} = \sigma_{sx} + \frac{\sigma_{c1} + \sigma_{cr} + \tau_{cr}\cot\theta}{\rho_x} \le f_{sdx}$ with $\rho_x = \frac{A_{sx}}{b_w s_x}$	f_x = yield at crack $f_{sx} + \frac{f_1 + [f_1 - \rho_v(f_{vy} - f_v)]\cot^2\theta}{\rho_x} \le f_y$ $\rho_x = \frac{A_{sx}}{b_w jd}$ This equation limits f_1.

NS does not provide any guidance on calculation of θ and is even more general than MCFT:

- there may be compressive stresses perpendicular to crack interface, and
- reinforcement can be below yield at cracks.

3.3.4 Minimum Shear Reinforcement

Due to the higher tensile strength of high strength concrete, a HSC member will have a higher cracking shear and hence will require a larger amount of minimum reinforcement than an identical member made with NSC.

At least half of the shear reinforcement is to be provided by stirrups (Clause 12.3.1.5) whose cross-sectional area must exceed (Clause 18.3.6):

$$A_s \ge 0.2 A_c f_{tk} \sin\alpha / f_{sk}$$

In North American notation and practice, $A_c = b_w s$, $f_{sk} = f_y$ and $\alpha = 90°$:

$$A_{vmin} = 0.2 \frac{f_{tk}}{f_y} b_w s$$

Concrete tensile strength f_{tk} is measured by the split cylinder test and is about 1.5 times smaller than the beam rupture test: $f_r \approx 1.5 f_{tk}$. NS does not give a formula relating f_{tk} to f'_c, but rather a table (Table 3.3).

Fig.3.17 compares concrete tensile strength as a function of compressive strength for various national codes. It is also interesting to compare the minimum stirrup requirement of the Norwegian, European, American and Canadian Standards for high strength concrete.

$$\text{NS, CEB} \quad A_v f_y / (b_w s) = 0.2 f_{tk}$$
$$\text{ACI} \quad A_v f_y / (b_w s) = 0.01 f_c'$$
$$\text{CSA} \quad A_v f_y / (b_w s) = 0.06 \sqrt{f_c'}$$
$$\text{AASHTO} \quad A_v f_y / (b_w s) = 0.083 \sqrt{f_c'}$$

f'_c (MPa)	36	44	54	64	74	84	94
f_{tk} (MPa)	2.95	3.30	3.65	4.00	4.30	4.60	4.90
f_{tn} (MPa)	2.00	2.25	2.50	2.60	2.70	2.70	2.70
NS, CEB	0.59	0.66	0.73	0.80	0.86	0.92	0.98
AASHTO	0.50	0.55	0.61	0.66	0.71	0.76	0.81
ACI	0.36	0.44	0.54	0.64	0.74	0.84	0.94
CSA	0.36	0.40	0.44	0.48	0.52	0.55	0.58

Table 3.3 Concrete Tensile Strengths (expected f_{tk} nominal f_{tn}) and Minimum Shear Reinforcement Ratios $A_v f_y / (b_w s)$ required by various Codes for various Compressive Strengths f'_c.

The ACI requirements fall between the Norwegian and the Canadian requirements. Also the increase in tensile strength is fairly linear versus the increase in compressive strength.

3.3.5 Strut-and-Tie Method § 12.6

In regions with discontinuity in geometry or loads, internal forces shall be calculated based on an assumed force model of compression struts of concrete and tension ties of reinforcement. Calculated concrete stresses in struts shall not exceed f_{c2d}:

$$f_{c2d} = \frac{f_{cd}}{0.8 + 100\varepsilon_1} < f_{cd}$$

If the reduced compressive concrete strength f_{c2d} is not derived from the strain condition, the calculated compressive concrete stress in the assumed joints shall not exceed the following values:

$1.1 f_{cd}$ in joints where no tensile reinforcement is anchored;

$0.9 f_{cd}$ in joints where tensile reinforcement in only one direction is anchored;

$0.7 f_{cd}$ in joints where tensile reinforcement in more than one direction is anchored.

Tensile forces caused by possible deviation in the assumed compressive field shall be considered. Examples of strut and tie models are provided in the *Commentary* of the Code.

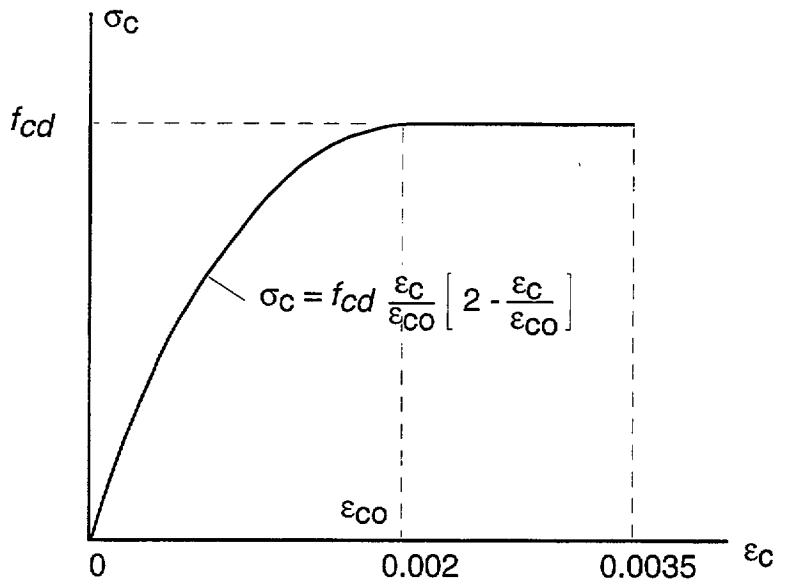

Figure 3.14 — Simplified compressive stress-strain curve for normal density concrete (grades C25 to C55) according to NS 3473E

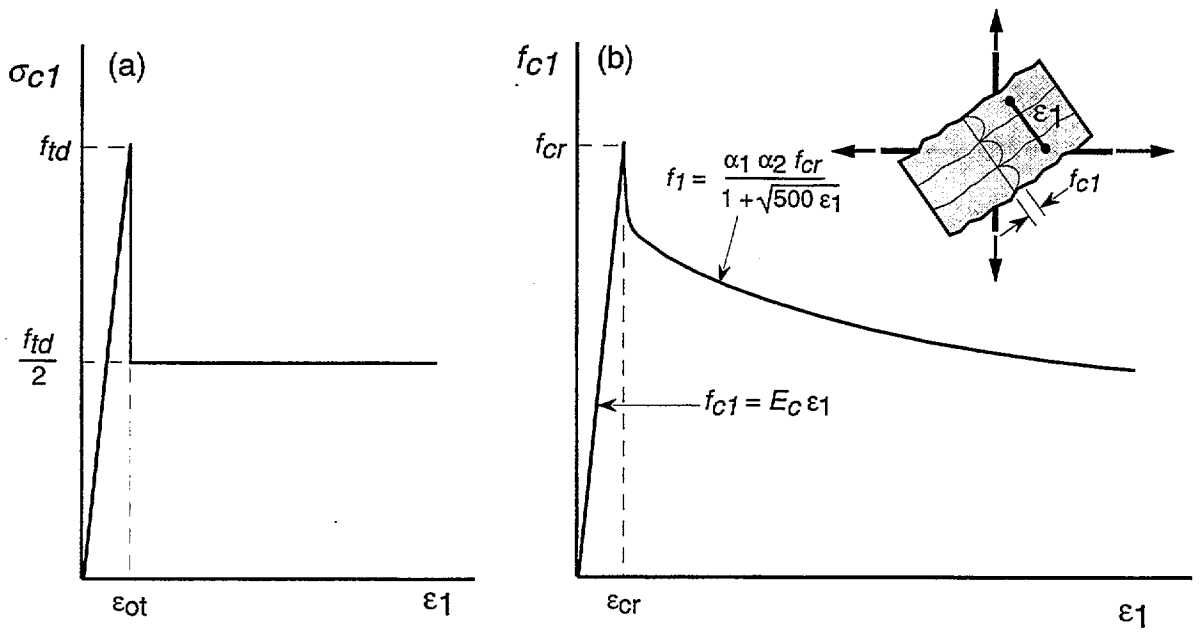

Figure 3.15 — Tensile stress-strain curves according to (a) NS 3473E and (b) modified compression field theory

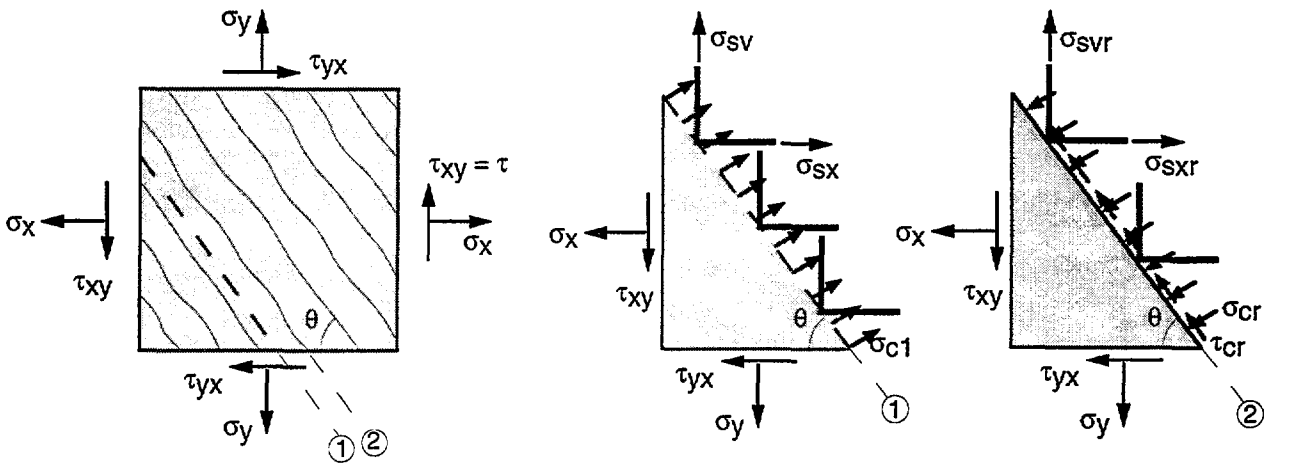

Figure 3.16 — Basis for determination of equilibrium in cracked concrete according to NS 3473E (compare with Fig. 2.20)

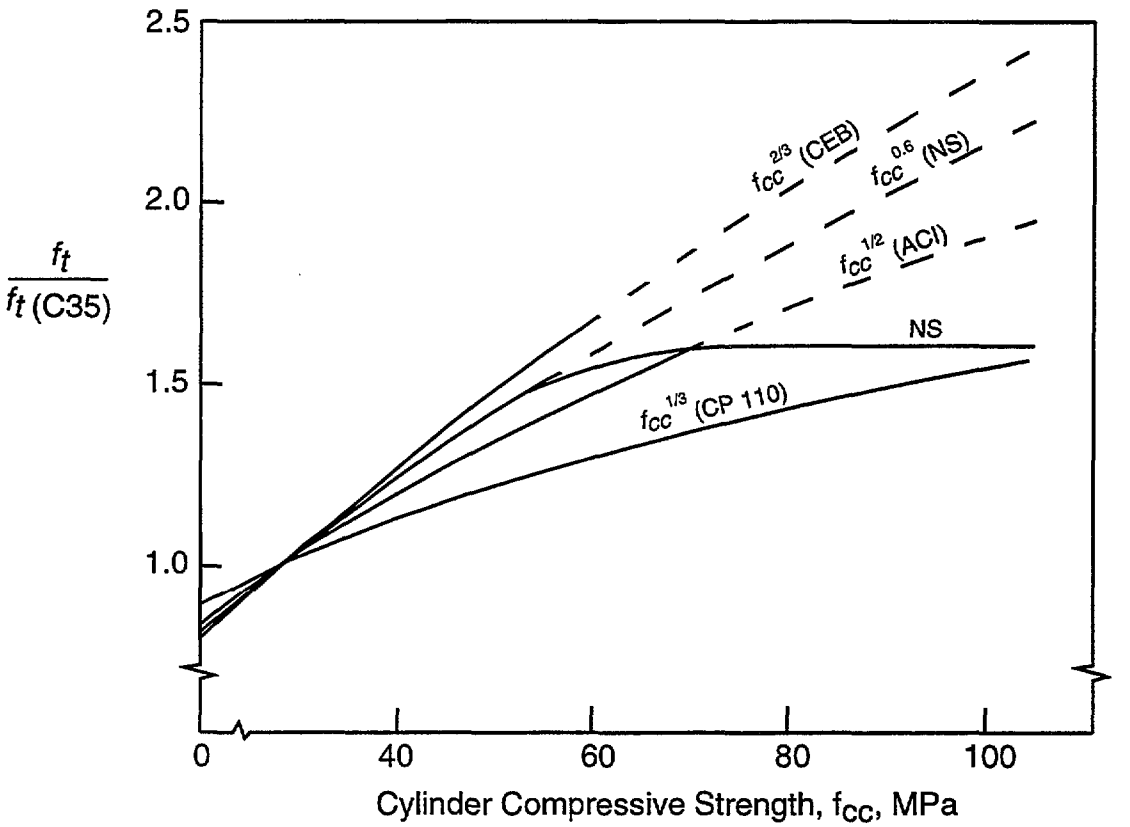

Figure 3.17 — Comparison of concrete tensile strength parameter as a function of compressive strength for different codes (adapted from CEB-FIP 1990)

3.4 AASHTO'S LRFD BRIDGE DESIGN SPECIFICATION (1994)

AASHTO (American Association of State Highway and Transportation Officials), in its *LRFD Bridge Design Specification (1994)*, recommends the Modified Compression Field Theory as the design method for shear, or shear combined with torsion, for reinforced concrete or prestressed concrete members. For non-prestressed sections, a simplified procedure is allowed which results in the expression for shear strength being essentially identical to the ACI traditional equations or the 1996 16th Edition AASHTO *Standard Specifications for Highway Bridges* (by using a strut angle of 45° and coefficient $\beta = 2.0$ where $v_c = \beta\sqrt{f'_c}$ psi).

The minimum amount of transverse reinforcement is proportional to $\sqrt{f'_c}$:

$$A_v = 0.0316\sqrt{f'_c}\frac{b_v s}{f_y} = \sqrt{\frac{f'_c}{1000}}\frac{b_v s}{f_y} \qquad \text{inch-kips system}$$

$$A_v = 0.0830\sqrt{f'_c}\frac{b_v s}{f_y} \qquad \text{mm-Newton system}$$

where b_v is the effective web width. This is 38 % more than required by the Canadian 1994 Code. See Table 3.3.

The concrete contribution to shear resistance is:

$$V_c = 0.0316\,\beta'\sqrt{f'_c}\,b_v d_v \qquad \text{inch-kips system}$$

$$V_c = (\beta'/12)\sqrt{f'_c}\,b_v d_v \qquad \text{mm-Newton system}$$

where d_v is the effective shear depth. Note that $\beta'_{\text{AASHTO}} = 12\,\beta_{\text{CSA}}$.

Designers may also use the strut-and-tie method, with provisions identical to the Canadian Code of 1994.

3.5 Japanese Code (1988)

Aoyama (1992) explains the philosophy behind the 1988 Japanese *Design Guideline for Earthquake Resistant Reinforced Concrete Buildings Based on Ultimate Strength Concept* proposed by the Architectural Institute of Japan (AIJ). Essentially, shear resistance is provided by a combination of truss action and arch action. One remarkable feature of the *Guideline* is its consideration of inelastic deformation capacity. It is otherwise an equilibrium theory with no consideration of strain compatibility.

Arch action

A straight arch, inclined at an angle θ with respect to the horizontal, and of vertical depth equal to half of the beam depth is assumed. If the axial compression in the arch is σ_a , then the shear carried by arch action is:

$$V_a = b\,\frac{D}{2}\,\sigma_a \tan\theta$$

$$\text{where} \quad \tan\theta = \frac{\sqrt{L^2 + D^2} - L}{D} \simeq \frac{D}{2L}$$

and b, D, L are beam dimensions (Fig. 3.18).

Truss action (variable angle truss)

The truss mechanism depends on the amount of web reinforcement; if no web reinforcement is provided, this mechanism does not exist. As the amount of web reinforcement increases, the share for the arch mechanism must be reduced.

Equilibrium of a joint in the upper chord gives (Fig 3.19):

$$\sigma_t = \frac{\rho_w \sigma_{wy}}{\sin^2\phi} = \rho_w \sigma_{wy}(1 + \cot^2\phi) \tag{3.2}$$

where σ_t = average diagonal compression,

ρ_w = web reinforcement ratio,

ϕ = inclination of the compression strut, and

$25 f_c' \geq \sigma_{wy}$ = yield strength of web reinforcement.

The shear carried by truss action is:

$$V_t = b j_t \rho_w \sigma_{wy} \cot\phi$$

where j_t is the distance between the centroids of the axial reinforcement.

The total shear carried by the member is:

$$V_u = V_t + V_a = b j_t \rho_w \sigma_{wy} \cot\phi + b \frac{D}{2} \sigma_a \tan\theta \tag{3.3}$$

Provisions for non-ductile members

The ultimate shear V_u is attained when the web reinforcement stress reaches the yield point σ_{wy} and the concrete reaches its maximum capacity, which is reduced from cylinder strength $\sigma_B = f_c'$ by a factor ν_o because of diagonal cracking.

$$\sigma_t + \sigma_a = \nu_o \sigma_B \tag{3.4}$$

Note that the difference between the truss inclination ϕ and the arch inclination θ is neglected here for simplicity. The reduction factor is adopted from Nielsen's shear tests of T-beams (Nielsen 1984): $\nu_o = 0.7 - \sigma_B / 200$ (MPa) = strength reduction factor for web concrete of non-ductile members. The above equation gives increasing effective strength $\nu_o \sigma_B$ up to $\sigma_B = 70$ MPa at which point $\nu_o \sigma_B$ reaches a maximum of 24.5 MPa

Introducing

$$\beta = \frac{\sigma_t}{\nu_o \sigma_B} = \frac{\rho_w \sigma_{wy}(1 + \cot^2\phi)}{\nu_o \sigma_B} \tag{3.5}$$

Eq. 3.3 can be rewritten as

$$V_u = b j_t \rho_w \sigma_{wy} \cot\phi + b \frac{D}{2}(1-\beta) \nu_o \sigma_B \tan\theta \tag{3.6}$$

where the truss angle ϕ is the only unknown.

Considering the possible limitation of aggregate interlock with increasing crack width, Thürlimann (1979) sets the limit:

$$\cot\phi \leq 2 \qquad (\text{or } \phi \geq 26.5°) \tag{3.7}$$

From Eq. 3.4, σ_t must be less than $\nu_o \sigma_B$. From Eq. 3.2

$$\cot\phi \le \sqrt{\frac{\nu_o \sigma_b}{\rho_w \sigma_{wy}} - 1} \tag{3.8}$$

With Eq. 3.5, Eq. 3.6 is a quadratic equation in $\cot\phi$. The solution of that equation is

$$\cot\phi = \frac{b j_t \rho_w \sigma_{wy} + \sqrt{\Delta}}{b D \rho_w \sigma_{wy} \tan\theta}$$

$$\text{where} \quad \Delta = (b j_t \rho_w \sigma_{wy})^2 - b D \rho_w \sigma_{wy} \tan\theta \, [2V_u - b D \tan\theta \, (\nu_o \sigma_B - \rho_w \sigma_{wy})]$$

$$\text{which leads to} \quad \cot\phi \ge \frac{j_t}{D \tan\theta}. \tag{3.9}$$

According to the lower bound theorem of the theory of plasticity, $\cot\phi$ may be taken to be the largest value within the range of Eqs. 3.7, 3.8 and 3.9 in order to maximize the ultimate shear V_u of Eq. 3.6.

Figure 3.20a illustrates the relationship between the normalized ultimate shear and the normalized web reinforcement for members in which Eq. 3.7 controls over Eq. 3.9, i.e. members of ordinary length $j_t / (D \tan\theta) \ge 2$.

Eq. 3.6 can be rewritten as follows:

$$\frac{V_u}{b j_t \nu_o \sigma_B} = \frac{\rho_w \sigma_{wy}}{\nu_o \sigma_B} \cot\phi + (1-\beta) \frac{D \tan\theta}{2 j_t} \tag{3.10}$$

When $\rho_w \sigma_{wy} = 0$, $\beta = 0$ (Eq. 3.5), hence point A in Fig. 3.20a is obtained (which cannot be greater than 0.25 due to the above-mentioned member length limitation $j_t / (D \tan\theta) \ge 2 \Rightarrow D \tan\theta / (2 j_t) \le 1/4$). Between points A and B, Eq. 3.7 governs. Hence $\cot\phi = 2.0$ and $\beta < 1$, and the ultimate shear consists of the truss mechanism of line OB and the arch mechanism of the shaded zone OAB. Beyond point B, Eq. 3.8 governs:

$$\cot\phi = \sqrt{\frac{\nu_o \sigma_B}{\rho_w \sigma_{wy}} - 1}$$

From Eq. 3.5, $\beta = 1$. The arch action term disappears from Eq. 3.10 and the first term gives a circle centered at G. Let

$$Y = \frac{V_u}{b j_t \nu_o \sigma_B} \quad \text{and} \quad X = \frac{\rho_w \sigma_{wy}}{\nu_o \sigma_B}$$

Eq. 3.10 becomes the familiar plastic solution, Eq. 2.12:

$$Y = X \sqrt{\frac{1}{X} - 1} \quad \Rightarrow \quad Y^2 = X - X^2 \quad \Rightarrow \quad \left(X - \frac{1}{2}\right)^2 + Y^2 = \frac{1}{4}$$

In this range, shear is carried by the truss mechanism only. The upper bound for shear reinforcement is given by point C, or $\rho_w \sigma_{wy} = \nu_o \sigma_B / 2$.

Figure 3.21b illustrates a similar relationship for very short members (with $j_t / (D \tan\theta) < 2$), for which Eq. 3.9 controls over Eq. 3.7 .

Provisions for ductile members (Ichinose 1990)

Ductile members develop yield hinges estimated to be 1.5 D in length and characterized by a criss-cross set of inclined cracks. Two modifications are made to the previous case to account for such cracks.

First, the effective strength of web concrete $\nu\,\sigma_B$ is lowered by the following equations:

$$\nu = (1 - 15R_p)\nu_o \qquad \text{for} \quad R_p \le 0.05$$

$$\nu = \frac{\nu_o}{4} \qquad \text{for} \quad R_p \ge 0.05$$

where R_p = expected maximum hinge rotation angle.

Secondly, the upper limit of $\cot\phi$ in Eq.3.7 is reduced as follows :

$$\cot\phi = \lambda$$

$$\text{where} \quad \lambda = 2 - 50R_p \qquad \text{for} \quad R_p \le 0.02$$

$$\lambda = 1 \qquad \text{for} \quad R_p > 0.02$$

The commentary of Chapter 4 of the *Guideline* recommends maximum expected rotations, from which values of ν and $\cot\phi$ can be derived.

	$1 / R_p$	ν / ν_o	$\cot\phi$
Columns:	67	0.775	1.25
Beams:	50	0.700	1
Beams connected to walls:	40	0.625	1

Reduced $\cot\phi$ in the hinge zones corresponds to the reduction of aggregate interlock due to the large rotations of the hinge zones. Beyond the hinge zones, $\cot\phi$ gradually increases to a constant value determined by Eqs. 3.7, 3.8 and 3.9.

Experimental Confirmation

Experimental data include beams of concrete strength 16.5 - 62.9 MPa, tensile reinforcement ratio 0.39 - 3.21 %, web reinforcement ratio 0 - 2.44%, web reinforcement yield strength 253 - 1470 MPa, product of the last two variables 0 - 19.1 MPa and axial stress ratio to concrete strength 0 - 0.732. The comparison between theory and experiments is satisfactory, in spite of the absence of axial force in the theory. Also, experimental observations show that the design methods of the *Guideline* generally provide sufficient deformation capacity for the yield hinges.

Figs. 3.21-3.24 from Takagi and Kanoh (1992) show test data versus the ACI and the AIJ Code equations. Also shown are Fukuhara's formulas (Fukuhara 1985, Fukuhara and Kokusho 1982) for shear tension failure:

$$Q_{u,st} = \left(k_u k_p \frac{0.12\,(18 + f_c')}{a/D + 0.12} + \alpha \rho_w \sigma_{wy} \right) bj$$

$$\alpha = -5.1 * 10^{-4} \sigma_{wy} + 1.7 \qquad \text{mm, N}$$

and for shear compression failure:

$$Q_{u,sc} = (0.124\,\rho_w \sigma_{wy} + 82\,\rho_c + 0.14 f_c' \sqrt{D/a})\, bj \qquad \text{mm, N}$$

where

f'_c = specified cylinder strength of concrete,
σ_{wy} = yield strength of web reinforcement,
D = total depth,
a = shear span = M/Q,
b = section width,
j = 7/8 of effective depth d,
k_u = coefficient modified by d,
k_p = coefficient modified by ρ_w,
ρ_c = longitudinal compression reinforcement ratio,
ρ_t = longitudinal tension reinforcement ratio,
ρ_w = web reinforcement ratio.

Fukuhara's formulas fit the experimental data well. Logically, the shear-compression failure formula should not depend on σ_{wy}. The dependence is, however, small. The AIJ formula also fits experimental data well. However, the formula may overestimate the shear strength of heavily reinforced (high values of $\rho_w \sigma_{wy}$) columns under high axial stress.

Alternate method (in Commentary of *Guideline*).
An alternate method developed by Minami and Kuramoto (1987) differs from the above by:

1. truss angle $\phi = 45°$ at all times,
2. the strength reduction factor for web concrete is a function of the shear span ratio, and
3. shear design in the hinge zone is carried out by expressing the ratio of shear versus flexural strength as a function of the expected maximum hinge rotation angle.

Authors' note: Since HSC is more brittle than NSC, v may have to be adjusted in vf_c' (plastic plateau). This has implications for the amount of ductility available in struts .

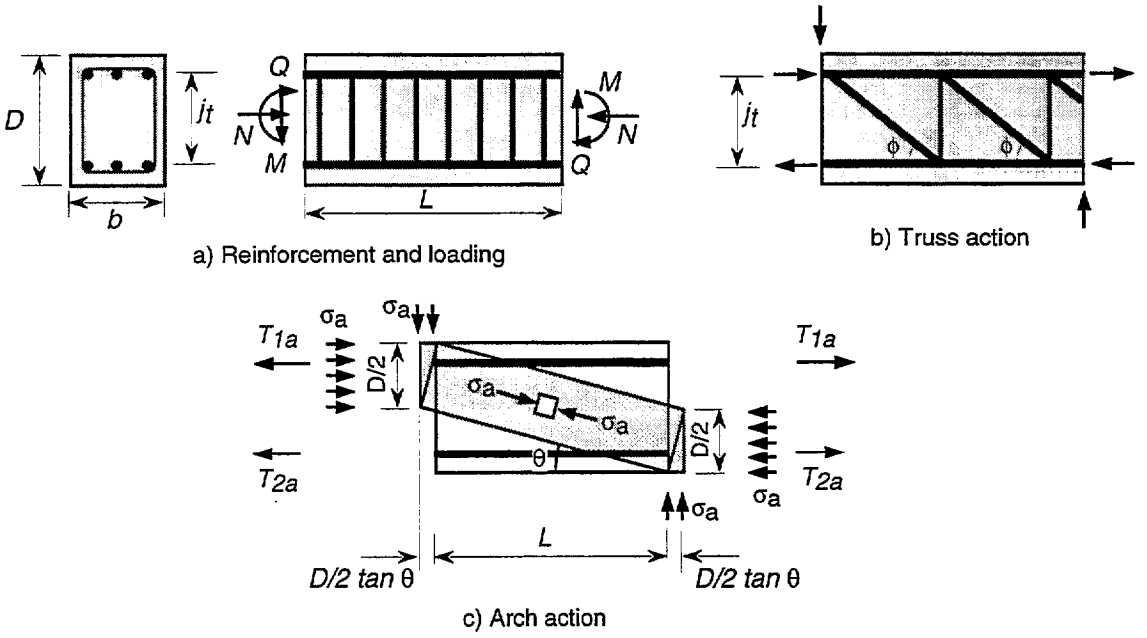

Figure 3.18 — Truss action and arch action in a member subjected to bending moment and shear force (adapted from Aoyama 1992)

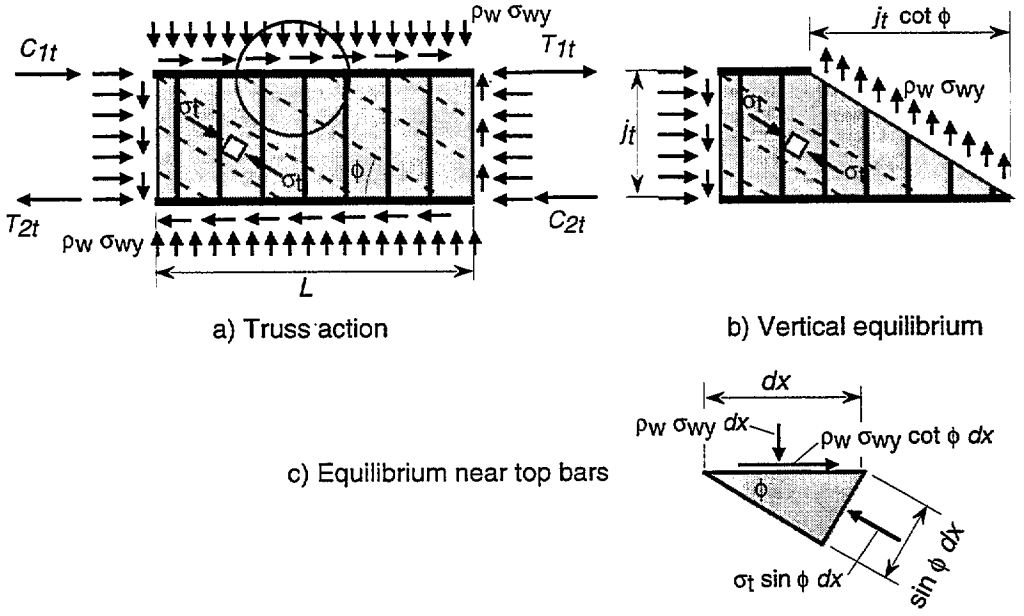

Figure 3.19 — Equilibrium in truss action (adapted from Aoyama 1992)

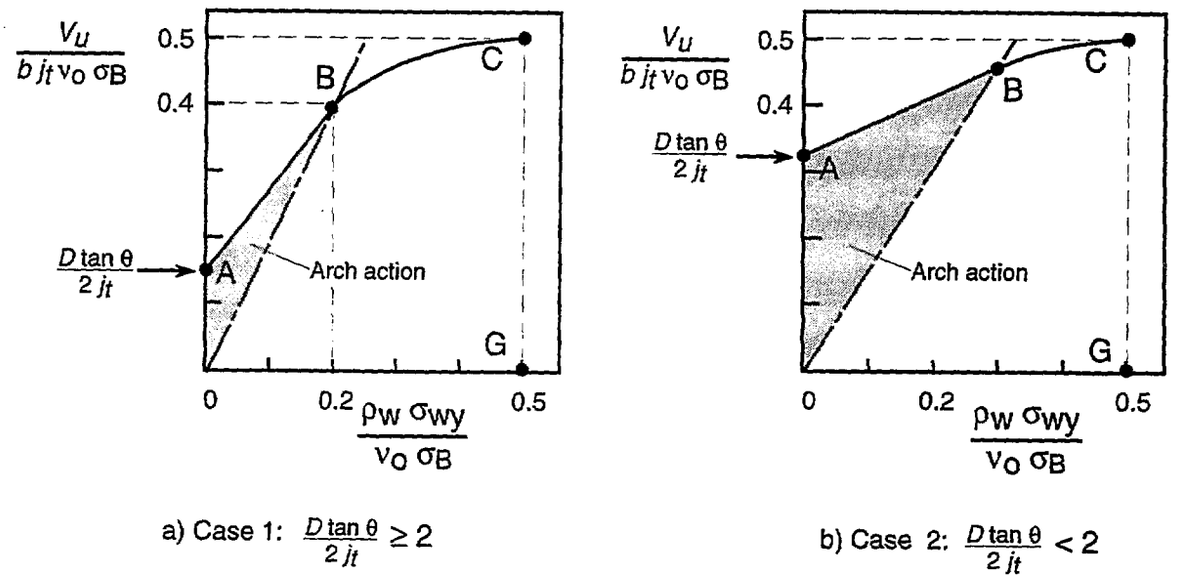

Figure 3.20 — Relationship between shear reinforcement and shear strength in a non-ductile member (adapted from Aoyama 1992)

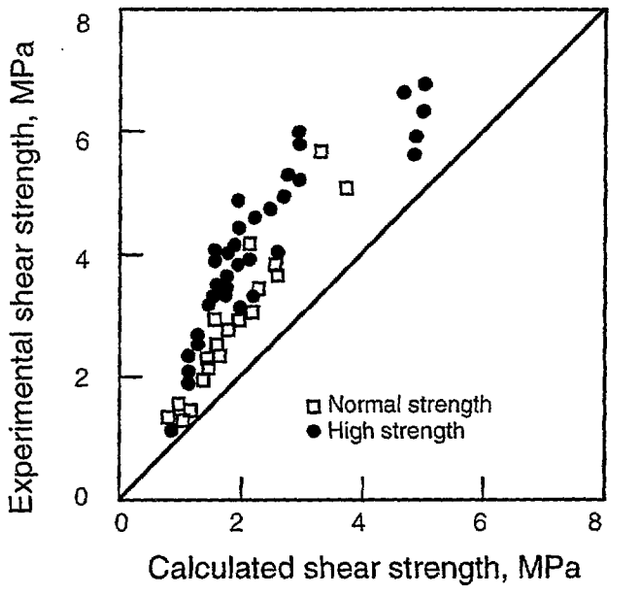

Figure 3.21 — Comparison of experimental shear strength with calculated values by ACI formula (adapted from Takagi and Kanoh 1991)

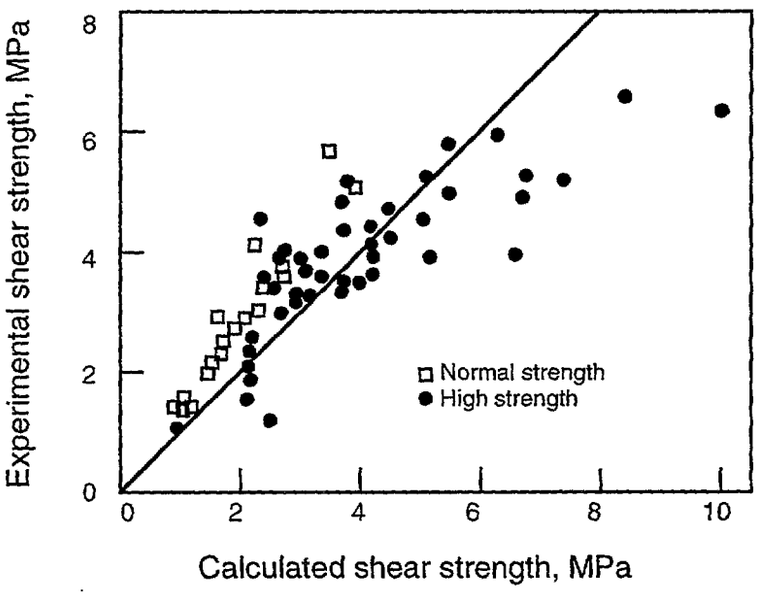

Figure 3.22 — Comparison of experimental shear strength with calculated values by ACI formula based on actual yield strength of transverse reinforcement (adapted from Takagi and Kanoh 1991)

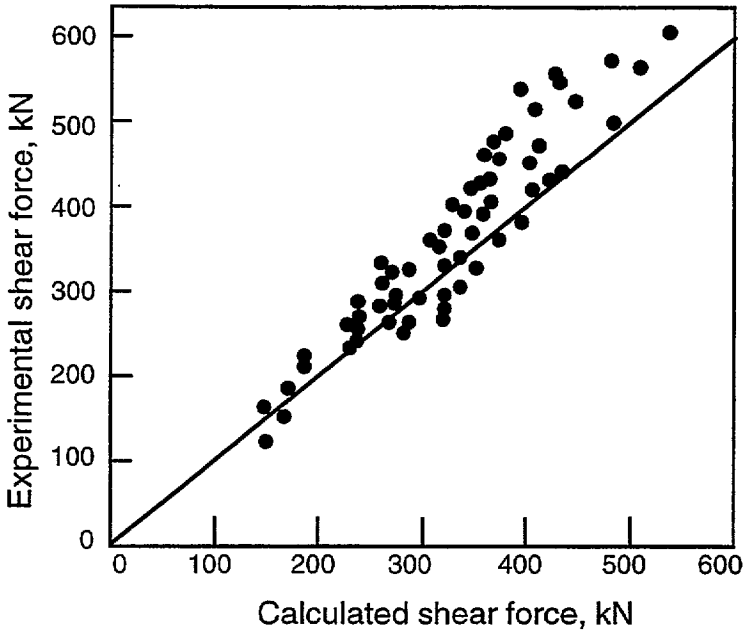

Figure 3.23 — Comparison of experimental shear force with calculated values by Fukuhara's formula (adapted from Takagi and Kanoh 1991)

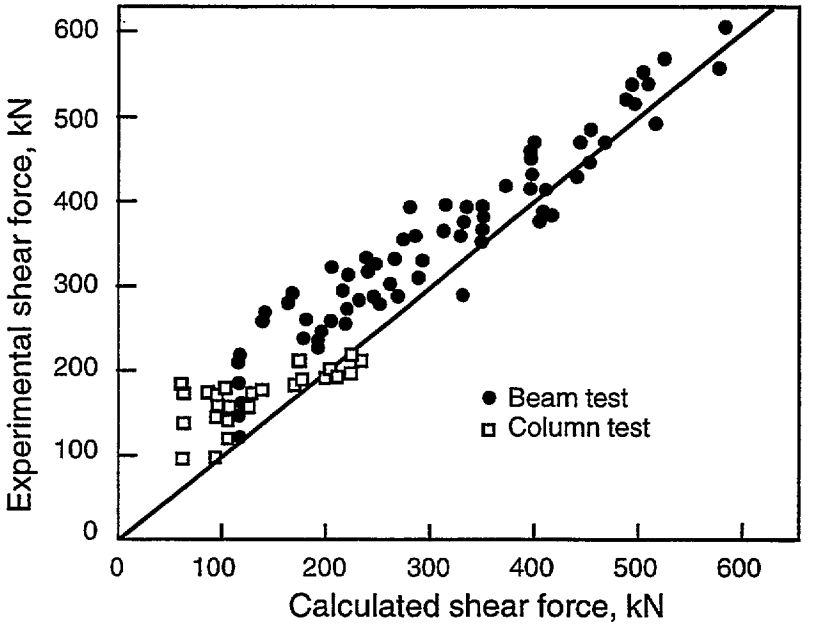

Figure 3.24 — Comparison of experimental shear force with calculated values by Architectural Institute of Japan formula (adapted from Takagi and Kanoh 1991)

3.6 European CEB-FIP Model Code (1990)

Although it can be used directly by designers, the CEB-FIP Model Code is mainly intended as a model for various national and international codes. For this reason it adopts a more theoretical approach than typical national codes. The CEB-FIP uses a variable angle truss model (§ 6.3.3.1), where the angle of inclination θ of the struts is allowed to vary between 18.4° and 45° to the longitudinal axis ($18.4° \leq \theta \leq 45°$ or $3 \geq \cot\theta \geq 1$). No V_c term is required, which would be necessary to correct the $\theta = 45°$ truss, as in the ACI Code. This is an equilibrium model with no attempt at satisfying strain compatibility. In the following, for simplicity, load and resistance factors are set to 1 and the angle of the stirrups is set to 90°:

Concrete compression (Fig. 2.15):

$$\frac{V_{Sd}}{\sin\theta} = f_{cd2}\, b_w\, z \cos\theta$$

where b_w = web width,
f_{cd2} = reduced concrete compressive strength due to transverse tension,
V_{Sd} = design shear load, and
z = shear depth.

Tension in transverse reinforcement (Fig.2.15):

$$V_{Sd} = \frac{A_{Sw} f_{yd}}{s} z \cot\theta$$

where A_{Sw} = area of transverse reinforcement,
f_{yd} = design yield stress of transverse reinforcement,
s = spacing of transverse reinforcement.

Chords (Fig. 2.15):

Tension due to shear $(V_{sd}/2)\cot\theta$ must be added to the tension or compression due to axial load and bending in the chords.

Reduced concrete strength (§ 3.4):

For cracking parallel to the direction of applied compression, the reduced design concrete strength due to transverse tension can be taken as:

$$f_{cd2} = \frac{f_{cd}}{1 + k\,\varepsilon_1 / \varepsilon_o}$$

where f_{cd} = concrete design compressive strength,
ε_o = concrete strain (about 0.002) at maximum compressive stress,
ε_1 = smeared tensile strain of cracked RC perpendicular to applied compression,
k = coefficient which depends on surface roughness and diameter of bars.
For medium deformed bars, $k = 0.1$.

If cracks are not parallel to the compressive stresses, the latter will have to be transferred across cracks by a combination of concrete - concrete friction (interface shear and compression normal to cracks) and dowel action. This results in a further reduction of concrete strength. This reduction is

greatest when cracks are at 45° to the applied compressive stresses, and smallest when they are parallel to them.

The nominal concrete shear strength in the absence of shear reinforcement is:

$$\tau_c = (1.6 - d)(1 + 50\,\rho)\,\tau_{RD}$$

where d is the section depth, ρ is the flexural reinforcement ratio, τ_{RD}, which is proportional to $(f_{ck})^{2/3}$, is the concrete shear strength and f_{ck} is the 28-day cube strength of concrete.

For comparison, the Norwegian Code formula is:

$$\tau_c = (1.5 - d)\left(1 + \frac{100}{f_{tn}}\right) 0.33 f_{td}$$

with $f_{tn} = 2$ MPa for C45.

Strut and Tie (§ 5.6.3):

If a stress field is chosen which satisfies the equilibrium conditions, a lower bound solution of limit analysis is considered. For the structure and its loads, an equivalent truss may be investigated, consisting of concrete struts and arches as compressive members, and of steel ties, formed by the reinforcement, as tensile elements, and their connections (nodes).

3.7 BPEL 91 (FRENCH PRESTRESSED CONCRETE CODE, 1991)

This code applies to concrete with strength up to 60 MPa (8700 psi). Shear design specifications are based on a variable angle truss of $\beta_u \geq 30°$ with an additional concrete contribution $v_c = f_{tj}/3$ carried by the compressed part of the beam.

Notation for BPEL Code

A_t = area of transverse reinforcement,
b_n = net width of web,
f_e = yield strength of reinforcement,
f_{cj} = concrete compressive strength at j days,
f_{tj} = concrete tensile strength at j days,
s_t = spacing of transverse reinforcement,
γ_b, γ_s = material coefficients for concrete and steel,
$\tau_{red,u}$ = mean shear stress on uncracked section.

BPEL 91 § 7.3.2	Collins and Mitchell, 1991
Stirrups $\frac{A_t}{b_n s_t}\frac{f_e}{\gamma_s} \geq \left(\tau_{red,u} - \frac{f_{tj}}{3}\right)\tan\beta_u$ ≥ 0.4 MPa	Stirrups $\frac{A_v f_v}{s} = \frac{V}{jd}\tan\theta$

Concrete	Concrete
$\frac{0.85 f_{cj}}{3\gamma_b} \sin 2\beta_u \geq \tau_{red,u}$	$\frac{f_2}{2} \sin 2\theta = \frac{V}{b_w jd}$

The design concrete compressive strength, according to BPEL 91, is:

$$\frac{2}{3}\frac{0.85}{\gamma_b} f_{cj}$$

3.8 BAEL 91 (FRENCH REINFORCED CONCRETE CODE, 1991)

This code also applies to concrete with strength up to 60 MPa (8700 psi). Shear design specifications (§ A5.1,2) are based on the Mörsch-Ritter 45° truss with an additional concrete contribution $v_c = f_{tj} / 3$ carried by the compressed part of the beam.

Stirrups

For stirrups at 90° to the longitudinal axis, the following is required for ultimate strength:

$$\frac{A_t}{b_o s_t} \geq \frac{\gamma_s (\tau_u - 0.3 f_{tj} k)}{0.9 f_c} \quad \text{with} \quad f_{tj} \leq 3.3 \text{ MPa}$$

where b_o = total width of web and τ_u = ultimate shear stress.

The coefficient 0.9 is an approximation to the ratio z/d where z = flexure lever arm and d = distance from tension steel to the most compressed fiber. The coefficient k is:

$k = 1$ for pure flexure,

$k = 1 + 3\ \sigma_{cm}/f_{cj}$ for flexure combined with axial compression, where σ_{cm} = mean compressive stress on entire concrete section,

$k = 1 - 10\ \sigma_{tm}/f_{cj}$ for flexure combined with axial tension, where σ_{tm} = mean tensile stress on entire concrete section.

Concrete

For stirrups at 90°, the concrete requirement is:

$$\frac{0.2 f_{cj}}{\gamma_b} \geq \tau_u$$

$$5 \text{ MPa} \geq \tau_u$$

In severely cracked webs, the above expressions are further reduced to:

$$\frac{0.15 f_{cj}}{\gamma_b} \geq \tau_u$$

$$4 \text{ MPa} \geq \tau_u$$

For stirrups at 45 °, the requirement is relaxed to:

$$\frac{0.27 f_{cj}}{\gamma_b} \geq \tau_u$$

$$7 \text{ MPa} \geq \tau_u$$

This last expression is consistent with the BPEL 91 Code.

3.9 Shear Friction

3.9.1 ACI Code 318-95 §11.7

In design, a crack is assumed along the shear plane and reinforcement is provided across that crack. The amount of reinforcement is computed using (Fig.3.25):

$$\phi V_n \geq V_u$$

$$V_n = A_{vf} f_y \mu \leq 0.2 f_c' A_c \qquad \text{(ACI 11.25)}$$

$$\leq 800 A_c \text{ pound} \quad (5.5 A_c \text{ Newton})$$

where V_n is the nominal shear strength, V_u the factored shear force at section, A_c the area of concrete section resisting shear transfer, A_{vf} the area of shear-friction reinforcement, $\phi = 0.85$ for shear and μ the coefficient of friction taken equal to:

a) $\mu = 1.4\,\lambda$ for concrete placed monolithically,
b) $\mu = 1.0\,\lambda$ for concrete placed against hardened concrete with the surface intentionally roughened to an amplitude of approximately 1/4 inch,
c) $\mu = 0.6\,\lambda$ for concrete placed against hardened concrete not intentionally roughened, and
d) $\mu = 0.7\,\lambda$ for concrete anchored to as-rolled structural steel by headed studs or reinforcement bars, where $\lambda = 1.0$ for normal weight concrete,
0.85 for "sand-lightweight" concrete, and
0.75 for "all-lightweight" concrete.

The values of $\mu = 1.4$ and 1.0 are larger than the true coefficient of friction which is given by Eq. 4.23 (§ 4.3.1 of this report) as about 0.8.

When shear friction reinforcement is inclined to the shear plane, the shear strength becomes:

$$V_n = A_{vf} f_y (\mu \sin\alpha_f + \cos\alpha_f) \qquad \text{(ACI 11.26)}$$

where α_f is the angle between the assumed crack plane and the shear friction reinforcement. In the above equation, only the normal component is multiplied by μ since it causes friction. Only those bars that are stressed in tension by the sliding motion can be included in A_{vf}. Permanent net compression across the shear plane can be added to the clamping force provided by the reinforcement in the above equations.

3.9.2 Canadian Standards CSA A23.3-94 §11.6

Relative displacement along the shear plane is resisted by *cohesion* and *friction* maintained by the shear friction reinforcement crossing the crack. The factored shear stress resistance of the plane is:

$$v_r = \lambda \phi_c (c + \mu \sigma) + \phi_s \rho_v f_y \cos\alpha_f$$

$$\text{with} \quad \lambda \phi_c (c + \mu \sigma) \leq 0.25\, \phi_c f_c'$$

$$\leq 7.0\, \phi_c \quad \text{MPa}$$

where α_f is the angle between the shear friction reinforcement and the shear plane, c the cohesion, μ the friction coefficient, f_y the yield strength of the reinforcement, ϕ_c and ϕ_s material factors for concrete and steel and λ a factor to account for low density concrete.

The normal stress is:

$$\sigma = \rho_v f_y \sin\alpha_f + \frac{N}{A_g}$$

$$\text{where} \quad \rho_v = \frac{A_{vf}}{A_{cv}}$$

and N is the unfactored permanent load perpendicular to the shear plane, positive for compression and negative for tension. A_g is the gross area of the section, A_{cv} the area of concrete section resisting shear transfer and A_{vf} the area of shear friction reinforcement. The following values are taken for c and μ:

a) $\mu = 0.60$, $c = 0.25$ MPa for concrete placed against hardened concrete with the surface clean but not intentionally roughened,
b) $\mu = 1.00$, $c = 0.50$ MPa for concrete placed against hardened concrete with the surface clean and intentionally roughened to a full amplitude of at least 5 mm,
c) $\mu = 1.40$, $c = 1.00$ MPa for concrete placed monolithically, and
d) $\mu = 0.60$, $c = 0.00$ MPa for concrete anchored to as-rolled structural steel by headed studs or by reinforcing bars.

An alternative based on Loov's work (see § 4.3.7) is also allowed:

$$v_r = \lambda \phi_c k \sqrt{\sigma f_c'} + \phi_s \rho_v f_y \cos\alpha_f \qquad \text{(CSA 11.33)}$$

$$\text{with} \qquad \lambda \phi_c k \sqrt{\sigma f_c'} \le 0.25 \phi_c f_c' \quad \text{or} \quad 7.0 \phi_c \quad \text{MPa}$$

where $k = 0.5$ for concrete placed against hardened concrete, and
$k = 0.6$ for concrete placed monolithically.

3.9.3 Norwegian Standards NS 3473E 1992 §12.7.2

The shear force capacity parallel to a construction joint with an effective area A_c and reinforcement area A_s through the joint surface is taken as:

$$V_d = \tau_{cd} A_c + f_{sd} A_s (\cos\alpha + \mu \sin\alpha) - \mu \sigma_c \le 0.3 f_{cd} A_c$$

where

α is the angle between the reinforcement area and the contact surface, where only reinforcement with an angle between 90° and 45° to the direction of the force is taken into account,
f_{cd} is the design compressive strength of concrete,
f_{td} is the design tensile strength of concrete,
τ_{cd} is the design shear strength of concrete (cohesion term),
μ is the friction coefficient, and
σ_c is the lowest simultaneously acting concrete stress perpendicular to the contact surface.
The combination of values, listed below, that gives the minimum capacity is used in design:

Contact surface	$\sum A_s \geq 0.001\, A_c$ or $\sigma_c < -0.4$ MPa			
	Combination 1		Combination 2	
	τ_{cd}	μ	τ_{cd}	μ
Smooth	0	0.70	0	0.70
Rough	0	1.50	$0.6 f_{td}$	0.80
Toothed	0	1.80	$1.5 f_{td}$	0.80

3.9.4 CEB-FIP Model Code 1990 §3.9.2

Smooth interfaces

The shear resistance of an interface due to concrete-concrete friction may be evaluated by:

$$\tau_{fu,d} = 0.40\, \sigma_{cd}$$

where σ_{cd} is the averaged normal compressive stress acting on the interface.

The shear slip needed for the mobilization of $\tau_{fu,d}$ may be calculated by:

$$s_u = 0.15 \sqrt{\sigma_{cd}}$$

Rough interfaces

The shear resistance of an interface due to concrete-concrete friction may be evaluated by:

$$\tau_{fu,d} = 0.40\, f_{cd}^{2/3}\, (\sigma_{cd} + \rho f_{yd})^{1/3}$$

where f_{cd} is the design value of the compressive strength of concrete, f_{yd} the design yield strength of the reinforcement perpendicular to the interface, σ_{cd} the average normal stress acting on the interface and ρ the reinforcement ratio. The shear stress given by the above equation corresponds to a shear slip of about 2.0 mm.

Where the slip is less than s_u, the mobilized shear stress τ_{fd} corresponding to the actual slip can be calculated as follows (Fig. 3.26):

For $s < 0.10$ mm $\quad \tau_{fd} = 5\, \tau_{fu,d}\, s$

For $s \geq 0.10$ mm $\quad \left(\frac{\tau_{fd}}{\tau_{fu,d}}\right)^4 - 0.5 \left(\frac{\tau_{fd}}{\tau_{fu,d}}\right)^3 = 0.3\, s - 0.03$

The shear slip along a rough interface is accompanied by a crack opening $w = 0.6\, s^{2/3}$. The CEB-FIP rules are more complicated than those of other codes.

3.10 Summary

From this brief review of several national codes, it is clear that the concept of shear being resisted by a truss formed by concrete struts and steel ties is used widely. Whereas ACI uses a 45° truss and thus requires a V_c term, CEB -FIP uses a variable angle truss with $18.4° \leq \theta \leq 45°$. In addition a number of codes have moved ahead to more rational methods, such as the Modified Compression Field Theory (Canada, Norway, AASHTO).

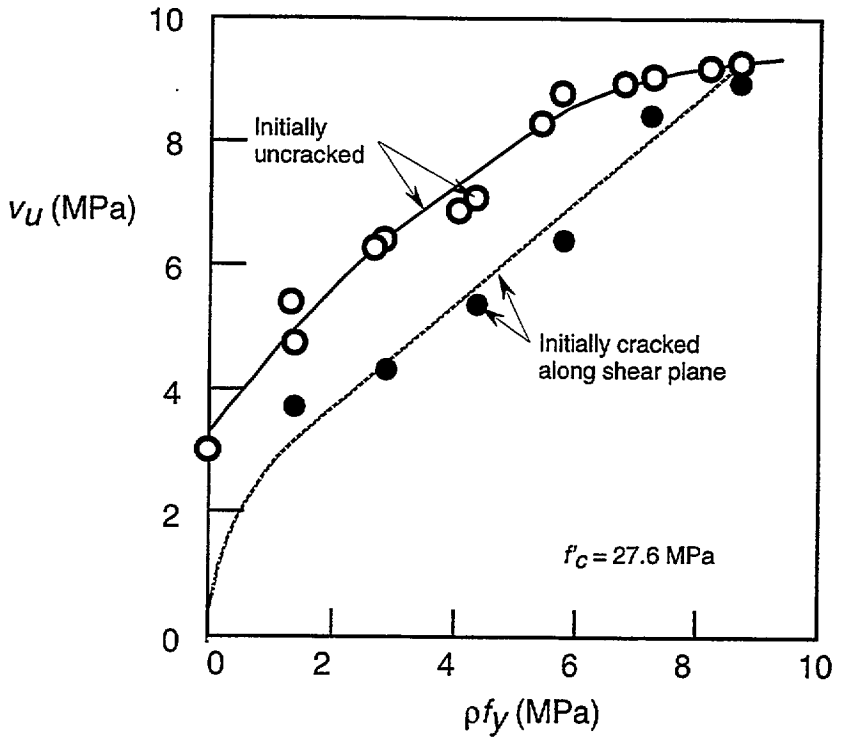

Figure 3.25 — (a) Variation of shear strength with reinforcement ratio (adapted from Hofbeck, Ibrahim, and Mattock 1969)

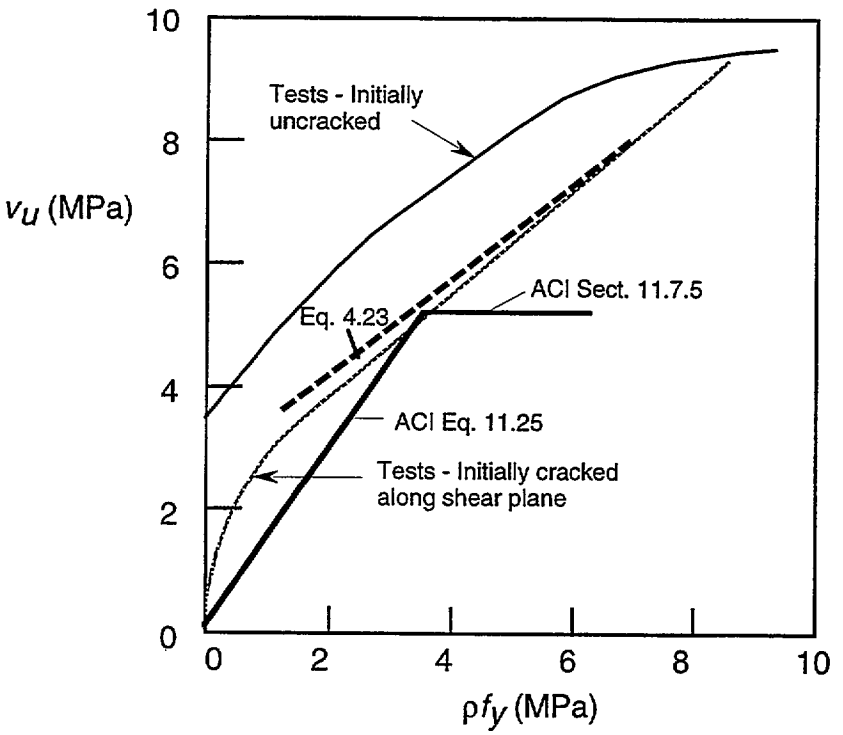

Figure 3.25 — (b) Comparison of test results and design equations (adapted from MacGregor 1992)

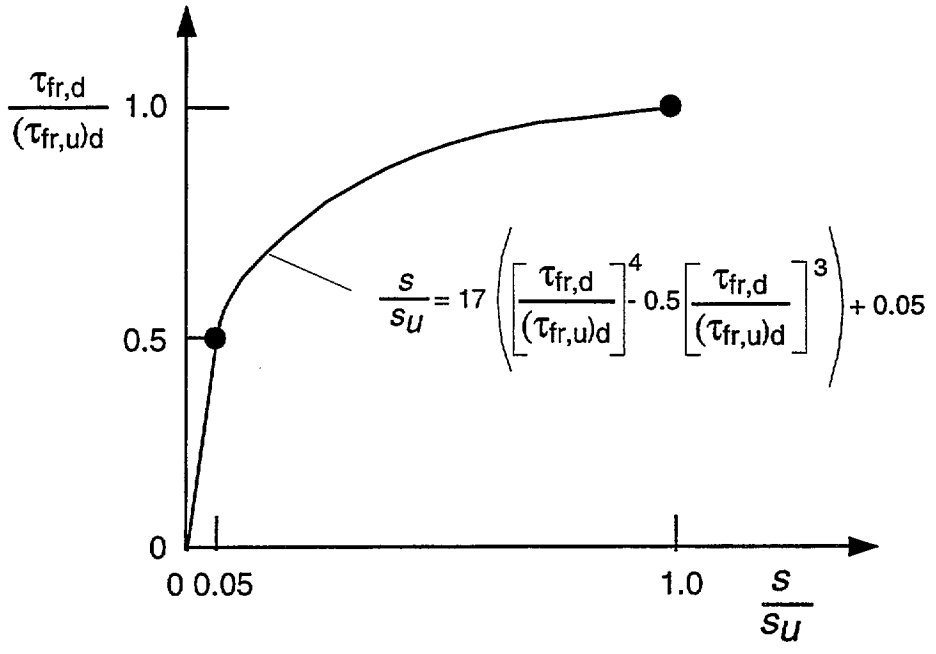

Figure 3.26 — Mobilized shear stress as a function of shear slip (CEB-FIP Model Code 1990)

4. Research Results

Results of tests of beams and panels made of HSC are reported here, as well as experimental and theoretical results on shear friction, and some work on size effect..

4.1 Beam Tests

4.1.1 Cornell University Tests

Beams without web reinforcement

Nilson (1987) and Elzanati, Nilson and Slate (1986) tested 9 reinforced concrete beams with f_c' ≥ 9500 psi (65 MPa) for shear strength and compared the results with 6 beams with $f_c' \leq$ 5800 psi (40 MPa). As Figs. 4.1 and 4.2 show, the ACI Code equation (ACI 11.5) is unconservative by 10 to 30% for many of the test beams, notably those combining high strength concrete with medium to high shear span ratios and typical or low longitudinal steel ratios.

Beams with web reinforcement

One beam with $f_c' = 9100$ psi (63 MPa) was tested for shear strength and the results compared with two beams with $f_c' \leq$ 5800 psi (40 MPa). As Fig. 4.3 shows, the ACI Code equation (ACI 11.5) is safe because the increase in the steel contribution V_s more than compensates for the decrease in the concrete contribution V_c as f_c' increases. The use of HSC tends to prevent shear-compression failure and to insure a diagonal tension failure instead, thus increasing the effectiveness of shear reinforcement. The concrete contribution V_c is lower than calculated by ACI Code equations. Figure 4.3 shows clearly the gain in $V_n = V_c + V_s$ as concrete strength increases. The transverse reinforcement index for these beams is $v_s = \rho_v f_y = 94$ psi (650 kPa). In addition, test results for 34 prestressed concrete beams with 6 000 ≤ $f_c' \leq$ 12 000 psi (41 ≤ $f_c' \leq$ 83 MPa) were reported.

4.1.2 University of Connecticut Tests

Beams without web reinforcement

Mphonde and Frantz (1984) tested the following beams for shear under a load at midspan and simple supports:

a/d	Number of tests	
	$f_c' \leq$ 6500 psi (45 MPa)	$f_c' \geq$ 9500 psi (65 MPa)
3.6	4	5
2.5	2	3
1.5	2	3

Table 4.1 Test Specimens

Results of the tests with $a/d = 3.6$ were compared with ACI Eq. 11.5 and Zsutti's (1968) equation, where ρ is the ratio of tension reinforcement. See Fig. 4.4.

$$v_u = 63.4 \sqrt[3]{f_c' \rho \frac{d}{a}} \quad \text{inch-pound system}$$

$$v_u = 2.3 \sqrt[3]{f_c' \rho \frac{d}{a}} \quad \text{mm-Newton system} \qquad (4.1)$$

The ACI equation is conservative, less so at high strengths than at low strengths. The regression equations

$$v_u = 10.10 \sqrt[3]{f_c'} + 71 \quad \text{inch-pound system}$$

$$v_u = 0.366 \sqrt[3]{f_c'} + 0.49 \quad \text{mm-Newton system}$$

or $$v_u = 1.52 \sqrt{f_c'} + 135 \quad \text{inch-pound system}$$

$$v_u = 0.126 \sqrt{f_c'} + 0.931 \quad \text{mm-Newton system}$$

best describe the test results.

Test results for short beams are also compared with ACI Eq. 11.29 and Zsutti's equation (Figs. 4.5 and 4.6).

$$v_u = \left(\frac{2.5}{a/d}\right) 59 \sqrt[3]{f_c' \rho \frac{d}{a}} \quad \text{inch-pound system}$$

$$v_u = \left(\frac{2.5}{a/d}\right) 2.1 \sqrt[3]{f_c' \rho \frac{d}{a}} \quad \text{mm-Newton system}$$

As complete arching action cannot be guaranteed in all deep beams, design values must be a lower bound of the test results. At $a/d = 2.5$ both the ACI and Zsutti's equations predict the inclined cracking loads well. At $a/d = 1.5$, both the ACI and Zsutti's equations significantly under-predict the ultimate shear strength, which is approximately proportional to the concrete compressive strength. Results are consistent with the Cornell work (Nilson 1987).

Beams with web reinforcement

Mphonde and Frantz (1985) also tested 12 reinforced concrete beams with shear reinforcement index $v_s = A_v f_y / (bs)$ of 50, 100, or 150 psi (0.34, 0.69, 1.03 MPa) and f_c' ranging from 3500 to 13000 psi (24 to 90 MPa). Only 3 of these beams had $f_c' < 6000$ psi (41 MPa).

Figure 4.7 shows that the ACI Code equations (ACI 11.2, 11.5 and 11.15) are conservative for all values of f_c'. The ratio of measured to predicted shear strengths varies from 1.11 to 1.61. The scatter in the data is such that no trend can be detected in the variation of this ratio with f_c' or with v_s. These conclusions differ from the Cornell results (Elzanaty, Nilson and Slate 1986).

A design equation is proposed, based on regression analysis:

$$v_n = 1.51\sqrt{f_c'} + 90 + 1.6\frac{A_v f_y}{bs} \quad \text{inch-pound system}$$

$$v_n = 0.125\sqrt{f_c'} + 0.62 + 1.6\frac{A_v f_y}{bs} \quad \text{mm-Newton system}$$

Notice that the shear resistance of stirrups is more than additive to that of concrete (coefficient 1.6 > 1). The average ratio of measured shear strength to that predicted by the above equation is 1.006 with a standard deviation of 0.085.

4.1.3 Measurement of Components of V_c

Mphonde (1988) tested 24 beams to quantify the effect of high compressive strengths on the various shear transfer mechanisms which add up to V_c (the concrete contribution), namely:

a) the shear carried by the concrete in the uncracked compression zone above the crack tip, V_{cz},
b) the interface shear or aggregate interlock across the crack face V_a, and
c) the shear carried by the dowel action of the longitudinal flexural steel V_d.

(The shear not carried by the concrete is carried by the stirrups. So:

$V_u = V_c + V_s$ with $V_c = V_{cz} + V_a + V_d$).

The concrete compressive strength ranges from 3 000 psi (21 MPa) to 13 600 psi (94 MPa).

Three series of beams were tested: Series A has no stirrups, whereas series B has transverse reinforcement ratio $A_v f_y / (bs) = 50$ or 100 psi (345 or 690 kPa). Series C has the same reinforcement as series B, but in addition has two pre-sawed diagonal cracks, one on each half of the span. (The beams are loaded at midspan). The pre-sawed cracks are based on observed cracks in beam series B. The difference in shear capacity between series B and C is the aggregate interlock V_a.

The steel contribution is measured by strain gaging the stirrups. It is always less than the difference between the shear capacity of series B and A.

The V_{cz} contribution requires elaborate measurements. The shear stress carried by the compression zone is

$$\tau_{xy} = E_c \int_0^{h_c} \frac{\partial \varepsilon}{\partial M}\frac{\partial M}{\partial x}\,dy$$

where $\varepsilon\,(x,y)$ is the strain, x the span direction, y the depth direction measured from the most compressed fiber, $M\,(x)$ the moment, $h_c\,(x)$ the depth of the uncracked compressive zone and E_c the concrete modulus of elasticity. ε is measured at one x and five y's for various values of M.

Finally, the dowel contribution V_d is obtained by subtraction. The measurements show that:

a) V_{cz} is rather insensitive to f_c'. This is the result of two opposing trends: as f_c' increases, the strain in the uncracked concrete decreases but the modulus of elasticity E_c increases. $V_{cz}/V_c \approx 25\%$.

b) V_a is significant at low concrete strengths: for 3 000 $< f_c' <$ 6 000 psi or 21 $< f_c' <$ 41 MPa,

$V_a / V_c = 53 - 25\%$ for $A_v f_y / (bs) = 50$ psi or 0.35 MPa, and

$V_a / V_c = 46 - 22\%$ for $A_v f_y / (bs) = 100$ psi or 0.69 MPa

but is virtually non-existent at higher concrete strengths ($f_c' >$ 9000 psi or 62 MPa).

c) The dowel contribution more than doubles as f_c' increases from 3 000 psi (21 MPa) to 13 000 psi (90 MPa). (V_d/V_c increases from 30 to 75%).

4.1.4 Roller and Russell's Tests

Roller and Russell (1990) reviewed 150 tests and confirmed the validity of the ACI Code equations for shear (Fig. 4.8). The same conclusion holds if only tests of beams that meet all ACI

318-83 design requirements are used (Fig. 4.9). They performed 10 more tests of beams with f_c' ranging from 10 500 psi (72 MPa) to 18 000 psi (124 MPa). The new tests confirm the appropriateness of ACI 318-95 §11.1.2.1 that requires an increase in the minimum amount of web reinforcement for concrete with $f_c' > 10\,000$ psi (69 MPa).

4.1.5 North Carolina State University Tests

Ahmad et al. (1986) presented the results of an experimental program that examined the effect of concrete of high strength ($f_c' = 10\,000$ psi or 69 MPa) with various longitudinal steel ratios, on the diagonal cracking capacity and the ultimate shear capacity of 36 beams without web reinforcement. The tests were performed for 6 shear span/depth ratios a/d ranging from 1 to 4.

Results showed that the then current ACI Code provided a conservative estimate of the shear capacity of HSC short beams ($1 < a/d < 2.5$). For slender beams ($a/d > 2.5$) of HSC, the ratio of measured to predicted capacity dropped to about 1.0. Also, for slender beams, the Code provisions did not accurately estimate the effect of longitudinal steel on shear capacity, especially for low ratios of reinforcement.

4.1.6 Purdue University Tests

Johnson and Ramirez (1989) tested 8 rectangular beams in shear with concrete strength in the range of 5 000 - 10 500 psi (34 - 72 MPa) and with web reinforcement ratios v_s of 0 to 100 psi (0.69 MPa).

Results indicate that the overall reserve shear strength after diagonal cracking $V_{fail} - V_c$ diminishes with the increase in concrete compressive strength for a constant $v_s = 50$ psi (0.35 MPa). The data were used to justify ACI §11.1.2.1 which limits f_c' to 10 000 psi (69 MPa) or increases the minimum amount of reinforcement by a factor equal to f_c' / 5000 psi (34.5 MPa) but less than 3 times the amount provided for concrete with $f_c' < 5000$ psi (34.5 MPa).

4.1.7 Norwegian Institute of Technology Tests

Thorenfeldt and Drangsholt (1990) tested 28 reinforced concrete beams without shear reinforcement in shear by two-point loading. The concrete strengths ranged from 54 to 98 MPa, the shear span to depth ratio ranged from 2.3 to 4.0 and the longitudinal reinforcement ratio was either 1.8% or 3.2%.

For members made of concrete with $f'_c > 80$ MPa, the diagonal cracking strength remained largely constant (with a minor decrease), in spite of the increasing tensile strength of the concrete. (This is why the Norwegian Standards keep the in-situ tensile strength constant for concrete with $f_c' > 74$ MPa). Surprisingly, the ultimate shear strength decreased as the concrete compressive strength increased above 80 MPa, probably because of the increasing brittleness with increasing strength. No difference between the roughness of the shear crack surfaces of concrete of different strengths could be detected visually. Also, as expected, the ultimate shear strength increased with decreasing shear span to depth ratio and with increasing longitudinal reinforcement. The diagonal cracking strength increased significantly with the longitudinal reinforcement ratio, but was practically independent of the shear span to depth ratio. The authors recommended that future research should be aimed at explaining the decrease in ultimate shear strength with increasing concrete compressive strength above 80 MPa and the greater dependency on scale of the shear strength of HSC beams versus NSC beams.

4.1.8 Nanyang University of Technology (Singapore) Tests

Tan et al. (1995) tested 19 reinforced concrete deep beams with compressive strengths ranging from 41 to 59 MPa (6 000-8 000 psi) under two-point loadings. The beams were tested for 7 shear span to depth ratios a/d ranging from 0.27 to 2.70 and 4 effective span to depth ratios l_e/d ranging from 2.15 to 5.3 (l_e is the distance between the two centers of support).

Test results indicate that l_e/d has little influence on the magnitude of the failure load. They also show that the ACI deep-beam provisions, although based on concrete strengths less than 40 MPa (6000 psi), will insure safe and rather conservative designs for higher- strength deep beams.

4.1.9 Darmstadt University of Technology Tests

König et al. (1993) tested 14 beams without stirrups in shear. In a first series, small beams with various shear span ratios ($2.3 \leq a/d \leq 4.0$) and reinforcement ratios ($\rho = 1.87, 4.09$) were tested. The concrete strength was 85 MPa. In a second series, the beam depth was varied while a/d and f'_c were kept nearly constant (3.8 and 92 MPa respectively).

The observed crack pattern was used as input to a finite-element model which modeled concrete as a linear elastic material with discrete (as opposed to smeared) cracks. The finite-element results showed that the tensile behavior of concrete was the most important factor governing the shear behavior of beams without stirrups. The influence of aggregate interlock and the dowel action of the longitudinal reinforcement were very small. Results from 150 tests produced the following empirical relationships:

$$f_{ct} = 2.12 \ln (1 + 0.1 f'_c)$$

where f_{ct} = concrete tensile strength

f'_c = concrete compressive strength

$$G_f = 65 \ln (1 + 0.1 f'_c)$$

where G_f = fracture energy (N/m)

$$l_{ch} = \frac{E * G_f}{f_{ct}^2} = \text{characteristic length}$$

where $E = 10\,000 (f'_c)^{0.3}$ = modulus of elasticity

and finally $v_u = 1.1 \sqrt[3]{\frac{l_{ch}\rho}{d}} f_{ct}$ = shear capacity

where ρ = reinforcement ratio

d = beam depth

4.1.10 Italian Tests

Marro (1987) tested 10 beams in shear, of which 4 had $f_c' = 35$ MPa, 5 had $f_c' = 70$ MPa and one had $f_c' = 120$ MPa. They were loaded by 2 concentrated loads at the third points.

All beams exhibited stirrup yielding. The crack angle ranged from 34 to 38°. Post-yielding strength was often considerable: $1.17 < V_{max}/V_y < 1.58$.

Marro concluded that:

- Early diagonal cracking occurs because the opening of cracks is associated with tensile strength

which increases only slightly with increasing compressive strength. However, the ratio of shear stress at diagonal cracking to mean tensile strength τ_{cr}/f_{ctm} is always greater than 0.25, which is the value specified by the Model Code for members without stirrups.

- The standard method of the Model Code, which assumes a 45° truss, is always on the safe side, but the accurate method when used with the minimum allowable crack angle (31°), is unconservative.

4.1.11 Nordic Concrete Research

Bernhardt and Fynboe (1986) reported test results of 11 beams failing in shear. The 28-day cube strength is 104 MPa corresponding to a cylinder strength of 90 MPa (13 000 psi). One beam was reported to have a 570-day cube strength of 123 MPa (18 000 psi). Six of the beams had no shear reinforcement. Analysis of the results and comparison with Code values were not presented.

4.1.12 Korean Tests

Kim and Park (1994) reported the results of 20 beam tests and compared them to various code predictions. The beams tested used a concrete strength of $f_c' = 53.7$ MPa, had no web reinforcement, and were loaded by two equal concentrated loads. The following design equations were studied:

British Standards 8110

$$v_c = \frac{0.79}{\gamma_m}\left(\frac{100A_s}{b_v d}\right)^{1/3}\left(\frac{400}{d}\right)^{1/4}\left(\frac{f_{cu}}{25}\right)^{1/3} \quad \text{for } a/d \geq 2.0 \tag{4.2}$$

$$v_c = 2.0\,\frac{d}{a} * \text{Eq. (4.2)} \quad \text{for } \frac{a}{d} \leq 2.0 \quad \text{MPa}$$

ACI

$$v_c = 0.1578\sqrt{f_c'} + 17.25\,\rho_w\frac{V_u d}{M_u} \quad \text{for } \frac{l_n}{d} \geq 5.0 \quad \text{MPa} \tag{4.3}$$

$$v_c = \left(3.5 - 2.5\,\frac{M_u}{V_u d}\right) * \text{Eq. (4.3)} \quad \text{for } \frac{l_n}{d} < 5.0 \quad \text{MPa}$$

CEB-FIP

$$v_{cr} = 0.15\left(\frac{3d}{a}\right)^{1/3}\left(1 + \sqrt{\frac{200}{d}}\right)(100\,\rho f_{ck})^{1/3} \quad \text{MPa}$$

Zsutti

$$v_u = 2.1746\left(f_c'\,\rho\,\frac{d}{a}\right)^{1/3} \quad \text{for } a/d \geq 2.5 \quad \text{MPa} \tag{4.4}$$

$$v_u = 2.5\,\frac{d}{a} * \text{Eq. (4.4)} \quad \text{for } a/d < 2.5 \quad \text{MPa}$$

Note: In Eq. 4.4 the coefficient in front of the cube root ought to be 2.3 (as in Eq. 4.1) for ultimate stress or 2.2 (as in Eq. 4.9) for diagonal tension failure stress.

Bažant

$$v_u = 0.54\sqrt[3]{\rho}\left(\sqrt{f_c'} + 249\sqrt{\frac{\rho}{(a/d)^5}}\right)\frac{1 + \sqrt{5.08/d_a}}{\sqrt{1 + d/(25\,d_a)}} \quad \text{MPa}$$

Notation:

A_s = area of tension reinforcement,
a = shear span,
d = effective depth,
d_a = maximum aggregate size,
f_{ch} = characteristic compressive strength of concrete,
f_{cu} = cube compressive strength of concrete,
f'_c = cylinder compressive strength of concrete,
l_n = clear span, measured from face to face of supports,
M_u = ultimate moment,
V_u = ultimate shear force,
v_u = ultimate shear stress,
γ_m = material factor = 1.25
ρ = ratio of flexural tension reinforcement.

Test results of this study (Figs. 4.10, 4.11 and 4.12) indicate that the CEB-FIP Model Code equation predicts the shear strength of test beams relatively well; the BS 8110 equation is excessively conservative, the ACI equation is unsafe for large beams (d = 915 mm); the effects of ρ and a/d on the shear strength of beams are not significantly influenced by the concrete strength; and the effect of size on shear strength is the same for NSC as for HSC.

4.1.13 Sarsam and Al-Musawi's Tests

Sarsam and Al-Musawi (1992) reported the test results of 14 beams with stirrups failing in shear and also reviewed the results of 107 beam tests from the literature. These included NSC (f_c' < 41 MPa or 6000 psi) as well as HSC (f_c' up to 83 MPa or 12 000 psi). They evaluated the predictions of six design equations in light of these test results. SI units are used, except where indicated.

$$\text{ACI} \quad V_{ACI} = 0.85\left(\sqrt{f'_c} + 120\ \rho_w V_u d/M_u\right) b_w d/7 + 0.85\ A_v f_y d/s \qquad (4.5)$$

$$\text{INCH-LB} \quad V_{ACI} = 0.85\left(1.9\sqrt{f'_c} + 2500\ \rho_w V_u d/M_u\right) b_w d + 0.85\ A_v f_y d/s \qquad (\text{ACI } 11.5)$$

$$\text{CANADA} \quad V_{CSA1984} = 0.60\left(0.20\sqrt{f'_c}\ b_w d\right) + 0.85\ A_v f_y d/s \qquad (4.6)$$

$$\text{NEW-ZEALAND} \quad V_{NZ} = 0.85\,(0.07 + 10\ \rho_w)\sqrt{f'_c}\ b_w d + 0.85\ A_v f_y d/s \qquad (4.7)$$

$$\text{BRITISH} \quad V_{BS} = 0.79\ \sqrt[3]{100\rho_w}\ \sqrt[3]{f'_c/20}\ \sqrt[4]{400/d}\ b_w d/1.25 + 0.87\, A_v f_y d/s \qquad (4.8)$$

with $\quad (cylinder)\ f'_c = 0.8\ f_{cu}\ (cube)$

$$\text{ZSUTTI} \quad V_{ZST} = 0.85\left(2.2\ \sqrt[3]{f'_c \rho_w d/a}\right) b_w d + 0.85\, A_v f_y d/s \qquad (4.9)$$

$$\text{SARSAM} \quad V_{SAR} = 0.85 * 1.8\,(f'_c \rho_w V_u d/M_u)^{0.38}\ b_w d + 0.85\, A_v f_y d/s \qquad (4.10)$$

Ratios of measured to predicted strengths are listed in Tables 4.2 and 4.3 for HSC beams and for all beams. Also, the influence of f'_c on the predictions is shown in Fig. 4.13. Sarsam and Al-Musawi concluded that the ACI design equation is adequate even up to f'_c = 83 MPa (12 000 psi).

Ratio	V_{TEST} / V_{ACI}	V_{TEST} / V_{CSA}	V_{TEST} / V_{NZ}	V_{TEST} / V_{BS}	V_{TEST} / V_{ZST}	V_{TEST} / V_{SAR}
Equation	4.5	4.6	4.7	4.8	4.9	4.10
Mean	1.77	1.93	1.54	1.74	1.41	1.63
Stan. Dev.	0.523	0.586	0.490	0.535	0.401	0.414
COV	0.296	0.304	0.318	0.308	0.285	0.254
Maximum	3.16	3.57	2.85	3.13	2.35	2.57
Minimum	1.00	1.09	0.84	0.93	0.81	1.00
Max / Min	3.16	3.29	3.40	3.37	2.89	2.57
Number <1	0	0	2	1	4	0

Number < 1 indicates the number of specimens (out of 33) for which $V_{TEST} < V_{DESIGN}$.

Table 4.2 Comparison between V_{TEST} and V_{DESIGN} for 33 HSC Beams

Ratio	V_{TEST} / V_{ACI}	V_{TEST} / V_{CSA}	V_{TEST} / V_{NZ}	V_{TEST} / V_{BS}	V_{TEST} / V_{ZST}	V_{TEST} / V_{SAR}
Equation	4.5	4.6	4.7	4.8	4.9	4.10
Mean	1.63	1.78	1.48	1.47	1.32	1.56
Stan. Dev.	0.391	0.441	0.361	0.389	0.297	0.322
COV	0.239	0.248	0.245	0.265	0.224	0.207
Maximum	3.16	3.57	2.85	3.13	2.35	2.68
Minimum	1.00	1.09	0.84	0.93	0.81	1.00
Max / Min	3.16	3.29	3.40	3.37	2.89	2.68
Number <1	0	0	4	3	12	0

Table 4.3 Comparison between V_{TEST} and V_{DESIGN} for 121 Beams

4.1.14 Sakaguchi and others' tests

Sakaguchi et al. (1990) tested 6 beams and 10 columns with and without shear reinforcement to determine their diagonal cracking strengths and ultimate shear capacities. Most of the members tested were made of HSC (f_c' up to 90 MPa) and reinforced with high strength steel (HSS with σ_y up to 1000 MPa). The shear reinforcement quantity $\rho_w\sigma_y$ varied from 0 to 11.2 MPa, the axial stress

in the columns had values of 0, 18.4 or 36.8 MPa, and the depth ratio was 1.0 for beams and 1.14 for columns.

Notation:

b,d = width, depth of section,
F_c = nominal compressive strength of concrete,
f'_c = compressive strength of concrete,
f_{wt} = allowable tensile stress in shear reinforcement,
j = $7d/8$ = distance between centroids of tension and compression steel,
K_c = size coefficient (= 0.72 here),
M = maximum moment in member,
M' = moment occurring simultaneously with shear force at critical section,
V_a = allowable shear force,
V_c = shear strength provided by concrete,
V_u = ultimate shear force,
α = coefficient due to shear span/depth ratio,
θ = angle of critical shear crack,
ρ_t = tension reinforcement ratio,
ρ_w = shear reinforcement ratio,
σ_o = axial stress,
σ_y = yield strength of shear reinforcement,
τ_a = allowable shear stress, and
τ_u = ultimate shear stress.

The following design equations were compared to experimental results:

Diagonal Cracking Strength

ACI :

$$\frac{7}{8}\tau_c = \frac{V_c}{bd} = 2\left(1+\frac{\sigma_o}{2000}\right)\sqrt{f'_c} \quad \text{psi}$$

$$\frac{7}{8}\tau_c = \frac{V_c}{bd} = 0.166\left(1+\frac{\sigma_o}{13.8}\right)\sqrt{f'_c} \quad \text{MPa} \qquad \text{(ACI 11.4)}$$

with the cracking shear stress :

$$\tau_c = \frac{V_c}{bj} = \frac{V_c}{b(7d/8)}$$

The factor 7/8 serves to reconcile the ACI definition and this study.

ACI equation for deep beams:

$$\frac{7}{8}\tau_c = \frac{V_c}{bd} = \left(3.5 - 2.5\frac{M'}{Vd}\right)\left(1.9\sqrt{f'_c} + 2500\,\rho_t\frac{Vd}{M'}\right) \quad \text{psi}$$

$$\frac{7}{8}\tau_c = \frac{V_c}{bd} = \left(3.5 - 2.5\frac{M'}{Vd}\right)\left(0.158\sqrt{f'_c} + 17.2\,\rho_t\frac{Vd}{M'}\right) \quad \text{MPa} \qquad \text{(ACI 11.29)}$$

Ohno and Shibata (Uemura et al. 1978):

$$\tau_c = \frac{V_c}{bj} = \frac{0.085 K_c}{\frac{M}{Vd} + 1.7}\left(1 + \frac{\sigma_o}{14.7}\right)(49.1 + f_c') \tag{4.11}$$

Ultimate strength:

ACI Eq. 11.2, 11.4, 11.15:

$$\frac{7}{8}\tau_u = \frac{V_u}{bd} = \frac{V_c}{bd} \text{ [from Eq. ACI 11.4] } + \rho_w \sigma_y \tag{4.12}$$

ACI 426R-74 Deep Beams (Eqs. 4.9 and 4.11a p.1157 Joint ASCE-ACI Com. 426).

$$\frac{7}{8}\tau_u = \frac{V_u}{bd} = \frac{V_c}{bd} \text{ [from Eq. ACI 11.29] } + \rho_w \sigma_y \tan\phi \cos^2\theta \tag{4.13}$$

where θ = shear crack angle (= 30° here),
and $\tan\phi$ = apparent coefficient of friction between concrete surfaces (=1 here).

AIJ (Architectural Institute of Japan):

$$\tau_a = \frac{V_a}{bj} = \alpha\left(\frac{F_c}{67} + 0.74\right) + 0.5 f_{wt}(\rho_w - 0.002)$$

$$\text{where} \quad \alpha = \frac{4}{\frac{M}{Vd} + 1} \quad \text{and} \quad 1 \le \alpha \le 2 \tag{4.14}$$

For ultimate shear stress, based on experimental data, Sakaguchi et al. modified Eq. 4.14 as follows:

Sakaguchi et al. :

$$\tau_u = \frac{V_u}{bj} = \alpha\left(\frac{f_c'}{45} + 0.78\right) + 0.8\,\rho_w \sigma_y + 0.1\,\sigma_o \tag{4.15}$$

Results are shown in Figs. 4.14 - 4.22 .

1. The diagonal cracking strength is underestimated by ACI Eq. 11.4, but better predicted by Ohno-Shibata Eq. 4.11. For the specimens without axial load, ACI Eq. 11.29 is the best predictor.
2. Eq. 4.12 from ACI underestimates the ultimate shear capacity of members having a low $\rho_w\sigma_y$ and high axial load.
3. Eq. 4.13 from ASCE-ACI, used with a crack angle of 30°, predicts well the ultimate shear capacity of members without axial stress.
4. The ultimate shear capacity of the HSC beams reinforced with HSS is best predicted by the proposed Eq. 4.15.

4.1.15 Comparison between ACI Method and MCFT

Shahawy and Batchelor (1996) performed full scale tests of 20 AASHTO Type II pretensioned concrete girders and compared the measured shear strength with the values predicted by the *1989 AASHTO Standard Specifications*, which use the ACI method, and the *1994 AASHTO LRFD (Load and Resistance Factor Design) Specifications*, which uses the Modified Compression Field Theory (MCFT).

The main variables of the study were the amounts of shear reinforcement, shear span and strand diameter. Six girders were designed according to the provisions of the *1989 Standard* and were provided with the required *(R)* shear reinforcement. The other 14 girders had various shear reinforcement ρ_v from 0 to 3*R*. 13 girders were 12.5 m (41 ft) long, 2 girders were 7.62 m (25 ft) long and the other 5 girders were 6.40 m (21 ft) long. Both the girder and cast-in-place concrete slab were designed for a 28-day cylinder concrete strength of $f'_c = 41$ MPa (6000 psi).

Results are shown in Figs. 4.23 - 4.25. From Fig. 4.23, it is clear that the *1989 Standard* provides excellent predictions for girders having shear reinforcement $R < \rho_v < 3R$ and conservative estimates for girders with $0 < \rho_v < R$. On the other hand, the *LRFD Code* considerably overestimates the shear strength of over-designed girders ($2R < \rho_v < 3R$) and grossly underestimates the shear strength of under-designed girders ($0 < \rho_v < R/2$). The latter suggests that the *LRFD* estimate for V_c is too low. For $\rho_v = R$, the *1989 Standard* also provides better estimates than the *LRFD Code* (Fig. 4.24). The effect of *a/d* is also accounted for much better by the *1989 Standard* than by the *LRFD Code* (Figs. 4.24 - 4.25).

Note that as ρ_v increases from *R* to 3*R*, the shear strength only increases slightly. This justifies the imposition of a cap on shear reinforcement. The code requires the upper limit to prevent the concrete in the web from crushing prior to yielding of the shear reinforcement. However, the maximum amount of shear reinforcement was significantly exceeded without any sign of concrete crushing in the webs at failure. When the maximum specified shear reinforcement is imposed, the *1989 Standard* compares very well with test results, but the *LRFD Code* significantly overestimates the shear strength, suggesting that the *LRFD* limit is too high.

In regions near supports, the *LRFD Code* predicts higher values of shear strength than does the *1989 Standard*, because the *LRFD Code* assumes smaller strut angles than does the *1989 Standard*, which uses $\theta = 45°$. However, away from the support regions, the concrete contribution V_c is relatively small compared to the shear reinforcement contribution V_s, and θ approaches 45° in both codes. The *LRFD Code* underestimates V_c in these regions, thereby resulting in lower predicted shear strength than provided by the *1989 Standard*.

The authors recognize the appeal of the greater rationality of the MCFT but question if the increased complexity and the greater discrepancy with test results justify the extensive changes to the code.

4.1.16 Strength of Nodes and Struts

Yun and Ramirez (1996) used the results of a finite-element analysis (FEA) to guide them in the dimensioning of a strut-and-tie model of the D-region of a beam with $a/d = 2.15$ and loaded at the third points. Of particular concern was the allowable stresses and dimensions of the struts and the nodal zones.

Struts — Yun and Ramirez used the biaxial stress failure envelope of Kupfer and Gerstle: the effective stress level of a concrete strut in a biaxially stressed web is a function of the ratio of the principal stresses. This ratio was evaluated from the FEA of a plain concrete model of the beam. If the strut angle deviates by an angle $\alpha \geq 10°$ from the direction of principal compression, then the effective

stress is scaled down by cosα.
Nodal Zones — Detailed FEA of nodal zones were also performed. Ties anchored into a node were modeled as compression applied through a bearing plate from the opposite face. Because the struts intersecting at a node were loaded to different stress levels, the end faces of the struts did not have to be perpendicular to the struts. Again, the strength envelope of Kupfer and Gerstle was used.
Results — Two different strut-and-tie models were tried for the same load. Tension in the longitudinal reinforcement predicted by the models compared reasonably well with experiments.

4.1.17 High Strength Shear Reinforcement

Takagi and Kanoh (1991) investigated the effectiveness of high strength web reinforcement (up to 800 MPa). They concluded that:

- As the concrete strength f'_c increases and / or the amount of stirrups decreases, the stresses in the shear reinforcement increases. The use of high strength stirrups is efficient for HSC.
- It is doubtful, however, whether high strength shear reinforcement is as effective as normal strength shear reinforcement when used in reduced quantities. This is due to the splitting bond failure of longitudinal bars, caused by the reduction in confinement.

4.1.18 Summary

A great number of beams have been and continue to be tested, resulting in almost as many empirical equations as investigators. In general, code equations do a reasonably conservative job of predicting the shear strength of beams. However, extrapolation beyond the range of test variables can sometimes be unconservative.

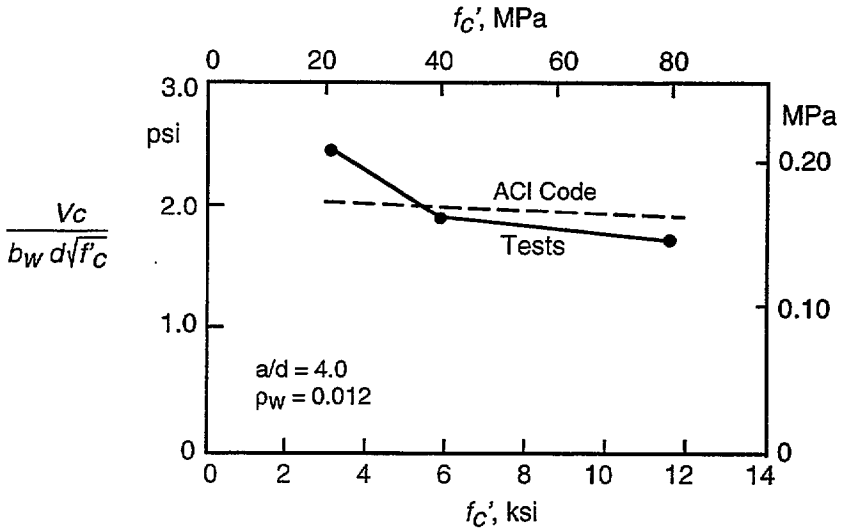

Figure 4.1 — Effect of concrete strength on shear strength of reinforced concrete beams (adapted from Nilson 1985)

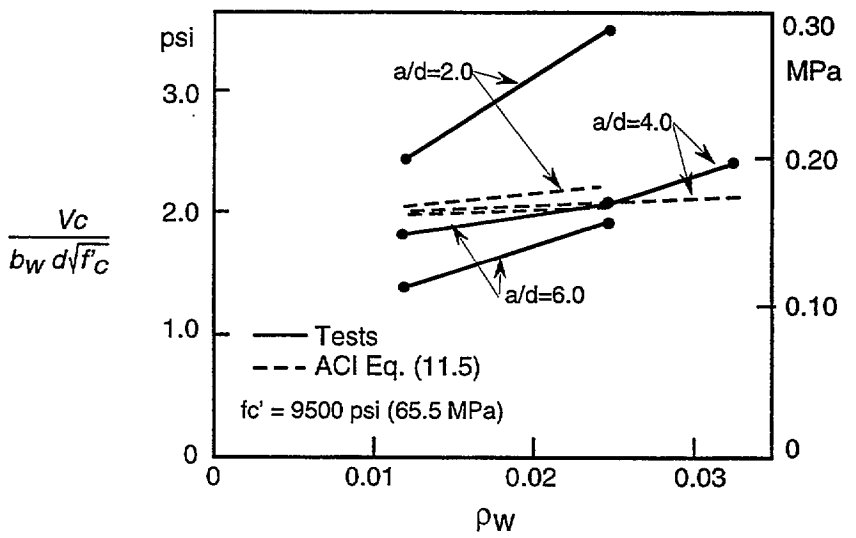

Figure 4.2 — Effect of steel ratio and shear span-to-depth ratio on shear strength of reinforced concrete beams (adapted from Nilson 1985)

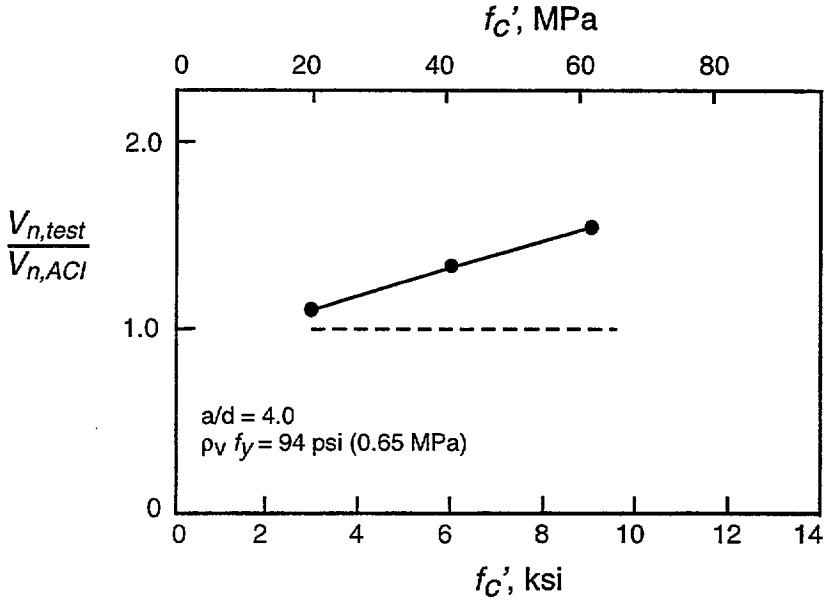

Figure 4.3 — Effect of concrete strength on shear strength of web-reinforced concrete beams (adapted from Nilson 1985)

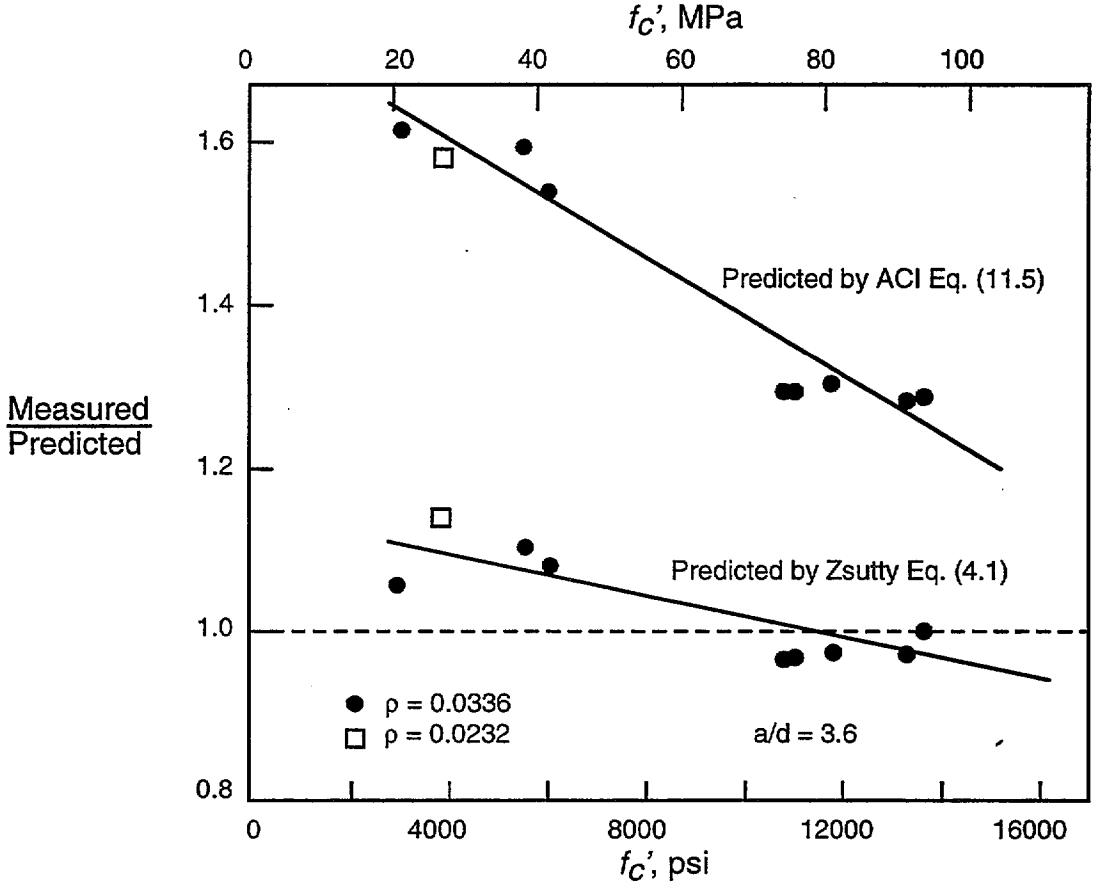

Figure 4.4 — Comparison of shear strength predictions using ACI and Zsutty equations (adapted from Mphonde and Frantz 1984)

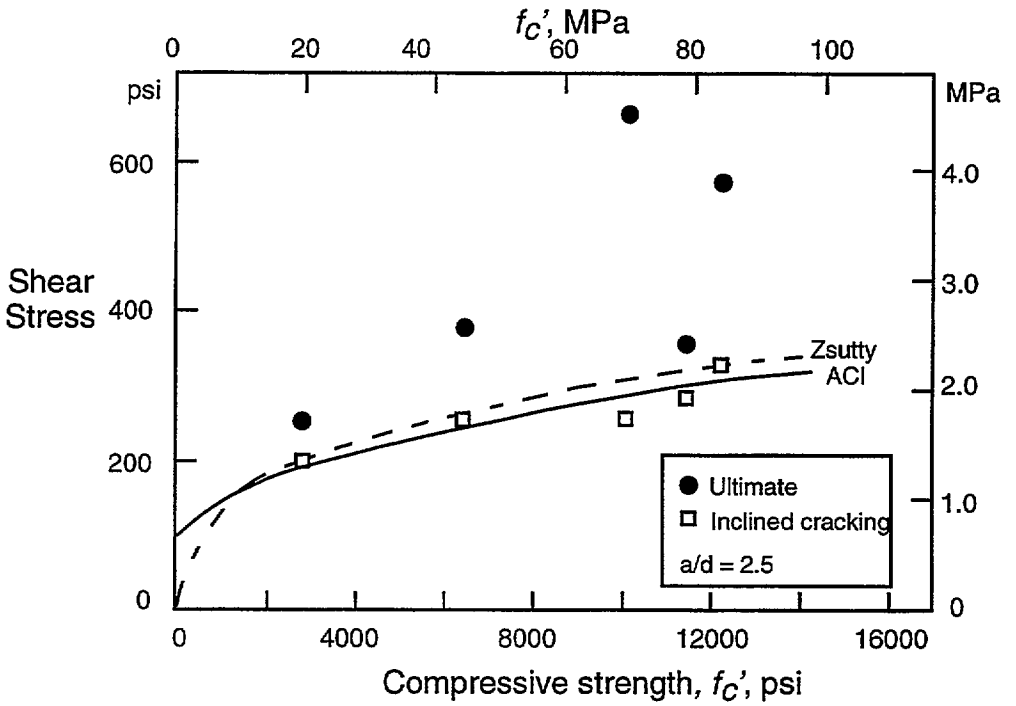

Figure 4.5 — Test results by Mphonde and Frantz (1984) for $a/d = 2.5$

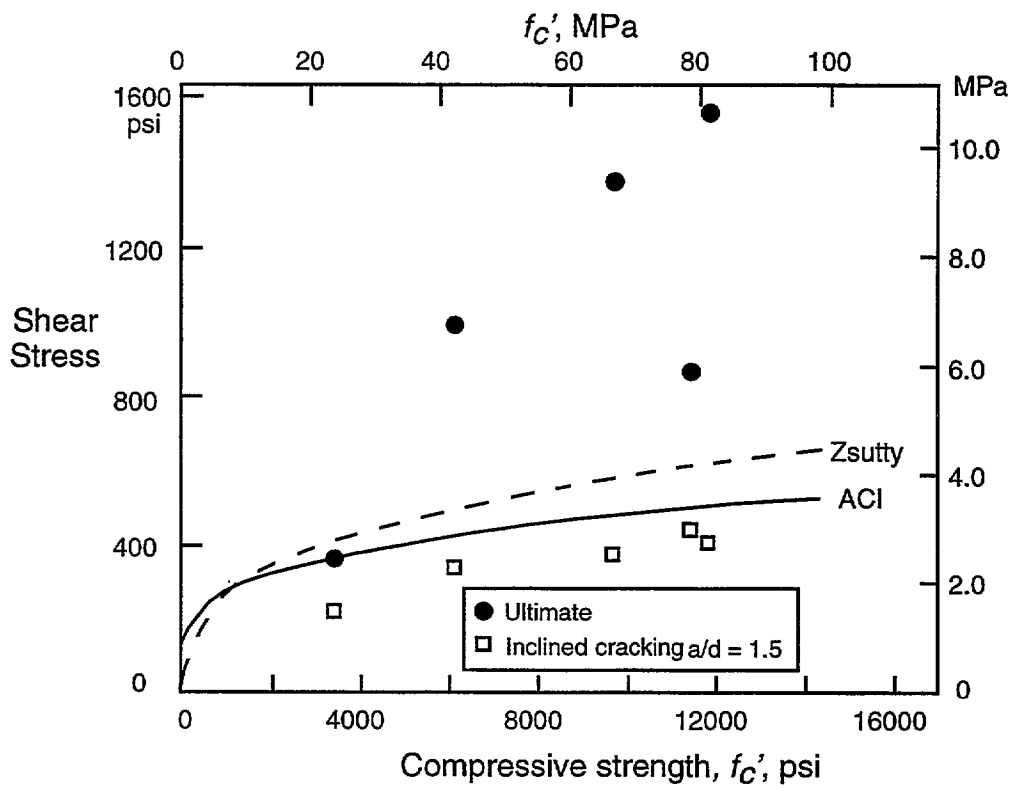

Figure 4.6 — Test results by Mphonde and Frantz (1984) for $a/d = 1.5$

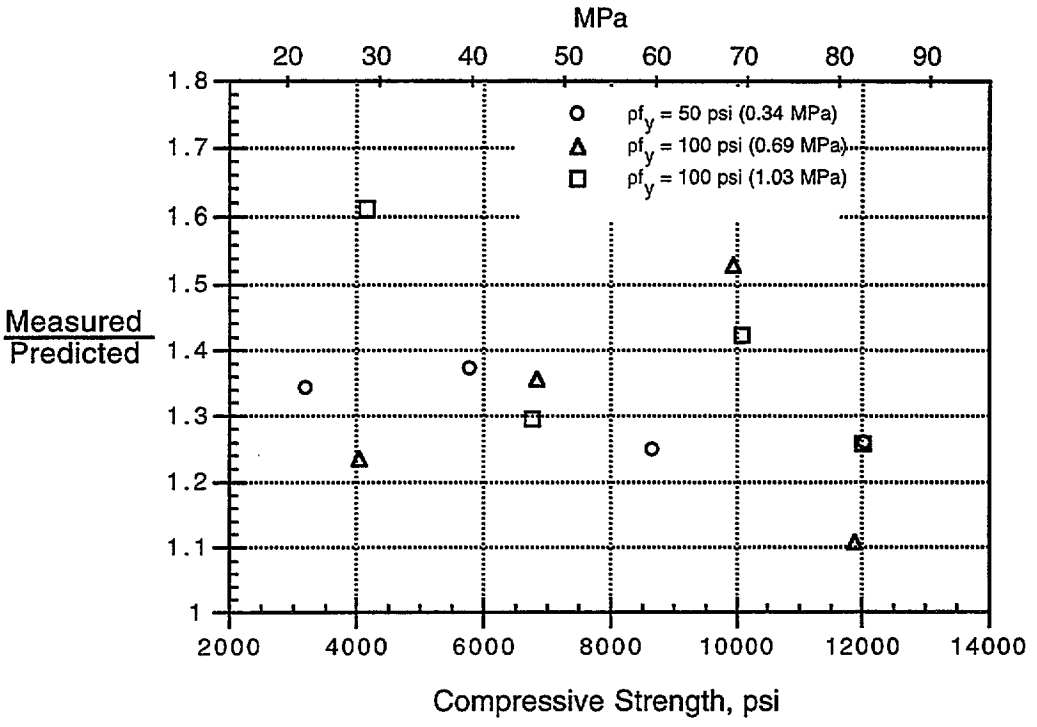

Figure 4.7 — Ratio of measured to predicted shear strength (based on ACI equation) as a function of concrete strength (Mphonde and Frantz 1985)

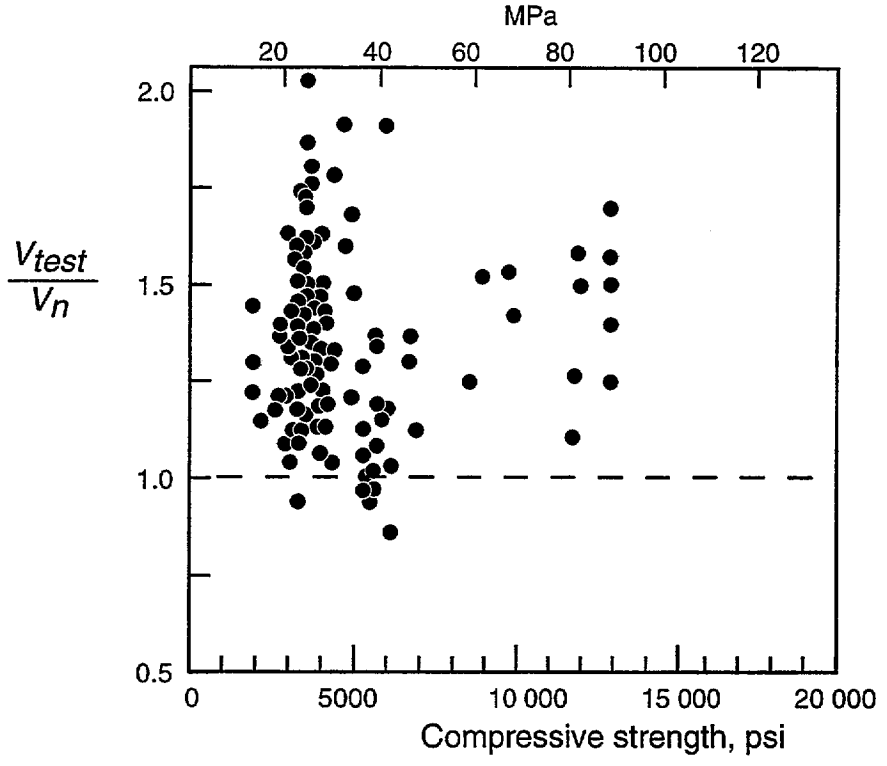

Figure 4.8 — Test results from beams that failed in shear, V_n according to ACI (adapted from Roller and Russell 1990)

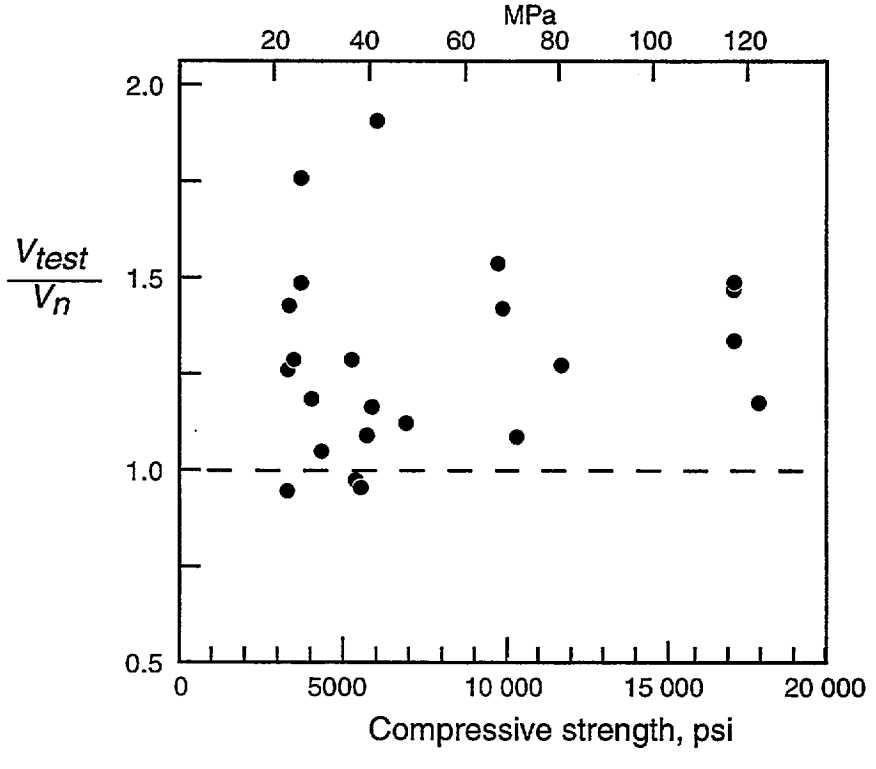

Figure 4.9 — Test results from beams that failed in shear and met all the requirements of ACI Code including minimum web reinforcement provision, V_n according to ACI (adapted from Roller and Russell 1990)

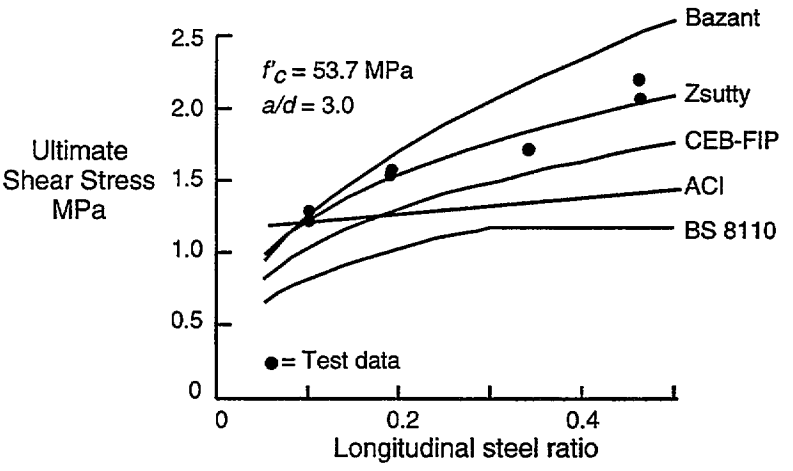

Figure 4.10 — Effect of longitudinal reinforcement ratio on shear strength (Kim and Park 1994)

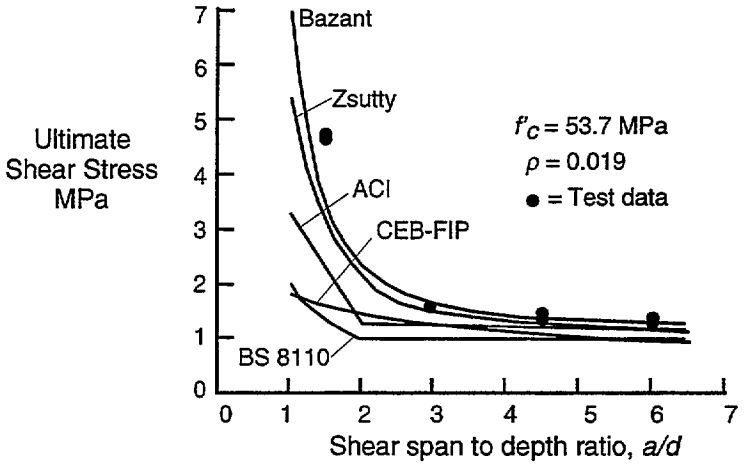

Figure 4.11 — Effect of shear span to depth ratio on shear strength (Kim and Park 1994)

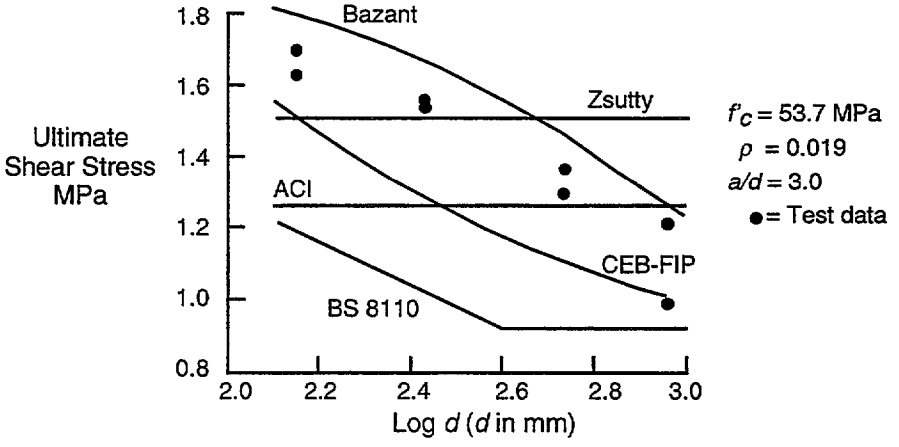

Figure 4.12 — Effect of depth *d* on shear strength (Kim and Park 1994)

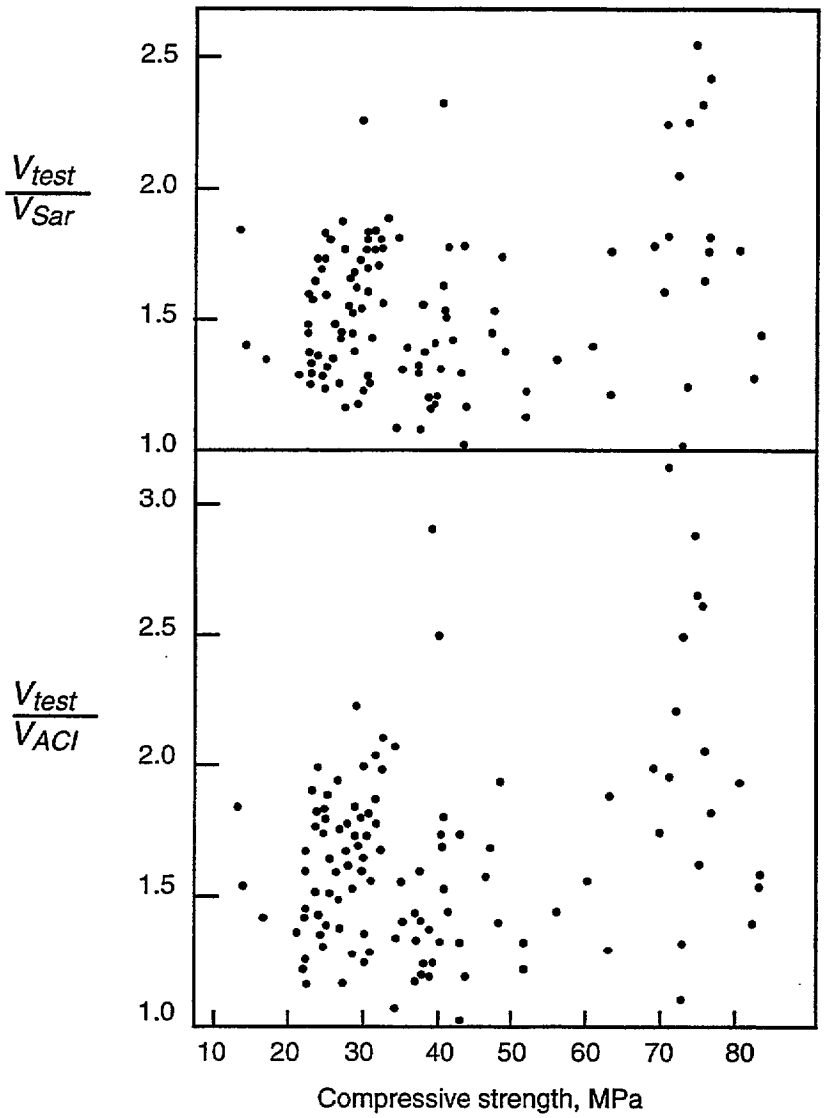

Figure 4.13 — Influence of compressive strength on ratio of experimental to computed shear strength (Sarsam and Al-Musawi 1992)

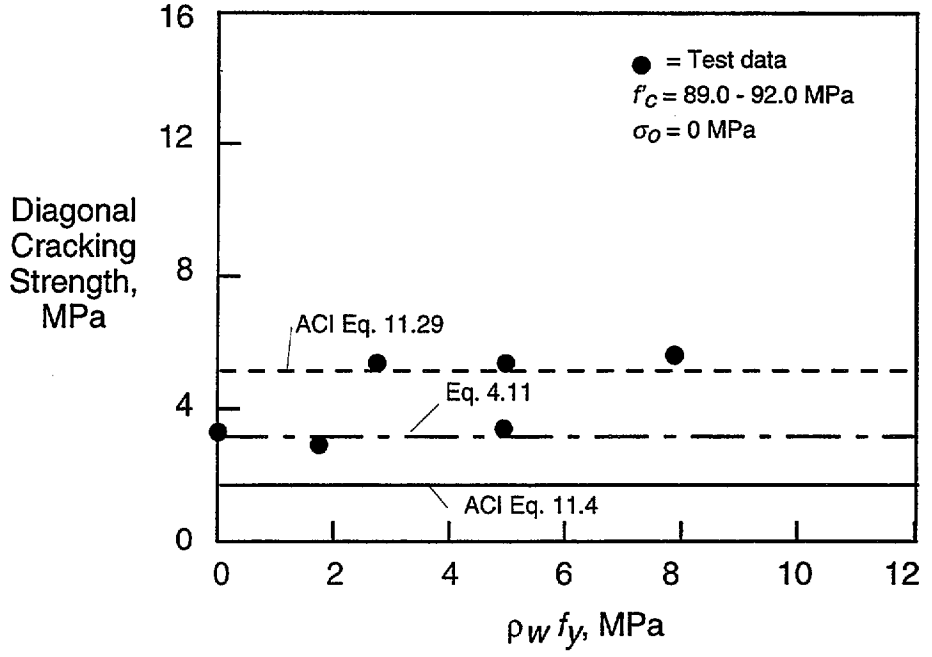

Figure 4.14 — Effect of transverse reinforcement ($\rho_w f_y$) on diagonal cracking strength of beam specimens (Sakaguchi et al. 1990)

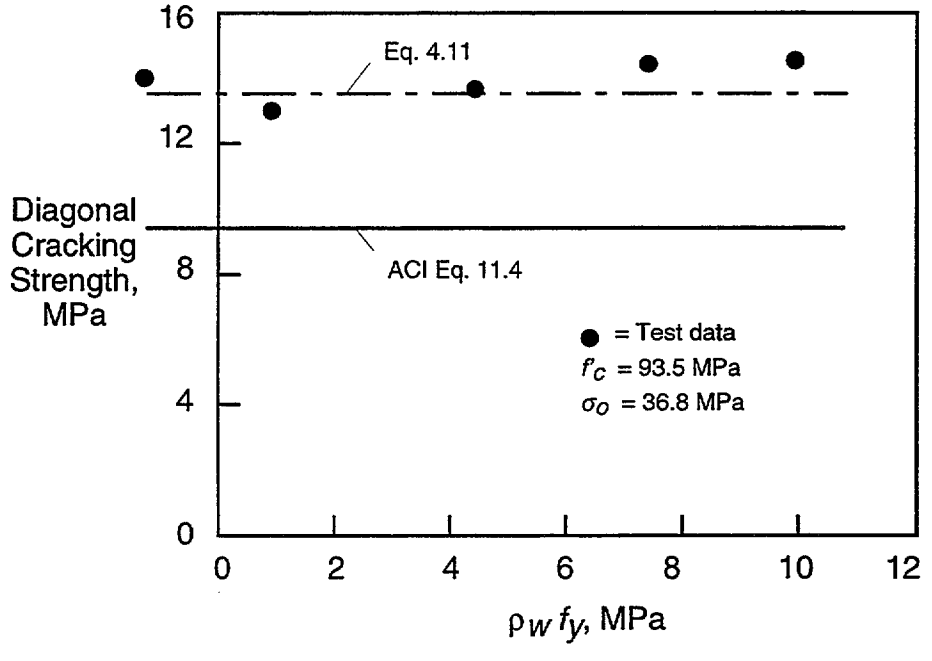

Figure 4.15 — Effect of transverse reinforcement ($\rho_w f_y$) on diagonal cracking strength of column specimens (Sakaguchi et al. 1990)

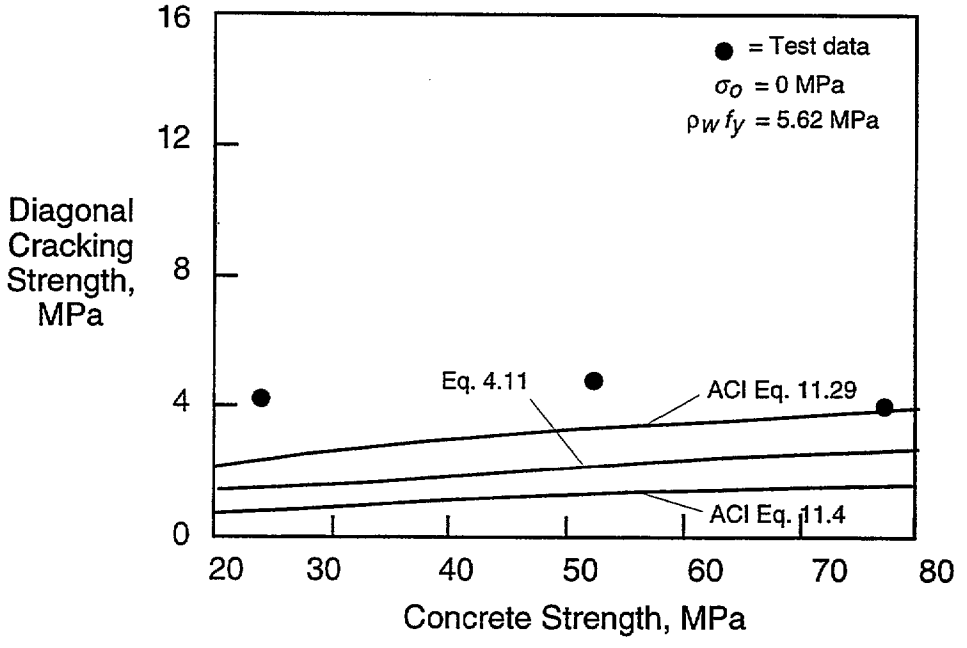

Figure 4.16 — Effect of concrete strength on diagonal cracking strength of column specimens (Sakaguchi et al. 1990)

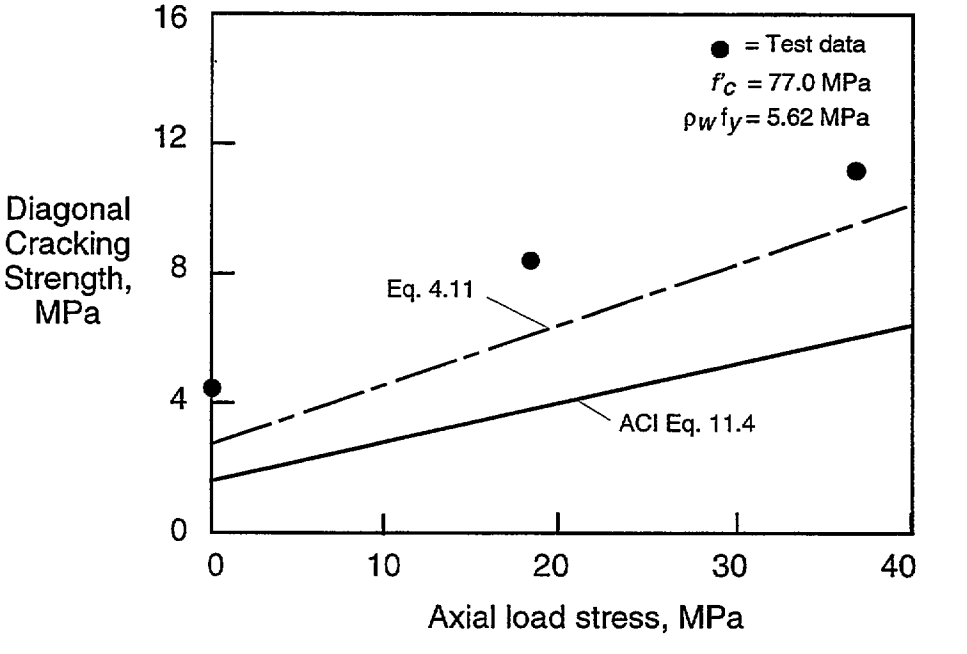

Figure 4.17 — Effect of axial load on diagonal cracking strength of column specimens (Sakaguchi et al. 1990)

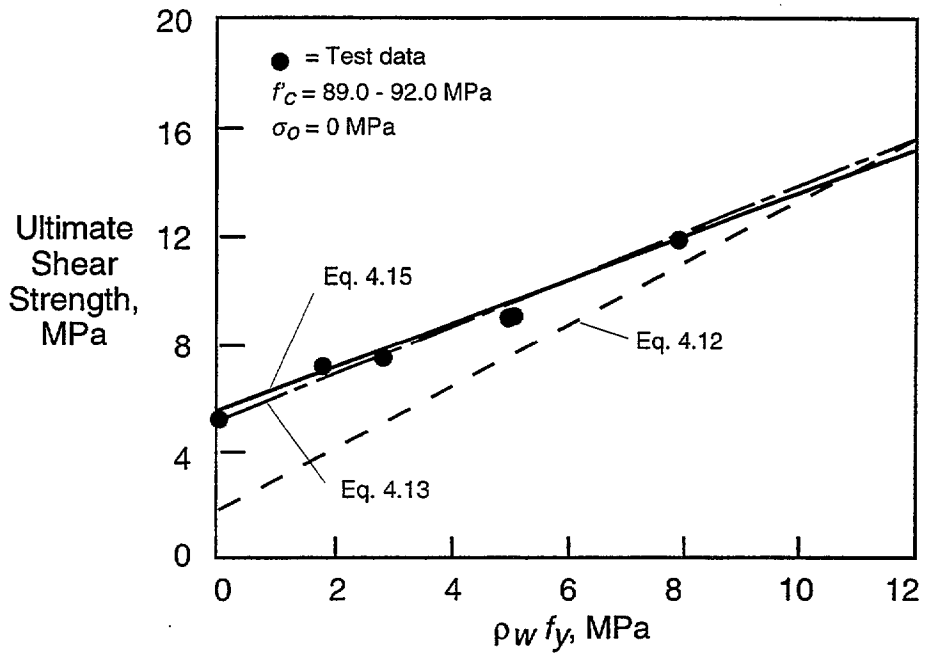

Figure 4.18 — Effect of transverse reinforcement ($\rho_w f_y$) on ultimate shear strength of beam specimens (Sakaguchi et al. 1990)

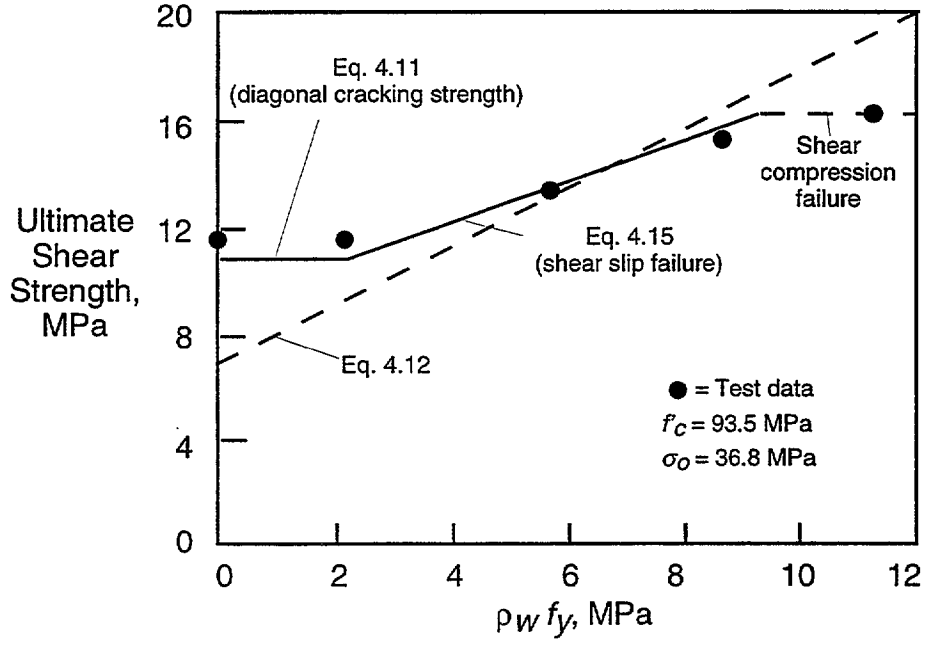

Figure 4.19 — Effect transverse reinforcement ($\rho_w f_y$) on ultimate shear strength of column specimens (Sakaguchi et al. 1990)

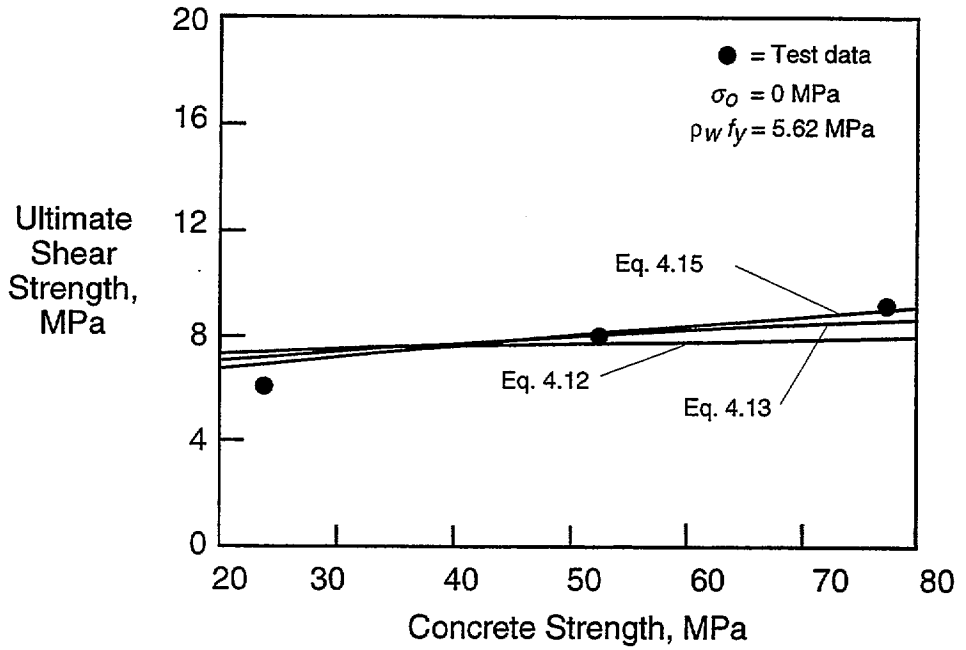

Figure 4.20 — Effect of concrete strength on ultimate shear strength (Sakaguchi et al. 1990)

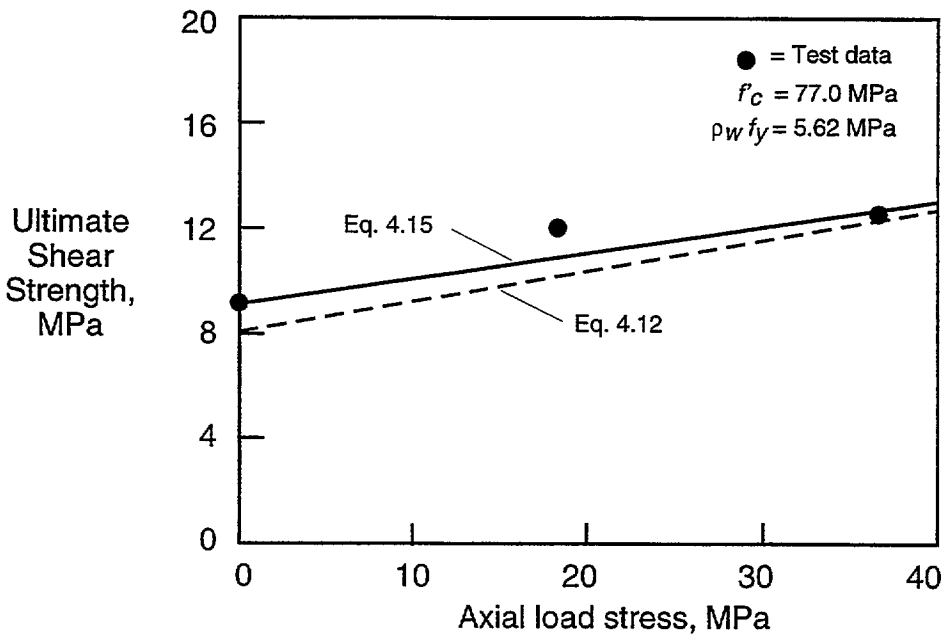

Figure 4.21 — Effect of axial load stress on ultimate shear strength (Sakaguchi et al. 1990)

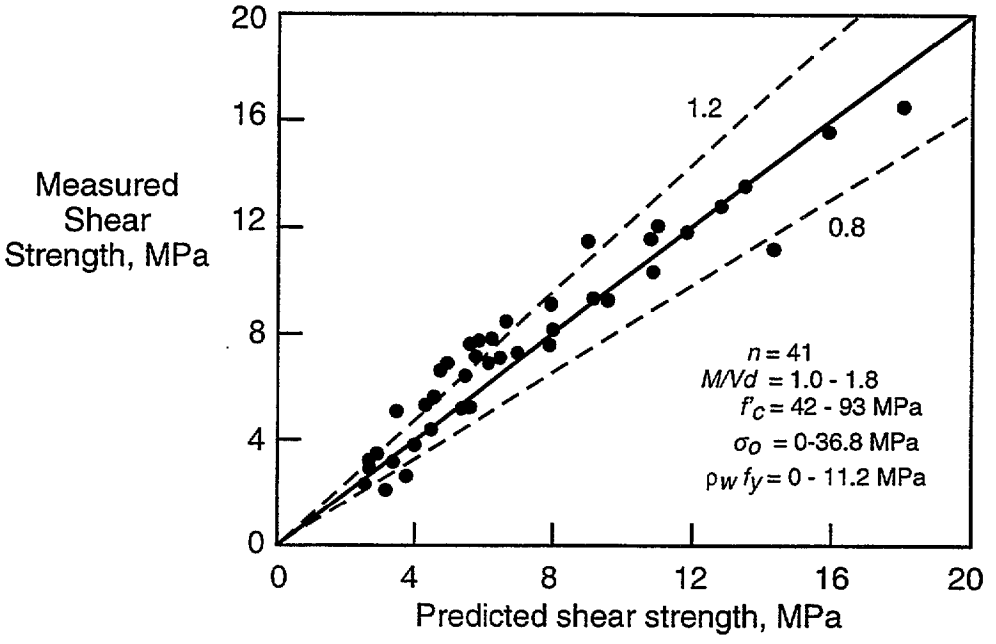

Figure 4.22 — Comparison of experimental results with predicted shear strength using Eq. 4.15 (Sakaguchi et al. 1990)

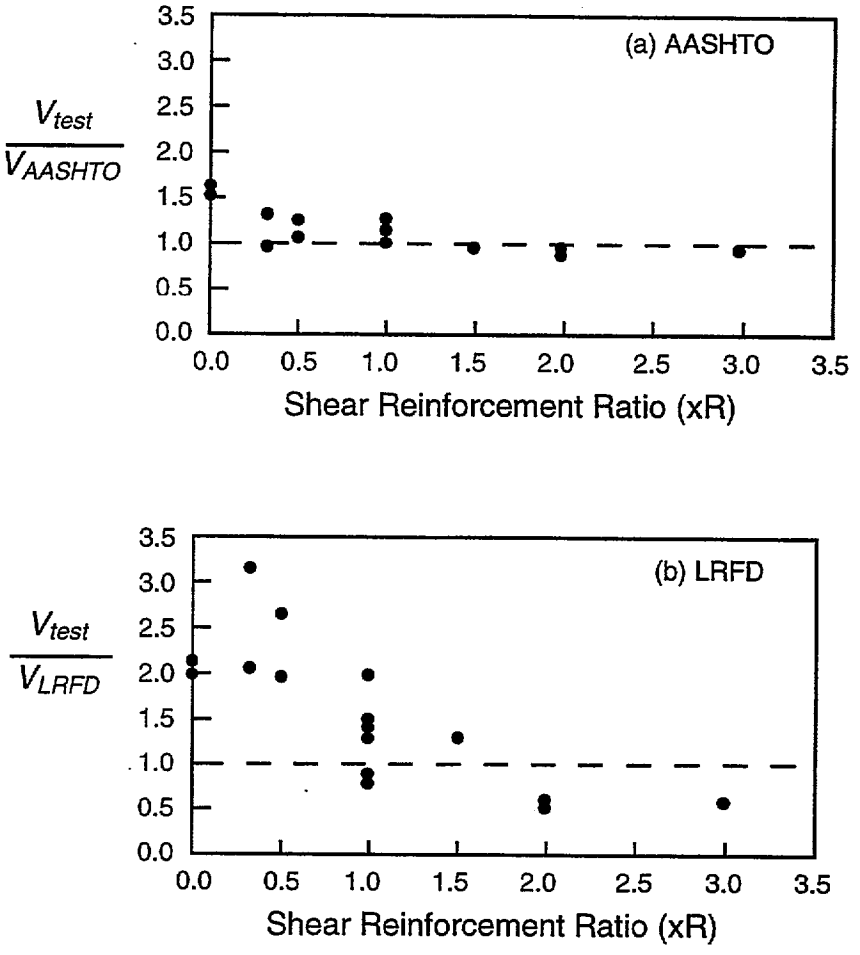

Figure 4.23 — Comparison of experimental shear strengths with predictions by (a) 1989 AASHTO Specifications and (b) 1994 LRFD Specifications (reinforcement ratio in terms of AASHTO requirement) (Shahawy and Batchelor 1996)

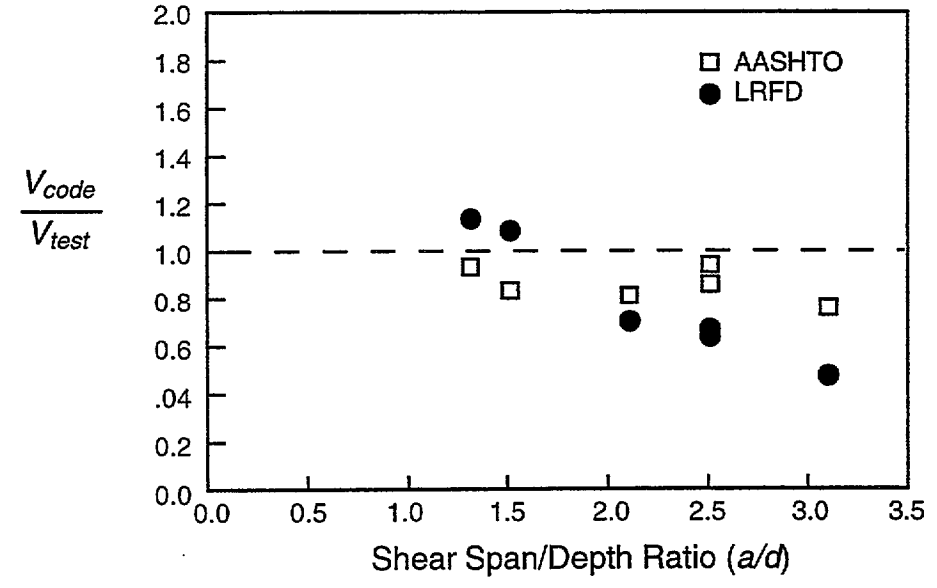

Figure 4.24 — Comparison of predicted shear strength with test results for beams with shear reinforcement as required by 1989 AASHTO Specifications (Shahawy and Batchelor 1996)

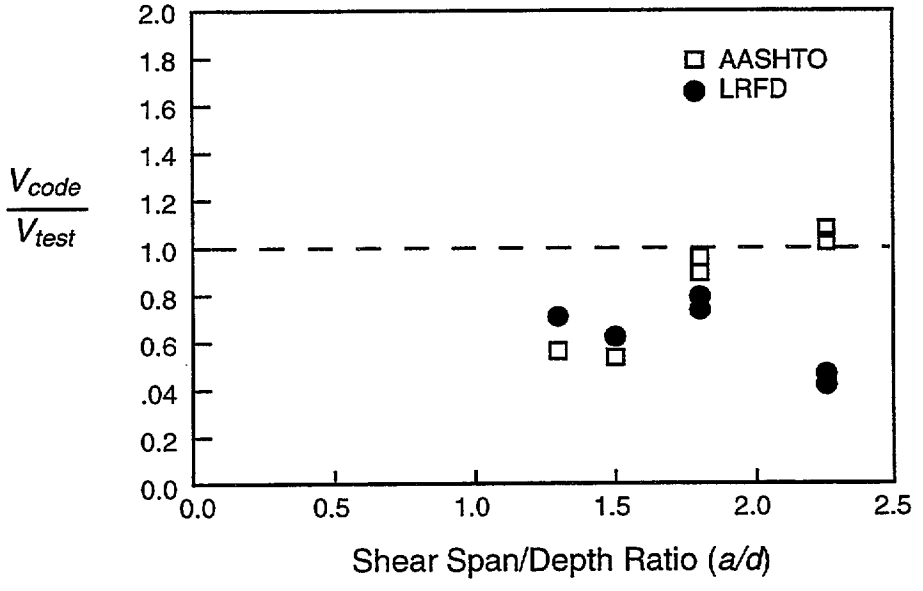

Figure 4.25 — Comparison of predicted shear strength with test results for beams with no shear reinforcement (Shahawy and Batchelor 1996)

4.2 Panel Tests

The web of concrete beams under shear is in a state of biaxial tension-compression. The presence of simultaneous transverse tensile strain leads to a deterioration of the compressive strength of the cracked concrete (Fig. 4.26). The main cause is probably that concrete cracks are irregularly shaped, resulting in irregular shapes of the concrete between the cracks. This engenders eccentric loads and stress concentration in the concrete struts. This behavior is investigated in panel tests.

4.2.1 Vecchio and Collins (1993) reviewed various models of compression softening of cracked reinforced concrete panels due to transverse tension. A softening parameter β is defined as the ratio of the compressive strength in biaxial tension (direction 1) - compression (direction 2) f_{c2max} to the uniaxial cylinder compressive strength f'_c.

$$\beta = \frac{f_{c2max}}{f'_c}$$

1) Vecchio and Collins (1982) expressed β as a function of the ratio of the principal strains:

$$\beta = \frac{1}{0.85 - 0.27\,\varepsilon_1/\varepsilon_2}$$

They used Hognestad's (1951) parabola, Eq. 4.21, as the cylinder stress-strain curve. Both peak stress f'_c and its associated strain ε_o were multiplied by β. Good agreement was found with 178 experimental data points (mean ratio = 1.01, coefficient of variation = 0.15).

2) Vecchio and Collins (1986) simplified the expression for β to:

$$\beta = \frac{1}{0.80 + 0.34\,\varepsilon_1/\varepsilon_o} = \frac{1}{0.8 + 170\,\varepsilon_1} \quad \text{for} \quad \varepsilon_0 = 0.002 \qquad (4.16)$$

The latter expression is now used in the Canadian Code (CSA 1994). Again good agreement with experiments was obtained (mean ratio = 0.98, coefficient of variation 0.16).

3) Kollegger and Mehlhorn (1990) concluded that the effective compressive strength did not reduce beyond $0.8f_c'$ and that the prime influencing factor appeared to be the principal tensile stress f_{c1} rather than the principal tensile strain ε_1. They based their conclusions on 55 panel tests which had the tension-compression loads applied parallel to the reinforcement on most of them, but with some applied at 45°. All reinforcement crossing the cracks yielded before large tensile strains were attained and hence, significant softening could not be achieved. Kollegger and Mehlhorn (1990) stated that the low strength of Vecchio and Collins's (1986) panels was actually due to yielding of the reinforcement and not crushing of the concrete.

4) Miyahara (1988) proposed a softening model also based on the principal tensile strain:

$$\begin{aligned} &\beta = 1.0 && \varepsilon_1 < 0.0012 \\ &\beta = 1.15 - 125\,\varepsilon_1 && 0.012 < \varepsilon_1 < 0.0044 \\ &\beta = 0.60 && 0.0044 < \varepsilon_1 \end{aligned} \qquad (4.17)$$

The degree of softening is much less than that predicted by Vecchio and Collins. It should be noted, however, that this model is used together with a shear transfer model. In cases where appreciable levels of shear transfer act on the crack plane, the reduction effect is greater than predicted by the compression model alone.

5) Shirai and Noguchi (1989) and Mikame (1991) proposed the following softening parameter:

$$\beta = \frac{1}{0.27 + 0.96\,(\varepsilon_1/\varepsilon_o)^{0.167}} \tag{4.18}$$

They noted that the softening is greater for HSC than for NSC.

6) For HSC, Ueda (1991) proposed the following:

$$\beta = \frac{1}{0.8 + 0.6\,(1\,000\,\varepsilon_1 + 0.2)^{0.39}}$$

7) Belarbi and Hsu (1991) used Hognestad's parabola as a basis and suggested one softening parameter for stress and another for strain:

$$\beta_\sigma = \frac{0.9}{\sqrt{1 + K_\sigma \varepsilon_1}} \quad \text{and} \quad \beta_\varepsilon = \frac{1}{\sqrt{1 + K_\varepsilon \varepsilon_1}}$$

where K_σ and K_ε depend on the orientation θ of the cracks to the reinforcement and the type of loading as follows:

	Proportional Loading		Sequential Loading	
θ	K_σ	K_ε	K_σ	K_ε
45°	400	160	400	160
90°	400	550	250	0

Balarbi and Hsu (1995) updated their model in a recent paper. See § 4.2.2 of this report.

8) Vecchio and Collins (1993) updated their model as follows:
Their base curve is now the Thorenfeldt (1987) curve, which is more appropriate for HSC (more linear in its pre-ultimate response) than Hognestad's parabola. The Thorenfeldt curve was calibrated by Collins and Porasz (1989). See § 4.2.3 and Fig. 4.27.

$$f_{c2base} = -f_p \frac{n\,(-\varepsilon_2/\varepsilon_p)}{n - 1 + (-\varepsilon_2/\varepsilon_p)^{nk}} \tag{4.19}$$

where n = $0.80 + f_p / 17$ (MPa)

k = 1.0 for $-\varepsilon_p < \varepsilon_2 < 0$,

k = $0.67 + f_p / 62$ (MPa) for $\varepsilon_2 < -\varepsilon_p$, (4.20)

f_p = maximum compressive stress in softened concrete, and

ε_p = strain corresponding to f_p.

The base curve is modified in two possible ways:

Model A: strength and strain softening:

$$\beta = \frac{1}{1.0 + K_c K_f}$$

$$\text{where} \quad K_c = 0.35\left(\frac{-\varepsilon_1}{\varepsilon_2} - 0.28\right)^{0.80} \geq 1.0 \quad \text{for} \quad \varepsilon_1 < \varepsilon_{1L}, \quad \text{and}$$

$$K_f = 0.1825\sqrt{f_c'\,(\text{MPa})} \geq 1.0.$$

ε_{1L} is the limiting tensile strain in the concrete at which the reinforcement at a crack begins to yield and the concrete suffers little additional cracking.

For $-\varepsilon_2 < \beta\varepsilon_o$, f_{c2} is calculated from Eq. 4.19 with $f_p = \beta f_c'$ and $\varepsilon_p = \beta\varepsilon_o$.

For $-\varepsilon_2 > \beta\varepsilon_o$, $f_{c2} = \beta f_{c2\,base}$ with $f_{c2\,base}$ calculated from Eq. 4.19 using $f_p = f_c'$ and $\varepsilon_p = \varepsilon_o$.

For the 443 data sets considered, the ratio of experimental to calculated stress has a mean of 0.996 and a coefficient of variation (COV) of 0.188. If only the ultimate load stages of the 45 specimens failing by concrete crushing are considered, then the mean is 1.06 and the COV is 0.178.

Model B uses strength only softening:

$$\beta = \frac{1}{1 + K_c} \quad \text{where} \quad K_c = 0.27\left(\frac{\varepsilon_1}{\varepsilon_o} - 0.37\right)$$

Note that Eqs. 4.19 and 4.20 are used with $f_p = \beta f_c'$ and $\varepsilon_p = \varepsilon_o$ = strain in concrete cylinder at peak stress f_c'. No correlation could be found with f_c' and thus a K_f factor was not included. Considering all load stages, the ratio of experimental to calculated values of principal compressive stress has a mean of 1.022 and a COV of 0.211. Considering the ultimate stress conditions of the panels failing in concrete crushing, the stress ratio has a mean of 1.018 and a COV of 0.227.

In a later update, Vecchio, Collins and Aspiotis (1994) conducted 12 shear tests of panels 890 mm x 89 mm x 70 mm made of 55 MPa (8000 psi) concrete. The panels were reinforced by two orthogonal grids at 45° to their edges. Results show that the compression-softening formulation developed for normal strength concrete elements apply equally well to HSC elements. Now Model B also has a K_f factor:

$$K_f = 2.55 - 0.2629\sqrt{f_c'\,(\text{MPa})} \leq 1.11$$

Both models agree well with experiments, with Model B being slightly superior.

9) Parametric study

Influence of f_c':

Of 443 experimental data points, more than half correspond to $20 < f_c' < 30$ MPa. Of the 16 data points above 70 MPa, the prediction with or without the K_f factor is not as good as for NSC. (The theory overestimates strength and the scatter is large). In general, though, the inclusion of K_f improves the prediction at all strength levels.

Other parameters were investigated and found to have minor effects:

- type of loading (proportional or not),
- inclination of stress field to reinforcement,
- crack rotation,
- type of reinforcement (deformed or mesh), and
- size of panel.

10) Comparison of models

Model A gave the strongest correlation. The Maekawa (see § 4.2.5) and the Noguchi (Shirai and Noguchi 1989) models also gave good predictions of the mean stresses, but with a somewhat higher scatter (COV = 0.23). The Hsu model (Belarbi and Hsu 1995) showed weaker correlation, over predicting the softening effect and producing higher scatter (COV = 0.26). Limiting the softening to $0.80 f_c'$ or ignoring it, produces poor results.

11) Prediction of element behavior

Analyses of overall element behavior by non-linear FEA showed an accuracy better than the compression softening models used. The dependence of the element behavior on the reinforcement tended to reduce the error in predicting response.

4.2.2 Belarbi and Hsu (1995) tested 22 panels 55 x 55 x 7 in. (1400 x 1400 x 178 mm) under biaxial tension-compression. The panels had a concrete strength of 6000 psi (40 MPa), minimal reinforcement (0.54%) in the compression (transverse) direction and various reinforcement ratios in the tension (longitudinal) direction. The purpose of the tests was to determine the principal parameters and the constitutive equations of cracked concrete in biaxial, orthogonal tension-compression. The following conclusions were reached:

1) Two planes of loading jacks are recommended to prevent bending of the panels.
2) LVDT's attached to rods spanning the length of the panels are recommended to measure average strains. A minimum of eight (four on each side) is recommended for the compressive strains, which can vary widely depending on whether the rod is between cracks or approximately on top of a crack.
3) It is the tensile strain, and not the tensile stress, that affects the orthogonal compressive softening. In one series of tests, the tension was released after the concrete had cracked and before the compression was applied. The compression behavior was similar to the tests in which the tension was maintained while the orthogonal compression was applied.
4) The load path makes little difference. Sequential loading (tension followed by orthogonal compression) produces the same behavior as proportional loading. However, significant differences in behavior are observed when a small release of tensile stress occurs just prior to failure.
5) The amount and spacing of the longitudinal reinforcement has only a minor effect on the behavior.

The following notation is used:

f_c' = cylinder compressive strength,
σ_d = principal compressive stress of concrete under orthogonal biaxial tension-compression,
ε_o = cylinder strain corresponding to cylinder strength f_c',
ε_d = average principal compressive strain under orthogonal biaxial tension-compression,
ε_r = average principal tensile strain of concrete under orthogonal biaxial tension-compression,
β = softening coefficient, and
K_o = 400 for proportional loading,
250 for sequential loading with some tension release just prior to failure.

The following stress-strain relationship is proposed for cracked reinforced concrete under orthogonal biaxial tension-compression (see Fig. 4.27a):

For a non-softened, standard cylinder, strength is a parabolic function of strain:

$$\sigma_d = f_c' \left[2 \left(\frac{\varepsilon_d}{\varepsilon_o} \right) - \left(\frac{\varepsilon_d}{\varepsilon_o} \right)^2 \right] \tag{4.21}$$

The softening is of the form:

$$\text{For } \varepsilon_d \le \beta\varepsilon_o \qquad \sigma_d = \beta f_c' \left[2\left(\frac{\varepsilon_d}{\beta\varepsilon_o}\right) - \left(\frac{\varepsilon_d}{\beta\varepsilon_o}\right)^2 \right]$$

$$\text{For } \varepsilon_d > \beta\varepsilon_o \qquad \sigma_d = \beta f_c' \left[1 - \left(\frac{\frac{\varepsilon_d}{\beta\varepsilon_o} - 1}{\frac{2}{\beta} - 1} \right)^2 \right] \tag{4.22}$$

$$\beta = \frac{0.9}{\sqrt{1 + K_o \varepsilon_r}}$$

6) This softening is less severe than that proposed by Vecchio and Collins (1986). This may be attributed to the orientation of the reinforcements: 45° to the principal directions for Vecchio and Collins and parallel to the principal directions here. The amount of reinforcement, especially transverse, is therefore also different between Vecchio and Collins and here. A comparison with other softening coefficients is shown in Fig. 4.28.
7) It would be interesting to pursue this kind of tests further for HSC ($f_c' > 40$ MPa).

Hsu (1991) also developed a general method to perform non-linear analysis of concrete membrane elements.

4.2.3 Collins and Porasz (1989)

The modified compression field theory (MCFT), in its normal strength concrete (NSC) version, is slightly unconservative when applied to high strength concrete (HSC). This conclusion was reached from test results of four panels 1.6 m x 1.6 m x 2.9 m, made of 70 MPa concrete and reinforced with two orthogonal grids of reinforcement oriented at 45° to the edges of the element. The authors suggest abandoning the parabolic stress-strain curve of NSC, Eq. 4.21, in favor of the one proposed by Thorenfeldt, Tomaszewicz and Jensen (1987):

$$\frac{f_c}{f_c'} = \frac{n(\varepsilon_c/\varepsilon_o)}{n - 1 + (\varepsilon_c/\varepsilon_o)^{nk}}$$

where f'_c = peak stress obtained from cylinder tests,
ε_o = strain corresponding to $f_c = f'_c$,
n = $0.8 + f'_c / 17$ (f'_c in MPa) = curve fitting factor and
k = 1.0 for $\varepsilon_c \le \varepsilon_o$ (ascending branch),
= $0.67 + f'_c / 62$ for $\varepsilon_c > \varepsilon_o$ (descending branch).

Test results indicate that HSC is somewhat more sensitive to transverse straining than lower strength concrete. The authors suggest the following adjustments to the stress-strain curve:

$$\frac{f_{c2}}{f_c} = \frac{1}{\lambda} \quad \text{or} \quad \frac{f_{c2}}{f_c'} = \frac{1}{\lambda} \frac{n(\varepsilon_{c2}/\varepsilon_o)}{n-1+(\varepsilon_{c2}/\varepsilon_o)^{nk}}$$

$$\lambda = \left(0.8 - 0.34\frac{\varepsilon_1}{\varepsilon_o}\right)\left(0.9 + 0.0045 f_c'\right) \geq 1$$

4.2.4 Stroband

Stroband (1995) tested rectangular concrete panels reinforced longitudinally under longitudinal tension and transverse compression. The range of cube strength is 30 MPa (4 panels), 65 MPa (4 panels) and 110 MPa (12 panels). He found that:

1. The biaxial compressive strength is, on the average, 70% of the uniaxial prism strength (100 x 100 x 400 mm prism).
2. Taking into account the fairly high standard deviation of the results, there is no indication that behavior under biaxial loading is dependent on the concrete compressive strength.
3. The ultimate compressive strength is almost independent of the level of the tensile stress. This contradicts Kollegger and Mehlhorn's (1990) conclusions. It should be noted that the maximum crack width did not exceed 0.4 mm and thus the yield strength of the steel was not reached.
4. The panels typically fail with the formation of an inclined shear failure plane. With increasing concrete strength, a more brittle failure occurred.

4.2.5 Tanabe and Wu (1991)

Tanabe and Wu (1991) presented some Japanese experimental results for biaxial tension-compression and corresponding softening coefficient.

1) Maekawa and Okamura proposed the following softening coefficient, based on measurements on cylindrical specimens under axial compression and internal pressure.

$$\beta = 1.0 \qquad \varepsilon_1 < \varepsilon_a$$

$$\beta = 1.0 - 0.4\frac{\varepsilon_1 - \varepsilon_a}{\varepsilon_b - \varepsilon_a} \qquad \varepsilon_a \leq \varepsilon_1 \leq \varepsilon_b$$

$$\beta = 0.6 \qquad \varepsilon_o < \varepsilon_1$$

where ε_1 = transverse tensile strain, $\varepsilon_a = 0.0012$ and $\varepsilon_b = 0.0044$.

2) Sumi and Kawamata tested panels with equal reinforcement in two perpendicular directions and proposed a softening of the form:

$$\frac{\sigma_2}{f_c'} = f(\varepsilon_2)\left(1.5 + \frac{\varepsilon_{cr}}{\varepsilon_o}\right) - \left(\frac{\varepsilon_2}{\varepsilon_o}\right)^2$$

where σ_1 = stress in transverse direction,
σ_2, ε_2 = compressive stress and strain of cracked element, and
ε_{cr} = compressive strain in cracked element at initiation of transverse strain.

They also tested panels with unequal reinforcement in directions 1 and 2, for which they proposed the following softening:

$$\frac{\sigma_2}{f_c'} = \lambda f(\varepsilon_2) \qquad \lambda = \frac{4\,\sigma_1 + \sigma_{2max}}{\sigma_{2max}}$$

Surprisingly, this equation gives higher compressive strength when the orthogonal tensile stress is increased.

Shirai performed tests of small panels and proposed:

$$\beta_1 = -\left(\frac{0.31}{\pi}\right)\tan^{-1}(4820\,\varepsilon_1 - 11.82) + 0.84$$

$$\beta_2 = -5.9\,\frac{\sigma_1}{f_c'} + 1.0$$

$$\beta = \beta_1 * \beta_2$$

4.2.6 Tension Stiffening

So far, we have only looked at the softening of the concrete struts due to transverse tension. Hsu and Zhang (1996) improved on the modeling of the biaxial behavior of concrete membranes under biaxial tension-compression by also accounting for the tension stiffening of the reinforcement bars due to the tensile resistance of the concrete between cracks. Indeed, the behavior of a steel bar embedded in concrete is quite different from that of a bare bar. To properly account for this behavior, Hsu and Zhang modeled the concrete tensile stress-strain curve by:

$$\sigma_r = E_c\,\varepsilon_r \qquad \varepsilon_r \le \varepsilon_{cr}$$

$$\sigma_r = f_{cr}\left(\frac{\varepsilon_{cr}}{\varepsilon_r}\right)^{0.4} \qquad \varepsilon_r > \varepsilon_{cr}$$

where E_c = $47\,000\sqrt{f'_c}$ (psi) = $3\,900\sqrt{f'_c}$ (MPa) = concrete elastic modulus,
f_{cr} = $3.75\sqrt{f'_c}$ (psi) = $0.31\sqrt{f'_c}$ (MPa) = concrete tensile strength,
f_r = principal tensile stress averaged from a crack to midpoint between cracks,
ε_{cr} = 80×10^{-6} = average tensile strain at which concrete begins to crack, and
ε_r = principal tensile strain averaged over a length that traverses several cracks.

Also, they described the stress-strain curve of an embedded bar by a bilinear model:

$$f_s = E_s\,\varepsilon_s \qquad \text{for} \quad \varepsilon_s \le \varepsilon_n$$
$$f_s = f_y' = f_y\,C\,D \qquad \text{for} \quad \varepsilon_s > \varepsilon_n$$

where $C = (0.91 - 2B) + (0.02 + 0.25B)\,\varepsilon_s/\varepsilon_y$

$$D = 1 - \frac{2 - \alpha_2/45°}{1000\rho}$$

$$\varepsilon_n = \varepsilon_y\,(0.93 - 2B)\,D$$

and $$B = \frac{1}{\rho}\left(\frac{f_{cr}}{f_y}\right)^{1.5}$$

Factor C accounts for the averaging of steel stresses in the post-yield branch; D is a "kinking" factor and is equal to 1 when $\alpha_2 = 90°$; α_2 is the angle between the most compressive principal applied stress and the longitudinal reinforcement; and ε_n is the average strain at the intersection of the two straight lines in the bilinear model. Also,

E_s = elastic modulus of steel,
ε_s = average tensile strain of reinforcement bar,
f_y = yield strength of bare steel bar,
f'_y = average yield stress of bar embedded in concrete = a linear function of ε_s, and
ρ = reinforcement ratio.

These material relations were used with the concrete softening Eq. 4.22. Hsu and Zhang obtained good agreement with experimental results over the entire load-deformation history. The results were much improved compared to either ignoring the tensile strength of concrete or using the stress-strain curve of bare steel.

This conclusion agrees with earlier finite-element results by Kollegger and Mehlhorn (1990) who obtained equally good agreement with experiments by considering tension stiffening in the material model of the reinforcement or the concrete, as a function of the strain in the reinforcement direction (as opposed to the principal tensile strain direction). However, if tension stiffening is associated with the reinforcement, then the concrete compressive stresses are overestimated by the amount which should be carried by the concrete in tension. The agreement with experimental results is much worse when tension stiffening is ignored. Tension stiffening is also present in the models of Dei Poli, Prisco and Gambarova (1990) and Prisco and Gambarova (1995). See § 2.5.3.

4.2.7 Summary

From this review, it is seen that the behavior of concrete panels in biaxial tension-compression is not a settled issue. There is substantial disagreement on the extent of softening due to transverse tension. Hsu (1992) identifies the following reasons for these differences:

1) The concrete principal tensile strain is less than the yield strain of the reinforcement in some experiments, and exceeds it in others. The larger the principal tensile strain, the lower the softening coefficient.

2) The reinforcement is at 90° to the cracks in some experiments, and at 45° in others. Because 45° bars tend to kink at a crack, they result in a lower softening coefficient.

3) Load sequence also has an effect. Sequential loading with a small release of tension just prior to failure tends to produce a higher softening coefficient than does proportional loading.

4) The reinforcement ratios in the two orthogonal directions, equal or unequal, are also important. When the ratios are unequal, shear stresses develop between the concrete struts, thus weakening them and causing a lower softening coefficient. (For unequal ratios, the fixed crack angle differs from the rotating crack angle. The fixed angle is defined by the *applied* membrane stresses, whereas the rotating angle is the angle between the longitudinal steel and the *actual* principal compressive stress in the concrete. Cracks initially form in the fixed direction, but because of their formation, the stress field changes and future cracks form in a new direction. Thus, the name rotating angle.)

5) The concrete strength, the extent of restraint at the edges, and possible out-of-plane bending may also be significant parameters.

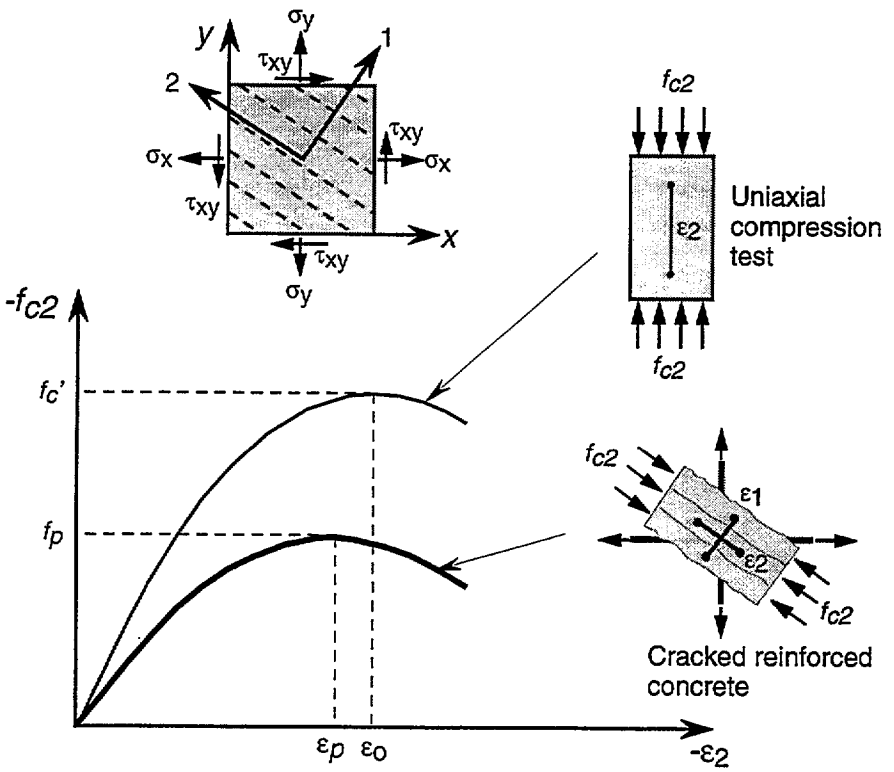

Figure 4.26 — Deteriorated compression response in cracked reinforced concrete elements (Vecchio and Collins 1993).

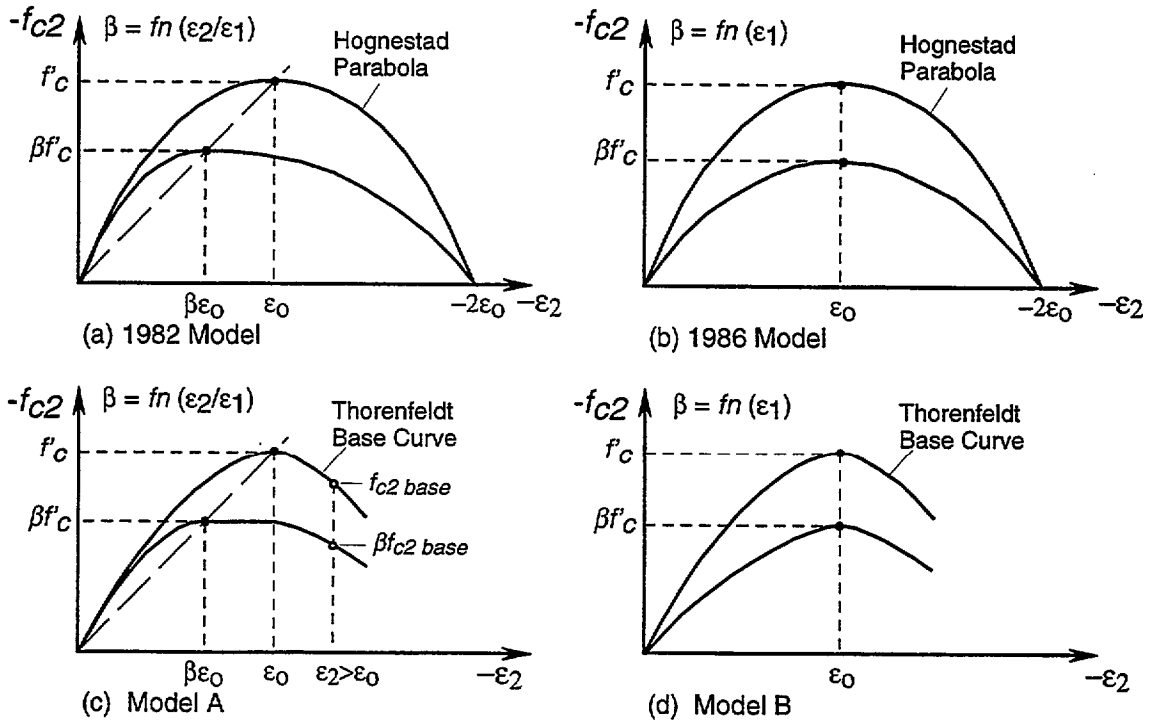

Figure 4.27 — Compression softening models: (a) 1982 model; (b) 1986 model; (c) proposed model A; and (d) proposed model B (Vecchio and Collins 1993).

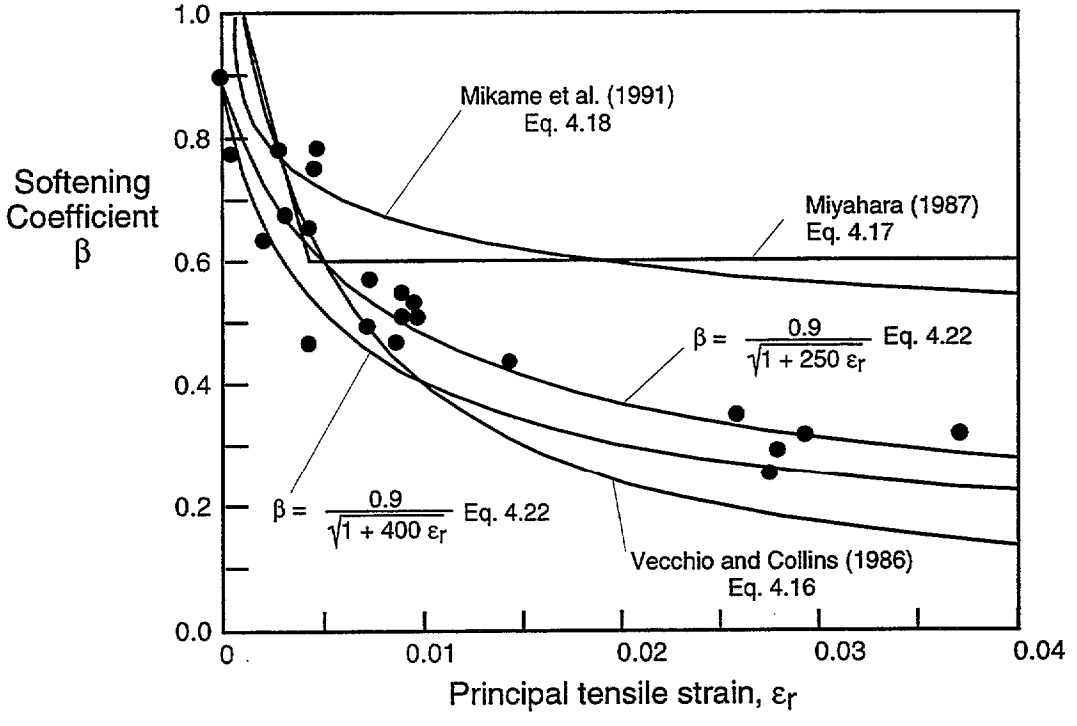

Figure 4.28 — Peak stress softening coefficient as a function of principal tensile strain (Belarbi and Hsu 1995)

4.3 Shear Friction Studies

4.3.1 Mattock (1972)

By transmitting normal and shear stresses across their faces, shear cracks contribute to shear resistance. This process is called aggregate interlock, interface shear transfer or more generally, shear friction. Hofbeck, Ibrahim and Mattock (1969) and Mattock and Hawkins (1972) carried out extensive tests on uncracked and precracked sections. They performed push-off, pull-off and modified push-off tests (Fig. 4.29). The latter combined a shear force $P\cos\theta$ with a normal compressive force $P\sin\theta$ transverse to the shear plane. The concrete strength varied from 21 to 37 MPa (3100 to 5400 psi).

In comparing the results of push-off tests to those of pull-off tests, Mattock et al. concluded that direct tension stress parallel to the shear plane reduces the shear transfer strength of initially *uncracked* concrete, but not that of initially *cracked* concrete.

In comparing the results of push-off tests to those of modified push-off tests, Mattock et al. concluded that an externally applied compressive stress, acting transversely to the shear plane, is additive to the compressive stress provided by the stirrups, assumed at yield, in calculations of the ultimate shear transfer strength of both initially cracked and uncracked concrete.

In initially cracked concrete, the concrete strength sets an upper limit value for the reinforcement ratio ρf_y, below which the relationship between the shear strength v_u and ρf_y is independent of concrete strength. Above this value of ρf_y, the shear transfer strength increases at a much reduced rate for lower strength concrete and is equal to that of similarly reinforced, initially uncracked concrete (Fig.4.30).

The shear transfer mechanisms of initially cracked concrete and initially uncracked concrete are completely different. In initially uncracked concrete, the shear transfer strength is developed by a truss action after diagonal tension cracking. Failure occurs when the inclined concrete struts fail under a combination of shear and axial force. In initially cracked concrete with moderate amounts of reinforcement, the shear transfer strength is developed primarily by frictional resistance to sliding between the faces of the crack and by dowel action of the reinforcement crossing the crack. When large amounts of reinforcement, or sufficient externally applied compressive stresses normal to the shear plane are provided, then the crack in the shear plane "locks up" and shear transfer strength is developed as in initially uncracked concrete. A pre-existing crack along the shear plane will both reduce the ultimate shear transfer strength and increase the slip at all levels of load (Fig. 3.25).

If the transverse reinforcement is perpendicular to the shear plane, Mattock et al. suggest that the shear strength of a precracked surface is:

$$V_n = 0.8 A_{vf} f_y + A_c K_1$$
$$\text{with} \quad \rho_v f_y = A_{vf} f_y / A_c \geq 1.38 \text{ MPa (200 psi)} \tag{4.23}$$

where

A_{vf} = area of reinforcement crossing the crack,
A_c = area of the concrete surface resisting shear friction,
K_1 = 2.76 MPa (400 psi) for normal weight concrete,
1.38 MPa (200 psi) for "all-lightweight" concrete,
1.72 MPa (250 psi) for "sand-lightweight"concrete.

The first term of Eq. 4.23 represents friction, with the coefficient of friction taken as 0.8 for concrete sliding on concrete. The second term represents the shear transferred by shearing off surface protrusions and by dowel action. A simplified version of this equation is adopted by the ACI Code

(see § 3.9.1 of this report).

It should be noted that a linear shear friction was first introduced by Mast and was later developed further by Birkeland, Anderson and their co-workers:

$$v_n = \mu \rho_v f_y$$

where μ is the coefficient of friction. This equation is very conservative for low clamping stresses and unsafe for high clamping stresses (Loov and Patnaik 1994).

4.3.2 Delft University of Technology Tests on NSC (1981)

Walraven (1981) and Walraven and Reinhardt (1981) performed some fundamental and convincing work on aggregate interlock, dowel action and axial tension of the reinforcement at a shear crack. The work combines experiment and theory and shows good agreement between the two. It also shows how to use the results in a finite-element analysis of cracked reinforced concrete members.

Pure shear tests with no bending were conducted on precracked, push-off, rectangular specimens 400 x 600 x 120 mm with a shear area of 300 x 120 mm, similar to Mattock's specimens. The two applied loads were collinear with the crack, and wedges on the upper and lower faces of the specimen channeled the loads to either side of the crack (Fig. 4.31). The specimens were either internally or externally reinforced. The concrete ranged from 20 to 56 MPa cube strength (f_{cc}) and included a lightweight concrete and one mix with a discontinuous grading of gravel size (no aggregate between 0.25 mm and 1.00 mm). The reinforcement ranged in ratio from 0.56 to 3.35% and in inclination from 45° to 135° to the crack plane. In one series of experiments, the reinforcement bars were covered with soft sleeves extending 20 mm on both sides of the crack to eliminate dowel action.

The analytical study assumes the concrete to be a mix of rigid, perfectly plastic mortar and rigid spherical aggregates of various sizes (Fig. 4.32). Knowing the volumetric ratio of aggregate to concrete and the size distribution of the aggregate, one can work out the average number of aggregate particles encountered by a crack of a given length. The portion of the mortar that interferes geometrically with the aggregate when the crack faces open and slide with respect to one another is assumed to yield, thus engendering normal and shear stresses which are related by a coefficient of friction. Equilibrium is related to frictional sliding and crushing of matrix material along the contact areas a_x and a_y. These depend on the crack displacement δ_t, δ_n (tangential and normal) or on the mix proportions (maximum aggregate size and volumetric percentage of aggregate).

The constitutive equations of the cracks are:

$$\sigma_u = \sigma_{pu}(A_x - \mu A_y) \quad \text{and} \quad \tau_a = \sigma_{pu}(A_y + \mu A_x)$$

where $A_x = \sum a_x$ and $A_y = \sum a_y$ depend on the crack width, the shear displacement, the maximum particle diameter and the total aggregate volume per unit volume of concrete. The strength of the mortar σ_{pu} and the coefficient of friction μ between mortar and aggregate are found from fitting curves to the experimental results.

$$\mu = \tau_{pu} / \sigma_{pu} = 0.40 \text{ and } \sigma_{pu} = 6.39 f_{cc}^{0.56} \text{ (elastic-perfectly plastic).}$$

Physically reasonable values can be found that fit *all* experimental curves well, thus lending credibility to the theory. (The indeterminacy of *two* parameters means that *two* curves can always be

fitted well. The credibility of the theory lies in the good fit of *all* the curves.)

Some of the conclusions of the study follow:

1) For reinforced cracks, the crack displacement path (sliding versus opening) is approximately constant, irrespective of the reinforcement ratio. For cracks in plain concrete, the crack displacement path depends clearly on the stiffness of the external restraint.
2) In reinforced cracks, variation of the bar diameter for a constant reinforcement ratio has no significant influence on the behavior.
3) Variation of the aggregate composition (doubling the maximum diameter from 16 to 32 mm or removing all particles between 0.25 and 1.00 mm) does not significantly influence the behavior.
4) The normal and shear displacements in reinforced cracks subjected to an external shear force decrease with increasing reinforcement ratio and concrete strength. The ultimate shear resistance is increased by higher concrete strength.
5) The efficiency of the reinforcement increases as its inclination with respect to the crack decreases, i.e. a bar at 45° to a crack is put into tension by the shear displacement, whereas a bar at 135° tends to kink.
6) Dowel action is of minor importance compared to aggregate interlock.
7) For light-weight concrete (LWC), cracks cross the aggregate. For a given shear displacement, the shear stress, normal stress and crack width are smaller in LWC than in a normal-weight concrete (NWC) of similar strength.

4.3.3 Walraven and others (1987)

From 88 push-off tests of specimens with compressive strengths ranging from 17 to 60 MPa, Walraven, Frénay and Pruijssers (1987) developed the following empirical expression:

$$v_{u,th} = C_1(\rho_v f_y)^{C_2} \tag{4.24}$$

in which $C_1 = 0.822 f_{cc}^{0.406}$ and $C_2 = 0.159\ f_{cc}^{0.303}$ in MPa

or $C_1 = 15.686 f_{cc}^{0.406}$ and $C_2 = 0.0353 f_{cc}^{0.303}$ in psi.

f_{cc} is the concrete compressive strength of 150 mm (5.9 in) cubes, and $f'_c = 0.85 f_{cc}$.

Concrete strength does not appear to influence Eq. 4.23, according to Walraven and others (1987), because the strength of Mattock's specimens varied between narrow limits ($21 < f'_c < 37$ MPa) and therefore a possible effect of the concrete strength is hidden by the natural scatter of the experimental results. Mattock (1988) recognized this fact, and carried out further tests on specimens made from 41 MPa (6000 psi) concrete. Based on these, he proposed a refinement to Eq. 4.23 which accounted for the effect of concrete strength:

$$v_u = 0.467\left(f'_c\right)^{0.545} + 0.8\,(0.8\,\rho_v f_y + \sigma_n) < 0.3 f'_c \quad \text{mm-N system}$$

$$v_u = 4.5\left(f'_c\right)^{0.545} + 0.8\,(0.8\,\rho_v f_y + \sigma_n) < 0.3 f'_c \quad \text{in-lb system} \tag{4.25}$$

$$v_u \le 0.3 f'_c$$

Comparison between experimental and theoretical values of v_u according to Eq. 4.24 is given in Table 4.4.

Reference	Number of Specimens	Mean	Standard Deviation
Hofbeck, Ibrahim and Mattock (1969), Walraven and Reinhardt (1981)	55	0.991	0.105
Frénay (1985)	20	1.032	0.135
Pruijssers and Liqui Lung (1985)	13	0.999	0.084
All tests	88	1.001	0.109

Table 4.4 Ratio of measured to ultimate shear stress

A 5 % lower bound expression is obtained by:

$$v_{u\,5\%,\,th} = 0.82\ v_{u,\,th} \tag{4.26}$$

Design charts based on Eq. 4.26 area shown in Fig. 4.33.

As shown in Fig. 4.32b, the mechanism of shear transfer across cracks depends predominantly upon the interaction between aggregate particles and the concrete matrix at the opposing faces of the crack. It is therefore essential that the major part of the particles does not break through. An inspection of the crack faces after precracking showed that the percentage of broken particles in the tests considered was always lower than 30 %.

Comparison with existing equations:

Ratios of experimental results to predictions from the following equations are plotted in Figs. 4.34, 4.35 and 4.36:

ACI - PCI Equation (Fig. 4.34):

$$\frac{V_u}{\phi A_c} = 1.4\,\rho_v f_y \quad \text{where} \quad \phi = 0.85 \tag{ACI 11.25}$$

for normal-weight concrete placed monolithically. The expression is a safe lower bound, but the scatter is large. There is a tendency towards increased conservatism for HSC.

Mattock's equation (Eq. 4.23, Fig. 4.35):

$$\frac{V_u}{\phi A_c} = 0.8\,\rho_v f_y + 2.76 \quad \text{MPa}$$

$$\text{or} \quad \frac{V_u}{\phi A_c} = 0.8\,\rho_v f_y + 400 \quad \text{psi} \tag{4.27}$$

For concrete strengths up to $f'_c = 35$ MPa (5000 psi), a good lower bound with low scatter is obtained. With increasing concrete strength, however, more conservatism is observed.

Finally, Fig. 4.36 uses Eq. 4.26. Over the whole range of values,

$$0.35 < \rho_v f_y < 15.17 \text{ and } 17 < f'_c < 68 \text{ MPa}$$

$$(50 < \rho_v f_y < 2167 \text{ and } 2416 < f'_c < 11474 \text{ psi}),$$

very good agreement with low scatter is obtained.

4.3.4 Delft University of Technology Long Term Tests (Frénay 1990)

This is a study of the behavior of cracked concrete subjected to in-plane, sustained (long term) shear loading. The shear resistance mechanisms of interest here are aggregate interlock and dowel action of the reinforcement. Comparison of Walraven's push-off tests for two concrete cube strengths f_{cc} = 31 MPa and f_{cc} = 56 MPa shows a significant decrease in shear force carried by aggregate interlock for the same crack slip and the same reinforcement ratio as concrete strength decreases. See Fig. 4.37. However, the crack width (or opening) is rather similar for the two cases, since cracks go around the aggregate in both cases.

Frénay's work has to do with sustained or long term shear load. For our purpose, the results at time = 0 are of interest. Fig. 4.38 compares shear friction stresses for two concrete strengths f_{cc} = 51 MPa and f_{cc} = 70 MPa. All other things being equal, Fig. 4.38 shows *greater* shear stress for the higher strength concrete. This theoretical result is supported by experimental observations. Based on push-off tests performed on concrete with cylinder strength ranging from 43 to 60 MPa, Frénay and others observed that for these strengths, concrete exhibited crack surfaces that are similar with regard to the percentage of aggregate fractured in the crack plane. However, this no longer holds true for higher concrete strengths.

Tassios and Vintzěleou (1987) confirmed Walraven's experimental values and the increase in shear stress with an increase in concrete strength ($16 < f_{cc} < 40$ MPa).

4.3.5 Delft University of Technology Tests on HSC (Walraven 1995)

Since crack surfaces are smoother in HSC than in NSC (cracks tend to go through the aggregate in HSC whereas they go around the aggregate in NSC), one would expect a decrease in shear friction as the concrete strength increases. This is indeed the case, as was borne out by shear friction tests on precracked, push-off experiments made of concrete with a cylinder strength of 100 MPa (14 500 psi) or a cube strength of 115 MPa (16 700 psi).

In unreinforced concrete, shear-friction at a given crack slip and opening is reduced by 35% for HSC (say 100 MPa) compared to NSC (say 40 - 60 MPa). See Fig. 4.39. For reinforced concrete, the reduction is about the same, in the range of 25-45%.

Mau and Hsu's formula (1988) works well for the shear capacity of cracks in NSC:

$$\frac{v_u}{f_c'} = 0.66\sqrt{\omega} < 0.3 \quad \text{with} \quad \omega = \frac{\rho f_y}{f_c'} .$$

When applied to all the test results of Table 4.4, it performs almost as well as Eq. 4.24 and is much simpler to use (mean = 1.019, standard deviation = 0.127).

Authors' note: For HSC, a 35 % reduction of this equation gives:

$$\frac{v_u}{f_c'} = 0.43\sqrt{\omega} .$$

4.3.6 Bažant and Gambarova

Based on tests by Paulay and Leober (1974), Bažant and Gambarova (1980) suggested the following formulas for shear (σ^c_{nt}) and normal compressive stress (σ^c_{nn}) in cracks of concrete members, as functions of crack opening (δ_n) and slip (δ_t):

$$\sigma^c_{nn} = -\frac{a_1}{\delta_n}(a_2\,|\sigma^c_{nt}|)^p \quad \text{and} \quad \sigma^c_{nt} = \tau_u r\,\frac{a_3 + a_4\,|r|^3}{1 + a_4 r^4}$$

$$\text{with} \quad r = \frac{\delta_t}{\delta_n}; \quad \tau_u = \tau_o\,\frac{a_o}{a_o + \delta_n^2}; \quad p = 1.30\left(1 - \frac{0.231}{1 + 0.185\,\delta_n + 5.63\,\delta_n^2}\right)$$

where

$a_o = 0.01\,D_a^2$ $\quad a_1 = 0.000534$ N/mm $\quad a_2 = 145$ mm^2/N

$a_3 = 2.45/\tau_o$ N/mm^2 $\quad a_4 = 2.44\,(1 - 4/\tau_o$ N/mm$^2)$ $\quad \tau_o = 0.245 f_c'$

τ_u = maximum shear stress $\quad \delta_n, \delta_t$ = crack opening ($\delta_n \geq 0$) and slip

f_c' = cylinder compressive strength $\quad D_a$ = maximum aggregate size.

Application of these relations to reinforced concrete shows that the principal axes of stress and strain increments are not parallel because of coupling between shear and normal stresses. This is to be expected since cracked concrete is not isotropic.

Frénay (1990) reviewed other mathematical models:

Paulay and Loeber's (1974) expression, which is based on variable crack width but constant stress to crack width ratio:

$$\tau_a = 0.51 + 7.07\sqrt{\delta_t}$$

where τ_a is the shear stress due to aggregate interlock.

Houde and Mirza (1974) performed similar push-off tests and found that τ_a is almost proportional to $\sqrt{f_{cyl}}$ and $(\delta_{no})^{-1.5}$ where δ_{no} is the initial separation. A more complete review of various mathematical models of shear friction and dowel action can be found in Gambarova and Prisco (1991).

4.3.7 University of Calgary Tests

Loov and Patnaik (1994) tested 16 composite concrete beams with a rough interface to measure their horizontal shear strength. 12 of the beams were made of concrete of compressive strength f'_c = 35 MPa (5000 psi), two had f'_c = 20 MPa (2900 psi) and two had f'_c = 45 MPa (6500 psi). Loov and Patnaik proposed the following design equations:

$$v_n = k\lambda\sqrt{(0.1 + \rho_v f_y) f_c'} \leq 0.25 f_c' \quad \text{MPa}$$
$$v_n = k\lambda\sqrt{(15 + \rho_v f_y) f_c'} \leq 0.25 f_c' \quad \text{psi} \qquad (4.28)$$

where v_n = nominal shear strength,

k = 0.6 for concrete placed monotonically,
0.5 for concrete placed against hardened concrete with a rough surface, and

ρ_v = $A_v/(b_v s)$ = transverse reinforcement ratio.

This is an extension to unreinforced joints of a previous equation also proposed by Loov:

$$v_n = k\sqrt{\rho_v f_y f_c'} \qquad (4.29)$$

This equation was the first to account for the influence of concrete strength. A value of $k = 0.5$ was suggested for uncracked shear interfaces.

These equations fall into a family of parabolic equations which started with Birkeland:

$$v_n = 2.78\sqrt{\rho_v f_y} \quad \text{MPa}$$
$$v_n = 33.5\sqrt{\rho_v f_y} \quad \text{psi}$$

For $f'_c = 30.9$ MPa, Loov's Eq. 4.29 is identical to Birkeland's equation.

The present PCI equation, which is based on Shaikh's work, is also parabolic:

$$v_u = \phi\, \rho_v f_y\, \mu_e$$
$$\text{with} \quad \mu_e = \frac{6.9\,\lambda^2}{v_u} \quad \text{MPa} \qquad \text{(PCI 6.7.1)}$$
$$\text{or} \quad \mu_e = \frac{1000\,\lambda^2}{v_u} \quad \text{psi}$$

where $\phi = 0.85$ for shear and λ accounts for the effects of concrete density:

$\lambda = 1.0$ for normal weight concrete,

$\lambda = 0.85$ for sand-lightweight concrete, and

$\lambda = 0.75$ for all-lightweight concrete.

The above equation is a specialized version of the PCI equation, obtained by setting the coefficient of friction μ equal to $1.0\,\lambda$ for friction between concrete and hardened concrete with a roughened surface. If the last three equations (PCI 6.7.1) are combined, a parabolic equation for v_u with respect to the clamping force is obtained:

$$v_u = \lambda\sqrt{6.9\,\phi\,\rho_v f_y} \le 0.25 f'_c \lambda^2 \quad \text{and} \quad 6.9\,\lambda^2 \quad \text{MPa}$$
$$v_u = \lambda\sqrt{1000\,\phi\,\rho_v f_y} \le 0.25 f'_c \lambda^2 \quad \text{and} \quad 1000\,\lambda^2 \quad \text{psi}$$

Figs. 4.40 and 4.41 compare test data with various design equations. The ACI provisions are a combination of special provisions for horizontal shear from §17.5 (1 to 3 in the following list), along with shear-friction provisions from §11.7 (4 and 5 here):

1)	0	$\le \rho_v f_y \le$	0.33	MPa	$v_u = 0.6$	MPa
	0	$\le \rho_v f_y \le$	50	psi	$v_u = 80$	psi
2)	0.33	$\le \rho_v f_y \le$	2.83	MPa	$v_u = 1.8 + 0.6\,\rho_v f_y$	MPa
	50	$\le \rho_v f_y \le$	400	psi	$v_u = 260 + 0.6\,\rho_v f_y$	psi
3)	2.83	$\le \rho_v f_y \le$	3.5	MPa	$v_u = 3.5$	MPa
	400	$\le \rho_v f_y \le$	500	psi	$v_u = 500$	psi
4)	3.5	$\le \rho_v f_y \le$	5.5	MPa	$v_u = \rho_v f_y$	MPa
	500	$\le \rho_v f_y \le$	800	psi	$v_u = \rho_v f_y$	psi
5)	5.5	$< \rho_v f_y$		MPa	$v_u = 5.5$	MPa
	800	$< \rho_v f_y$		psi	$v_u = 800$	psi.

Figs. 4.42 and 4.43 compare Eq. 4.28 with results of push-off tests for uncracked and precracked specimens. The proposed equation represents the test data better than do previous shear-friction equations. For a concrete strength exceeding about 30 MPa (4350 psi), it will result in designs with less stirrup reinforcing than those obtained using the current ACI or PCI equations. The authors also observe that:

- Slip and stirrup stresses in the test beams were insignificant until the beams attained a horizontal shear stress of about 1.5 to 2 MPa (220 to 290 psi).
- For beams designed with the proposed equation, a slip of 0.5 mm is likely to yield the stirrups if the yield strength is less than about 440 MPa (64 ksi).

4.3.8 University of Warwick Tests

Millard and Johnson (1984) studied experimentally shear transfer across cracks in reinforced concrete due to aggregate interlock (19 specimens) and dowel action (7 specimens). Concrete cube strength f_{cc} ranged from 28 MPa to 54 MPa. In the aggregate interlock tests, dowel action was removed by placing the reinforcement in oversize ducts in the concrete so that only an axial restraint normal to the plane of cracking was provided. In the dowel action tests, aggregate interlock was eliminated by the artificial creation of a smooth crack.

Aggregate Interlock

- Test results do not support the local/global roughness model (Laible, White and Gergely 1977). According to this theory, local roughness causes interlocking of the fine aggregate particles, principally a bearing or crushing action, and global roughness causes interlocking of the coarse aggregate particles, principally a sliding and overriding action. The demarcation between local roughness behavior and global roughness behavior is thought to occur at a crack width of 0.25 mm. However, test results show no radical difference between the behavior of specimens with an initial crack width less than 0.25 mm and those with a greater initial crack width.
- Test results do not support either the theory that the resistance to shear is provided principally by a bearing/crushing action of the local asperities of the crack faces. These surfaces have been represented by a sawtooth shape (Jimenez, Gergely and White 1978) and by a series of parabolic segments (Fardis and Buyukozturk 1979).
- Fairly consistent agreement is found between test results and the simplified two-phase aggregate interlock model (Walraven and Reinhardt 1981. See § 4.3.2).

Dowel Action

The non-linear shear stiffness of the dowel action specimens was attributed to:

- crushing or splitting of the concrete supporting the bar, and/or
- plastic yielding of the reinforcement.

The beam on an elastic foundation model was used to predict the initial shear stiffness K_i of each dowel action specimen:

$$F_d = 0.166\ \Delta s\ G_f^{0.75}\ \phi^{1.75}\ E_s^{0.25}$$

where E_s = elastic modulus of steel,
F_d = dowel force,
G_f = foundation modulus of concrete,
Δs = shear displacement across crack, and
ϕ = bar diameter.

The plastic moment M_p of a bar with an axial force of αf_y is:

$$M_p = \phi^3 f_y (1 - \alpha^2)/6$$

where f_y is the bar yield strength.

The ultimate dowel force F_{du} in a bar with an axial force is:

$$F_{du} = 1.30\ \phi^2 \sqrt{f_{cc} f_y (1 - \alpha^2)}$$

The measured dowel force at various stages of loading is fitted well by:

$$F_d = F_{du}[1 - \exp(-K_i \Delta s / F_{du})]$$

Millard and Johnson (1985) performed 13 more tests where aggregate interlock and dowel action were both present. They concluded that there is an interaction between the two modes of behavior. Aggregate interlock causes additional tensile forces in the reinforcement due to overriding of the crack faces. This causes a reduction in the dowel action shear stiffness and strength. Likewise, local bond between the reinforcement and the concrete, which is absent from the aggregate interlock tests, produces a higher tensile stiffness normal to the plane of cracking. This results in an increase in the aggregate interlock shear stiffness and strength, but this is sensitive to deterioration of the local bond. When the tensile stiffness of the reinforcement normal to the plane of cracking is known, the two-phase aggregate interlock model and the elasto-plastic dowel action model can be used to predict the behavior of cracked RC specimens. The limit of applicability of these results may be reached when the in-plane shear transferred across a set of parallel tension cracks becomes high enough to cause additional diagonal shear cracking to occur between these cracks. The flexibility due to widening of these diagonal cracks may exceed that due to shear slip across the original tensile cracks (Perdikaris, White and Gergely 1980).

4.3.9 Cornell University Tests

White and Holley (1972) conducted friction tests on unreinforced, externally clamped, precracked specimens measuring 457 mm x 610 mm x 915 mm (18 in. x 26 in. x 36 in.). Concrete strength was about 20 MPa (3 000 psi). The shear area was 1810 cm^2 (280 in^2) for specimens 1-6, and 1550 cm^2 (240 in^2) for specimens 7-16. Following cyclic loading, each specimen was loaded to a maximum (not ultimate) load. The conclusions were:

1. Crack slip and opening both increased under cyclic shear loading.
2. The clamping forces remained low during cycling (about 30 - 50% of applied shear).
3. The most significant damage to the shearing surfaces occurred during the final load application, and not during the cyclic loading.
4. With two exceptions, the increase in crack width after 25 cycles was less than or equal to 0.25 mm (0.010 in).
5. Crack slip did not return to zero during unloading of the specimen.
6. Slip decreased with increasing aggregate size, increasing size of the clamping rods (stiffness effect) and decreasing initial crack width.
7. A specimen with variable crack width across its thickness exhibits less slip than a similar specimen with a uniform crack width equal to the average of the variable crack width.

4.3.10 Impact Shear Friction Tests

In a very original paper, Krauthammer (1992) examines the ACI 318-89 minimum shear reinforcement requirement $A_v = 0.35\, b_w s / f_y$ (mm-N system) or $A_v = 50\, b_w s / f_y$ (in-lb system), which is intended to require reinforcement to resist 0.35 MPa (50 psi) shear stress.

Analysis

The shear resistance V_n provided by a bar crossing a shear crack at an angle α_f is:

$$V_n = A_{vf} f_y (\mu \sin\alpha_f + \cos\alpha_f) \tag{4.30}$$

where A_{vf} = bar area,
f_y = bar yield strength, and
μ = concrete-to-concrete friction coefficient.

The minimum requirement ensures that V_n equals the full shear transfer due to concrete friction

(aggregate interlock).

$$V_n = \mu f_n b_w s \tag{4.31}$$

where $b_w s$ = contact area and f_n = externally induced normal stress across shear interface.

Equating (4.30) and (4.31) gives:

$$A_{vf} = K_{sh} b_w s / f_y \tag{4.32}$$

where

$$K_{sh} = f_n \frac{\mu}{\mu \sin \alpha_f + \cos \alpha_f} \tag{4.33}$$

Krauthammer also defines a factored coefficient $K_{sh}' = K_{sh} / 0.85$. By taking derivatives of Eq. 4.33 with respect to α_f, he finds that K_{sh}, and consequently A_{vf}, reaches a minimum for tan $\alpha_f = \mu$. If μ ranges between 0.6 and 1.4, α_f ranges between 30 and 55°.

Experiments

The goal of the experiments is to determine f_n. Two normal weight concrete slabs 762 mm x 762 mm x 152 mm (30 inch x 30 inch x 6 inch) are used to model an unreinforced concrete-to-concrete interface. The two slabs are placed side by side on a 305 mm (one foot) deep sand bed for support. Various in-place compressive forces N are applied to the system to simulate different conditions of shear transfer between the two slabs. A vertical, dynamic load is generated by dropping a 133 N (30 lb) weight from a height of 914 mm (3 ft) on one side of the interface. Acceleration histories are recorded for both slabs and analyzed by fast Fourier transform. A first peak occurs at 244 Hz for all values of compression N. However, the second peak varies with N for low values of N. For $N \geq 53.4$ kN (12 000 lb), the second peak remains at 1098 Hz and the two slabs behave as one unit. Thus:

$$f_n = \frac{12000}{6*30} = 66.67 \text{ psi} \quad (460 \text{ kPa})$$

Minimum shear requirement

The crack angle of α_f is unknown

1. Assume $\alpha_f = 45°$. Then $241 < K_{sh} < 379$ kPa $(35 \leq K_{sh} \leq 55$ psi) and
   $287 \leq K_{sh}' \leq 446$ kPa $(42 \leq K_{sh}' \leq 65$ psi).
2. Assume $30 \leq \alpha_f \leq 55°$. Then $236 \leq K_{sh} \leq 378$ kPa $(34.3 \leq K_{sh} \leq 54.8$ psi) and
   $278 \leq K_{sh}' \leq 445$ kPa $(40.4 \leq K_{sh}' \leq 64.5$ psi).
3. Assume $\alpha_f = 90°$. Then $K_{sh} = 460$ kPa (66.7 psi) and $K_{sh}' = 540$ kPa (78.4 psi).

Recommendation Assume $\alpha_f = 45°$.

According to ACI, $\mu = 1.4$ for monolithic construction, leading to $K_{sh}' = 448$ kPa (65 psi). So $A_v = 0.45\, b_w s / f_y$ (mm-N system) or $A_v = 65\, b_w s / f_y$ (in-lb system) is recommended.

4.3.11 Summary

As demonstrated by the various research results mentioned above, the relationship between compressive stress across a crack and the shear which can be transmitted as a function of crack displacements is more complex than the simple shear friction model suggests (see Eq. ACI 11.25 § 3.9.1 of this report). Fig. 4.44 (Collins and Mitchell 1991) compares various results.

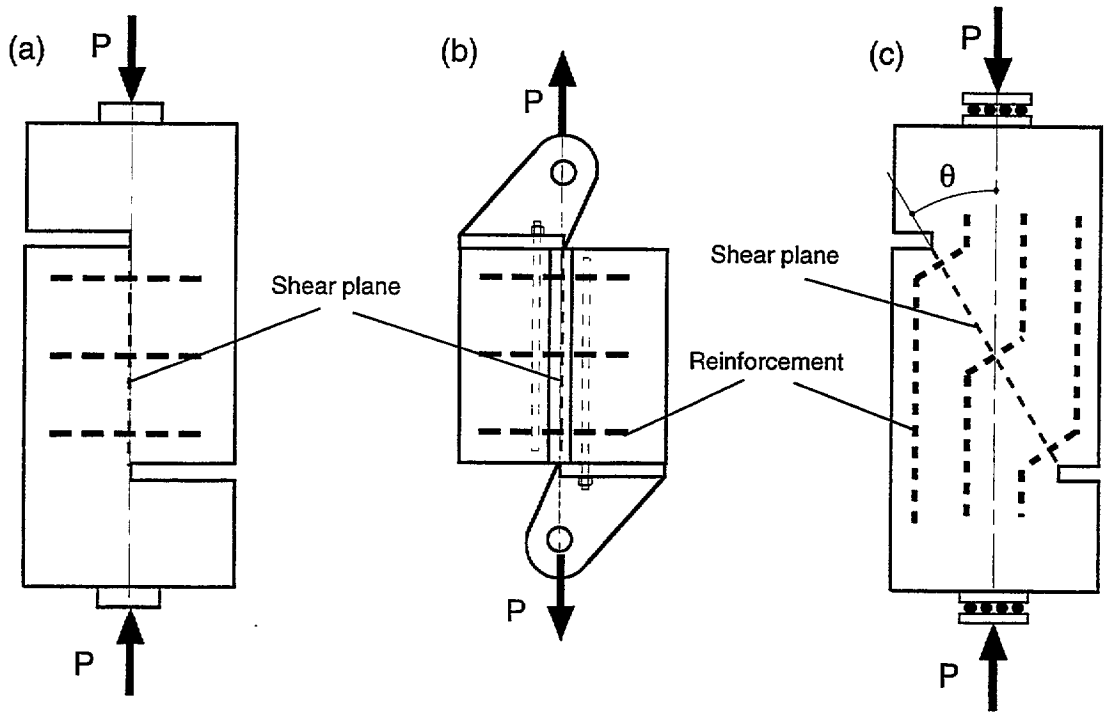

Figure 4.29 Shear transfer specimens (a) push-off, (b) pull-off, and (c) modified push-off (Mattock and Hawkins 1972)

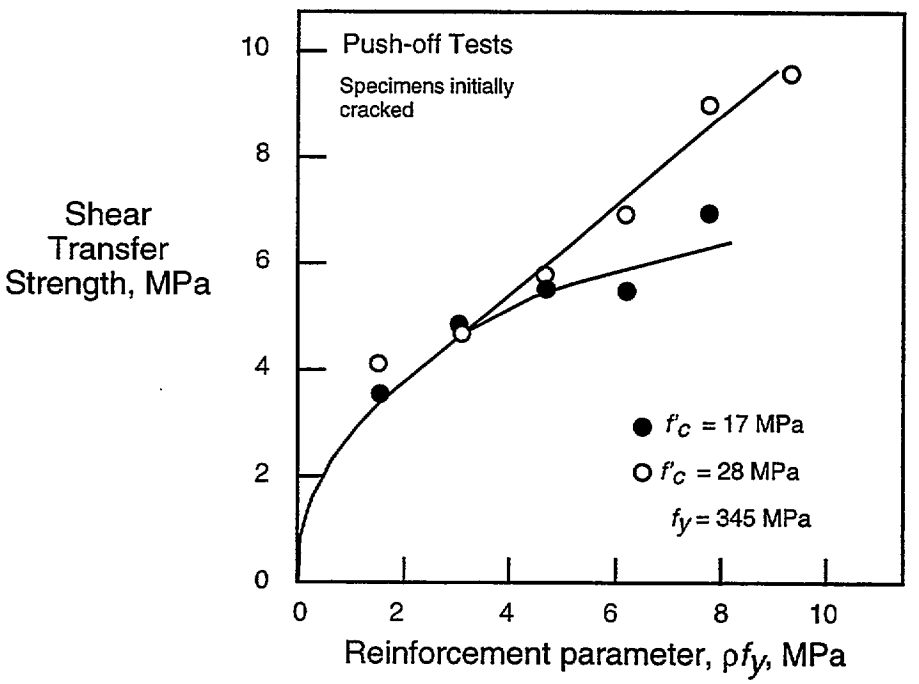

Figure 4.30 — Effect of concrete strength on the shear transfer strength of initially cracked push-off specimens (Mattock and Hawkins 1972)

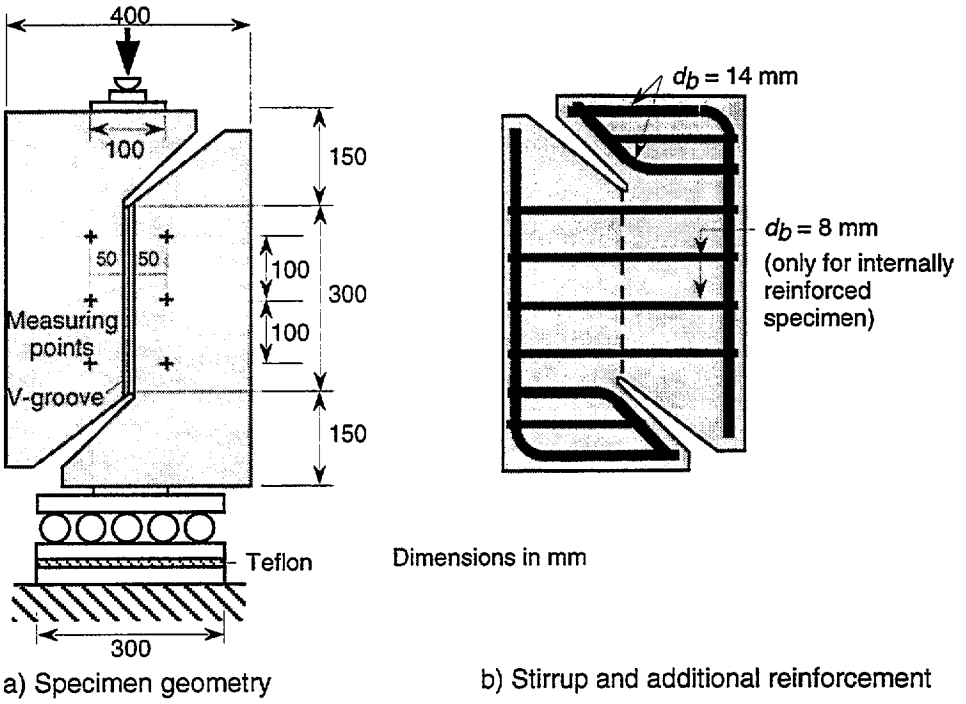

Figure 4.31 — Push-off test specimens to study aggregate interlock in cracked reinforced concrete: (a) geometry ; (b) reinforcement (Walraven and Reinhardt 1981)

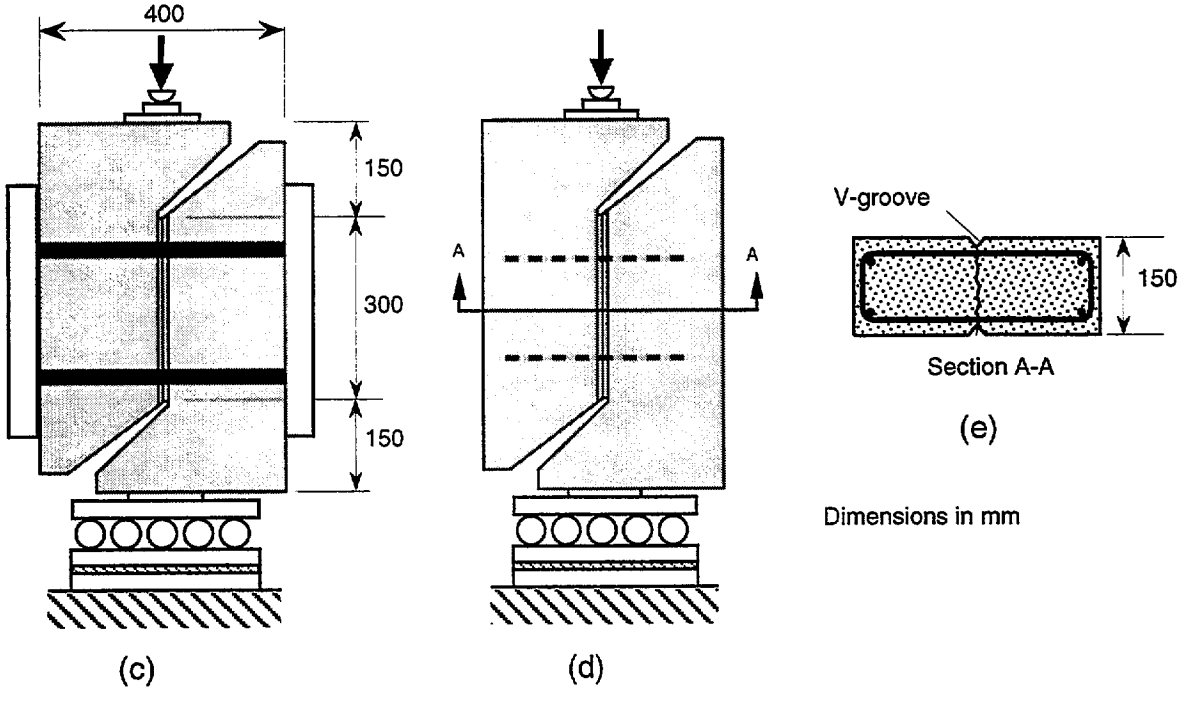

Figure 4.31 — Push-off specimen with (c) external reinforcement and (d) internal reinforcement; (e) cross-section of internally reinforced specimen (Walraven 1995)

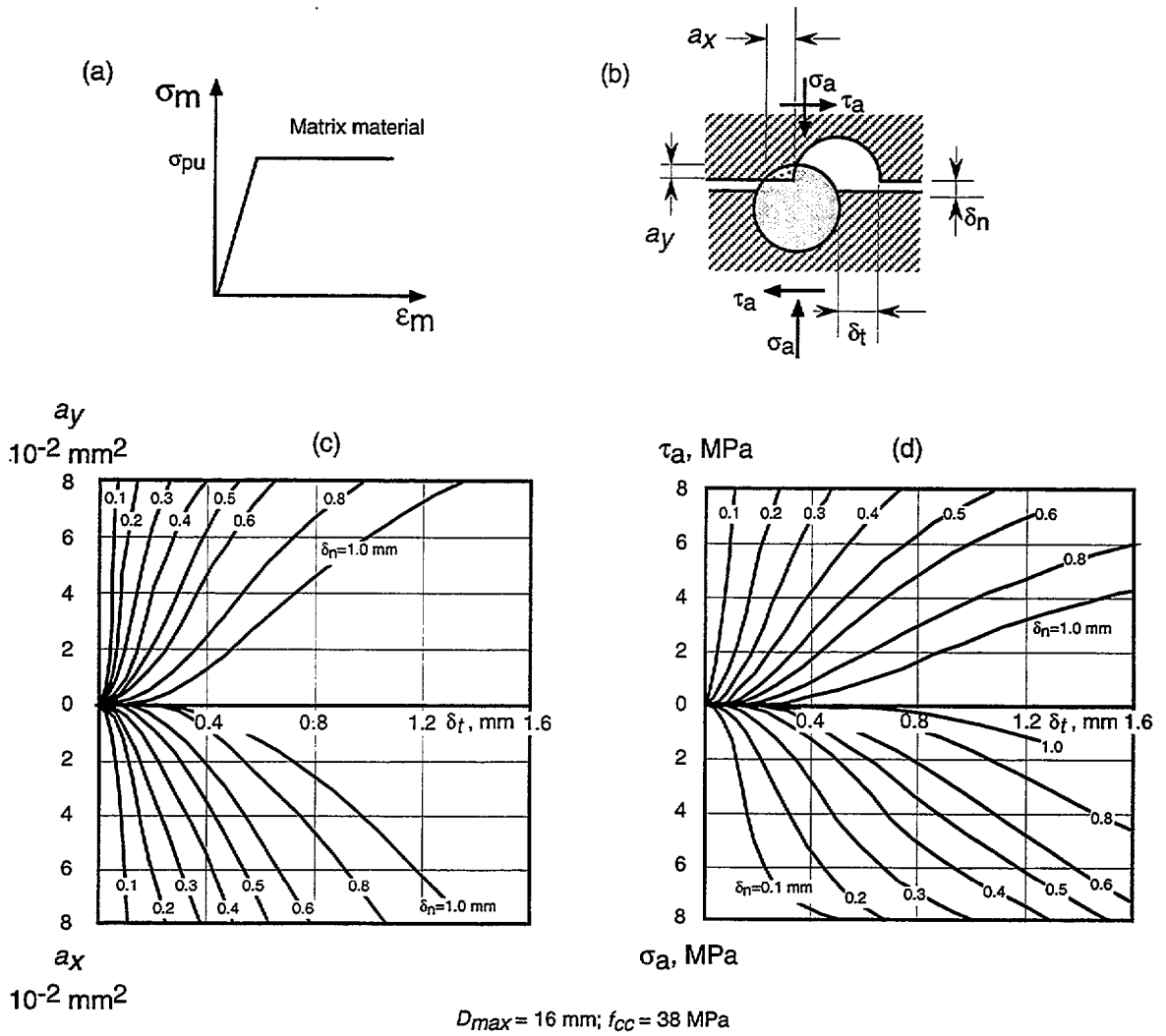

D_{max} = 16 mm; f_{cc} = 38 MPa

Figure 4.32 — Walraven's model for shear transfer across crack: (a) stress-strain curve of matrix material; (b) deformation at crack; (c) contact areas as functions of crack width and slip; and (d) normal and shearing stress as functions of crack width and slip (adapted from Frénay 1990)

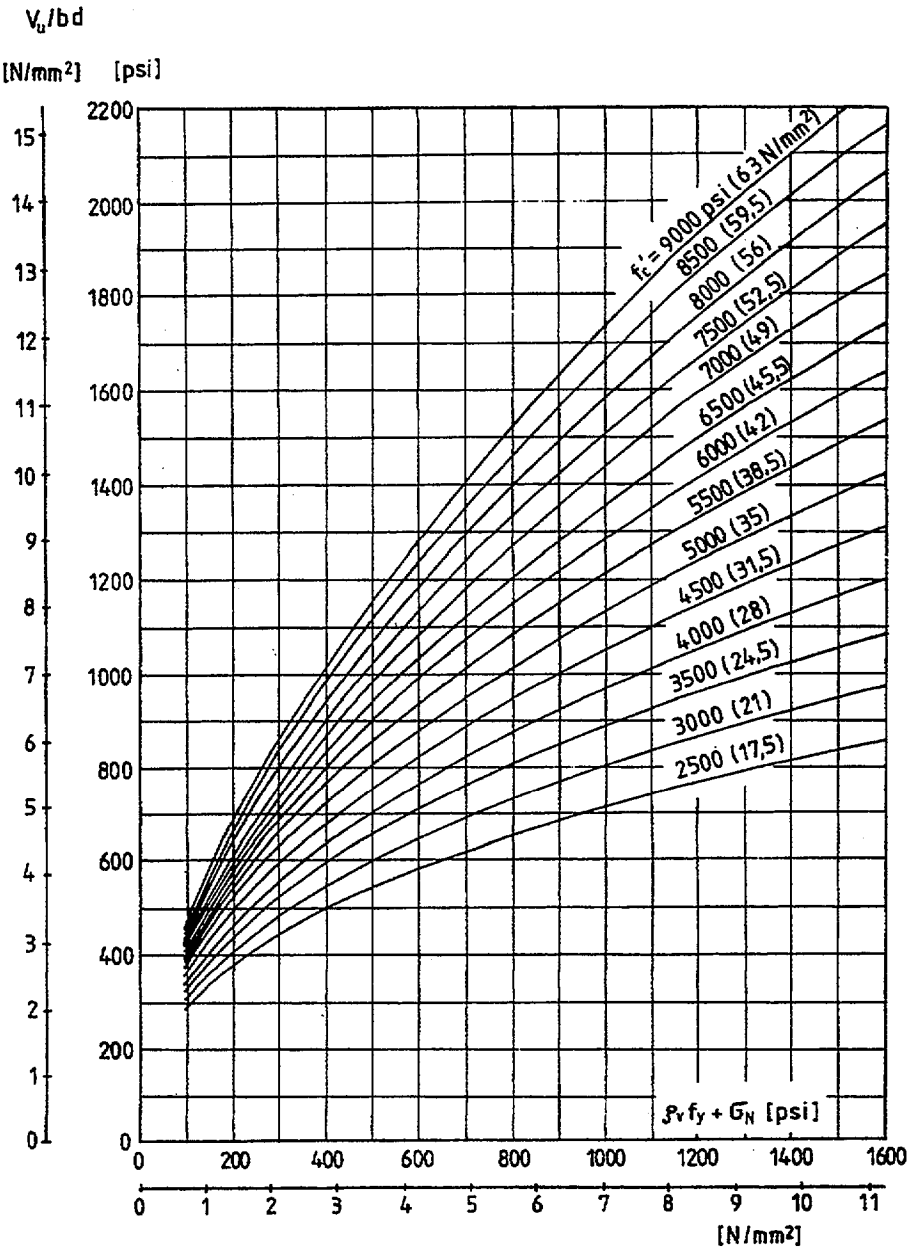

Figure 4.33 — Design chart, accounting for concrete strength, for determining shear friction capacity (Walraven et al. 1987)

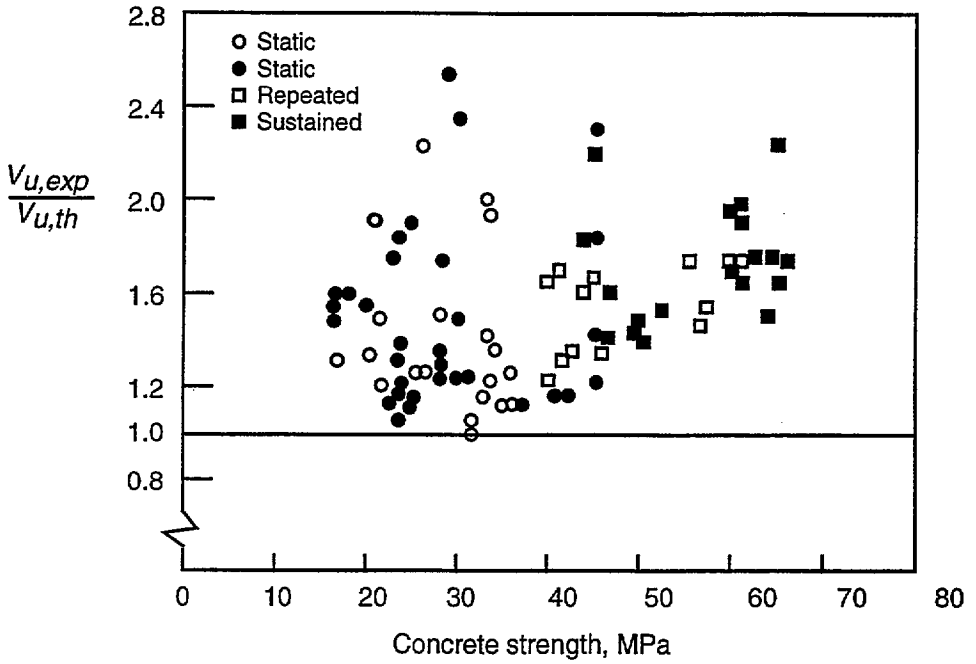

Figure 4.34 — Comparison of experimental shear stress, $V_{u,exp}$, with values calculated by shear friction method from PCI Design Handbook (Walraven et al. 1987)

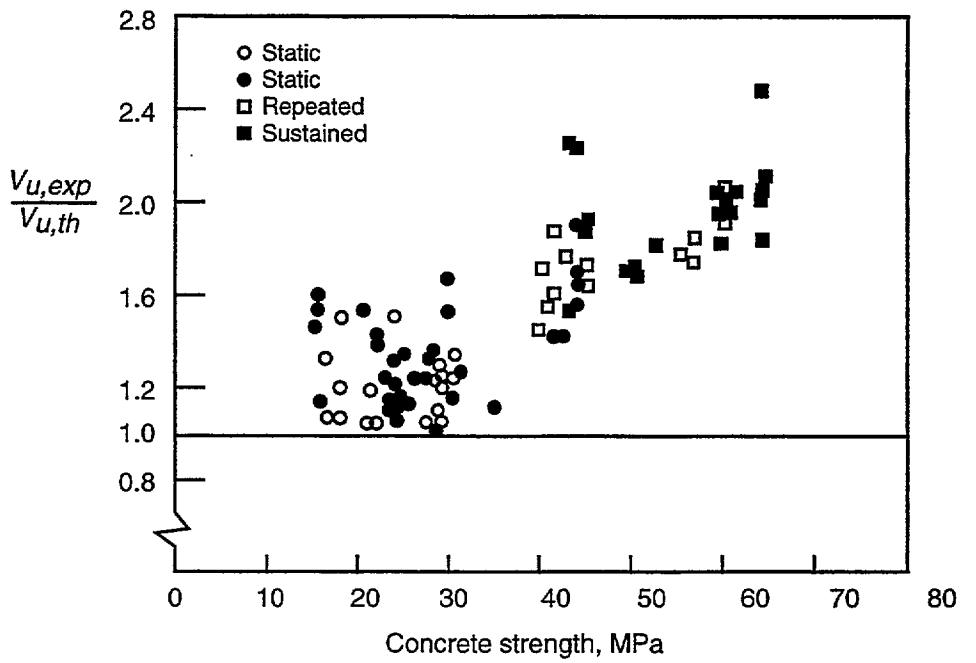

Figure 4.35 — Comparison of experimental shear stress, $V_{u,exp}$, with values calculated by modified shear friction method by Mattock (Walraven et al. 1987)

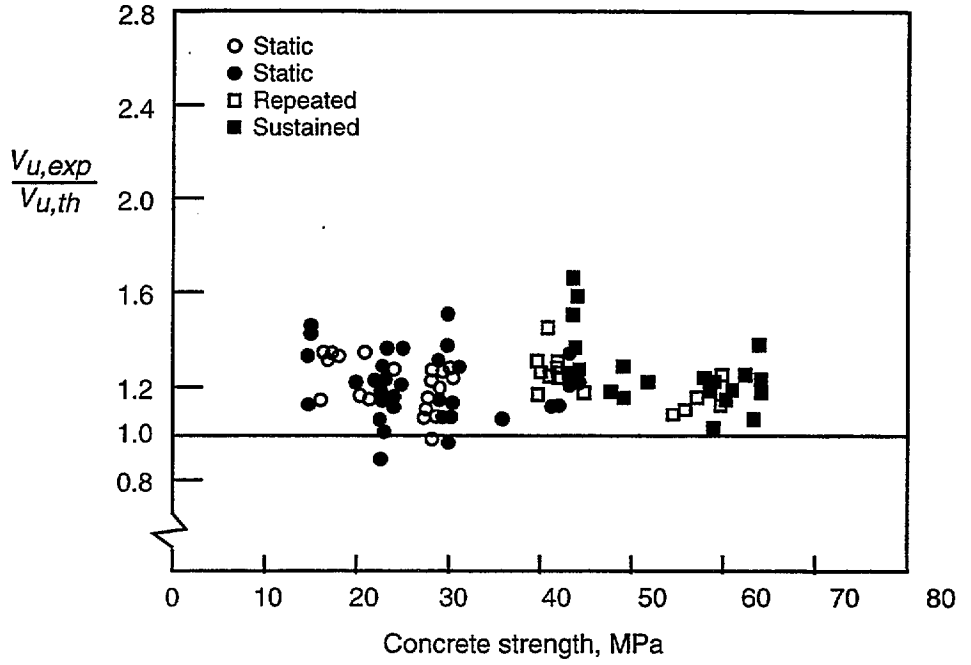

Figure 4.36 — Comparison of experimental shear stress, $V_{u,exp}$, with values obtained from design chart of Fig. 4.33 (Walraven et al. 1987)

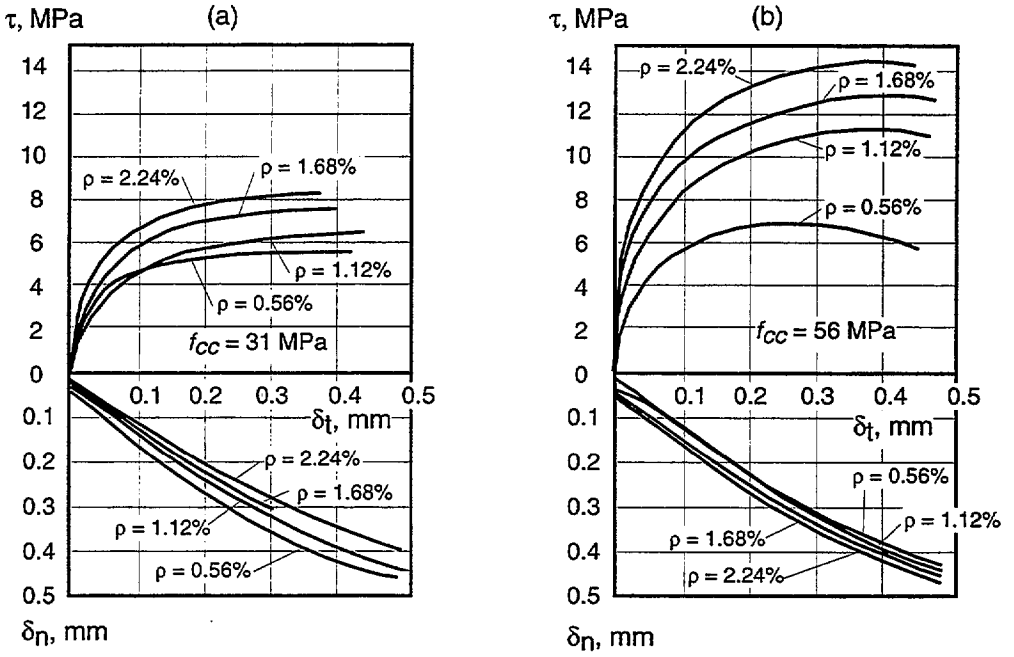

Figure 4.37 — Push-off test results by Walraven; (a) f_{cc} = 31 MPa and (b) f_{cc} = 56 MPa (Frénay 1990)

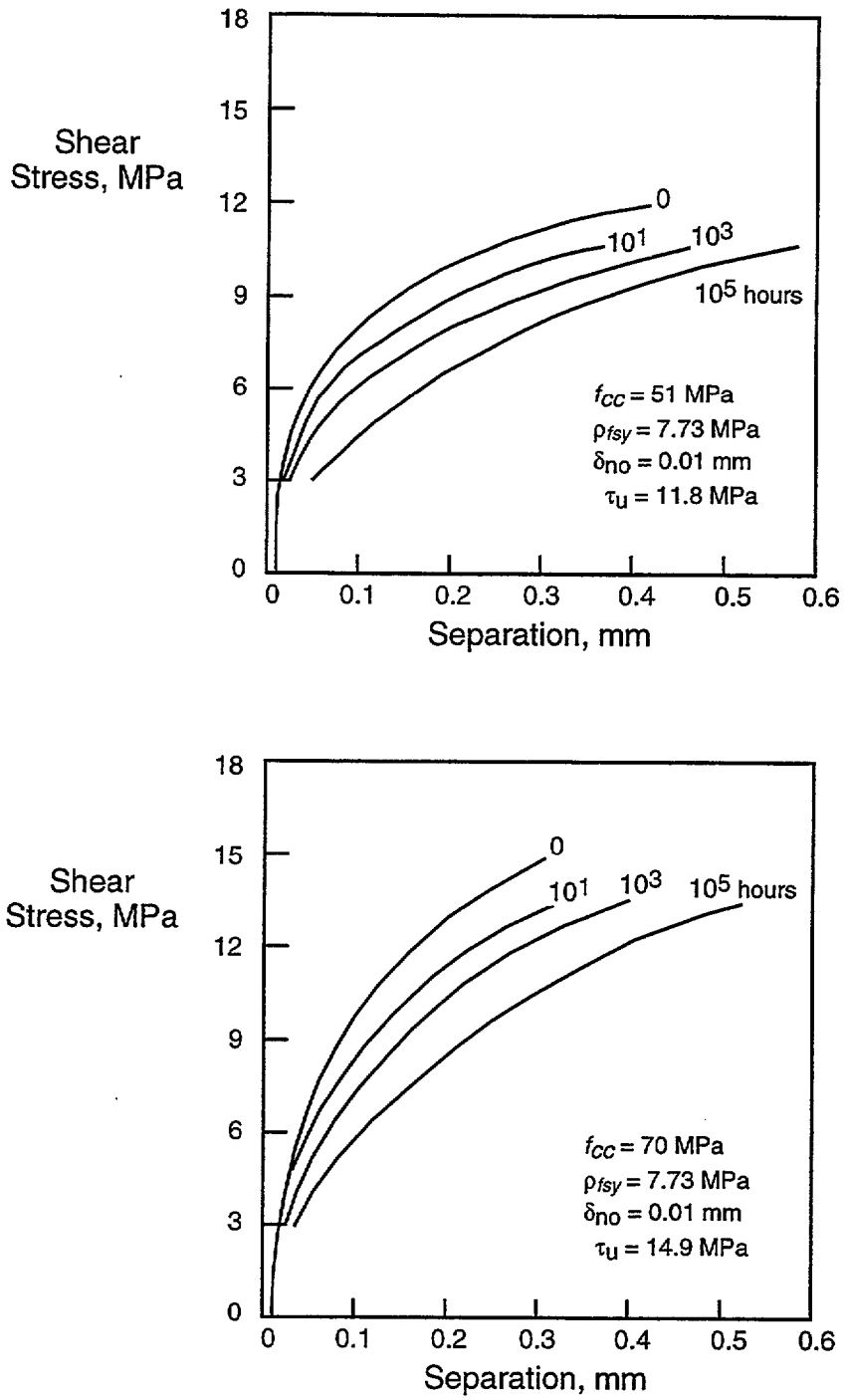

Figure 4.38 — Computed shear stress-separation relationships for two concrete mixtures (Frénay 1990)

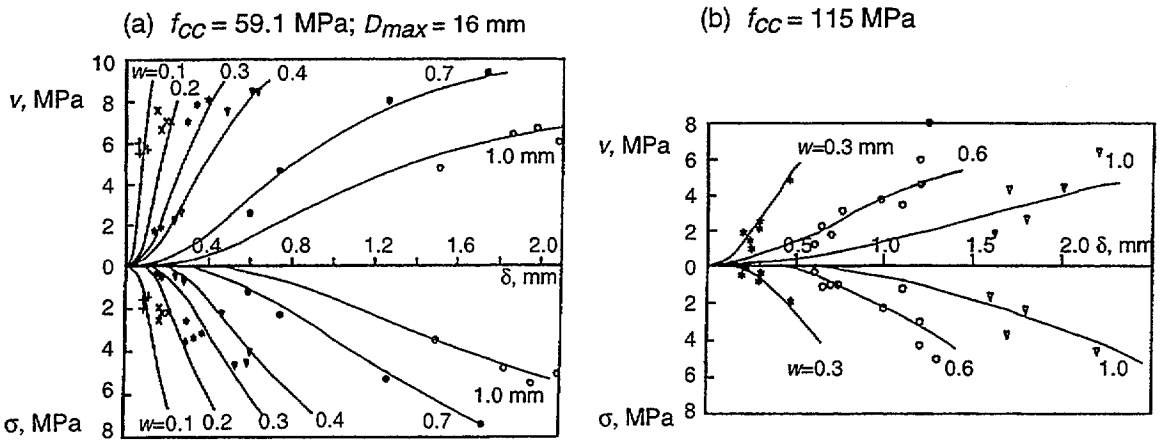

Figure 4.39 — Shear stress, v, normal stress, σ, and shear displacement, δ, at different constant crack widths for unreinforced concrete at two strength levels: (a) 59 MPa and (b) 115 MPa (Walraven 1995)

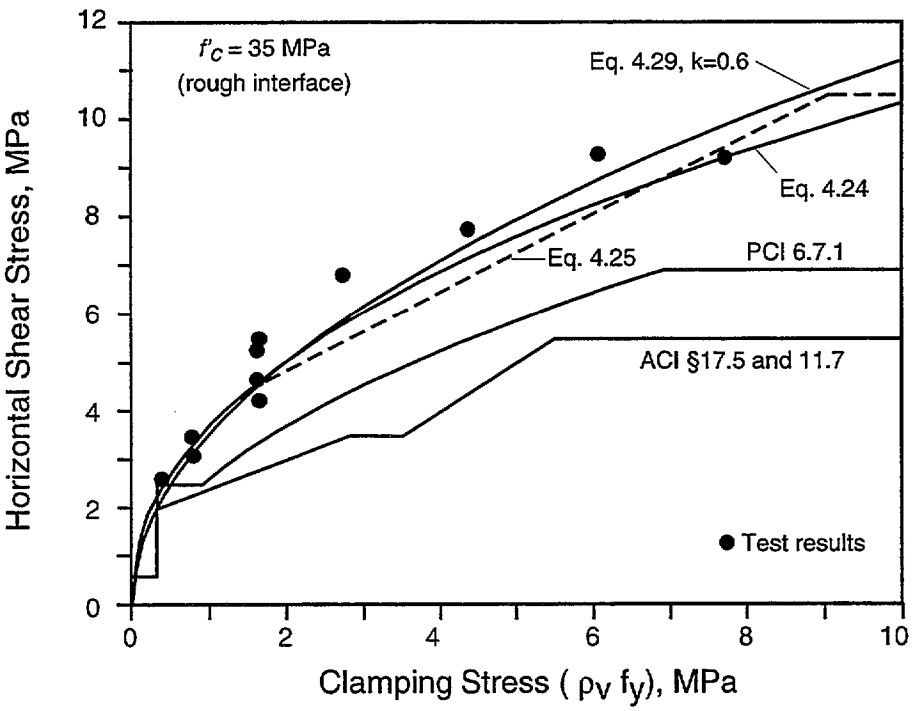

Figure 4.40 — Comparison of horizontal shear strength test results with different equations (Loov and Patnaik 1994)

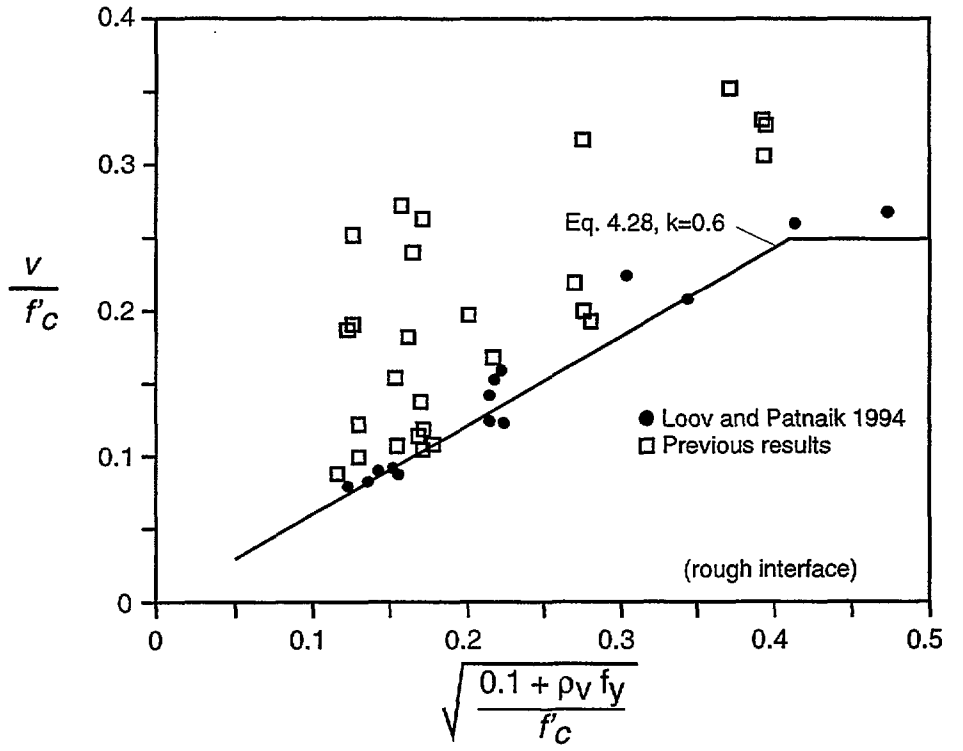

Figure 4.41 — Comparison of horizontal shear strength test results with equation of Loov and Patnaik (1994)

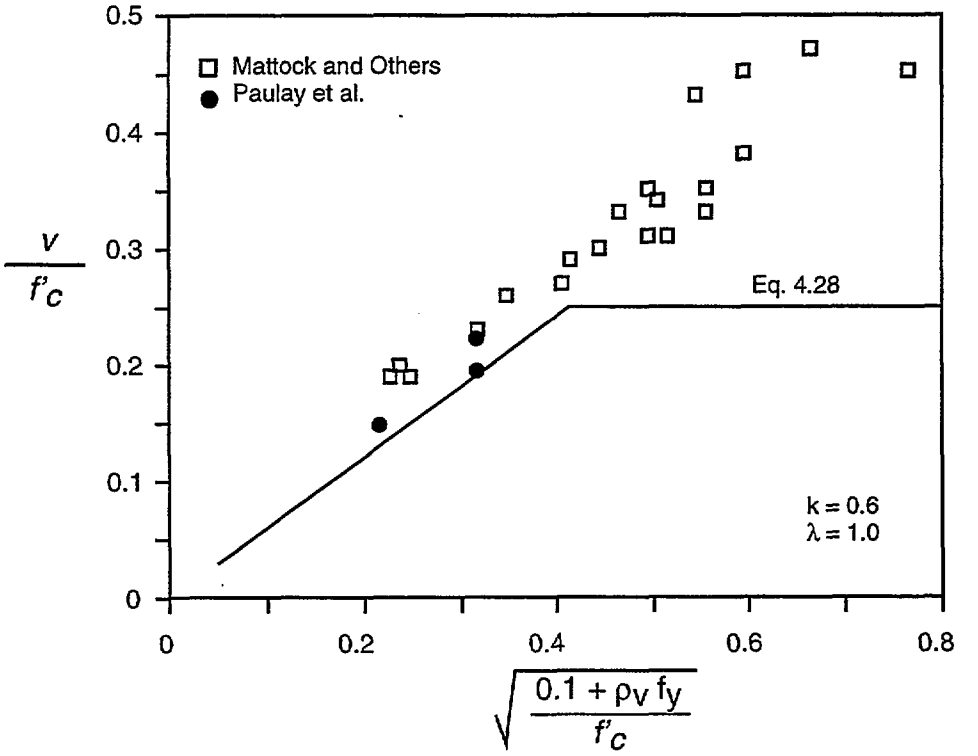

Figure 4.42 — Comparison of equation suggested by Loov and Patnaik with results of uncracked push-off tests (Loov and Patnaik 1994)

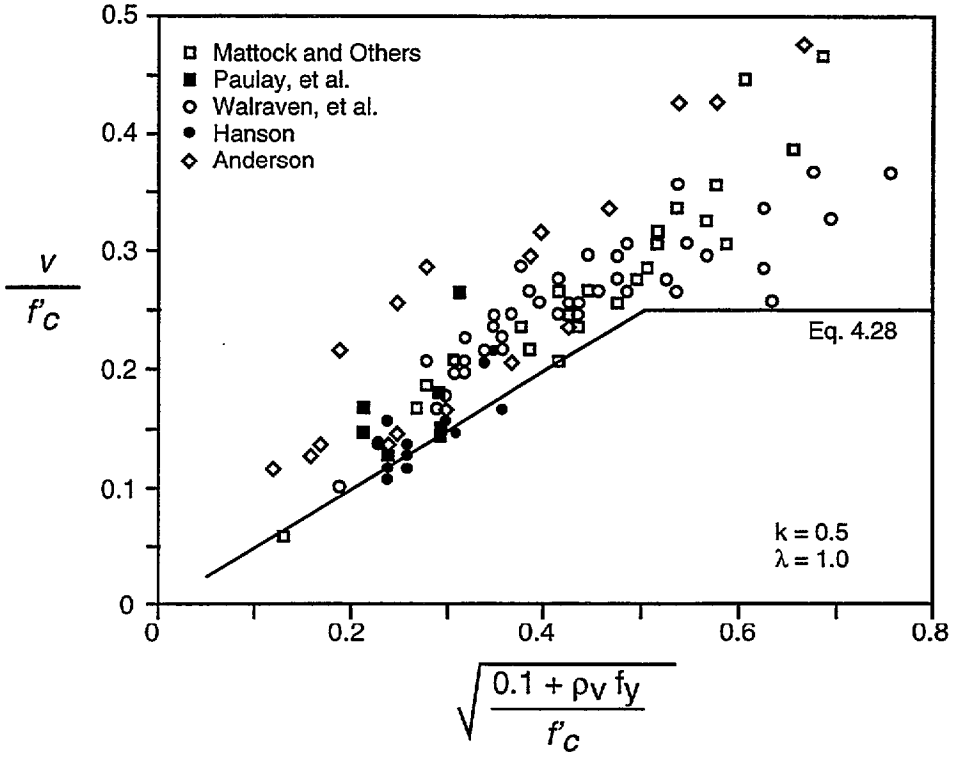

Figure 4.43 — Comparison of equation suggested by Loov and Patnaik with results of cracked push-off tests (Loov and Patnaik 1994)

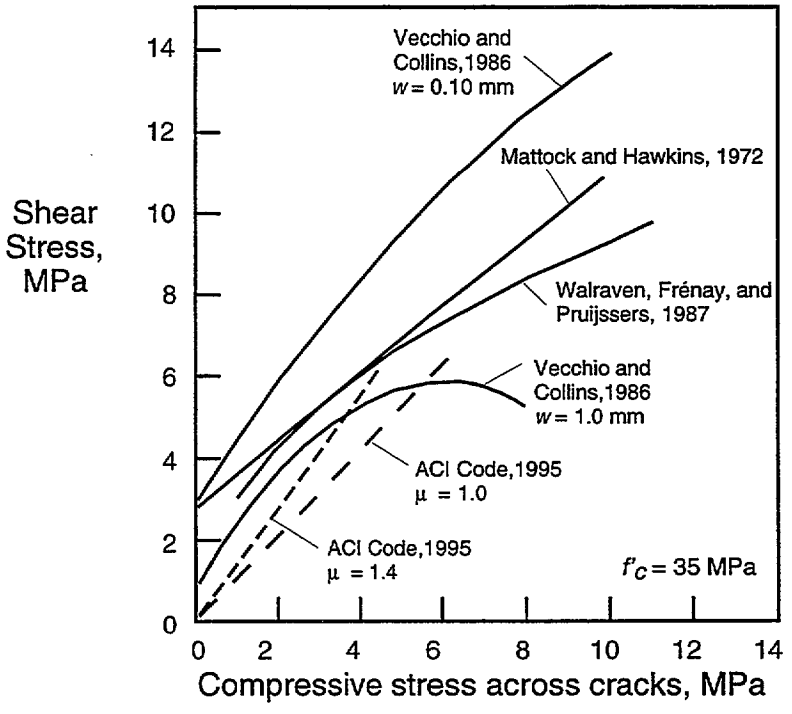

Figure 4.44 — Comparison of suggested relationships of shear stress that can be transmitted across a crack as a function of the compressive stress across crack, w = crack width (Collins and Mitchell 1991)

4.4 Fracture Mechanics - Size Effect

4.4.1 Jenq and Shah (1989) used fracture mechanics to explain the size effect of RC beams, without stirrups, failing in shear. They found that an important factor in the model is the bond strength of the longitudinal reinforcement to concrete. Also the relative shear resistance $v_u / \sqrt{f'_c}$ decreases as f_c' increases. For example, for a reinforcement ratio of 0.015,

$$v_u = 3.22\sqrt{f'_c} \quad \text{for} \quad f'_c = 2500 \quad \text{psi}$$

$$v_u = 0.267\sqrt{f'_c} \quad \text{for} \quad f'_c = 17 \quad \text{MPa}$$

$$\text{and} \quad v_u = 2.17\sqrt{f'_c} \quad \text{for} \quad f'_c = 10\,000 \quad \text{psi}$$

$$v_u = 0.180\sqrt{f'_c} \quad \text{for} \quad f'_c = 69 \quad \text{MPa.}$$

4.4.2 Gustafson and Hillerborg (1988)

The ratio of the slope of the ascending branch of the stress-*strain* curve (in the entire specimen) to that of the descending branch of the stress-*displacement* curve (in the fracture zone) in a tensile test of concrete produces a characteristic length which is a measure of concrete brittleness.

$$l_{ch} = 2EG_f / f_t^2$$

where E = modulus of elasticity,
f_t = tensile strength, and
G_f = fracture energy = area under descending branch of stress-displacement curve.

G_f is determined experimentally by the energy required to break a notched three-point bend specimen into two pieces. Typically, HSC would have shorter characteristic lengths ($\sim$ 0.5 m) than NSC ($\sim$ 1 m), indicating that HSC is more brittle than NSC.

"A key to a rational approach with respect to ductility is the fracture energy, as measured by a characteristic length which expresses the widening of the fracture zone in tension. The characteristic length varies over a large range from about 1000 mm for very ductile concretes and about 600-100 mm for a normal case, to 70 mm for a concrete unit with a cube strength of 170 MPa manufactured by high pressure steam curing."

The characteristic length is incorporated into a finite-element program which assumes an *a priori* chosen crack path to calculate the shear strength f_v of beams of various depths without stirrups. Various crack paths were investigated to minimize the strength. Results show the following trend:

$$\frac{f_v}{f_t} = k\left(\frac{d}{l_{ch}}\right)^{-0.25}$$

where k = proportionality coefficient and d = beam depth.

This formula quantifies the size effect and links it to the characteristic length, l_{ch}. Although the exponent agrees with the Weibull strength theory, it is merely a coincidence. The Weibull theory does not provide an explanation of the size effect in shear strength.

4.4.3 Hillerborg (1989) presents a convincing case of the use of the fracture energy G_F as a measure of the tensile toughness of concrete. The characteristic length l_{ch}, which can be derived from the fracture energy, provides a good scaling factor which can explain the size effect in the tensile failure of concrete (shear or cracking strength of beams).

The shear strength f_v of a beam without stirrups is:

$$f_v = f_t \left(\frac{d}{l_{ch}} \right)^{-1/4} = \left(\frac{E G_F f_c'}{d} \right)^{1/4}$$

Agreement with experiments is good. The author notes that the CEB 1978 Model Code takes more explicit account of the size effect than does the ACI code.

5. Future Research

5.1 Analytical Work

Great progress has been made, especially in the last 20 years, in the analytical solution of shear problems in reinforced concrete, since Mörsch and Ritter laid the foundation at the beginning of the 20th century. Research tools of great sophistication have been developed (e.g., Prisco and Gambarova 1995), but their implementation into design codes would require considerable simplification. Of particular note is the Modified Compression Field Theory which combines "rationality", in the sense that it satisfies equilibrium, compatibility and stress-strain relationships, with certain simplifying assumptions (principal stresses and strains are parallel, verify the ability of cracks in the direction of principal compression to transmit shear) that make it amenable to Code formulation. In addition, extensive verification with experimental results (Fig. 3.12) has led to the adoption of the MCFT in a number of Codes (Canada, Norway, AASHTO LRFD, although with some reservation for the last one. See § 4.1.15).

Further progress will no doubt be achieved, to mention a few examples: in simplifying and implementing some of the German work into Code provisions (e.g., Kupfer et al. 1992, Reineck 1991); in developing computer programs that track the "rotating" crack angle to predict shear behavior even more accurately (Kollegger 1992); in accounting for arch action to the same level of accuracy as truss action (e.g. Prisco and Gambarova 1995). However, Schlaich's (1987) remark ought to perhaps be kept in mind, that the shear problem for B-regions is probably overworked already, and surpasses in exactness the solutions available for D-regions.

Regarding D-regions, there is a need for greater automation of the design of strut-and-tie models. Presently, the process is a manual one, which has the advantage of allowing the designer to visualize the flow of forces. In practice, however, multiple load cases create a daunting challenge. Whereas procedures exist for B-regions to select governing load cases and to ensure that the design meets all criteria for strength and serviceability for all load cases, such procedures remain to be developed for D-regions. Relying on experience and judgement, designers would select a few critical load cases and dimension accordingly. Practical detailing considerations sometimes govern and the resulting strut-and-tie model may be quite different from the stress flow obtained by an elastic finite-element analysis of the remaining load cases. There is often no easy way to ensure that the concrete has adequate ductility, or that the ensuing crack widths will meet serviceability requirements. Some of this work is being undertaken at NIST in collaboration with Cornell University.

5.2 Experimental Work

More experimental research needs to be done on the strength of struts and nodes. Consensus has been difficult to achieve because several strut-and-tie models are usually possible to match an experiment.

The strength of concrete under biaxial tension-compression is common to D- and B-regions and is an essential element of all modern theories of shear. Again, more work needs to be done to achieve consensus on a softening model.

An important mechanism of shear resistance is the capacity of cracks to transmit shear, or shear friction. In the MCFT, concrete tension is limited by shear across cracks. Transverse reinforcement

provides a clamping force, restrains crack width, and thus influences interface shear capacity. For members with little or no transverse reinforcement, the dowel action of the longitudinal steel limits the crack width. Loss of dowel action allows the crack to open up rapidly and lose its interface shear capacity, thus triggering splitting along the longitudinal reinforcement and failure.

Although both the strength of concrete under biaxial tension-compression and shear friction are important, the research priority for HSC ought to be shear friction. Tests at the University of Delft (§ 4.3.5) have shown a decrease in shear friction of 35 % for HSC compared with NSC, because HSC fractures along much smoother surfaces than NSC. This affects shear strength adversely and could be the reason why the shear strength decreases as the compressive strength increases above 80 MPa, as observed at the Norwegian Institute of Technology (§ 4.1.7). On the other hand, tests at Delft (§ 4.2.4) show no marked difference between HSC and NSC as far as biaxial tension-compression behavior is concerned. In addition, shear friction tests require a much smaller capital expenditure than biaxial panel tests and fewer centers are presently investigating shear friction than biaxial behavior.

For these reasons we recommend that NIST initiate an experimental research program to improve our knowledge of shear transfer across cracks of HSC, and a parametric study of the shear strength of beams, using the MCFT, to determine the influence of shear friction and various biaxial softening models.

6. Acknowledgments

Drs. Richard Marshall, Andrew Taylor and Long Phan of NIST, Professors Michael Collins of the University of Toronto and Julio Ramirez of Purdue University reviewed earlier drafts of this report. The final report is much improved thanks to their comments and criticisms. Guy Pham of Doris Engineering, Paris, provided the French Concrete Codes, Lisa Sier and Nancy Fleegle helped with the typing. To all of them, the authors express their gratitude.

7. References

AASHTO (American Association of State Highway and Transportation Officials) (1994): "LRFD Bridge Design Specifications." 1st ed., Washington, D.C., 1091 pp.

ACI (American Concrete Institute) (1995): "ACI Building Code Requirements for Reinforced Concrete ." ACI 318-95.

ACI Committee 363 (1992): "State of the Art Report on High-Strength Concrete." ACI 363R-92, 55 pp.

ACI-ASCE Committee 326 (1962): "Shear and Diagonal Tension." ACI J., v. 59, no. 1 and 2, Jan. and Feb. 1962. See also Joint ASCE-ACI Committee.

Adebar, P. and Collins, M.P. (1996): "Shear Strength of Members without Transverse Reinforcement." Canadian J. Civil Eng. v. 23, pp. 30-41.

Adebar, P. and Collins, M.P. (1994): "Shear Design of Concrete Offshore Structures." ACI St. J. v. 91, no. 3, May-June 1994, pp. 324-335.

Adebar, P. and Collins, M.P. (1991): "A Consistent Shear Design Model for Concrete Offshore Structures." IABSE Colloq. on *Structural Concrete*, IABSE Rep., v. 62, pp. 513-518.

Ahmad, S.H., Khaloo, A.R., and Poveda, A. (1986): "Shear Capacity of Reinforced High Strength Concrete Beams. "ACI J., v. 83, no. 2, Mar.-Apr. 1986, pp. 297-305.

Aoyagi, Y. (1992): "State of the Art Experimental Study Related to In-Plane Shear in Reinforced Concrete Shell Elements in Japan." Proc. Symp. on *Concrete Shear in Earthquake*, Houston, pp. 3-12.

Aoyama, H. (1992): " Design Philosophy for Shear in Earthquake Resistance in Japan." Proc. Symp. on *Concrete Shear in Earthquake*, Houston, pp. 407-418.

BAEL (Béton Armé aux Etats Limites) (1991):"Règles Techniques de Conception et de Calcul des Ouvrages et Constructions en Béton Armé suivant la Méthode des Etats Limites." CCTG (Cahier des Clauses Techniques Générales) fasc. 62 N.

Bažant, Z. and Gambarova, P. (1980): "Rough Cracks in Reinforced Concrete" ASCE ST 4, v. 106, Apr.1980, pp. 819-841.

Belarbi, A., and Hsu, T.C. (1995): "Softened Concrete in Biaxial Tension-Compression."ACI St. J., v. 92 , no. 5, Sep.-Oct. 1995, pp. 562-573.

Belarbi, A., and Hsu, T.C. (1991): "Constitutive Laws of RC in Biaxial Tension-Compression." Research Report UHCEE 91-2, Univ. of Houston, Texas.

Bernhardt, C.J. and Fynboe, C.C. (1986): "High Strength Concrete Beams." Nordic Concrete Research, no. 5, Dec. 1986, pp. 19-26.

Bhide, S.B. and Collins, M.P. (1989): "Influence of Axial Tension on the Shear Capacity of Reinforced Concrete Members." ACI St.J., Sep.-Oct. 1989, pp. 570-581.

Bjerkeli, L., Dyngeland ,T., Drangsholt, G., Lenshow, R., Maage, M., Smeplass, S., Stemland, H. and Thorenfeldt, E. (1989): "High Strength Concrete: State of the Art." SINTEF Rep. PB89-220768 by the Norwegian University of Technology, Trondheim, for the Norwegian Hydro Technical Lab. Trondheim, Jan. 1989.

Bonneau, O., Poulin, C., Dugat, J., Richard, P. and Aïtcin, P.C. (1996): "Reactive Powder Concretes: From Theory to Practice." Concrete International, v. 18, no. 4, Apr. 1996, pp. 47-49.

Braestrup, M.W. (1994): "Concrete Plasticity: The Copenhagen Shear Group, 1973-79." *Concrete Plasticity: A Tribute to Professor Nielsen on his 60th Birthday.* Danish J. of Structural Engineering, v. 65, no. 2-3-4, pp. 33-87.

BPEL (Béton Précontraint aux Etats Limites) (1991):"Règles Techniques de Conception et de Calcul des Ouvrages et Constructions en Béton Précontraint suivant la Méthode des Etats Limites." CCTG (Cahier des Clauses Techniques Générales) fasc. 62.

CEB (Comité Euro-International du Béton, 1991): "CEB-FIP Model Code 1990." CEB Bull. d'Information, no. 203, 204 and 205, July 1991.

Chana, P.S.(1987): "Investigation of the Mechanism of Shear Failure of Reinforced Concrete Beams." Mag. of Concrete Research, v. 39, no. 141, Dec. 1987, pp. 196-204.

Collins, M.P. (1993): "The Use of Rational Design Methods for Shear." ACI SP 157 Proc. Thomas Paulay Symp. *Recent Developments in Lateral Force Transfer in Buildings,* Univ. California San Diego, Sep. 1993, pp. 351-374.

Collins, M.P. (1992): "The Response of Reinforced Concrete Elements Subjected to Shear." Proc. Symp. on *Concrete Shear in Earthquake*, Houston, pp. 13-23.

Collins, M.P. (1987): "Shear Design of Complex HSC Structures."Proc. Symp. on *Utilization of High Strength Concrete*, Stavanger, Norway, June 1987, pp. 345-364.

Collins, M.P. (1978): "Towards a Rational Theory for RC Members in Shear."ASCE, v. 104, ST 4, Apr. 1978, pp. 649-666.

Collins, M.P. and Aïtcin, P.C. (1993): "Design and Construction Using High-Performance Concrete: Some Lessons from Offshore Concrete Structures." Proc. Conf. on *Structural Concrete,* Toronto, May 1993.

Collins, M.P., Mitchell, D., Adebar, P. and Vecchio, F.J. (1996): "General Shear Design Method." ACI St. J., v. 93, no.1, Jan.-Feb.1996, pp. 36-45.

Collins, M.P., Mitchell, D. and MacGregor, J.G. (1993): "Structural Design Considerations for High-Strength Concrete." Concrete Int., May 1993, pp. 27-34.

Collins, M.P. and Mitchell, D. (1991): Prestressed Concrete Structures. Prentice-Hall Inc, Englewood Cliffs, N.J., 1991, 766 pp.

Collins, M.P. and Mitchell, D. (1986): "A Rational Approach to Shear Design: The 1984 Canadian Code Provisions." ACIJ., Nov.-Dec. 1986, pp. 925-933.

Collins, M.P. and Mitchell, D. (1980): "Shear and Torsion Design of Prestressed and Non-Prestressed Concrete Beams."PCIJ., v. 25, no. 5, Sep.-Oct. 1980, pp. 32-100.

Collins, M.P. and Porasz, A. (1989): "Shear Design for High Strength Concrete." CEB Bull. d'Information no. 193: *Design Aspects of High Strength Concrete*, pp. 75-83. Presented at the 26th Plenary Session of CEB, Dubrovnik, Sep. 1988.

Collins, M.P., Vecchio, F.J., Adebar, P. and Mitchell, D. (1991): "A Consistent Shear Design Model."Colloq. on *Structural Concrete*, Stuttgart, IABSE Rep., v. 62, pp. 457-462.

CSA (Canadian Standards Association) (1994):" Design of Concrete Structures." CSA A23.3-94, Dec. 1994, 200 pp.

Elzanaty, A.H., Nilson, A.H. and Slate, F.O. (1986): "Shear Capacity of Reinforced Concrete Beams using High Strength Concrete." ACI J., v. 83, Mar.-Apr. 1986, pp. 290-296.

Eurocode No.2 (1991): Design of Concrete Structures. Part 1: General Rules and Rules for Buildings, Commission of the European Communities, ENV 1992-1-1, Dec. 1991, p.253.

Fardis, M.N., and Buyukozturk, O. (1979): "Shear Transfer Model for RC." Proc. ASCE EM 2, v.105, Apr. 1979, pp. 255-275.

Ferguson, P.M. (1973): Reinforced Concrete Fundamentals John Wiley, 3rd ed.

FIP-CEB Working Group on HSC (1990): "High Strength Concrete: State of the Art." Draft 5B CEB Bull. d'Information no. 197, Apr. 1990.

Frénay, J.W. (1985): "Shear Transfer Across a Single Crack in Reinforced Concrete under Sustained Loading." Part I, Experiments, Stevin Report, 5-85-5, 114 pp.

Frénay, J.W. (1990): "Theory and Experiments on the Behavior of Cracks in Concrete Subjected to Sustained Shear Loading." Delft Univ. of Technology, Heron, v. 35, no. 1, 80 pp.

Frénay, J.W., Pruijssers, A.F., Reinhardt, H.W. and Walraven, J.C. (1987): "Shear Transfer in High

Strength Concrete."Proc. Symp. on *Utilization of High Strength Concrete*, Stavanger, Norway, June 1987, pp. 225-235.

Fukuhara, M. (1985): "A Proposition about the Value Formula for the Ultimate Shear Strength of RC Beams with High Tension Shear Reinforcement." Proc. Japan Concrete Institute, no. 7, pp. 525-528.

Fukuhara, M., Kokusho, S. (1982.12): "Effectiveness of High Tension Shear Reinforcement in Reinforced Concrete Members." J. Structural and Construction Engineering (Transactions of AIJ) no. 320, pp. 12-20.

Gambarova, P. and Prisco, M. Di (1991): "Interface Behavior."CEB Bulletin d'Information no.210, v.1, ch.5, July 1991, pp. 161-209.

Gustafson, P.J., and Hillerborg, A. (1988): "Sensitivity in Shear Strength of Longitudinally Reinforced Concrete Beams to Fracture Energy of Concrete." ACI St. J., May-June 1988, pp. 286-294.

Han, K.J., Mau, S.T. and Hsu, T.T. (1992): "Ductile and Brittle Failures of RC Wall Elements Subjected to Shear." Proc. Symp. on *Concrete Shear in Earthquake*, Houston, pp. 375-384.

Holand, I. (1989): "State of the Art of Design Aspects and Research Needs in the Future."CEB Bull. d'Information, no. 193: *Design Aspects of HSC*, Dec 1989, pp. 145-163. Presented at the 26th Plenary Session of CEB, Dubrovnik, Sep. 1988.

Hillerborg, A. (1989): "Fracture Mechanics and the Concrete Codes." ACI SP 118.7: *Fracture Mechanics: Application to Concrete*, pp. 157-169.

Hofbeck, J.A., Ibrahim, I.O. and Mattock, A.H. (1969): "Shear Transfer in Reinforced Concrete." ACIJ, v.66, no. 2, Feb. 1969, pp. 119-128.

Hognestad, E. (1952): "What do we know about Diagonal Tension and Web Reinforcement in Concrete ? " Univ. Of Illinois Engrg. Exp. Station, Circular Series no.64, 47 pp.

Hognestad, E. (1951): "A Study of Combined Bending and Axial Load in RC Members." Univ. of Illinois Engrg. Exp. Station, Bulletin Series no. 399, Bull. no.1, 28 pp.

Houde, J. and Mirza, M.S. (1974): "A Finite-Element Analysis of the Shear Strength of Reinforced Concrete Beams." ACI SP 42.5: *Shear in Reinforced Concrete*, pp. 103-128

Hsu, T. (1993): Unified Theory of Reinforced Concrete. CRC Press, 1993, 313 pp.

Hsu, T. (1992): Discussion. Proc. Symp. on *Concrete Shear in Earthquake*, Houston, pp. 498-499.

Hsu, T. (1988): "Softened Truss Model Theory for Shear and Torsion." ACI St. J., v. 85, no.6, Nov.-Dec. 1988, pp. 624-635.

Hsu, T. (1991): "Non-linear Analysis of Concrete Membrane Elements."ACI St. J., v. 88, no.5, Sep.-Oct. 1991, pp. 552-561.

Hsu, T., Belarbi, A. and Pang, X.B. (1992): "Stress-Strain Relationships for Reinforced Concrete Elements." Proc. Symp. on *Concrete Shear in Earthquake*, Houston, pp. 43-54.

Hsu, T.C. and Mo, Y.L. (1985): "Softening of Concrete in Low-Rise Shear Walls." ACIJ., Nov.-Dec. 1985, pp. 883-889.

Hsu, T.C. and Zhang, L.X. (1996): "Tension Stiffening in RC Membrane Elements." ACIJ., v. 93, no. 1 , Jan.-Feb. 1996, pp. 108-115.

Ichinose, T. (1990): "A Shear Design Equation for Ductile Reinforced Concrete Members." *Earthquake Engrg. and Structural Dynamics*, Wiley, Oct. 1990.

Jakobsen, B. (1989): "High Strength Concrete in Offshore Structures." CEB Bull. d'Information no. 193*: Design Aspects of HSC*, Dec. 1989.

Jenq, Y.S., and Shah, S.P. (1989): "Shear Resistance of Reinforced Concrete Beams: A Fracture Mechanics Approach." ACI SP 118.11: *Fracture Mechanics: Application to Concrete,* pp. 237-287.

Jensen, J.F. (1979): "Plastic Solutions for Reinforced Concrete Beams in Shear." IABSE Colloq. *Plasticity in Reinforced Concrete*, Copenhagen.

Jimenez, R., Gergely, P. and White. R.N. (1978): "Shear Transfer across Cracks in RC." Cornell University Report 78-4, 357 pp.

Jirsa, J., Breen, J., Bergmeister, K., Barton, D., Anderson, R. and Bouadi, H. (1991): "Experimental Studies of Nodes in Strut-and-Tie Models." IABSE Colloq. on *Structural Concrete*, IABSE Rep., v. 62, pp. 525-532.

Johnson, M.K., and Ramirez, J.A.(1989): "Minimum Shear Reinforcement in Beams with Higher Strength Concrete." ACI St.J., v.86, no.4, Jul.-Aug.1989, pp. 378-382.

Joint ASCE-ACI Task Committee 426 on Shear and Diagonal Tension (1973,1990): "The Shear Strength of Reinforced Concrete Members." J. Struct. Div., ASCE ST6, June 1973, reapproved 1990.

Kim, J.K. and Park, Y.D. (1994): "Shear Strength of Reinforced High Strength Concrete Beams without Web Reinforcement." Mag. of Concrete Research, v. 46, no.166, pp. 7-16.

Kolleger, J.(1992): "Comparison of Fixed and Rotating Crack Models in the Analysis of Panels, Plates and Shells Subjected to Shear." Proc. Symp. on *Concrete Shear in Earthquake*, Houston, pp. 216-225.

Kolleger, J. and Mehlhorn, G. (1990): "Material Model for the Analysis of RC Surface Structures."

Computational Mechanics, no. 6, pp. 341-357, Springer Verlag.

Kolleger, J. and Mehlhorn, G. (1987): "Material Model for Cracked RC." IABSE Colloq. on *Computational Mechanics of Concrete Structures: Advances and Applications*, Delft, Report no. 54, pp. 63-74.

König, G., Grimm, R. and Ramal, G. (1993): "Shear Behavior of Longitudinally Reinforced Concrete Members of High Strength Concrete." Darmstadt Concrete, v. 8, pp. 27-42.

Kotsovos, M. (1991): "Shear in Structural Concrete: a Reappraisal of Current Concepts."IABSE Colloq. on *Structural Concrete*, IABSE Rep., v. 62, pp. 667-672.

Kotsovos, M. (1988): "Compressive Force Path Concept: Basis for Reinforced Concrete Ultimate Limit State Design." ACI St. J., Jan.-Feb. 1988, pp.68-75.

Krauthammer, T. (1992): "Minimum Shear Reinforcement based on Interface Shear Transfer." ACI St.J., v. 89, no. 1, Jan.-Feb. 1992, pp. 99-105.

Kupfer, H. and Bulicek, H. (1992): "A Consistent Model for the Design of Shear Reinforcement in Slender Beams with I- or Box-Shaped Cross-Section." Proc. Symp. on *Concrete Shear in Earthquake*, Houston, pp. 256-265.

Kupfer, H., Mang, R. and Karavesyroglou, M. (1983): "Ultimate Limit State of the Shear Zone of Reinforced and Prestressed Concrete Girders - An Analysis taking Aggregate Interlock into Account." Bauingenieur 58, pp. 143-149, (In German).

Laible, J.P., White, R.N. and Gergely, P. (1977): "Experimental Investigation of Seismic Shear Transfer across Cracks in Concrete Nuclear Containment Vessels." ACI SP 53: *RC Structures in Seismic Zones*, pp. 203-226.

Leivestad, S.,Vik, B. and Ekeberg, P.K. (1987): "The Utilization of HSC: A Survey of International Codes and Regulations." Proc. Symp. on *Utilization of High Strength Concrete*, Stavanger, Norway, June 1987, pp.379-391.

Levi, F. and Marro, P. (1989): "Shear Tests up to Failure of Beams made with Normal and High Strength Concrete." CEB Bull. d'Information no.193: *Design Aspects of HSC*, Dec 1989, pp. 11-24 Presented at the 26th Plenary Session of CEB, Dubrovnik, Sep. 1988.

Loov, R.E. and Patnaik, A.K. (1994): "Horizontal Shear Strength of Composite Concrete Beams with a Rough Interface." PCIJ v.39, no.1, Jan-Feb.1994, pp.48-69.

MacGregor, J.G. (1992): Reinforced Concrete: Mechanics and Design. 2nd ed., Prentice Hall, Englewood Cliff, N.J., 1992, 848 pp.

MacGregor, J.G. (1991): "Dimensioning and Detailing." Colloq. on *Structural Concrete*, Stuttgart, IABSE Rep., v. 62 , pp. 391- 410.

MacGregor, J.G. and Gergely, P. (1977): "Suggested Revisions to ACI Building Code Clauses Dealing with Shear in Beams." ACIJ. v. 74, no. 10, Oct. 1977, pp. 493-500.

Marro, P. (1987): "Bending and Shear Tests up to Failure of Beams made with High-Strength Concrete." Proc. Symp. on *Utilization of High- Strength Concrete*, Stavanger, Norway, June 1987, pp. 183-193.

Marti, P. (1992): "State of the Art of Membrane Shear Behavior - European Work." Proc. Symp. on *Concrete Shear in Earthquake*, Houston, pp. 187-195.

Marti, P. (1991): "Dimensioning and Detailing."Colloq. on *Structural Concrete*, Stuttgart, IABSE Rep., v. 62, pp. 411- 444.

Marti, P.(1985): "Truss Models in Detailing." Concrete International, v. 7, no.12, Dec.1985, pp. 66-73.

Marti, P.(1985): "Basic Tools of Reinforced Concrete Beam Design." ACIJ. v. 82, no. 1, Jan.-Feb. 1985, pp. 46-56.

Marti, P. (1982): "Strength and Deformations of Reinforced Concrete Members under Torsion and Combined Actions." CEB Bull. d'Information no. 146, Jan. 1982, pp. 97-138.

Mattock, A.H. and Hawkins, N.M. (1972): "Shear Transfer in RC - Recent Research." PCIJ. v. 17, no. 2, Mar.-Apr. 1972, pp. 55-75.

Mattock, A.H. (1988): Discussion of paper by Walraven, J.C., Frénay, J. and Pruijssers, A. (1987): "Influence of Concrete Strength and Load History on the Shear Friction Capacity of Concrete Members."PCIJ. v. 22, no. 1, Jan.-Feb. 1988, pp.165-166.

Mau, S.T. and Hsu, T.T. (1988): Discussion of paper by Walraven, J.C., Frénay, J. and Pruijssers, A. (1987): "Influence of Concrete Strength and Load History on the Shear Friction Capacity of Concrete Members."PCIJ. v. 22, no. 1, Jan.-Feb. 1988, pp. 166-170.

Mehlhorn, G. (1988): "Two-Dimensional FE-Analysis of Reinforced Concrete Membrane Elements." Int. Conf. on Computational Engrg. Science, Atlanta, Apr. 10-14, 1988.

Mikame, A., Uchida, K. and Noguchi, H. (1991): "A Study of Compressive Deterioration of Cracked Concrete." Proc. Int. Workshop on *FEA of RC*, Columbia Univ., New York, N.Y.

Millard, S.G., and Johnson, R.P. (1984): "Shear Transfer across Cracks in Reinforced Concrete due to Aggregate Interlock and to Dowel Action." Mag. of Concrete Research, v. 36, no.126, Mar. 1985, pp. 9-21.

Millard, S.G., and Johnson, R.P. (1985): "Shear Transfer in cracked Reinforced Concrete." Mag. of Concrete Research, v. 37, no.130, Mar. 1985, pp. 3-15.

Mirami, K., and Kuramoto, H. (1987): "A Shear Design Equation for Reinforced Concrete Members." Proc. Japan Concrete Institute, v. 9, no. 2, June 1987, pp. 347-352.

Mitchell, D. and Bickley, J. (1993): "Code Implications: High Performance Concrete" Proc. CPCA/CSCE Conf. on *Structural Concrete,* Toronto, May 1993.

Mitchell, D. and Collins, M.P. (1974): "Diagonal Compression Field Theory - A Rational Model for Structural Concrete in Pure Torsion." ACIJ. v. 71, Aug. 1974, pp. 396-408.

Mitchell, D. And Cook, W. (1991): "Design of Disturbed Regions." IABSE Colloq. on *Structural Concrete*, Stuttgart, IABSE Rep., v. 62, pp. 533-536.

Miyahara, T., Kawakami, T. and Maekawa, K. (1988): "Non Linear Behavior of Cracked RC Plate Element under Uniaxial Compression." Proc. Japan Society of Civil Engineers, v. 11, pp. 306-319. Also in Concrete Library Int., JSCE, no.11, June 1988, pp. 131-144.

Mokhtarzadeh, A. and French, C.W. (1994): "Bibliography on HSC" PCIJ., May 1994, pp. 130-137.

Mörsch, E. (1909): Concrete Steel Construction. McGraw-Hill, N.Y.,1909, 368 pp (English translation by E.P. Goodrich, from 3rd. ed. of Der Eisenbeton, 1st ed., 1902).

Mphonde, A.G. (1988): "Aggregate Interlock in High Strength Reinforced Concrete Beams." Proc. Inst. Civil Engr., Part 2, v. 85, Sep. 1988, pp. 397-413.

Mphonde, A.G.and Frantz, G.C. (1984): "Shear Tests of High and Low Strength Concrete Beams without Stirrups." ACI J., v. 81, no. 4, Jul.-Aug. 1984, pp. 350-357.

Mphonde, A.G. and Frantz, G.C. (1985):" Shear Tests of High and Low Strength Concrete Beams with Stirrups." ACI SP 87.10 on *High Strength Concrete*, pp. 179-196.

Nakamura, H. and Higai, T. (1995): "Evaluation of Shear Strength of RC Beam Section Based on Extended Modified Compression Field Theory." Concrete Library of Japan Soc. of Civil Engineers, no. 25, June 1995, pp. 93-105.

Nielsen, M.P. (1984): Limit Analysis and Concrete Plasticity. Prentice-Hall Inc, Englewood Cliffs, N.J., 1984, 620 pp.

Nilson, A.H. (1987): "High Strength Concrete: An Overview of Cornell Research." Proc. Symp. on *Utilization of High Strength Concrete*, Stavanger, Norway, June 1987, pp. 27-38.

Nilson, A.H. (1985): "Design Implications of Current Research on High Strength Concrete." ACI SP 87.7 on *High Strength Concrete,* pp. 85-118.

Norwegian Council for Building Standardization (1992): Norwegian Standard NS 3473 E, 4th ed., Nov. 1992.

Pang, X.B. and Hsu, T.C. (1996): "Fixed Angle Softened Truss Model for Reinforced Concrete." ACIJ. v. 93, no. 2, Mar.-Apr. 1996, pp. 197-207.

Park, R. and Paulay, T. (1975): Reinforced Concrete Structures. Wiley-Interscience, New York, 769 pp.

Paulay, T., Loeber, P.J. (1974): "Shear Transfer by Aggregate Interlock." ACI SP 42.1: *Shear in Reinforced Concrete,* pp. 1-15.

Perdikaris, P.C., White, R.N. and Gergely, P. (1980): "Strength and Stiffness of Tensioned RC Panels Subjected to Membrane Shear, Two Way Reinforcing." Nuclear Regulatory Research Report NUREG/CR-1602, Washington, 393 pp.

Poli, S.D., Gambarova, P.G. and Karakoç, C. (1987): "Aggregate Interlock: Role in Reinforced Concrete Thin-Webbed Beams in Shear." J. Struct. Engrg., v. 113, no. 1, Jan. 1987, pp. 1-19.

Poli, S.D., Prisco, M.D. and Gambarova, P.G. (1990): "Stress Fields In Web of Reinforced Concrete Thin-Webbed Beams Failing in Shear." J. Struct. Engrg., v. 116, no. 9, Sept. 1990, pp. 2496-2515.

Prisco, M.D. and Gambarova, P.G. (1995): "Comprehensive Model for Study of Shear in Thin-Webbed RC and PC Beams ." J. Struct. Engrg., v. 121, no. 12, Dec. 1995, pp. 1822-1831.

Prisco, M.D. and Gambarova, P.G. (1992): "Optimum Design of Stirrups in RC and PC Thin-Webbed Beams Failing in Shear."Proc. Symp. on *Concrete Shear in Earthquake*, Houston, pp. 246-255

Pruijssers, A.F., and Liqui Lung, G. (1985): "Shear Transfer Across a Crack in Concrete Subjected to Repeated Loading - Experimental Results." Part I, Stevin Report 5-85-12, 178 pp.

Ramirez, J. and Breen, J. (1991): "Evaluation of a Modified Truss Model Approach for Beams in Shear." ACI St. J. v.88, no.5, Sept.-Oct. 1991, pp. 562- 571.

Regan, P.E. (1993): "Research on Shear: A Benefit to Humanity or a Waste of Time ?"The Structural Engineer, v. 71, no.19/5, Oct. 1993, pp. 337-347.

Reineck, K.H. (1991a): "Modeling of Members with Transverse Reinforcement." IABSE Colloq. on *Structural Concrete*, Stuttgart, IABSE Rep., v. 62, pp. 481-488.

Reineck, K.H. (1991b): "Modeling of Members without Transverse Reinforcement." IABSE Colloq. on *Structural Concrete*, Stuttgart, IABSE Rep., v. 62, pp. 643-648.

Reineck, K.H. (1991c): "Ultimate Shear of Members without Transverse Reinforcement." ACI St.J. v.88, no.5, Sep.- Oct. 1991, pp.592-602.

Reineck, K.H. (1989): "Theoretical Considerations and Experimental Evidence on Web Comparison Failure of High Strength Concrete Beams." CEB Bull. d'Information no. 193: *Design Aspects of*

HSC, Dec. 1989, pp. 59-74. Presented at the 26th Plenary Session of CEB, Dubrovnik, Sep. 1988.

Reineck, K.H. (1982): "Models for the Design of Reinforced and Prestressed Concrete Members." Part 2 of Progress Report of Task Group IV/1 *Shear in Prestressed Concrete* CEB Bull. d'Information no. 146, Jan. 1982.

Rogowsky, D.M. and MacGregor, J.G. (1986): "Design of Reinforced Concrete Deep Beams." Concrete Int., v. 6, no.8, Aug. 1986, pp. 49-58.

Roller, J.J. and Russell, H.G. (1990): "Shear Strength of High Strength Concrete Beams with Web Reinforcement." ACI St.J., v. 87, no. 2, Mar.-Apr. 1990, pp. 191-198.

Russell, H.G. (1987): "HSC in North America."Proc. Symp. on *Utilization of High Strength Concrete*, Stavanger, Norway, June 1987, pp. 561-571.

Sakaguchi, N.,Yamanobe, K., Kitada, Y., Kawachi, T. and Koda, S. (1990): "Shear Strength of High Strength Concrete Members." ACI 2nd Int. Symp. on *HSC*, ACI SP 121.9, pp. 155-178.

Sarsam, K.F. and Al-Musawi, J.M.S. (1992): "Shear Design of High and Normal Strength Concrete Beams with Web Reinforcement." ACI St. J., v. 89, no. 6, Nov.-Dec. 1992, pp. 658-664.

Schlaich, J. (1991): "The Need for Consistent and Translucent Models." IABSE Colloq. on *Structural Concrete*, Stuttgart, IABSE Rep., v. 62, pp. 169-184.

Schlaich, M. and Anagostou, G. (1989): "Stress Fields for Nodes of Strut an d Tie Models."ASCE J. of Structural Engrg., v. 116, no. 1, Jan.1990, pp. 13-23.

Schlaich, J, Schäfer, K., and Jennewein, M. (1987): "Toward a Consistent Design of Structural Concrete." PCI J., v. 32, no. 3, May-June 1987, pp. 74-150.

Shahawy, M.A. and Batchelor, B. deV (1996): "Shear Behavior of Full-Scale Prestressed Concrete Girders: Comparison between AASHTO Specifications and LRFD Code." PCI J. v. 41, no.3, May-June 1996, pp. 48-53.

Shirai, S. and Noguchi, H. (1989): "Compressive Deterioration of Cracked Concrete." *Structures Congress: Design, Analysis and Testing*, Proc. ASCE, New York, N.Y., pp. 1-10.

Stroband, J.(1995): "Biaxially Loaded Reinforced Panels in High Strength Concrete." Progress in Concrete Research, Delft Univ. of Technology, v. 4, pp. 67-74.

Takagi, H. and Kanoh,Y. (1991): "Use of Super High-Strength Rebars as Web Reinforcements." ACI Int. Symp. on *Evaluation and Rehabilitation of Concrete Structures and Innovations in Design*, Hongkong, ACI SP 128-65, pp. 1049-1063.

Tan, K.H., Kong, F.K., Teng, S. and Guan, L. (1995): "High Strength Concrete Deep Beams with Effective Span and Shear Span Variations." ACI St.J., Jul.-Aug. 1995, pp. 395-405.

Tanabe, T., and Wu, Z. (1991): "Strain Softening under Biaxial Tension and Compression." IABSE Colloq. on *Structural Concrete*, Stuttgart, IABSE Reports, v. 62, pp. 623-636.

Tassios, T.P., and Vintzĕleou, E.N. (1987): "Concrete-to-Concrete Friction." ASCE J. of Structural Engineering, v. 113, no.4, April 1987, pp. 832-849.

Thorenfeldt, E., and Drangsholt, G. (1990):" Shear Capacity of Reinforced High Strength Concrete Beams." ACI 2nd Int. Symp. on *HSC*, ACI SP 121.8, pp. 129-154.

Thorenfeldt, E., Tomasziewicz, A. and Jensen, J.J. (1987): "Mechanical Properties of HSC and Application in Design." Proc. Symp. on *Utilization of HSC*, Stavanger, Norway, June 1987, pp. 149-159.

Thürlimann, B. (1979):" Plastic Analysis of Reinforced Concrete Beams." IABSE Colloq. *Plasticity in Reinforced Concrete*, Copenhagen, pp. 71-90.

Ueda, M., Noguchi, H., Shirai, N. and Morita, S. (1991): "Introduction to Activity of new RC." Proc. Int. Workshop on *FEA of RC*, Columbia Univ., New York, N.Y.

Uemura, T., Sakurai, S., Hattori, T., Shibata, T., Ohno, K. (1978): "Investigation on the Equations of Ultimate Shear Strength of RC Columns." Annual Meeting of Hokkaido Branch, Architectural Institute of Japan, Sept. 1978, pp. 91-94.

Vecchio, F.J. (1991): " Analysis based on the Modified Compression Field Theory." IABSE Colloq. on *Structural Concrete*, Stuttgart, 1991, IABSE Report, v. 62, pp. 321-326.

Vecchio, F.J. and Collins, M.P. (1993):" Compression Response of Cracked Reinforced Concrete." ASCE J.St. Engrg., v. 119, no.12, Dec. 1993, pp. 3590-3610.

Vecchio, F.J. and Collins, M.P. (1986): "The Modified Compression Field Theory for Reinforced Concrete Elements Subjected to Shear." ACIJ. v. 83, no. 2, March-April 1986, pp. 219-231.

Vecchio, F.J. and Collins, M.P. (1982): "The Response of Reinforced Concrete to In-Place Shear and Normal Stresses." Pub 82.03, Dept. of Civil Engineering, Univ. of Toronto, March 1982, 332 pp.

Vecchio, F.J., Collins, M.P.and Aspiotis, J. (1994): " High Strength Concrete Elements Subjected to Shear." ACI St.J., Jul.-Aug.1994, pp. 423-433.

Vecchio, F.J. and De Roo, A. (1995): "Smeared-Crack Modeling of Concrete Tension Splitting." ASCE J. Engrg. Mech., June 1995, pp. 702-708.

Wagner, H. (1929): "Metal Beams with Very Thin Webs." Zeitschrift für Flugtechnik und Motorluftshiffahr, v. 20, no. 8 to 12, 1929 (in German).

Walraven, J.C. (1995): "Shear Friction in High Strength Concrete." Progress in Concrete Research, Deft University of Technology, v. 4, pp. 57-65.

Walraven, J.C. (1995): "High Performance Concrete: Exploring a New Material." Structural Engrg. Int., Mar. 1995, pp. 182-187.

Walraven, J.C. (1992): "Rough Cracks Subjected to Earthquake Loading." Proc. Symp. on *Concrete Shear in Earthquake*, Houston, pp. 236-245

Walraven, J.C. (1982): "Shear in Elements without Shear Reinforcement." Part 1 of Progress Report of Task Group IV/1 *Shear in Prestressed Concrete,* CEB Bull. d'Information no.146, Jan.1982, 41 pp.

Walraven, J.C. (1981):"Fundamental Analysis of Aggregate Interlock." J. Struct. Div., ASCE, v. 107, ST11, November 1981, pp. 2245-2270.

Walraven, J.C., Frénay, J. and Pruijssers, A. (1987): "Influence of Concrete Strength and Load History on the Shear Friction Capacity of Concrete Members." PCIJ. v. 32, no. 1, Jan.-Feb. 1987, pp. 66-85

Walraven, J.C. and Reinhardt, H.W.(1981): " Theory and Experiments on the Mechanical Behavior of Cracks in Plain and Reinforced Concrete Subjected to Shear Loading." Heron v. 26, no. 1A, 68 pp.

Walraven, J. and Stroband, J. (1994): "Shear Friction in High-Strength Concrete." Proc. ACI Int. Conf. on *High Performance Concrete,* Singapore, ACI SP 149-17, pp. 311-330.

Walther, R. (1989) :"Potentiality of using High Strength Concrete in Structures." CEB Bull. d'Information no.193 *Design Aspects of HSC,* Dec. 1989. Also in Proc. Symp. on *Utilization of High Strength Concrete*, Stavanger, Norway, June 1987, pp. 365-378.

Watanabe, F., and Ichinose, T. (1992): " Strength and Ductility Design of Reinforced Concrete Members subjected to Combined Bending and Shear." Proc. Symp. on *Concrete Shear in Earthquake,* pp. 429-438.

White, R.N. and Holley, M.J. (1972): "Experimental Studies of Membrane Shear Transfer." ASCE J. St. Div., v. 98, ST8, Aug. 1972, pp. 1835-1852.

Yun, Y.M. and Ramirez, J. (1996): "Strength of Struts and Nodes in Strut-Tie Model." ASCE J. of Structural Engineering, v.122, no.1, Jan.1996, pp.20-29.

Zsutti, T. (1968): "Beam Shear Strength Prediction by Analysis of Existing Data." ACIJ. v. 65, no. 11, Nov. 1968, pp. 942-951.